UNIVERSITY OF LIVERPOOL

BIOAVAILABILITY-BASED ENVIRONMENTAL RISK ASSESSMENT OF THE IMPACTS FROM METAL TOXICANTS AND NUTRIENTS IN LAKE TAI

Thesis submitted in accordance with the requirements of the University of Liverpool for the degree of Doctor in Philosophy

by

Xiaokai Zhang

May 2020

ABSTRACT

Environmental pollution has increasingly become a global issue in recent years. Heavy metals are the most prevalent pollutants and are persistent environmental contaminants since they cannot be degraded or destroyed. Environmental risk assessment (ERA) will pave the way for streamlined environmental impact assessment and environmental management of heavy metal contamination. Bioavailability is increasingly in use as an indicator of risk (the exposure of pollutants), and for this reason, whole-cell biosensors or bioreporters and speciation modelling have both become of increasing interest to determine the bioavailability of pollutants. While there is a great emphasis on metals as toxicants in the environment, some metals also serve as micronutrients. The same processes that introduce metals as pollutants into the environment also introduce metals that may function, in some cases, as micronutrients, which then have a role to play in eutrophication, i.e. excessive nutrient richness that is an impairment of many freshwater ecosystems and a prominent cause of harmful algal blooms. In this thesis, I cover a wide range of topics. A unifying theme is biological impacts of metals in the environment and what the implications are for environmental risk assessment.

This thesis begins with my initial work in which I conducted laboratory experiments using a bioreporter, genetically engineered bacterial that can produce dose-dependent signals in response to target chemicals to test the bioavailability of lead (Pb) in aqueous system containing Pb-complexing ligands. Lead serves as a good model because of its global prevalence and toxicity. The

studied ligands include ethylene diamine tetra-acetic acid (EDTA), meso-2,3 dimercaptosuccinic acid (DMSA), leucine (Leu), methionine (Met), cysteine (Cys), glutathione (GSH), and humic acid (HA). The results showed that EDTA, DMSA, Cys, GSH, and HA amendment significantly reduced Pb bioavailability to bioreporter with increasing ligand concentration, whereas Leu and Met had no notable effect on bioavailability at the concentrations tested. Natural water samples from Lake Tai (Taihu) were also been studied which displayed that dissolved organic carbon in Taihu water significantly reduced Pb bioavailability. Meanwhile, the bioreporter results are in accord with the reduction of aqueous Pb^{2+} that I expected from the relative complexation affinities of the different ligands tested. These findings represented a first step toward using bioreporter technology to streamline an approach to ERA.

Dissolved organic matter (DOM) plays an important role in both speciation modelling and bioavailability of heavy metals. Due to the variation of DOM properties in natural aquatic systems, improvements to the exiting standard one size fits-all approach to modelling metal-DOM interactions are needed for ERA. My next effort was to investigate variations in DOM and Pb-DOM binding across the regional expanse of Taihu. Results show that different DOM components are highly variable across different regions of Taihu, and bivariate and multivariate analyses confirm that water quality and DOM characterisation parameters are strongly interrelated. I find that the conditional stability constant of Pb-DOM binding is strongly affected by the water chemical properties and composition of DOM, though is not itself a parameter that differentiates lake water properties in different regions of the lake. The variability of DOM composition and Pb-DOM binding strength across Taihu is consistent with prior findings that a one-size-

fits-all approach to metal-DOM binding may lead to inaccuracies in commonly used speciation models, and therefore such generalised approaches need improvement for regional-level ERA in complex watersheds.

Based on the findings from the investigation of Pb-DOM complexation, I compared a one-size-fits-all approach to different methods of implementing site-specific variations in modelling. I was able to substantively improve the procedures to the existing speciation model commonly used in ERA applications. The results showed that the optimised model is much more accurate in agreement with bioreporter-measured bioavailable Pb. This streamlined approach to ERA that I developed has performed well in a first regional-scale freshwater demonstration.

There is a close connection between environmental water and sediment contamination, and I also studied Pb bioavailability in lake sediemnt with a focus on the ramifications regarding environmental risk. For this work, I studied sediment samples from Brothers Water lake in the United Kingdom, a much simpler lake system than Taihu that is severly impacted by centuries of Pb-mining in the immediate vicinity. The results showed that the total concentration of Pb in the sediment has an inverse relationship with bioavailable Pb in the test samples, has a positive relationship with sediment particle size and sand content and a negative relationship with clay content. I find that the relative amount of bioavailable Pb in the lake sediments are low, although surface sediments may have much higher bioavailable Pb than deeper sediments.

To address the issues of metals and other micronutrients on algal growth, I performed small-scale mesocosm nutrient limitation bioassays using boron (B),

iron (Fe), cobalt (Co), copper (Cu), molybdenum (Mo), nitrogen (N) and phosphorus (P) on phytoplankton communities sampled from different locations in Taihu to test the relative effects of micronutrients on in situ algal assemblages. I found a number of statistically significant effects for micronutrient stimulation on growth or shift in algal assemblage. The most notable finding concerned copper, which, to my knowledge is unique in the literature. However, I am unable to rule out a homeostatic link between copper and iron. The results from my study concur with a small and emerging body of literature suggesting that the potential role of micronutrientss in harmful algal blooms and eutrophication requires further consideration in ERA and environmental management.

The findings from this work are not only of interest to academics, but represent feasible approaches from which environmental practitioners may evaluate risk. My work on Pb needs further validation, however would be validatable through impact assessment studies and is therefore directly and immediately extensible to environmental risk. I am therefore hopeful that my work on ERA will drive tangible outcomes in the work of environmental management. Likewise, though my work on the affect of micronutrients on algal growth is more fundamental than applied at present, there are important and immediate implications for environmental management: at present, copper is used as an algicide. My work suggests the long term effect of copper at 20 $\mu g \cdot L^{-1}$ could possibly encourage rather than inhibit harmful algal blooms. It is satisfying to arrive at a scientifically interesting, and at the same time practically useful outcome from my years' of work, however, I hope that this and other similar work on risk and management interventions could inspire a shift to pollution prevention rather than "end of pipe" solutions.

ACKNOWLEDGEMENTS

Firstly, I would like to thank God for all his blessings. Secondly, I would like to thank everyone who helped me during this project. Foremost, I would like to express my gratitude to my supervisors, Drs Mona Wells and Boris Tefsen for the continuous support of my PhD study and research. I am very grateful to Mona Wells for her help with the good laboratory experience and prudential instruction. I will cherish this forever.

In addition, I would like to thank my committee member, Dr Zheng Chen for the assistance he provided on the measurement of samples by ICP-MS. I also would like to thank Professor Richard Chiverrell for offering me all the sediment samples from Brothers Water lake, and Drs Mal Horsburgh and James Cooper for offering me the workplace in the laboratory at the University of Liverpool.

My sincere thanks also goes to Professor Boqiang Qin, Professor Jianming Deng and Dr Hai Xu at the Nanjing Institute of Geography and Limnology, Chinese Academy of Sciences for their support with water quality data and their extensive expertise and assistance with all aspects of work on Taihu. I have greatly enjoyed my field work in Taihu Laboratory for Lake Ecosystem Research. I would like to thank Boling Li and other PhD students for their help during field work.

Finally, I would like to thank my father and my mother for continuous support during a busy four years. Many thanks to all my friends, especially like to thank my girlfriend Qing Zhang and my friends Xingwu Tang and Liyan Fang for their love and support.

PREFACE

When I was a high school student, many people told me that college students must choose a major of environmental science because it will be easy to find a good job in the future. However, when I chose an environment-related major in college, I found that everything was not what I expected. Students whose majors were related to the environment had difficulty finding good jobs. When I decided not to choose the environmental science major for my Master's degree, an unexpected opportunity made me choose an environment-related major. During the three-year study, I found myself liking my major more and more. It is coincidental and fortunate that my research during the Ph.D. was ERA, and my research target area is China's third largest freshwater lake, Taihu. During my study, I have felt quite confident that I am doing something that is of great significance to improving the human living environment.

This thesis is about the investigation of metal bioavailability on ERA. Moreover, risk assessment of lake pollution has been carried out from different perspectives. I believe that this research will provide evidence and guidance for future risk assessment on larger scale environment.

It is my pleasure to express my thanks to Dr Mona Wells who used to be my supervisor, and I want to thank her for all the help she gave me during my PhD. Her erudition is almost unbelievable. What I learned from her is not only how to do scientific research, but also the attitude towards research. I am also very grateful to my supervisor Dr Boris Tefsen for all his help.

In truth, I could not have achieved my current level of success without the support of my family and my friends. Thank you all for your unwavering support.

Suzhou, China Xiaokai Zhang

TABLE OF CONTENTS

LIST OF TABLES

LIST OF FIGURES

List of Abbreviations and Symbols

3DEEM	Three-dimensional excitation-emission matrix
ADOC	Active dissolved organic carbon
As	Arsenic
B	Boron
BIC	Bayesian information criterion
BIX	The index of recent autochthonous contribution
BLM	Biotic ligand model
BOD	Biological oxygen demand
Chl-a	Chlorophyll-a
COD_{Mn}	Chemical oxygen demand
Co	Cobalt
Cu	Copper
Cys	Cysteine
C_{ADOC}	Concentration of active dissolved organic carbon
$C_{Pb^{2+}}$	Concentration of Pb^{2+}
$C_{Pb}^{Tot,\,diss}$	Concentration of total dissolved Pb
DMSA	Meso-2,3 dimercaptosuccinic acid
DOC	Dissolved organic carbon
DOM	Dissolved organic matter
EDTA	Ethylene diamine tetra-acetic acid
EEM	Excitation emission matrix (synonymous with 3DEEM)
ERA	Environmental risk assessment
ESV	End-systolic volume
FA	Fulvic acid
FCM	Flow cytometry measurement
Fe	Iron
FI	Fluorescence index
FlInd	Fluorescent indices (BIX, HIX and FI)
GSH	Glutathione
HA	Humic acid
HIX	Humification index
HABs	Harmful algal blooms
ICL	Integrated completed likelihood criterion

ICP-MS	Inductively coupled plasma mass spectrometry
IUPAC	International Union of Pure and Applied Chemistry
K_{cond}^{HA}	Conditional stability constant of Pb-Humic acid complexation
K_{cond}^{FA}	Conditional stability constant of Pb-Fulvic acid complexation
K_{cond}^{Trp}	Conditional stability constant of Pb-Tryptophan complexation
K_{cond}^{Try}	Conditional stability constant of Pb-Tyrosine complexation
K_{cond}	Conditional stability constant of lead binding with dissolved organic matter
L_{ADOC}	Organic ligand type
Leu	Leucine
LOD	Limit of detection
LOQ	Limit of quantitation
Pb	Lead
Met	Methionine
MHPRC	Ministry of Health, People's Republic of China
MM	Optimised minimal medium
MN	Micronutrient
Mn	Manganese
Mo	Molybdenum
MOPS	3-[*N*-morpholino] propane sulfonic acid
MRR	Maximum response ratio
N	Nitrogen
Ni	Nickel
NLB	Nutrient limitation bioassays
NIGLAS	Nanjing Institute of Geography and Limnology, Chinese Academy of Sciences
OD_{600}	Optical density at 600 nm
OM	Organic matter
P	Phosphorus
PARAFAC	Parallel factor analysis
PCA	Principle component analysis
RLU	Relative luminescence units
RPD	Relative percent difference

RPD_{geom}	Corresponding geometric mean of Relative Percent difference
RSD	Relative standard deviation
Se	Selenium
SFS	Synchronous fluorescence spectroscopy
SHM	Stockholm humic model
SSR	Sum of squared residuals
St	Sample station
TIN	Total inorganic nitrogen
TLLER	Taihu Laboratory for Lake Ecosystem Research
TOC	Total organic carbon
TDB	Total dissolved boron
TDFe	Total dissolved iron
TDCu	Total dissolved copper
TDCo	Total dissolved cobalt
TDMo	Total dissolved molybdenum
TDN	Total dissolved nitrogen
TDP	Total dissolved phosphorus
TGA	Thermogravimetry
TN	Total nitrogen
TP	Total phosphorus
Trp	Tryptophan
Tyr	Tyrosine
UK	United Kingdom
USEPA	United States Environmental Protection Agency
USNRC	United States National Research Council
V	Vanadium
WHAM	Windemere humic acid model
WQC	Water quality criteria
WRT	Water retention time
WWTPs	Wastewater treatment plants
Zn	Zinc

1 INTRODUCTION

1.1 BACKGROUND

This thesis focuses on development of new approaches to Environmental Risk Assessment (ERA) that will pave the way for expedited environmental impact assessment, which has a crucial role in decision support for environmental management interventions. As the world burden of environmental contamination increases, it is of the utmost importance to develop streamlined approaches to ERA in order to prioritise mitigation measures. Biological effects, such as toxic response, are a consequence of pollutant bioavailability in the environment, hence bioavailability has been an increasing focus of ERA (United States Environmental Protection Agency, USEPA 2016; Zhang et al., 2017), particularly for heavy metals. Many different methods have been and are being developed to utilise bioavailability in ecological and human health risk assessment (USEPA 2007a; Fairbrother et al. 2007). In human health risk assessment, methods include, but are not limited to, methods to assess human oral bioavailability (the definition for which is different from environmental bioavailability, USEPA 2007a). In recent years, whole-cell bioreporters have become of increasing interest to determine the bioavailability of pollutants in environment (Al-Anizi et al. 2014; Van der Meer and Belkin 2010; Wells 2012).

Meanwhile, speciation models are also often used in ERA to evaluate the bioavailability of heavy metals (Di Toro et al. 2001; USEPA 2016), and those models include dissolved organic matter (DOM) in natural water as DOM binds heavy metals and thus reduces their bioavailability (Boggs et al. 1985; Mostofa et al. 2013a). In this research, I conducted some bioavailability-based experiments in the lab and combined them with the speciation modelling. Then, I extended my work to field studies that focused on lakes, as these sinks represent an endpoint for catchment-wide effects (pollution, land use and land use change).

1.2 Research Questions and Structure of Thesis

The structure of this thesis is framed around the following research questions:

I) Are bioreporter results able to reflect expectations based on chemical speciation modelling, i.e. the type of modelling used in ERA?

I report results from this work in Chapter 3, after the literature review in Chapter 2. This work consists of a lab-based case study to examine whether whole-cell bioreporter results are able to reflect expectations based on chemical speciation modelling, with the hope to extend the research into a wider framework of risk assessment. I studied a specific test case concerning the bioavailability of lead (Pb) in aqueous environments containing organic and inorganic Pb-complexing ligands. Inorganic ligands in the media that I used are those commonly encountered in natural waters and organic ligands studied included ethylene diamine tetra-acetic acid (EDTA), meso-2,3 dimercaptosuccinic acid (DMSA), leucine (Leu), methionine (Met), cysteine (Cys), glutathione (GSH), and humic acid (HA), and I also performed preliminary experiments using natural lake

water samples. I compared the results to expectations from theory and some results from speciation modelling.

II) How does the dissolved organic matter in natural water affect the metal speciation, and is there a suitable approach to account for dissolved organic matter variability in ERA modelling?

Having validated the bioreporter for my intended use, the next step in my project was to investigate whether validation could be achieved for a large freshwater system, i.e. using environmental samples rather than well-characterised lab proxies. I found that my results for Pb binding by DOM in natural waters are more complex than I had anticipated due to the possible and unknown variability of natural DOM from site-to-site. Speciation models in common use assume a relatively fixed nature for DOM. Chapter 4 summarises the work that I did to characterise DOM across my chosen field area of Taihu, including determination of site-specific conditional stability constants used in ERA for metal binding with DOM, by using fluorescence spectroscopic techniques combined with different approaches to multivariate data analysis.

III) How does my approach of using a bioreporter and modelling perform in an ERA context for freshwater?

Since a one-size-fits-all approach to metal-DOM binding may lead to inaccuracies in commonly used speciation models, therefore such generalised approaches need improvement for regional-level ERA in complex watersheds. In Chapter 5, I used results from Chapter 4 to test whether the obtained parameters are fit-for-purpose with respect to speciation modelling and ERA. Furthermore, I also used

the bioreporter to test the Pb bioavailability across the whole lake and checked whether the bioreporter results agree with the optimised speciation model.

IV) What does the bioreporter reveal about Pb bioavailability in heavily contaminated lake sediments and what are the implications for ERA?

Using the bioreporter for the measurement of bioavailable Pb in lake sediment is a logical extension of ERA on lake pollution and also an extension of my aqueous-phase work. During the course of this work, an opportunity arose to investigate a lake system in the United Kingdom called Brothers Water lake, in which Pb is specifically highly accumulated in the sediment (Schillereff et al. 2016). Therefore, I conducted such a study using Pb-polluted sediment from this lake and the results are described in Chapter 6. Until now, very few studies have conducted investigation from the standpoint of ERA as implemented by environmental practitioners. Therefore, my aim for this study was to develop methods that enable reaching fit-for-purpose ERA conclusions.

V) How do micronutrients, including metals, affect algae, and are there implications regarding the risk of harmful algal blooms?

Metal toxicity is not the only way in which metals pose a potential environmental risk. As is well-known, some heavy metals are micronutrients for phytoplankton. What is less-well known, but increasingly recognised as an ERA challenge, is that with increasing levels of anthropogenic disruption of biogeochemical cycles, metals and other micronutrients may in some cases be limiting. In Chapter 7, I describe mesocosm studies to investigate the effect of metal amendments on algae to understand whether or not metals might be a causative or aggravating factor in harmful algal blooms.

1.3 STATUS OF MANUSCRIPTS ARISING FROM WORK

All of the work reported in this thesis is either published or scheduled for publication. I am the first author for all the publications. The publication status of the work presented here, at the time of submission of this manuscript to the examiner, is listed below.

Work presented in Chapter 3, published:

Zhang X, Qin B, Deng J, Wells M (2017) Whole-cell bioreporters and risk assessment of environmental pollution: A proof-of-concept study using lead. Environ Pollut 229:902–910

Work presented in Chapter 4, revised manuscript under review:

Zhang X, Li B, Deng J, Qin B, Wells M, Tefsen B. Regional-scale investigation of dissolved organic carbon and lead binding in a large impacted lake with a focus on environmental risk assessment. Water Res 172:115478

Work presented in Chapter 5, manuscript prepared, improving first draft:

Zhang X, Li B, Deng J, Qin B, Wells M, Tefsen B. Advances in freshwater risk assessment: improved accuracy of dissolved organic matter-metal speciation prediction and rapid biological validation. Ecotoxi Environ Safe (reviewed positively, revision for resubmission in progress).

Work presented in Chapter 6, manuscript prepared, improving first draft:

Zhang X, Li B, Schillereff DN, Chiverrell RC, Wells M, Tefsen B. Risk assessment of Pb pollution in lake sediment (manuscript under minor revision after first internal review of authors; I intend to submit this manuscript to Journal of Hazardous Materials in February, 2020).

Work presented in Chapter 7, published:

Zhang X, Li B, Xu H, Wells M, Tefsen B, Qin B (2019) Effect of micronutrients on algae in different regions of Taihu, a large, spatially diverse, hypereutrophic lake. Water Res 151:500–514

2 LITERATURE REVIEW

Environmental pollution has increasingly become one of the severe global issues (Briggs 2003; Hill 2010). Recent years have witnessed rapid industrialisation, urbanisation, and population growth, mining activities, the use of large number of pesticides and chemicals for agricultural production, resulting in the deterioration of environment (Hill 2010). Therefore, it is important to conduct ERA. The ERA process can be complicated, being time and resource intensive, yet, it is often driven by immediate needs such as reducing human and ecosystem exposure to unacceptable levels of pollutants. Because of the ever increasing scale of environmental pollution and in the increasing immediacy of ERA needs, it is essential to develop streamlined approaches to ERA.

2.1 AN ERA PROBLEM – HEAVY METAL POLLUTION

Since 2008, according to various reports from the Pure Earth Institute and partners, heavy metals[1] topped the list of the world's biggest pollution problems, inclusive of health effects, with contaminated surface water being a key issue

[1] There is no generally accepted definition for what a heavy metal is, however, in environmental analysis, testing labs often analyse a screening group for heavy metal for contamination including arsenic (technically a metalloid), cadmium, chromium, copper, nickel, lead, zinc, and sometimes mercury. These also, normally, happen to be present at trace quantities and are therefore sometimes referred to as trace metals.

linking pollution to health effects. In addition to being the most abundant and toxic pollutants, heavy metals are persistant because metals cannot be degraded. Heavy metals are introduced to freshwater environments by many different industrial activities, viz. mining, refining ores, smelting, legacy sources such as leaded gasoline, fertilizer industries, tanneries, battery manufacture, paper industries, pesticides and wastewater (Pastircakova 2004; Pure Earth/Green Cross 2015). Many of the heavy metals (e.g. Copper or Cu) can be nutrients or toxicants, depending upon the concentration, organism, bioavailability, and other considerations (Procházková et al. 2014). Anthropogenic contributions of heavy metals that disrupt natural biogeochemical cycles have the ability to impact heavy metals' role as nutrient or toxicant.

In terms of heavy metals toxicants, Pb is ranked as the most abundant heavy metal pollutant in the world today (Pure Earth/Green Cross 2015, also, historically, see Tong et al. 2000). Pb's prevalence is aggravated by its particular toxicity to children (Grandjean and Landrigan 2014). Tiwari et al. (2012) report that Pb accounts for the majority of cases of pediatric heavy metal poisoning. The global annual costs of childhood Pb exposure from cognitive defects alone are estimated to be 1.15 trillion US dollars, most of which is borne by low- and middle-income countries (Grandjean and Bellange 2017). Cognitive defects are only one of several cost categories, and even for cognitive defects, this estimate does not consider cognitive losses within the normal range, which a recent sensitivity analysis suggests may result in a 200-fold underestimate for costs of Pb exposure from cognitive defects to children (Attina and Trasande 2013). USEPA has set the maximum allowable level for Pb in drinking water at a concentration of 15 ppb (USEPA 2002), and in China the maximum allowable

level is 10 ppb (Ministry of Health, People's Republic of China, MHPRC 2006), however, though limits are set, literature shows that no safe level of lead exposure exists (Grandjean 2010). Pb precipitates to insoluble species under alkaline conditions, and conversely the increasing occurrence of acid rain in some areas of the world, notably China, has enhanced the release of Pb into water and soil solution (Du et al. 2014; Li et al. 2015). China is one of the places most affected by Pb poisoning. Recent studies have shown that nearly 30% of urban children aged 3-5 years had a blood Pb level above the recommended 100 $\mu g \cdot L^{-1}$ ((Wang and Zhang, 2006; Ye et al. 2007). The major sources of Pb in the environment are from mining, historical use of Pb in vehicle fuel, smelters, and battery disposal (Adriano 2001; Joumard et al. 1983; Sud et al. 2008). In addition to posing risks to human health, high levels of Pb in soils and water threaten ecosystems (Sekar et al. 2004), and it is therefore important to be able to rapidly evaluate potential biological effects of Pb in the environment and on a site-to-site basis. These factors concerning the high risk profile of Pb determined its selection as the target metal for my work.

The role of heavy metals as micronutrients (MNs) is discussed further in Section 2.4 below.

2.2 Environmental Risk Assessment

As a seminal text on ERA states "the world is a dirty place, and getting dirtier all the time" (Lerche and Glaesser 2006; also see Biello 2009; Harvey 2007). With the increasing levels of contaminants prevalent globally, there is an increasing and urgent need to perform accurate ERA and to be able to set appropriate and

site-specific or even regional levels for metals that are protective, yet not unrealistically conservative (Briggs 2003; Critto and Suter 2009; Fairman et al. 1999; Janssen et al. 2003). Environmental risk involves the combined evaluation of hazards and exposure. ERA is a process that evaluates the interactions of hazards, humans, and ecological resources and is a crucial process that underpins environmental management (Muralikrishna and Manickam 2017). It consists of two parts; human health risk assessment and ecological risk assessment. The risk assessment process has been divided into four steps: hazard identification, dose–response assessment, exposure assessment and risk characterisation by USEPA (USNRC 1983). The identification of hazard may involve characterising the behaviour of a pollutant within the human body and chemical interactions within organs, cells, or even parts of cells (Frenich et al. 2007). However, exposure assessment is mainly estimates how often a person comes in contact with a pollutant (Frenich et al. 2007). Ecological risk assessment is different from human health risk assessment which can be considered single species, since only a few types of representative organisms are selected as assessment end-points (Muralikrishna and Manickam 2017; Stephen et al. 1985). Historically, ERA from potential exposure to toxic contaminants has been based on total chemical load (Critto and Suter 2009). For heavy metals, total concentration has been traditionally used as a predictor of the magnitude, frequency and duration of human exposure and used to define a level of acceptable carcinogenic or noncarcinogenic human health risk (USEPA 1992; 2007a). In addition to being concentration-based, the traditional methods for ERA often require large amounts of field data and usually obtained at significant effort and expense (Lerche and Glaesser 2006). With the ever-increasing amount of environmental

contamination in the world, it is of crucial interest to develop risk assessment methods that are streamlined and enable a sort of environmental triage or ranking of contaminant risk. A first step in this direction occurred with the recognition that risk relates more to bioavailability of pollutants rather than total concentration. Therefore, bioavailability has largely become the focus of ERA (Avio et al. 2015; Caussy et al. 2003; Janssen et al. 2003; USEPA 2003a). The "Bioavailability Processes" was defined by the US National Research Council (USNRC 2003) as an approach to ERA; they include the release of solid-bound pollutants and their subsequent transport, direct contact and uptake by passage through a biological membrane and incorporation into a living system. The factors that determine the bioavailability of heavy metals are complex, and may depend, on, for instance, the total concentration of metal, water chemistry, and physical conditions (e.g. temperature) (Coles and Young 2006; Sisombath 2014). While there are distinct advantages to using bioavailability rather than total chemical load as a basis for ERA, the measurement-intensive (therefore relatively time- and cost-intensive) nature of obtaining data remains.

Speciation modelling is increasingly used to effect streamlined ERA, and ERA modelling is now an accepted approach to heavy metals ERA (Niyogi and Wood 2004; Sander et al. 2015) and is being used to set Water Quality Criteria (WQC), i.e. safe operating levels (Di Toro et al. 2001; USEPA 2016) of heavy metals in freshwater, that may also be regional or even site-specific. The speciation modelling approach is implemented in a number of software packages, assessing bioavailability directly through speciation, or evaluating toxicity indirectly through speciation (e.g. Gustafsson 2014).

2.3 TOWARD STREAMLINING BIOAVAILABILITY-BASED ERA

Measurement of bioavailability using bioreporters

In recent years, whole-cell bioreporter has attract more attention for its role on measuring the bioavailability of pollutants in the environment. (Al-Anizi et al. 2014; Ding 2009; Deepthike et al. 2009; Kohlmeier et al. 2008; Selifonova et al. 1993; Van der Meer and Belkin 2010; Wells 2012). This approach is typically faster and cheaper than many other biological tests and also has the advantage of being able to measure bioavailability or toxicity, depending on the concentration range of the target molecule (Ding 2009; Wells 2012; Zhang et al. 2017). Bioreporters are organisms that are genetically engineered to give a "report" on target substances being capable of producing dose-dependent signals in response to target chemicals (Belkin 2003; Kessler et al. 2012; Magrisso et al. 2008; Van der Meer and Belkin 2010). Genetic construction of bacterial bioreporter strains is achieved by a combination of a promoter gene (a sensing element) and a reporter gene (signalling element) within a host cell. The most common strategy for the selection of the sensing element is to use the promoter of a gene known to be induced by the stress condition of interest, in this case Pb exposure (Kessler et al. 2012). Therefore, the bioreporter was constructed for the measurement of the target metal. Fusing the promoter to the reporter ensures that when the promoter senses the target, i.e. the promoter is "turned on", this then causes the reporter gene(s) to be expressed. In this process, the target chemical was detected in the periplasm by means of a receptor (or 'receiver') protein. Then, the receptor binding triggers an intracellular phosphorelay that is transmitted to the switch and promoter, leading to the expression of the reporter gene (van Der

Meer and Belkin 2010). Many studies reported that the bioreporters are very sensitive to target metal at low concentrations (Kessler et al. 2012; Magrisso et al. 2008; Zhang et al. 2017). When the sample contains multiple metals, it is necessary to further consider which bioreporter to use and how to optimize the detection method.

Figure 2-1 is a schematic representing the process of bioreporter signal activation. Reporter genes are chosen to produce reporter proteins that have a measurable signal, typically optical. Studies have shown that almost all of the promoter elements used for the construction of bioreporters drive the induction of genes involved in heavy metal resistance (Bontidean et al. 2004; Bruins et al. 2000), and many bioreporters specifically responsive to one or more heavy metals have been constructed (Selifonova et al. 1993; Magrisso et al. 2008; Rasmussen et al. 2000; Yoon et al. 2016a). Most heavy metal bioreporters detect concentrations of target pollutants below the respective drinking water safety limits (Ripp et al. 2011).

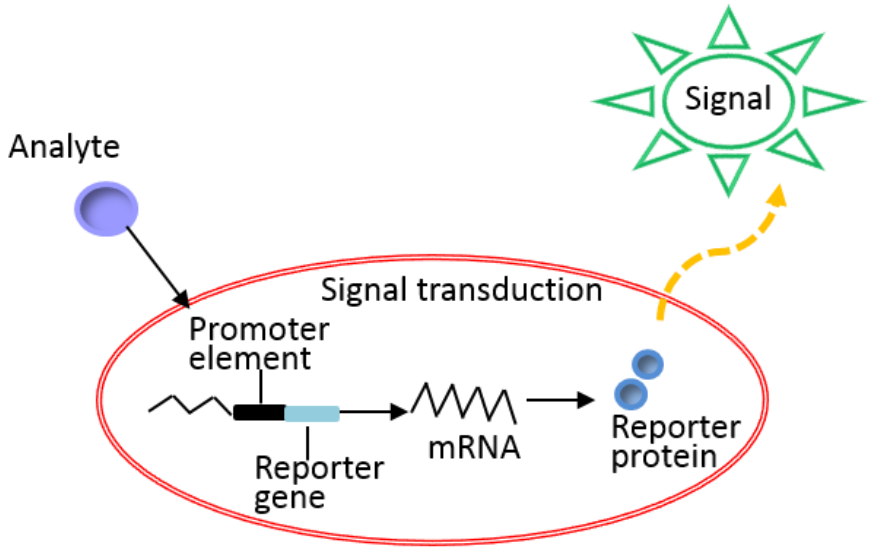

Figure 2-1. Schematic representing the process of bioreporter signal activation to measure bioavailability (after Belkin 2003).

Recently, some work has assessed the bioavailability and toxicity of arsenic (As), Cu, cobalt (Co), nickel (Ni), zinc (Zn) and Pb, using whole-cell bioreporters (Jia et al. 2016; Magrisso et al. 2009; Yoon et al. 2016a, b). A bioreporter for As was used for testing 194 different groundwater samples from Vietnam (Trang et al. 2005). The authors noted that after a 1.5 h incubation, the strain exhibited a limit of detection (LOD) of 7 $\mu g \cdot L^{-1}$. The bioreporter assay used for the testing was shown to more reliable than chemical field test kits, as validated using instrumental methods of chemical analysis. A *mer-lux* bioreporter was constructed by Ndu et al. (2012) to assess the bioavailability of methylmercury, $CH_3Hg(II)$, in *Escherichia coli* (*E. coli*). These authors found that the addition of chlorides resulted in an increase in $CH_3Hg(II)$ bioavailability, however, HA were found to reduce the bioavailability of $CH_3Hg(II)$ in varying degrees (Ndu et al. 2012). The work of Ndu et al. is an example demonstrating how bioreporter response follows the conceptual model wherein free-metal ions react with biological binding sites (Song et al. 2014a), and, for instance, presence of other ions or complexing ligands then affects the bioreporter signal in a manner consistent with expectations from theory (see discussion of speciation below).

In addition to measurements of bioavailability in aqueous media, bioreporters have been used to measure the bioavailability of heavy metals in soil and sediment. For example, Ivask et al. (2007) used an *E. coli merR-luxCDABE* strain and an *E. coli ars-luxCDABE* strain to examine the bioavailability of Hg and As in soil and sediment samples. They found only 1.2-6.7% of total Hg and 0.9-4.9% of total As was bioavailable (Ivask et al. 2007). The properties of soil and sediment can strongly affect the bioavailability of metals. For instance, Magrisso et al.

(2009) found that Fe-oxides, which have the highest affinity for Pb, make Pb biounavailable to microorganisms in the soil (Magrisso et al. 2009).

The various attributes of bioreporters that I describe here (rapid and sensitive response, economic feasibility, measurement of bioavailability, ability to use in a variety of environmental matrices) make them ideal with respect to their potential to streamline ERA.

Bioavailability, ERA, and speciation modelling

Modelling has become quite an important tool in ERA, and perhaps one of the most famous and often used models is referred to as the biotic ligand model (BLM). The BLM was developed to provide a scientific method for the assessment and prediction of metal toxicity to aquatic organisms (Di Toro et al. 2001; Sander et al. 2015). This is a bioavailability-based approach that first arose out of work that was maturing in the 1990s and culminated with the USEPA's 2003 publication of the BLM approach to formulation of BLM-based WQC used in management of environmental risk for heavy metals (see USEPA 2003a, and references therein, also see Niyogi and Wood 2004 for an early review). The USEPA now uses the BLM as a defensible and cost-effective way to develop WQC used in environmental risk management (USEPA, 2016).

A generally accepted conceptual model of the cause of metal toxicity involves free-metal ions reacting with a biological binding site or receptor (Song et al. 2014a). Some cations, such as H^+, Ca^{2+}, Mg^{2+}, Na^+ and K^+ compete with metal ions for these binding sites thereby decreasing bioavailability to organisms and associated toxic response (Celen et al. 2007; De Schamphelaere and Janssen 2002;

Santore et al. 2001; Song et al. 2014a). In natural waters, dissolved organic matter (DOM) primarily, and anions secondarily (e.g., Cl^-, SO_4^{2-}, CO_3^{2-}), are also known to complex or adsorb toxic free-metal ions and reduce bioavailability. The discovery that these effects could be accurately estimated through modelling led to the development of the BLM, a conceptual representation of which is given in Figure 2-2.

The BLM is run in one of two modes: speciation and toxicity, and the model has been implemented in a number of software packages. The most commonly used, which I used for my work, is Visual MINTEQ (Gustafsson 2001). Speciation mode does not depend on information about metal-receptor binding, which is organism-specific. In speciation mode, the chemical speciation, or form, of heavy metal toxicant is calculated, and, risk is based on the level of toxic free-metal ion present (Gustafsson 2001; USEPA 2003a). The parameters that describe metal-ligand, cation-ligand, cation-anion, etc, binding have been incorporated in the speciation mode-Visual MINTEQ, which enables calculation of the amounts of all different metal species on basis of commonly and inexpensively measured water properties.

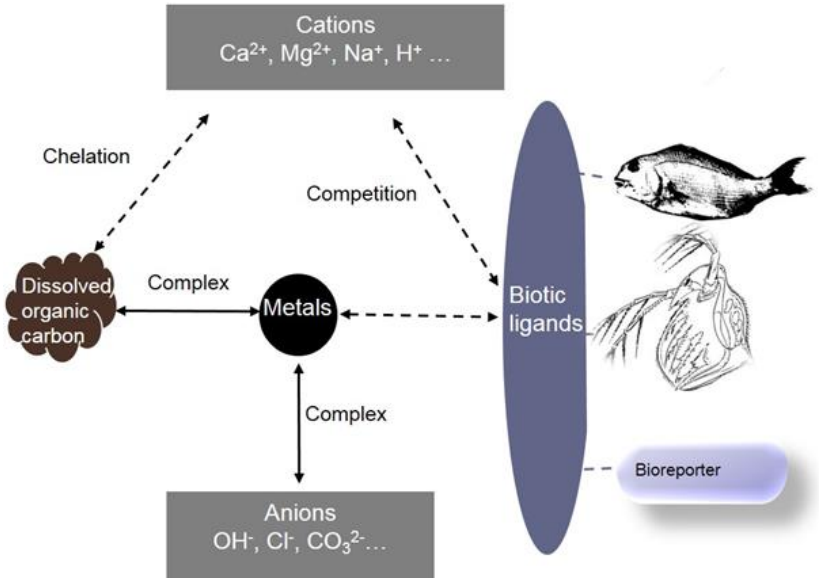

Figure 2-2. Schematic representing the concepts underlying the BLM. Cations compete with metal ions for binding sites on the biotic ligands present in organisms like fish, water flea and bacteria (including bioreporters). Anions and dissolved organic carbon (DOC) can complex with metals and thereby decrease metal bioavailability.

Toxicity mode requires additional parameters (Nys et al. 2014) that enable the model to calculate the total metal concentration that will result in a particular toxic effect for a specific organism. Many toxicity-mode BLMs originate from tests with fish (Santore et al. 2001; Smith et al. 2017). Some have been recalibrated for more sensitive daphnids by adjustment BLM parameters according to the relative sensitivity of toxic response (Clifford and Mcgeer 2010; Santore et al. 2001), and recently toxicity-mode BLMs have been constructed for algae and bacteria. Such calibration to run in toxicity mode can be very accurate, however may also be very time consuming (Niyogi and Wood 2004; Nys et al. 2014). For my work, I refer to speciation modelling in the context of ERA as the speciation modelling that I perform is the same as BLM speciation-mode. This is convenient since the bioreporter that I use reports bioavailable Pb (free-metal ion). To translate this to toxicity would involve performing a calculation in toxicity mode to produce the same level of free-metal ion Pb that is observed in speciation mode or developing

and adding parameters for toxicity-mode calculations for my organism. The latter is a work nearing completion that has been conducted by a fellow-PhD student (Boling Li, Xi'an Jiaotong-Liverpool University, upcoming thesis), and therefore is not a topic covered in this thesis.

Models require validation, and for ERA speciation and toxicity models this occurs by comparing model results with comparable biological results. Numerous biological techniques have been used to investigate the bioavailable fraction or toxicity of heavy metals (Heijerick et al. 2005; Nys et al. 2014; Smith et al. 2017). Most of this type of work is relatively unwieldy in terms of cultivating and maintaining test organisms for use, for example, the cultivation of *Daphnia magna* and rainbow trout (De Schamphelaere and Janssen 2002; Heijerick et al. 2005; Nys et al. 2014; Smith et al. 2017). In this respect, use of a whole-cell bioreporter to measure bioavailable Pb offers the advantage of being rapid and readily comparable to model results.

The role of dissolved organic matter in heavy metals' bioavailability

Studies have shown that DOM [2] plays an important role in the fate and biogeochemical cycling of metal ion in the aquatic environment (Christensen et al. 1999; Mostofa et al. 2013a; Mueller et al. 2012; Reuter and Perdue 1977; Zhang et al. 2014). For many metals, complexation, which reduces bioavailability and therefore risk, is primarily determined by complexation with DOM in natural

[2] The term dissolved is operational and is understood to be a size fraction that is small enough to pass a given filter size. Commonly, as relates to my work, the term dissolved applies to DOM and to heavy metals. The most common filter sizes for environmental work are 0.22 and 0.45 microns (e.g., see Kolka et al. 2008). It is generally acknowledged that this is operational, and that these filter sizes may entail that some colloidal materials (not technically dissolved species) are within the operationally defined dissolved fraction.

systems, and complexation can be quantified using chemical speciation models (Baken et al. 2011; Boggs et al. 1985; Mostofa et al. 2013a; Yamashita and Jaffé 2008; Zhang et al. 2017). A quantity associated with DOM and a term that will be used often in this thesis is DOC (see Figure 2-2). DOC is the primary component of that is used to quantify DOM and used in modelling studies (Chen et al. 2003a). In modelling, DOC is used as an input parameter, usually expressed in units of $mg \cdot L^{-1}$ as determined from total carbon analysis of combustion of DOM (Gustafsson 2001; 2014).

Fundamentally, DOM is an organic ligand, however, a difficulty in modelling metal-DOM interactions arises because DOM is not "one thing"; DOM is a complex, heterogeneous mixture of aromatic and aliphatic organic compounds of varied origin and includes humic substances such as HAs and fulvic acids (FAs) (Leenheer and Croué 2003; Zhang et al. 2014). One way to study the effect of organic ligands on bioavailability in a simple way is to use model ligands. In my work, I started experiments with simple model organic ligands prior to progressing to work with DOM. Initially I chose different ligands with different structures and types of functional groups that are known to complex Pb in aqueous environments (two chelators, three amino acids one peptide, and a commercially available HA). Literature provided a rationale for ligand choice. I chose ethylenediaminetetraacetic acid (EDTA) and dimercaptosuccinic acid (DMSA) as chelators. Sillanpää and Oikari (1996) studied the effect of EDTA on heavy metal toxicity and found that complexation by EDTA noticeably reduced the toxicity of Zn and Pb, whereas DMSA is a drug currently used for chelation therapy in Pb poisoning (Besunder et al. 1996). Amino acids, peptides and HA are two subgroups of DOM that occur in environmental settings and play an

important role in binding heavy metals due to the presence of metal-coordinating functional groups in their chemical structures. For amino acid and peptides choice, I followed the protocol of Ndu et al. (2012), who investigated the comparative effects of two thiol-containing compounds, the amino acid Cys and the peptide GSH (a Cys containing tri-peptide), to those of two non-thiol-containing amino acids, Leu and Met, on the response of a mercury-sensitive bioreporter. Leu with its α-amino group, α -carboxylic acid group and isobutyl side chain is classified as a non-polar amino acid, whereas Met is also non-polar, however has an *S*-methyl thioether side chain. Cys in turn has an active thiolate instead of the *S*-methyl thioether side chain and is variously classified as polar to hydrophobic. Cys and glycine having two carboxyl groups, a primary amine, two secondary amines, and a thiolate group, GSH is a tripeptide incorporating glutamate (Sisombath 2014; Wu et al. 2004). While the carboxylic acid and primary amine groups (e.g. as in Leu and Met) are capable of complexing metals, the thiol groups in particular (Cys, GSH) are thought to be largely implicated in the complexation of metals by thiolate-containing amino acids and peptides (Sisombath 2014). Studies have shown that Pb complexes strongly with HA, which serves to reduce bioavailable Pb (Coles and Yong 2006). Though HA itself is a class of compound with no specific chemical formula or structure, commercially available HA is purified, hence it represents one purified component of naturally occurring DOM and is therefore more uniform chemically than DOM itself.

Bivalent metals such as Pb^{2+} often complex strongly with HA and FA components of DOM, with HA's complexing heavy metals more strongly (Fasurová and Pospíšilová 2010). Some authors assert that when comparing modelling results

to experiment, the differences in metal complexing properties in natural waters have been found to be relatively small between different HAs and FAs, suggesting that to some extent generalisation within these groups is possible (Benedetti et al. 1996). The idea of generalisability has led to the development of speciation submodels for metal-DOM binding that have been able to be validated in the context of ERA (Di Toro et al. 2001; USEPA 2007b; Gustafsson 2001, Tipping 1994). Two common approaches to quantify metal-DOM binding and attendant metal bioavailability include the Stockholm Humic Model (SHM, Gustafsson 2001, implemented in Visual MINTEQ) and the Windemere Humic Acid Model (WHAM, Tipping 1994 and 1998). While the details of these models and model calculations are quite complicated, the key point is that these models rely on conditional stability constants, K_{cond}, which originate from thermodynamic quantities and are constant quantities that reflects the strength of an interaction between a given metal and DOM sample in coming together to form a metal-DOM complex. Models such as SHM and WHAM hold the assumption that for HA and FA, respectively, a single K_{cond} describes metal binding with phenolic- and carboxylic- acid type sites within HA and FA, and that the relative proportions of DOM that are HA and FA are generalisable, therefore, such an approach may be referred to as a "one-size-fits-all" approach.

The varying characteristics of DOM that relate to its origin, environmental conditions and aging processes have driven much work devoted to characterising DOM to provide a better understanding of metal-DOM complexation (Leenheer and Croué, 2003; He et al. 2015; Kikuchi et al. 2017; Mostofa et al. 2013a; Ren et al. 2015; Zhang et al. 2014). There is increasing evidence that extant speciation models do not always adequately predict metal-DOM binding due to the variable

nature of DOM (e.g. see Ahmed et al. 2014; Ndungu 2012). Natural waters with DOM that deviates in composition or binding strength from current model assumptions and specifications, inherent in the one-size-fits-all approach, will not be amenable to accurate calculation of speciation and assessment of risk, and recent studies call for site-specific binding parameters to ensure that ERA modelling meets environmental management needs (Ahmed et al. 2014; Mostofa et al. 2013a; Mueller et al. 2012; Zhang et al. 2014).

Common techniques for the characterization of DOM and metal-DOM binding include voltammetry (Sander et al. 2015; Sander et al. 2011), fluorescence (Mostofa et al. 2013b) and UV/vis spectroscopy (Birdwell and Engel 2010), Fourier transform ion cyclotron resonance (ultra-high resolution) or triple quadrupole mass spectrometry with electrospray ionization (Boija et al. 2014; D'Andrilli et al. 2010; Kujawinski et al. 2009) and different ultrafiltration and resin fractionation techniques combined with chemical analysis (Chow et al. 2004). Among these techniques, fluorescence spectroscopy has high sensitivity, is rapid and is semi-quantitative to quantitative (Chen et al. 2003a; Marhaba 2000; Mostofa et al. 2013b; Sanchez et al. 2014) and consequently is increasingly used to characterise properties and provenance of DOM in natural waters (Coble et al. 1990; Fellman et al. 2010; Hudson et al. 2007; Mostofa et al. 2013b). Additionally, the fluorescence characterization of metal-DOM binding has been demonstrated using high-throughput analysis (Neculita et al. 2011), which is quite cost-effective and would be ideal for ERA needs. Three-dimensional excitation-emission matrix (3DEEM) fluorescence spectroscopy (Coble et al. 2014) and synchronous fluorescence spectroscopy (SFS) are two techniques in particular that have been widely used to probe the chemical structure of DOM and to investigate water

pollution (Baker 2001; Baker et al. 2004; Manciulea et al. 2009; Mostofa et al. 2013b; Wu et al. 2003). The simplicity and potential for high-throughput were primary factors that led me to choose fluorescence techniques for the portion of my work that dealt with extracting parameters for use in Pb-DOM complexation modelling

2.4 Heavy Metals/Micronutrient Effects on Algae and Relation to Eutrophication Risk

Increasingly, harmful algal blooms (HABs) in freshwater and marine systems is an issue causing serious environmental and ecological problems. Eutrophication, identified as a major environmental problem for water resource management, is a term that typically indicates a process wherein a body of water becomes enriched in excess dissolved nutrients that stimulate excessive algal growth. This algal growth in turn causes reduced water transparency, and as algae die and decay, development of hypoxic/anoxic conditions leading to fish suffocation along with production and release of algal metabolites that are toxic to animals/humans; near-term and cumulative effects inclue decreased biodiversity (Qin et al. 2007; Tang et al. 2016).

For many years, phosphorus (P) was thought to be the primary limiting nutrient in terrestrial freshwater systems (Correll et al. 1998; Schindler 1977). It may be that, in an ideal and increasingly rare case of an anthropogenically undisturbed environment, an assumption of P-limitation would still prove valid. Increasingly, however, human activities are altering the Earth's pre-industrial balance. Of nine Earth systems characterised as planetary boundaries at risk of irreversible and potential catastrophic change, two count as systems in which the safe operating

space has been exceeded. One of these is biochemical flows of nitrogen (N) and P (Ahlström and Cornell 2018; Steffen et al. 2015). Human disruption of the global N cycle is greatest (Campbell et al. 2017; Kinzig and Socolow 1994; Steffen et al. 2015), and there is now a substantial amount of literature demonstrating that N is sometimes as important as P in contributing to eutrophication via the of development and persistence of HABs and in controlling phytoplankton species composition (Anderson et al. 2002; Chaffin et al. 2013; Conley et al. 2009; Havens et al. 2001; Paerl et al. 2011; Paerl et al. 2015; Smayda and Reynolds 2001; Xu et al. 2010). The dramatic increase of N- and P-inputs to lakes in the past several decades is mainly due to the increased use and abuse of chemical fertilizers during agricultural activities and inadequate environmental controls (Norse 2005; Smith and Siciliano, 2015).

The impact of chemical pollution, i.e. a category including heavy metals, in planetary boundaries has not yet been quantified (Steffen et al. 2015), however, as the research previously cited in Section 2.1 indicates, the increases in metal pollution and consequences of this pollution are dire. Anthropogenic disturbances of global geochemical cycles entail that assumptions about P-limitation, or even P- and/or N-limitation, may not be reliable, and this will affect water resource management needs (Campbell et al. 2017; Conley et al. 2009; Lewis et al. 2008). Compared to N and P, relatively little work has been done on the role of MNs, particularly in highly disturbed/impacted systems. In thinking about the issue of nutrient controls on eutrophication and HAB formation during the course of my PhD and discussing with collaborators, I became curious about the question of MNs. If the thinking on causes of HAB formation shifted from that of P-limitation (an early model) to P- and/or N-limitation (over the decades in

which the global biogeochemical N-cycle is increasingly disrupted), is it possible that other, similarly anthropogenically disrupted cycles, are now also contributing to the problem? Arguably, it is not possible to say not at present because the effect of MNs on algal growth tends to be overlooked as a research topic, particularly with respect to their role in HAB formation. In contrast, there has been so much work on N- and P- limitation, it would not be possible to provide a comprehensive overview within the scope of this thesis. The fundamental need for MNs by algae, the majority of which are heavy metals, is well-known (Anderson 2005; Axler et al. 1980; Goldman 1972; Twiss et al. 2000; Wurtsbaugh and Horne 1983).

The often-used text edited by Andersen (2005) on culturing algae lists boron (B), Co, Cu, iron (Fe), molybdenum (Mo), manganese (Mn), selenium (Se), vanadium (V), and Zn as important algal MNs, i.e. except for B and Se (a metalloid), seven of the nine of these would be considered as heavy or trace metals and three (Co, Cu, and Zn) are within the group of environmental heavy metal contaminants commonly screened. Some early research studies on algae in lakes have shown that the phytoplankton communities area affected in some way or potentially limited by the availability of MNs including Fe, B, Co, Mn, Mo, and Zn (Axler et al. 1980; Goldman 1972; Twiss et al. 2000; Wurtsbaugh and Horne 1983). The requirements of MNs appears to vary among phytoplankton species and groups, and Table 2-1 summarises representative information on MN limitation of algal growth. After some initial reading (key papers cited herein), I found I cannot work on all MNs that might be of interest. Therefore, I picked Fe due to its being the most studied MN, commonly known to be physiologically limiting in some situations. From some papers, there is a sense that cyanobacteria, mostly

responsible for the HABs, shows some limitation or co-limitation for B and Mo. The metals Co and Cu were interesting to me because both of them could either be nutrient or toxicant to algae.

Table 2-1. Available literature information on micronutrient limitation on algal growth.

Aqueous Media	Location	MN	Results	Reference
Lake Kasumigaura	Japan	Fe	Fe was a limiting nutrient, together with N and P for *Microcystis aeruginosa* and *Planktothrix agardhii*	(Nagai et al. 2006)
55 lakes	Canada	Fe	Fe serves as a possible cofactor that maintains cyanobacterial biomass across a lake trophic gradient.	(Sorichetti et al. 2016)
Lake Erken	Sweden	B	B addition increased the growth of cyanobacteria colonies in the presence of added iron, which was itself a limiting nutrient.	(Hyenstrand et al. 2001)
Lake Mahinerangi and LakeWaihola	New Zealand	B	The additions of B increased primary productivity by approximately 40% over the controls.	(Downs et al. 2008)
Godavari	India	Cu	At concentration of 1×10^{-7} M of metal, Cu acted as a nutrient and helped to increase the biomass of the algae.	(Chakraborty et al. 2010)
Castle Lake	America	Mo	The addition of Mo to the lake, primary productivity in the epilimnion increased 40% over the previous year.	(Goldman 1966)
Lake Tahoe, Walker Lake, and Clear Lake	America	Mo	N_2 fixation rates and Chl-a concentrations were positively correlated with Mo(V) concentrations	(Romero et al. 2011)
Eight lakes	South Island	Co	The availability of Co was found to limit primary productivity in eight of 10 South Island lakes.	(Goldman 1964; Goldman 1972)
Estuary	Swedish	Co	The growth of a bloom-forming alga in a Swedish estuary was stimulated by the addition of Co.	(Granéli and Haraldsson 1993)

For algae, Fe is needed for essential metabolic functions in photosynthetic electron transport, respiratory electron transport, nitrate and nitrite reduction,

sulphate reduction, N fixation, and detoxification of reactive oxygen species (Sunda et al. 2005). Work by Molot et al. (2010) and Pollingher et al. (1995) has shown that changes in Fe availability affect the outcome of competition among phytoplankton species (Molot et al. 2010; Pollingher et al. 1995). Cyanobacterial iron requirements are reported to exceed non-photosynthetic prokaryotes by ~10-fold and are described as "exceptionally high even among other photosynthetic organisms" (Kranzler et al. 2013; Moreno-Vivian 1999) due to mechanisms of intracellular homeostasis in these organisms. Xu et al. (2013) found that Fe is a primary limiting or co-limiting (with N and P) MN for *Microcystis* spp. growth in different regions of Taihu in China (Xu et al. 2013).

It has been demonstrated that the diazotrophic cyanobacteria have a specific need for Fe in enzymes required for atmospheric N_2 fixation (Sohm et al. 2011). In addition to studies that find Fe-limiting or co-limiting in freshwaters (Berman-Frank et al. 2001; Dang et al. 2012; De Wever et al. 2010; Evans and Prepas 1997; Goldman 1972; Ivanikova et al. 2007; Larson et al. 2015; Nagai et al. 2006; Nicolaisen et al. 2010; North et al. 2008; Stoddard 1987; Twiss et al. 2005; Verschoor 2017; Vrede and Tranvik 2006), a number of studies have looked at the effect of DOM, particularly siderophores, in affecting Fe bioavailability (Sorichetti et al. 2016; Ward et al. 2002) and hence algal community succession patterns (Molot et al. 2010; Murphy et al. 1976; Nagai et al. 2006; Sarkar et al. 2016). Another important line of enquiry concerns how Fe/P-linked biogeochemistry (e.g. Vivianite formation / dissolution) causes Fe limitation in some situations (Arbildua et al. 2017; Molot et al. 2014; Orihel et al. 2016). Reports indicate that in some cases a siderophore or P-related dose-response behaviour resembling toxicity is a consequence instead of the presence of these

substances in concentrations that decrease Fe bioavailability (Arbildua et al. 2017; Nagai et al. 2006; Ward et al. 2002).

With regard to some other MNs, as early as 1966 Lewin published a study reporting B to be a requirement for algal growth "generally" (Lewin 1966), and several studies have since been published looking finding B limitation or co-limitation in lakes (Bayer et al. 2008; Bonilla et al. 1990; Downs et al. 2008; Hyenstrand et al. 2001). Concerning HABs, Hyenstrand et al. (2001) reported that the addition of B increased the growth of cyanobacteria in the presence of added iron. Shortly after Hyenstrand's paper was published, another study reported findings concerning how the intake of one nutrient might also affect the status of another; Sterner et al. (2004) observed that quantities of N or P that caused only a small increase in algal phytoplankton growth rates were nonetheless sufficient to induce Fe limitation.

Another MN of essential importance to algae is Mo, which has been shown to be limiting and/or co-limiting (Axler et al. 1980; Downs et al. 2008; Glass et al. 2010 and 2012; Rueter and Petersen 1987; Song et al. 2012). Mo is a cofactor in N reduction (Moreno-Vivian et al. 1999) and similar to Fe, Mo contributes to N fixation for cyanobacteria. An early study showed that Mo stimulated N uptake rates and had the greatest effect when nitrate was the dominant N source (Axler et al. 1980). More recently Glass et al. have revisited the topic of Mo-limiting N fixation in freshwater and coastal cyanophytes (Glass et al. 2010; for a more detailed discussion of Mo, see Rueter and Petersen 1987, and references therein).

The MNs Co, Cu and Zn fall into the category of environmental heavy metal contaminants, and these nutrients stimulate algal growth at low concentrations

and are toxic to algae at high concentrations. All of these nutrients have been found to be growth-limiting nutrients to algae by some studies (Cavet et al. 2003; Chakraborty et al. 2010; Downs et al. 2008; Manahan and Smith 1973; Roussel et al. 2007; Sandmann and Böger 1980; Stoddard 1987). Chakraborty et al. (2010) found that at concentrations of 1×10^{-7} M, Cu acted as a nutrient and helped to increase the phytoplankton biomass followed by Co, Ni and Zn. However, a higher concentration of 1×10^{-6} M of metal resulted in toxic effect on phytoplankton; Cu acted as the most toxic metal followed by Zn, Co and Ni.

While the research on MN controls of HABs is comparatively (to N and P controls) sparse, the information that I could find nonetheless suggests that the effects of MNs on algal growth might play an important role in regulating HABs, and that therefore, studying these effects would be are important for the assessing the risk of HABs and evaluating possible management interventions.

2.5 Demonstration Project – Field Area

Field area characteristics and background

My work was designed around the idea of an ERA demonstration project, which imposes needs and desirable characteristics to consider in choosing a field site. The primary field study area for this work is Lake Tai (hereafter designated as Taihu, after 太湖 in Chinese), a system that is large enough (> 2,400 km^2) to reflect regional scale processes, has a complex aquatic ecosystem (Sun and Mao, 2008) and a long history of anthropogenic impacts (Qin, 2007). Lakes play an important role on the effect of ecosystem stability, providing important ecosystem services such as productivity from biodiversity, resilience to climate

change, fisheries, recreation and tourism, sediment and nutrient retention and processing, and hydrological regulation (Lévêque 2001; Schallenberg et al. 2013).

As China's third largest freshwater lake, Taihu provides a high degree of all of these ecosystem services, or at least it once did in its natural state. As shown in Figure 2-3, Taihu is situated in the south-eastern region of the Yangtze delta, the most industrialized area in China with high urbanisation, population density, and economic development (Qin et al. 2007). It has a volume of 4.4 billion m^3 and a drainage basin of 36,500 km^2, with a 68.5 km length (from north to south) and 56 km width (from east to west). The lake is the drinking water source for several cities, such as Wuxi, Suzhou and Shanghai and is also important for a variety of purposes including drinking water source, flood control, tourism and aquaculture (Gong and Lin 2009; Qin et al. 2007).

Taihu is a lake that is seriously disturbed by human activities. Studies have shown that due to the rapid development of industry and agriculture in this area, the lake has received more and more pollutants from industrial and agricultural activities, e.g. fertilizer and pesticide application (Jin et al. 2010; Liu et al. 2012; Qin et al. 2007). During the past several decades, most studies have focused on HABs in Taihu. However, the heavy metal contamination is substantial as well, if not as palpable. Many heavy metals have been deposited in lake sediments, however, since Taihu is a shallow lake (< 3 m maximum depth), wave action, especially during storms, is a key factor in interactions between the sediment and water (Qin et al. 2007), enhancing the risk of heavy metals in the sediment being released into the lake.

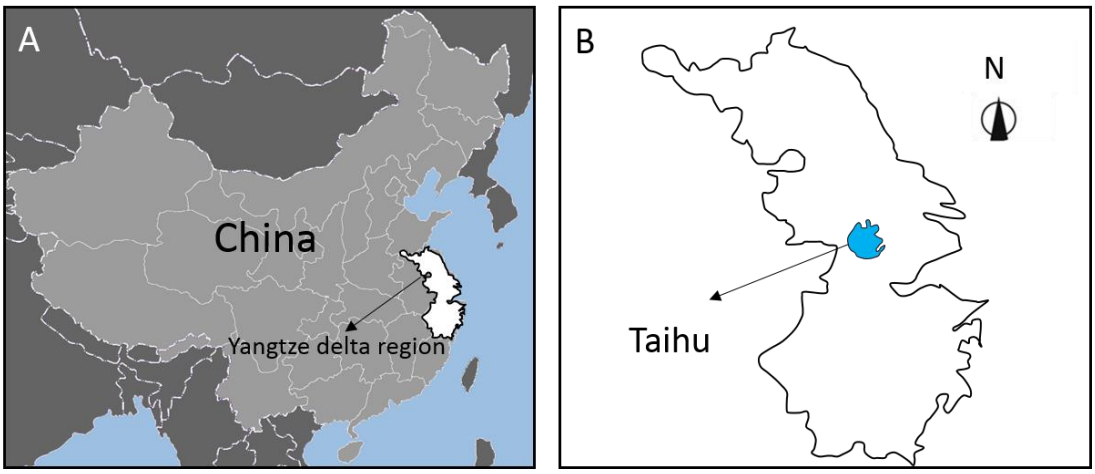

Figure 2-3. Location of Taihu. (A) Yangtze delta region, and (B) Map showing location of Taihu in the Yangtze delta.

The size, history of mixed impacts, and regional importance of Taihu is ideal for an ERA demonstration project. Additionally, however, the catchment complexity of Taihu makes it interesting and suitable for regional-scale ERA. Taihu has a complicated river and channel network with more than 170 rivers connecting to the lake. As Kothawala et al. (2014) have summarized regarding the importance of DOM's role in biogeochemical processes and the global carbon cycle, with particular emphasis on lakes, lakes may be viewed as sinks that may be used as catchment level indicators that receive and process DOM from catchment areas substantially greater than the area of any give lake itself. While these authors focus on DOM, a topic that is also very important to my work, the view of lakes as catchment level indicators is extensible, and Taihu serves as a sink for a particularly large and diverse catchment.

Heavy metal pollution in Taihu

With the development of the economy and increasing urbanisation, the regions surrounding Taihu have been faced with a serious problem of heavy metal contamination (Niu et al. 2015). An investigation conducted by Liu et al. (2004)

showed that the wastewater containing metals from papermaking, dyeing, leather and metallurgy industries were discharged to Taihu through rivers. This caused varying degrees of heavy metal pollution of the lake (Table 2-2). Especially during flooding season, flooding runoff from the west or southwest washes pollutants into the lake from west to the east.

Table 2-2. Summary of information from literature on heavy metal pollution in Taihu.

Object of study	Metals	Results	Reference
Water and sediment	Cu, Cd, Cr, Ni, Pb, Sn, Sb, Zn, Mn	The average concentration of all metals ranged from 0.047 μg·L^{-1} (Cd) to 8.778 μg·L^{-1} (Zn) in water, from 1.325 mg·L^{-1} (Cd) to 798.2 mg·L^{-1} (Mn) in sediment.	(Yu et al. 2012a)
Water column, interstitial water and surface sediment	Cu, Cd, Cr, As, Pb, Zn, Ni	In the surface sediment, the mean concentrations for Cr, Ni, Cu, Zn, As, Cd and Pb were 41.50, 28.72, 27.82, 65.46, 5.94, 0.82 and 41.17 mg·kg^{-1}, respectively.	(Jiang et al. 2012)
Sediment	Ag, As, Cd, Co, Cr, Cu, Hg, Ni, Pb, Zn	The nearby Meiliang Bay suffered from the worst heavy metal contamination (e.g. As, 64.0; Ag, 4.2; Cd, 0.93; Co, 14.2; Cr, 155.0; Cu, 144.0; Hg, 0.25; Ni, 79.8; Pb, 143.0 and Zn, 471 mg·kg^{-1}).	(Qu et al. 2001)
Sediment	Pb, Cd, Cu, Zn, Cr, Ni	The distribution areas of heavy metals with higher concentrations were mainly the north bays.	(Niu et al. 2015)
Water, sediments, *Ceratophyllum*, and *Bellamya* sp	Cd, Cr, Cu, Ni, Pb, Zn	Zn concentration was the highest, Cd concentration was the lowest among the six metals in water, sediments, and aquatic organisms.	(Bo et al.2015)

These heavy metals may be adsorbed or scavenged by suspended particles in lake water and subsequently deposit and accumulate in lake sediments. Previous studies have shown that a large amount of heavy metals are accumulated in Taihu sediment (Qu et al. 2001; Rose et al. 2004). Because Taihu is large and shallow/polymictic, these heavy metals in the sediment may be resuspended and released back to the lake water by frequent wind-blown waves, trawling and

large vessels (Qin et al. 2007). Resuspension events enable the metals to be adsorbed or incorporated by fish and other organisms in the water column, repeated cycles for which result in the contamination of food chains.

Studies have confirmed that concentrations of heavy metals have greatly increased in water of Taihu (Liu et al. 2012; Niu et al. 2015; Yu et al. 2012a) and a large amount of heavy metals have been accumulated in the sediment (Qu et al. 2001). A number of studies on heavy metals in Taihu focus on the investigation of bioaccumulation of different metals from water and sediment in phytoplankton, zooplankton, zoobenthos and fish (Bo et al. 2015; Chen et al. 2011; Qu et al. 2001; Yu et al. 2012b). Fu et al. (2013) found that fish from Taihu accumulated a much higher concentration of heavy metals than those from the Yangtze River. Chi et al. (2007) investigated the Zn content in edible parts of fishes sampled in Meiliang Bay, a polluted bay in north Taihu; the result showed that the Zn concentration had also surpassed the Chinese Food Health Criterion. Bo et al. (2015) measured the concentrations of Cd, Cr, Cu, Ni, Pb and Zn in water, sediments, *Ceratophyllum* and *Bellamya* sp. in Taihu. They found that Cd posed the highest ecological risk to the environment. Yu et al. (2012b) had similar findings (phytoplankton, zooplankton, two species of zoobenthos, and eight fish).

The concentration of heavy metals in Taihu varies with the seasons. Rajeshkumar et al. (2017) showed that total heavy metal (Pb, Cd, Cr and Cu) concentrations in water samples were higher in winter and summer than in the spring and autumn seasons. They also noted that oyster and fish tissues accumulated more metals during winter and summer relative to other seasons. Heavy metal pollution in Taihu also displays spatial differences. Many studies have shown that heavy

metal pollution in the northern part of the lake and in areas with river inflows was more serious than that in other parts of the lake (Hao et al. 2013; Shen et al. 2007). However, it needs more than just enforcement from above, more scientific studies are still needed to show the importance of taking action for improving the lake environment.

Effect of micronutrients on harmful algal blooms in Taihu

Investigation has shown that by 1981 the total inorganic nitrogen (TIN) in Taihu had increased dramatically by a factor of 18 over what is was in 1960. Over the same period, chemical oxygen demand (COD_{Mn}, determined by permanganate oxidation) increased by 49% (Sun and Huang 1993). The primary inputs of N and P in Taihu was river transport from the west or northwest. Studies have indicated that about 30-40% of N and P is retained inside the lake (Qin et al. 2007). The sources of the nutrient pollutants are industrial activities, domestic sewage, and non-point sources (agriculture production). The relative contributions of pollution vary. Huang (2004) showed that 49.5% of TN and 48% of TP produced in the basin were from agriculture.

The excessive nutrient inputs since the 1960s have led to the appearance of HABs and associated eutrophication in the lake. Figure 2-4 shows sampling in Taihu during part of my field work when an HAB was forming. It has been reported that during this period, Taihu has changed from a mesotrophic, diatom-dominated lake to hyper-eutrophic, cyanobacteria-dominated system (Chen et al. 2003b; Chen et al., 2003c). Since the mid-1980s, cyanobacteria (*Microcystis* spp.) HABs have occurred every summer in the northern part of the lake (Qin et al. 2007). In recent years, the HABs have expanded throughout northern part of the lake and

into the western and central regions, where the bloom is regular feature from May through October (Guo, 2007).

Figure 2-4. Pictures from my field sampling work showing what Taihu looks like during an HAB.

The eutrophication associated with HABs in Taihu has led to a serious reduction of the water quality, at times reading crisis levels. This has led to a large number of studies investigating the effects of N and P on algal growth and HABs. Since 2008, a series of nutrient limitation bioassays (NLBs) were conducted that were focused on the heavily polluted northern region and other selected lake locations (Paerl et al. 2015). Xu et al. (2010) and Paerl et al. (2011) found that P limitation happened in spring, followed by summer and autumn N and P co-limitation of *Microcystis* spp. blooms in Meiliang Bay. In most cases, the addition of combined N and P promoted maximum growth. In recent years, studies have been conducted to evaluate the potential role that Fe limitation might play in Taihu. Xu et al. (2013) demonstrated that addition of Fe alone significantly stimulated *Microcystis* spp. growth, indicating that Fe was a primary limiting nutrient in East Taihu. They also found that in East Taihu, N was not limiting, and Fe and P

supplies facilitated *Microcystis* spp. growth. With the exception of the Xu et al. (2013) work, other studies have been limited to the effects of N and P, and except for my work, other MNs have not been studied to my knowledge.

3 WHOLE-CELL BIOREPORTERS AND RISK ASSESSMENT OF ENVIRONMENTAL POLLUTION – A PROOF-OF-CONCEPT STUDY USING LEAD

The traditional approach to assessing ecological or human health risk associated with soil and water contaminants typically relies upon measuring the total concentration of contaminant present. Due to variations in bioavailability however, total concentration does not always relate to toxicity, and accordingly, the USEPA Framework for Metals Risk Assessment states that risk assessors should "explicitly incorporate factors that influence the bioavailability of a metal" (Fairbrother et al. 2007). To begin my work on risk assessment, first I wanted to examine whether bioreporter results, which reflect toxicant bioavailability, would be able to reflect expectations based on chemical reactivity and speciation modelling, with the hope to extend the research into a wider framework of risk assessment. For the work reported in this chapter I investigated the bioavailability of Pb, as measured with a Pb-sensitive bioreporter, in the presence

of different ligands that complex Pb in aqueous environments (EDTA, DMSA, amino acids/peptides, HA, and DOC).

I found that bioreporter results are in accord with the reduction of aqueous Pb^{2+} that I expect from the relative complexation affinities of the different ligands tested. Where possible, I compared bioreporter response with speciation modelling, results from which comparisons are in good agreement. This agreement was a first prerequisite to developing an approach to the biological validation of speciation modelling for ERA that is effectively high throughput compared to approaches such as those that I cited in Chapter 2 that are currently in common use.

3.1 Materials, Bioreporter Assay and Initial Speciation Calculation

Bioreporter strains, growth media, and assay conditions

In this research, *E. coli* strain zntA, which has the capacity to emit a dose-dependent bioluminescence in response to available Pb (Riether et al. 2001), was used for Pb bioavailability evaluation. The construction of the specific strain used is described in the studies by Kessler et al. (2012). The strain was stored on Lysogeny Broth (LB, Bertani 2004) agar amended with 40 $\mu g \cdot mL^{-1}$ ampicillin at 4°C. Overnight cultures (1 mL LB, 40 $\mu g \cdot mL^{-1}$ ampicillin) were grown at 30°C for 16 h. The overnight culture was diluted 100-fold in fresh LB and re-grown at 26°C with shaking at 200 rpm. At an optical density at 600 nm (OD_{600}) of 0.2, cells were harvested by centrifugation (10,625 × *g*). The supernatant was discarded, and the cells were resuspended in optimised minimal medium (MM). The MM contained

6.06 g of 3-[*N*-morpholino] propane sulfonic acid (MOPS), 2 g of sodium gluconate, 4.68 g of NaCl, 1.07 g of NH_4Cl, 0.43 g of Na_2SO_4, 0.2 g of $MgCl_2 \cdot 6H_2O$ and 0.03 g of $CaCl_2 \cdot 2H_2O$ in 1,000 mL of distilled water and adjusted to pH 7.0±0.1 (Magrisso et al. 2009; Mergeay et al. 1985). All chemicals were reagent grade and purchased from Alfa Aesar Co., Ltd (Shanghai, China).

Bioavailability calibration curves, as operationally defined by Magrisso et al. (2009), were used to assess bioreporter-measured bioavailability of Pb in this study. To construct these curves, 50 µL of bioreporter cell suspension was added to a 96-well opaque white microtiter plate (Nunc, Denmark) followed by another 50 µl of Pb standard, nominally containing 0 (blank), 0.0125, 0.025, 0.05, 0.1, 0.2, or 0.4 $mg \cdot L^{-1}$ of Pb in 0.002% HNO_3 (the latter confirmed low enough to be neutralised by MM) to each well. The microplate was incubated at 24°C with a shaking speed of 180 rpm, and bioluminescence was measured every 10 min for up to 7 h using a microtiter plate luminometer (Varioskan LUX, Thermo Fisher Scientific, USA).

Unless otherwise specified, samples subject to bioreporter measurements for Pb were spiked with Pb standard in order to conveniently achieve a final Pb concentration near the mid-point of the bioreporter linear range (0.2 $mg \cdot L^{-1}$ Pb^{2+}) which is effectively the speciation mode. To perform bioreporter measurements, 50 µL of Pb standard plus 25 µL ligand solution (EDTA, DMSA, Cys, Leu, GSH, Met, HA) were added to 25 µL bioreporter cell suspension in each microtiter plate well. HA was purchased from Alfa Aesar (Tianjin, China). The HA stock solution was prepared according to the method of (Chen and Elimelech 2007) before use. Final HA concentrations were verified using a total organic carbon (TOC) analyser

(multi N/C ®3100, Analytikjena, Germany). Bioreporter response was measured by the method described above. Measurements were also made to monitor response in the presence of ligands and absence of Pb (i.e., to see if the ligands alone had any effect on the bioreporter). Parallel experiments measuring OD_{600} were made a) for the bioreporter assays, and b) in experiments identical to the assays except without Pb (i.e., with ligands alone). In both cases, OD_{600} responses were identical to within experimental error and showed very slow and monotonic increase in OD_{600} with time, as I also observe in the same concentration of MM alone.

Collection and chemical analysis of natural water samples

Water samples were collected from Taihu in July 2016 from eight stations (St 0, St 1, St 3, St 4, St 5, St 6, St 7, and St 8) mostly in Meiliang Bay, with one station to the east of the Bay. These stations were chosen as being the primary focus of routine monitoring activities, and thus most well understood. For this initial work, my main focus was to obtain some natural water samples for controlled testing. I discuss Taihu as a freshwater system and results in that context in more detail in Chapters 4, 5, and 7. Subsequently all water samples were immediately brought to the laboratory and stored in the dark at 4°C for preliminary laboratory handling. Chemical properties were measured in the lab and included DOC, phosphate (PO_4^{3-}), ammoniacal nitrogen (NH_4^+), nitrate (NO_3^-) and nitrite (NO_2^-). NO_3^- and NO_2^- were measured using the cadmium reduction method and NH_4^+ was determined using the indophenol blue method (APHA 1995). PO_4^{3-} was determined by using the molybdenum blue method (APHA, 1995). Cations (Na^+, K^+, Ca^{2+}, Mg^{2+}) and anions (Cl^- and SO_4^{2-}) were analysed using ion

chromatography following the National Standards of the People's Republic of China (MHPRC 2016a, b). DOC was determined using the high-temperature combustion method with a Dohrmann DC-190 total organic carbon analyser (Rosemont Analytical Inc., Calif., USEPA, 1979). The total dissolved Pb concentrations in the water samples, $C_{\mathrm{Pb}}^{\mathrm{Tot,\ diss}}$, were determined by inductively coupled plasma mass spectrometry (ICP-MS, NexION300, PerkinElmer, USA). To investigate the effects of natural constituents in the samples on Pb bioavailability, samples were spiked to final Pb concentrations of 0.05, 0.2 and 0.8 mg·L^{-1} using 1000 mg·L^{-1} Pb standard solution and allowed to equilibrate overnight. This spike assay method is discussed further in Chapter 4. For measurement, 50 µL of water sample plus 50 µL bioreporter cell suspension was added to each microtiter well with bioluminescence subsequently measured as described above.

Chemical speciation calculations

Speciation was calculated using Visual MINTEQ 3.1 (Gustafsson 2014). Input data for Visual MINTEQ were pH, temperature (of assay) and the concentrations of , $C_{\mathrm{Pb}}^{\mathrm{Tot,\ diss}}$, Ca^{2+}, Mg^{2+}, K^{+}, Na^{+}, NH_4^{+}, Cl^{-}, SO_4^{2-}, NO_3^{-}, NO_2^{-} PO_4^{3-}, DOC, as well as concentrations of MM constituents and, as relevant, ligands/chelators described above. In this software, the Stockholm Humic Model (SHM) has been implemented to provide a more realistic assessment of metal-humic substances complexation (Gustafsson 2001). The SHM uses a discrete-site approach, wherein, in principle, humic substances are treated as impermeable spheres that may in part form gel-like structures. The electrostatic interactions on the surface are modelled using the Basic Stern Model. Equilibrium constants are defined for mono- and bidentate coordination, and an extra parameter accounts for binding-

site heterogeneity. HA concentration in water samples is estimated according to basic assumptions for terrestrial DOC in Visual MINTEQ.

3.2 EVALUATION OF BIOREPORTER RESPONSE TO PB

Figure 3-1 shows the bioluminescence response produced by the zntA bioreporter in response to different concentrations of Pb. Figure 3-1A and B display the kinetics of the bioluminescent response as a function of time and Pb concentration, respectively. After exposing the bioreporter to different concentrations of Pb, the luminescence response increases over time, typically reaching maximum luminescence at ~170 minutes. Figure 3-1C shows three representative bioavailability calibration curves (Magrisso et al. 2009), for which response is reported as the maximum response ratio (MRR), where MRR = $RLU_{C_{Pb},\ max}$ / $RLU_{0,\ max}$, $RLU_{C_{Pb},\ max}$ is the maximum response, in relative luminescence units (RLU), for $C_{Pb}^{Tot,\ diss}$, and $RLU_{0,\ max}$ is the maximum response of the blank. As for other methods of analysis (for instance, in high performance liquid chromatography response may be evaluated by peak height, peak area, and variations on these), there are different ways to calculate bioreporter response, and there are different ways to construct a bioavailability calibration curve (e.g. , ($C_{Pb}^{Tot,\ diss}$, Pb^{2+} or activity). Here I used MRR and $C_{Pb}^{Tot,\ diss}$ because when I published the work I wanted it to be comparable to that of Magrisso et al. (2009), who originally developed the calibration approach that I follow. The average relative standard deviation (RSD) for each measurement cycle was lower than 6%, which indicates the procedure of the experiment is repeatable and quite precise. For initial work, I used two methods to investigate the Pb LOD of the

bioreporter based on data from bioavailability calibration curves. Each method involved calculation according to LOD = 3 × $s_{C_{Pb=0}}$ (Shrivastava 2011). The first calculation utilised $s_{C_{Pb=0}}$ (standard deviation of blank) obtained as replicate measurements of $MRR_{C_{Pb=0}}$ and the second utilised s^{int}, the uncertainty in the linear regression intercept for the bioavailability calibration curve. Using standard deviation of blank replicates, the average LOD is 4 µg·L^{-1}; the linear regression method, displayed a lower value of 1.2 µg·L^{-1}. The first method is typically accepted, with the second being highly conservative. The USEPA has set the maximum allowable level for Pb in drinking water and aquatic life in freshwater at a concentration of 15 µg·L^{-1} and 3.2 µg·L^{-1}, repectively (USEPA 2002, 2017). Hence, these are reasonable LODs for detection of Pb in polluted waters or to test for exceedance of the USEPA drinking water standard, however these LODs are high for testing relatively unpolluted waters.

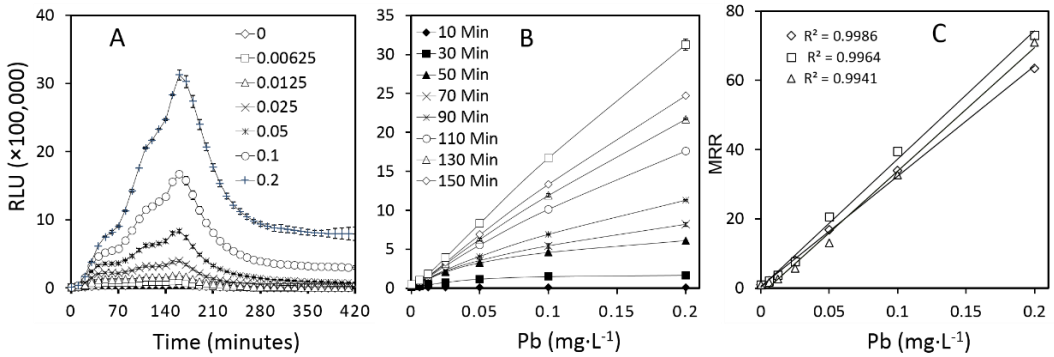

Figure 3-1. Response of the bioluminescent response of bioreporter strain zntA to Pb. Response kinetics (in relative luminescence units, RLU) as a function of (A) time, and (B) $C_{Pb}^{Tot,\,diss}$. Panel C shows a bioavailability calibration curve. Per the expression for MRR given in the text (where MRR = $RLU_{C_{Pb},\,max}$ / $RLU_{0,\,max}$), for $RLU_{C_{Pb},\,max}$ and $RLU_{0,\,max}$ the time of maximum intensity is not specified, as this may vary slightly from experiment to experiment and greatly from strain to strain. For these experiments $RLU_{C_{Pb},\,max}$ and $RLU_{0,\,max}$ are typically at ~170 min, as in Panel A. The unit in panel A is mg·L^{-1}.

Numerous studies have been conducted for the investigation of heavy metal bioavailability using whole-cell bioreporters (Ndu et al. 2012; Song et al. 2014b; Yoon et al. 2016a). As displayed in Figure 3-1, the strain zntA was effective to test for Pb bioavailability which in agreement with the previous studies using bioreporter as a tool to test the bioavailability of heavy metals. Directly after dosing cultures with Pb, the response is very low as the luminescent reporter proteins have not been synthesised by the bacteria yet. By 30 minutes, there is a marked difference in the amounts of luminescence given off by the bioreporter exposed to the higher concentration Pb. The luminescence signal increases until reaching a peak, diminishing thereafter, a circumstance anticipated from the cellular metabolic burden of expression of reporter protein and concomitant reduction of cellular activity from transferring cells to MM. The kinetics of strain zntA's response are comparable to those investigated for strain NMZA1 for Hg (Ndu et al. 2012) and strain AE1433 for Pb (Magrisso et al. 2009). In a previous study, Magrisso et al. (2009) used the strain AE1433 for the measurement of Pb bioavailability, and obtained an MRR of ~30 for the $C_{\mathrm{Pb}}^{\mathrm{Tot,\ diss}}$ of 3.25 mg·L^{-1}, which was approximately the top of the linear response range. In this study, the strain zntA produced an MRR of ~70 (Figure 3-1) for Pb at a total concentration of 0.2 mg·L^{-1}(Kessler et al. 2012), which is below the top of the linear range. The LOD for strain zntA is ~25 times lower than that of AE1433. The results thus demonstrate that the strain zntA is quite sensitive for Pb and is more suitable for the detection of bioavailable Pb in polluted waters, i.e., risk-related contexts.

3.3 Effects of Organic Ligands on the bioavailability of Pb

Effects of common chelating agents on the bioavailability of Pb

Generally, chelating agents can bind Pb, making Pb become less bioavailable. Figure 3-2 demonstrates the effects of two types of chelating agents, EDTA and DMSA, on Pb bioavailability for experiments wherein $C_{\mathrm{Pb}}^{\mathrm{Tot,\ diss}}$ was fixed at a concentration of 0.2 mg·L^{-1}. As the concentration of EDTA and DMSA increases, the bioavailability of Pb decreases according to a log-sigmoid trend. Using the EDTA ionisation and Pb complexation constants in the default thermodynamic database of Visual MINTEQ, the predicted response was calculated and is plotted for comparison to the bioreporter response for EDTA, along with the percent of $C_{\mathrm{Pb}}^{\mathrm{Tot,\ diss}}$complexed to EDTA (PbEDTA, second y-axis). The results are generally in very good agreement compared to the level of uncertainty that is acceptable for this type of modelling (USEPA 2007b), which is a promising initial result for the intended eventual application to risk assessment. For DMSA (meso form), there were no definitive results from modelling, which is not surprising since there is considerable disagreement about the appropriate thermodynamic constants, and even the most appropriate reactions (Fang and Fernando 1995). According to Fang and Fernando (1995) some possible dominant reactions are

$Pb^{2+} + DMSA^{4-} \rightarrow PbDMSA^{2-}$ $\log\beta_{1,1,0} = 18.2$,

$Pb^{2+} + DMSA^{4-} + H^{+} \rightarrow PbHDMSA^{-}$ $\log\beta_{1,1,1} = 24.82$,

$Pb^{2+} + DMSA^{4-} + 2H^{+} \rightarrow PbH_2DMSA$ $\log\beta_{1,1,2} = 27.5$

$Pb^{2+} + 2DMSA^{4-} + H^{+} \rightarrow PbHDMSA_2^{5-}$ $\log\beta_{1,2,1} = 32.2$.

In contrast, the β for $PbDMSA^{2-}$ is almost an order of magnitude different than that reported by Egorova (1972) and Harris et al. (1991), and in considerable disagreement with results from, for instance, De La Gala Morales et al. (2014). Since accurate ionisation and complexation constants are needed for modelling, I focused primarily on how modelling results compare to bioreporter response for Pb when in the presence of EDTA and HA, i.e. those species that are well studied and accounted for in Visual MINTEQ and its associated database. Since HA is highly variable, in particular it was important to me to see if results for EDTA would be accurate.

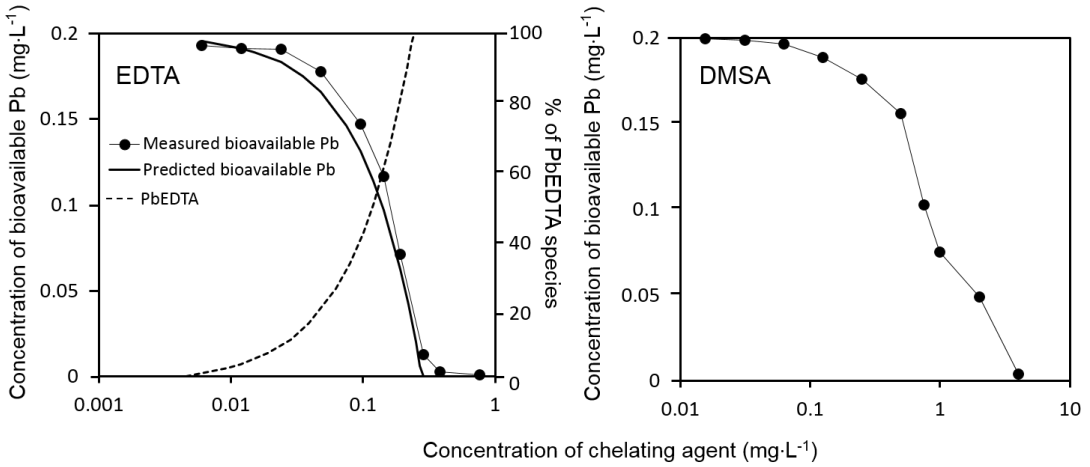

Figure 3-2. Effect of common chelating agents on Pb bioavailability to *E. coli* strain zntA and predicted data (for EDTA) based on speciation calculation. The concentration of Pb was kept constant at 0.2 $mg \cdot L^{-1}$, while the concentration of EDTA was increased from 0 to 0.76 $mg \cdot L^{-1}$ and DMSA concentration was increased from 0 to 4 $mg \cdot L^{-1}$. For calculation results bioavailable Pb is expressed as reduction in response to available Pb^{2+}. As detailed in the text, obtaining accurate speciation calculation results for DMSA is not possible due to large uncertainties in ionisation and complexation constants that are needed as input parameters.

Previous studies have demonstrated that, among various common chelators, EDTA is highly effective for Pb (Azhar et al. 2006; Lasat 2002; Palma and Mecozzi 2007). Azhar et al. (2006) found that 1:1and 3:4 molar ratio of EDTA to Pb

reduces the toxic effect of Pb on sunflower plants, which is consistent with the present study, wherein I find (Figure 3-2) that Pb becomes essentially biounavailable at a 1.37:1 molar ratio. While there is very good agreement between bioreporter results and results from speciation calculation for EDTA, small differences still exist. I find that, in practice, uncertainties in the concentration of chelator solutions are critical; even small errors in standard preparation for experiments can cause experimental results to appear to be quite different from calculated predictions. For the calculation the total chelator concentration is exact, and whatever one puts as input determines results. However, for calculations, uncertainties in the thermodynamic constants potentially have a strong effect, particularly for systems such as EDTA wherein there are six ionisation constants and one complexation constant in the database and uncertainties propagate non-linearly. With these considerations in mind, the agreement between measured bioreporter results and speciation calculations for EDTA is notable.

DMSA has been used for the detoxification of chronic metal overexposure in humans (Blaurockbusch 2014). In this study, I observed that there was a significant decrease of bioavailable Pb after the application of DMSA. At the concentration of 4 $mg \cdot L^{-1}$, DMSA complexed 98% of the total Pb (0.2 $mg \cdot L^{-1}$). Figure 3-2 shows that EDTA is more effective than DMSA to reduce the bioavailability of Pb, which is reasonable since the $\log\beta$ for formation of $PbDMSA^{2-}$ is estimated as being on the order of 17.4 to 18.2 (Fang and Fernando, 1995), whereas the $\log\beta$ for formation of $PbEDTA^{2-}$ is 19.8 (Allison et al. 1991). I find that Pb becomes essentially biounavailable at a 23:1 molar ratio of DMSA:Pb, compared to 1.37:1 for EDTA. These findings may be rationalised looking at the

proposed structure of EDTA and DMSA complexes with Pb^{2+} in Figure 3-4; EDTA is a hexavalent chelator, whereas DMSA is thought to be a bidentate chelator. It has been reported that, as a weaker chelating agent, DMSA is more suitable for Pb intoxicated children and sensitive adults (Blaurockbusch 2014). As noted above, the Pb complexation with DMSA includes several possible reactions, and the shape of the DMSA curve in Figure 3-2 is suggestive of two primary complexation reactions, as reported by Fang and Fernando (1995).

Effects of amino acids/peptide on the bioavailability of Pb

Amino acids, peptides and proteins are known as complexation agents for metal ions due to the presence of metal-coordinating functional groups in their chemical structures. In this study Leu, Met, Cys, and GSH were chosen as three target amino acids and one peptide for testing due to their different structural properties (see discussion of these ligands in Chapter 2 and work of Ndu et al. 2012). Figure 3-3 shows the effect of these amino acids/peptide on Pb bioavailability in the *E. coli* strain zntA. It can be observed that different amino acids affect the Pb bioavailability differently, and primarily according to the presence or absence of free thiolate. Leu and Met have little discernible dose-dependent effect on Pb bioavailability. I find that for both Cys and GSH, the raw response, as RLU, first increases, and then decreases (data not shown). Comparing the response of the bioreporter to Cys and GSH in the presence and absence of Pb however, I find that the trend is similar, i.e., it would appear that this response pattern reflects some effect of the compound itself on the bioreporter rather than a true effect related to Pb bioavailability. As such, for each concentration of Cys/GSH shown in Figure 3-3, the MRR is plotted according to

MRR= $\mathrm{RLU}_{C_{Pb=0.2}}^{C_{aa/peptide}}/\mathrm{RLU}_{C_{Pb=0}}^{C_{aa/peptide}}$, i.e. instead of normalising only to the blank response, there is a separate Pb blank response for each different concentration of Cys or GSH. This type of normalisation is non-optimal because the blank response is very low, and hence the trend of blank response is variable, and considerable uncertainties may be injected into the overall trend. Accordingly, the MRR trends for Cys and GSH in Figure 3-3 show the same log-sigmoid trend as for EDTA and DMSA in Figure 3-2, albeit there is still the indication of a slight increase in Pb bioavailability at low Cys concentrations. It seems likely that this is an artefact of the differential bioreporter response levels at the two different Pb concentrations (i.e. the response at $C_{\mathrm{Pb}}^{\mathrm{Tot,\ diss}} = 0.2$ being high are more precise versus $C_{\mathrm{Pb}}^{\mathrm{Tot,\ diss}} = 0$ being low and less precise).

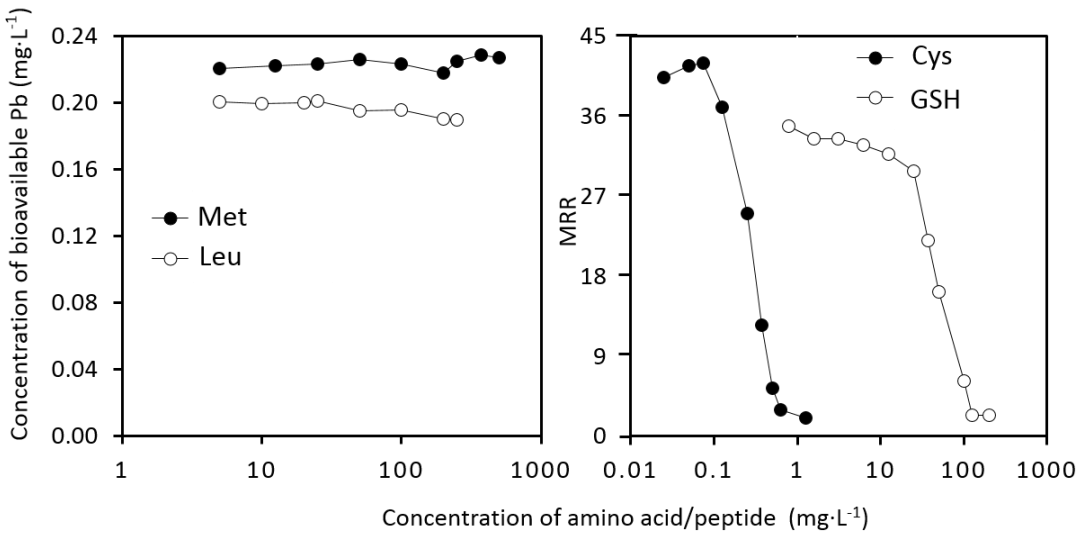

Figure 3-3. Effect of different amino acids and a peptide on Pb bioavailability in the *E. coli* strain zntA. The $C_{\mathrm{Pb}}^{\mathrm{Tot,\ diss}}$ was kept constant at 0.2 mg·L^{-1}, while the concentration of Leu was increased from 0 to 250 mg·L^{-1}, Met was increased from 0 to 500 mg·L^{-1}, Cys was increased from 0 to 1.25 mg·L^{-1}, and GSH was increased from 0 to 200 mg·L^{-1}.

The interaction between organic compounds such as amino acids, peptides and proteins with heavy metals may in some cases result in significant ecological

consequences (Dee 2016; Jia et al. 2016). In the case of Leu and Met, as shown in Figure 3-3, these have little effect on Pb bioavailability. While the carboxylic acid and primary amine groups in Leu and Met are capable of complexing metals, binding constants are low (the binding constants value for Pb are lowe than 4, see Berthon 1995), and in this study the Leu and Met have no effect on Pb complexation at the concentrations tested. A previous study conducted by Ndu et al. (2012) demonstrated that Leu and Met showed no effect on the bioavailability of CH_3Hg^+ and Hg^{2+}. Many amino acid-based compounds contain thiol groups, and Pb^{2+} has a high affinity for thiol-containing residues in biological conditions (Sisombath 2014). Ndu et al. (2012) demonstrated a trend of increasing bioavailability of Hg^{2+} and CH_3Hg^+ to bioreporter bacteria when Cys concentrations are increased. However, both the strain and the metal used in those studies differ from this study, and my results suggest that Cys reduces Pb^{2+} bioavailability, with the apparent slight increase at low concentrations likely artefactual.

However, I also find that the addition of GSH decreased Pb bioavailability, consistent with Ndu et al.'s finding that glutathione decreases the bioavailability of CH_3Hg^+ and Hg^{2+}. Reduction of bioavailability via Cys and GSH complexation is rationalised as primarily resulting from interaction of Pb^{2+} with the sulfhydryl group (Uzun et al. 2008). Reports indicate that complexes between Cys and GSH and Pb^{2+} involve multiple structures (Figure 3-4), all of which involve the thiol group, but which may also involve the carboxylic acid moiety. The stability constant of Pb complexation with Cys is 8.2 (Tewari 2005), which is higher than 7.8 for GSH (Singh 2001). I find that the molar ratio needed at which Pb is biounavailable for Cys is 11:1, whereas the molar ratio for GSH is 674:1. This is in

agreement with Crea et al. (2014), who found that GSH showed weaker Pb^{2+} binding affinity than Cys.

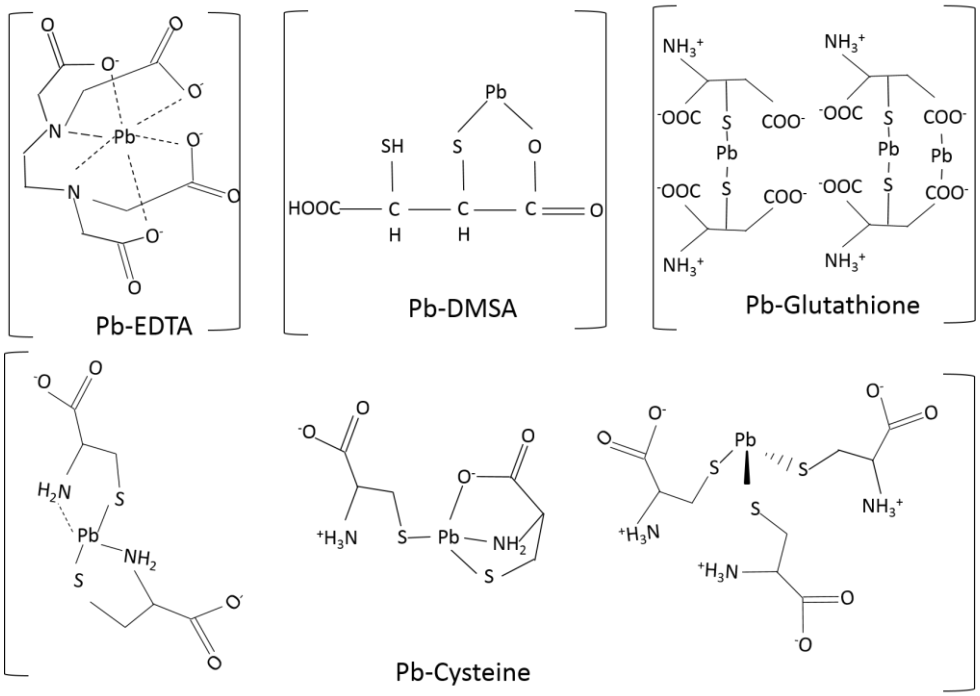

Figure 3-4. Proposed structure for Pb^{2+}-ligand complexes in aqueous solution. Structures from Bradberry and Vale 2009; Sisombath 2014; Vacek et al. 2004.

Effects of HA and DOC on the bioavailability of Pb

In aqueous systems, DOC is generically known to complex heavy metals and HA is a fraction of DOC that has been observed in many cases to dominate complexation with metals (Coles and Yong 2006; Di Toro et al. 2001; Gustafsson 2001, Tipping 1994). Figure 3-5 shows the effect of commercially available HA on Pb bioavailability, which follows the log-sigmoid trend observed for other binding agents above. Visual MINTEQ has reasonably well-studied thermodynamic constants that describe metal binding with HA, or at least an "average"/typical HA, and the Visual MINTEQ predicted response was calculated and is plotted for comparison to the bioreporter response for HA along with the

percent of total Pb complexed to HA (HA_2Pb, second y-axis). The results are in reasonable agreement with the bioreporter response, though not quite as good as for EDTA. Also plotted in Figure 3-5, are the effects of DOC on Pb bioavailability in water samples collected from Taihu sampling stations, which I plot in terms of estimated HA concentration (according to the implementation in Visual MINTEQ). In the eight Taihu samples analysed, estimated HA is proportional to DOC content, which was 6.88 mg·L^{-1} for St 4, 4.30 mg·L^{-1} for St 0, 3.99 mg·L^{-1} for St 1, 3.57 mg·L^{-1} for St 6, 3.43 mg·L^{-1} for St 3, 3.36 mg·L^{-1} for St 5, 2.45 mg·L^{-1} for St 7, and 2.44 mg·L^{-1} for St 8. I see the same trend for natural samples as for commercially available HA, however, the only sample that has enough DOC/HA to have a substantive effect is the one collected from St 4.

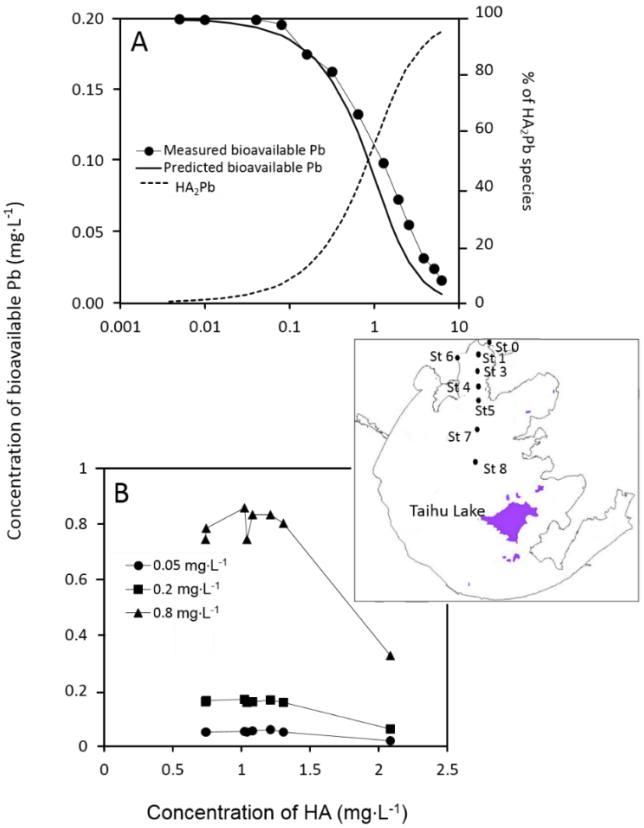

Figure 3-5. Effect of HA on Pb bioavailability in the *E. coli* strain zntA. Panel A is prepared HA solution and predicted data based on speciation calculation; Panel B is HA in Taihu water and the inset shows the locations of the sample sites.

HA is the most abundant organic constituent produced by the biodegradation of dead organic matter (present in the dissolved phase as DOC) and is a complex mixture of structures with a frequent motif of aromatic groups linked together and having carboxylic and phenolic acid substituents (Coles and Yong 2006). The considerable overall similarity among many individual HAs entails that they behave as mixtures of dibasic (carboxylic, phenolate) acids. The unique characteristics of HA make it a very efficient sorbent for heavy metals, and my results are consistent with the finding of Khokhotva and Waara (2010) that sorption of Zn, Ni, Pb and Cu is sensitive to DOC content. Visual MINTEQ results from speciation calculations, even using parameters for "generic" HA, were in reasonable agreement with bioreporter results. Results for Pb binding by DOC (expressed in Visual MINTEQ in terms of HA binding) in natural waters are more complex due to the possible and unknown variability of natural DOC from site-to-site. In this study, I noted that DOC in water samples can decrease the bioavailability of Pb in a manner that mimics the trend of the lab refined HA, as shown in Figure 3-5, and the differences in the effect on bioavailability at different $C_{\mathrm{Pb}}^{\mathrm{Tot,\ diss}}$ concentrations are consistent with model predictions. While all results reported herein are mutually consistent, further studies are still needed to increase the accuracy of modelling.

3.4 IMPLICATIONS FOR FIELD WORK

I have found that known chelators such as EDTA and DMSA, along with other complexing ligands including Cys, GSH, and commercially available HA, may significantly reduce the bioavailability of Pb or even render it biounavailable to a whole-cell bioreporter. In contrast, compounds that do not strongly complex Pb

(Leu, Met) do not affect bioavailability, or at least not at the concentrations tested here. I also found that bioavailability of Pb is reduced in natural waters at higher DOC concentrations. These findings are what would be expected based on the binding affinity of the ligands with Pb^{2+}, and in agreement with preliminary results from speciation modelling.

- These initial results indicate potential of being able to further develop a useful and cost-effective preliminary approach to water quality ERA for heavy metals, with rapid secondary validation from bioreporters.
- Given that biological methods currently in use for such validation are somewhat unwieldy, development of relatively higher throughput methods is of interest to complement, and potentially one day replace, methods in current use.
- In later chapters, I show how I combined this initial work with a geospatial view to examine Pb risk in Taihu. While Pb has been studied in Taihu, the work in this area has not been as comprehensive as for other forms of pollutants that threaten the lake, and moreover, the heavy metal pollution in a context of bio-toxicity in this drinking water lake has not been addressed to date.

4 THE EFFECT OF DOM IN TAIHU ON PB BINDING

After validating the bioreporter with model predictions through the work in Chapter 3, my intention had been to expand work to a full-scale regional level demonstrtaion in Taihu. Preliminary work, however, was not successful. I determined that the most likely cause of the problem was that the parameters describing Pb-DOM complexation in the models, though reasonably generalisable, are not correct for my field site. There is an emerging appreciation of this issue (as described in Chapter 2). This left me with the challenge that, if I wanted to proceed, I would need to find a way to rapidly obtain site-specific parameters (namely conditional binding constant, K_{cond}) for use in ERA models, and I determined that fluorescence techniques were most promising. In this work I 1) characterise the spatial distribution and variability of DOM across Taihu, i.e. at regional scale, 2) study the binding capacity of DOM with Pb in different parts of the lake to understand regional variability in K_{cond}, and 3) explore whether I can elucidate factors controlling Pb-DOM complexation, i.e. whether there are relationships between DOM fluorescence properties, water quality indicators and K_{cond} that provide insights on variability in K_{cond}. I find that K_{cond} varies over two

orders of magnitude at the regional level, contrary to established assumptions behind one-size-fits-all models of metal-DOM binding in current ERA speciation models that hold K_{cond} constant, and that K_{cond} varies in a manner that is consistent with other factors affecting DOM and water quality. Unlike other works that have studied metal-DOM complexation with fluorescence spectroscopic techniques, the approach I use here specifically addresses the needs of ERA in development of more accurate, yet rapid/streamlined ERA modelling. This work is novel as I do not know of any other studies that have employed as the wide array of indicators that might provide insights into K_{cond} variability or have used the approach that I use in the framework of ERA. The results are proof-of principle that the approach I take is sufficiently rapid and adaptable to be fit-for-purpose with respect to ERA applications.

4.1 Field Area, Sampling, Analysis and Fluorescence Techniques

Study area, sampling and water quality analyses

Taihu is located in one of the most rapidly developing urban and economic regions in China, with 0.4% of the land area of China, over 40 million inhabitants and ~13% of the nation's GDP (Gross Domestic Product) (Qin et al. 2010; Yang and Liu 2010). Taihu holds a crucial role in regional water security, however, Taihu has become hypertrophic (Qin et al. 2007) due to the influx of nutrient-rich wastes from urban, agricultural, and industrial activities within the Taihu watershed (Sun and Mao 2008). With more than 170 rivers and streams draining into Taihu, there is a substantial exogenous contribution to DOM in some parts of the Taihu ecological system. At the same time, the size and relative biological

productivity of Taihu entails that there is much endogenous contribution to DOM as well, particularly given that Taihu has experienced HABs every year since the mid-1980s (Sun and Mao 2008). These HABs have had a strong influence on the chemical nature and amount of DOM, particularly in the northern part of the lake (Zhang et al. 2014). In consequence of the highly variable sources of DOM across the very large lacustrine system, there is potential to observe a highly variable of DOM properties throughout the lake (Yao et al. 2011), and therefore different effects of metal-DOM binding and K_{cond}.

In addition to the highly variable sources of DOM to Taihu, the character of DOM is expected to be affected by the water retention time (WRT), which has been reported to be on the order of 5-10 months (Qin et al. 2004, 2007). As the lake is so large, the WRT is also variable in different regions of the lake. Urban pollutants discharge into northern Taihu, runoff sources are largely from the western and southwestern mountains, and outflows are located throughout East Taihu. Figure 4-1A shows the tributaries/drainage network for Taihu and prevailing summer current pattern (Qin et al. 2007). The greatest inflow rivers are the Chendong, Tiaoxi (net inflow), and Yincun in the west/southeast, though approximately 60% of river water inflow comes from western rivers along the Yixing shore (Figure 4-1B, notably the Chendong River and the Caoqiao are also important, see Qin et al. 2007; Sun and Mao 2008; Xu and Qin 2005). The main outflow rivers are the Taipu (accounting for ≥50% of the total outflow volume), Xinyun, and Xijiang in the east/southeast (Qin et al. 2007). By far the largest flow is the Taipu River, which results in shorter WRT times in the south. In consequence of inputs and residence times, water quality, therefore, is better in the south than in the north, and in the southeastern part of lake (Qin et al. 2007).

Water samples from 32 monitoring stations in Taihu that are monitored by NIGLAS (Nanjing Institute of Geography and Limnology, Chinese Academy of Sciences) quarterly (Zhang and Chen 2011) were collected in August, 2017 (Figure 4-1B). This sampling time was chosen to occur at the height of what has become a yearly occurrence of a cyanobacterial HAB in the north/northwestern part of the lake. The yearly HAB occurrence commences in the northern part of the lake, in the Meiliang Bay area where stations Sts 1, 3, 4 and 5 are located (Figure 4-1B), spreading toward the south and east thereafter. Despite the frequent HABs, the southeastern region of the lake is typically characterised by relatively clear water with floating and submersed macrophytes (Qin et al. 2007). The inflows and outflows of the lake are complex due to the networked nature of the watercourses connected to the lake (Sun and Mao 2008), however, the HAB is associated with inflow of nutrient-polluted waters, and its spread follows the predominant pattern of summer circulation, as shown in Figure 4-1B (Qin et al. 2007).

For taking water samples, at each station, a 1.5 L water sample was collected from 0.2 m below the water surface in a trace-metal clean polyethylene bottle, and water sample physical parameters including surface water temperature, Secchi-disk transparency (Transp), pH, electrical conductivity (Cond) and dissolved oxygen (DO), were measured using a YSI 6600 multisensor sonde. Water samples were returned to the laboratory within 6 h and 0.75 L of each sample was filtered through a pre-combusted 45 mm Whatman GF/F glass fibre filters (nominal pore size 0.7 μm) and kept at 4ºC in the dark until analysis for dissolved quantities. The remainder of each sample was subject to analysis of other water quality parameters.

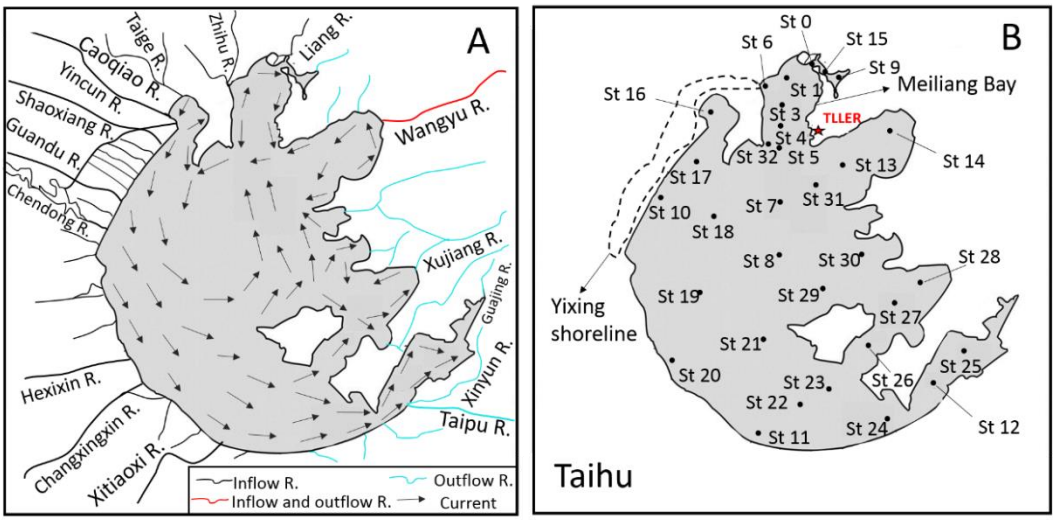

Figure 4-1. Maps of Taihu. Map shows (A) its tributaries/drainage network (R. is River) and prevailing summer current pattern (Qin et al., 2007), and (B) location of all 32 sampling stations (St) indicated with dots. TLLER is the location of the Taihu Laboratory for Lake Ecosystem Research, marked with a star.

The measurement of $C_{Pb}^{Tot,\ diss}$, DOC, NH_4^+, Na^+, K^+, Ca^{2+}, Mg^{2+}, NO_3^-, NO_2^-, PO_4^{3-}, Cl^- and SO_4^{2-} was conducted as described in detail in Chapter 3. Additional chemical properties that were measured in the lab included chlorophyll-a (Chl-a), total phosphorus (TP), total dissolved phosphorus (TDP), total nitrogen (TN), total dissolved nitrogen (TDN) 5-day biological oxygen demand (BOD) and COD_{Mn}. For the determination of Chl-a, water samples were filtered through Whatman GF/F glass fibre filters, then the concentration of Chl-a was determined by hot ethanol method (ISO 1992). The concentrations of TN, and TP were determined using a combined persulphate digestion (Ebina et al. 1983). BOD and COD_{Mn} were determined according to the corresponding standard methods (APHA 1995).

Fluorescence spectroscopy

Fluorescence spectra for the 32 stations were obtained in a 1 cm quartz cuvette using a Cary Eclipse fluorimeter (Agilent Technologies) equipped with a 150-W Xenon arc lamp light source and a PMT detector with voltage set at 700 V. For

3DEEM fluorescence spectra (3-D being excitation, emission, and intensity, hereafter EEM), the excitation wavelength range was scanned from 200 to 450 nm at 5 nm intervals, and the emission wavelength was scanned from 300 to 550 nm in 1 nm increments. For SFS quenching titration experiments to study Pb-DOM complexation (Esteves Da Silva et al. 1998; Fu et al. 2007), spectra were recorded scanning the excitation and emission monochromators over a 200 nm range starting at 250 nm with a $\Delta\lambda$ = 20 nm offset using a 5 nm slit width and a scan speed of 1200 nm·min^{-1}. Titration was carried out by adding a series of Pb spikes (final concentrations ranging from 9.5×10^{-7} to 3.8×10^{-5} M) to subsamples from each sample of the 32 stations. pH was adjusted to 7.00 ± 0.05 by adding MOPS buffer (Zhang et al. 2017). Prior to analysis, all samples were kept 24-h at room temperature in the dark to ensure complexation and avoid photolytic reactions. A sample of commercially available HA (8 mg·L^{-1}, Alfa Aesar, Tianjin, China) was also scanned under the same conditions, albeit without adding Pb, in order to have a comparator for spectral features.

Parallel factor analysis modelling

Stedmon et al. (2003) demonstrated the use of parallel factor (PARAFAC) analysis of EEM spectra to decompose or "unmix" the complex mixture of DOM fluorophores into contributions from underlying component fractions without any assumptions about the spectral shape or number of contributing components. In recent decades, this method has been widely used for the characterisation of DOM/DOC from both freshwater and marine aquatic environments (Cory and McKnight 2005; Kowalczuk et al. 2009; Yamashita et al. 2008). With regard to lakes in particular PARAFAC has been used to study land use change,

environmental processing of DOM, ecological processes taking place within and among lakes, and lake stratification and spatial variation in DOM sources within lakes (Jaffé et al. 2004). The PARAFAC model decomposes an EEM spectrum as follows:

$$X_{ijk} = \sum_{f=1}^{F} \left(a_{if} b_{jf} c_{kf}\right) + e_{ijk}, \qquad (4\text{-}1)$$

where X_{ijk} is an array with the fluorescence intensity for the *i*th sample at emission wavelength *j* and excitation wavelength *k*, the summation includes a set of trilinear terms a_{if}, directly proportional to the concentration of the *f*th analyte in the *i*th sample, b_{jf}, is linearly related to the emission spectra at wavelengths *j* for the *f*th analyte, and c_{kf} is linearly proportional to the specific absorption coefficient at excitation wavelength *k.* The term e_{ijk} represents an array containing the model residuals. For samples that have a wide range of DOC concentrations, a correlation of components may arise artefactually in proportion to DOC. To avoid that, the computational package used to perform PARAFAC analysis (staRdom, Pucher et al. 2019) is implemented so that samples may be normalised to DOC for determination of components, with normalisation being later reversed by multiplying samples loadings for each component with normalisation factors.

Theory of fluorescence quenching titrations

Fluorescence quenching is defined as any process that decreases the fluorescence intensity of a sample (Lakowicz 2006). There are many mechanisms by which quenching occurs, e.g. excited-state reactions, inner filter effect (autoabsorption proportional to the optical density of the sample at excitation and emission

wavelengths), self- and/or intramolecular absorbance, collisional/dynamic quenching and static quenching. Collisional/dynamic quenching occurs when an excited-state fluorophore experiences non-reactive contact with a species in solution (e.g. chloride, oxygen) that facilitates non-radiative relaxation to the ground state. Static quenching occurs when, for example, complexation between a metal ion and the main binding sites of DOM occurs and causes non-radiative relaxation.

It is well-known that DOM fluorescence is quenched by heavy metals, via both static and dynamic mechanisms (Lakowicz 2006), usually dominated by static quenching for bivalent metals that strongly form strong complexes with organic fluorophores (Cabaniss 1992; Esteves da Silva et al. 1998). Quenching (measured by SFS) is proportional to metal complexation, and this phenomenon has become well established as a method to determine K_{cond} of complexation (Cabaniss 1992; Esteves da Silva et al. 1998; Fu et al. 2007; Heibati et al. 2017; Lu and Jaffe´ 2001; Ryan and Weber 1982a and b). Studies have shown that both fluorescence lifetime (Lakowicz 2006) and thermal quenching (Carstea et al. 2014) are useful in verifying quenching mechanisms. Due to the various processes that may be affecting fluorescence, the use of quenching titrations is operationally bolstered by common matrix, i.e., when spiking metal into a sample solution, the only thing that is changing is metal concentration, hence mechanistic information is not operationally necessary.

The complexation reaction is described by (charges omitted)

$$M + L \leftrightarrow ML, \qquad (4\text{-}2a)$$

where M is the metal (Pb here), L represents a complexing ligand (in this case DOM), and ML is the complex (Pb-DOM). This chemical reaction is governed by the equilibrium expression

$$K_{\text{cond}} = \frac{[\text{ML}]}{[\text{M}]\cdot[\text{L}]}, \qquad \text{(4-2b)}$$

where binding is assumed to form 1:1 complexes, and brackets denote concentrations of the ML complex, uncomplexed metal ion, and uncomplexed ligand, respectively. The quenching of DOM fluorescence by complexation with a metal ion can be described by the modified Stern–Volmer equation (Esteves Da Silva et al. 1998) according to

$$\frac{I_0}{\Delta I} = \frac{1}{f\cdot K_{\text{cond}}\cdot C_{\text{M}}^{\text{Tot, diss}}} + \frac{1}{f}, \qquad \text{(4-3)}$$

where $\Delta I = I_0 - I$, I_0 and I are the fluorescence intensities of the sample, respectively, with and without M (Pb) present, f is the fraction of I_0 that corresponds to the fluorescent portion of DOM that participates in binding, K_{cond} is the conditional stability constant for the reaction shown in (2), and $C_{\text{M}}^{\text{Tot, diss}}$ is the total dissolved metal (Pb) concentration. Equation (3) may be plotted as a line for which $I_0/\Delta I$, $C_{\text{M}}^{\text{Tot, diss}}$, $1/(f\cdot K_{\text{cond}})$ and $1/f$ are the ordinate, abscissa, slope, and intercept, respectively. Thus K_{cond} and f are estimated from the slope and intercept of the linear plot. An alternate expression for static quenching (Ryan and Weber 1982b) is

$$I = \left(\frac{I_{\text{ML}}-100}{2K_{\text{cond}}C_{\text{L}}^{\text{Tot, diss}}}\right)\left[\left(K_{\text{cond}}C_{\text{L}}^{\text{Tot, diss}} + K_{\text{cond}}C_{\text{M}}^{\text{Tot, diss}} + 1\right) - \sqrt{\left(K_{\text{cond}}C_{\text{L}}^{\text{Tot,diss}} + K_{\text{cond}}C_{\text{M}}^{\text{Tot, diss}} + 1\right)^2 - 4{K_{\text{cond}}}^2 C_{\text{L}}^{\text{Tot, diss}} C_{\text{M}}^{\text{Tot, diss}}}\right] + 100, \qquad \text{(4-4)}$$

where I_{ML} is the fluorescence intensity (in %, i.e. when data is expressed such that I_0 = 100%) at which further addition of quencher produces no further diminution of fluorescence intensity, and $C_L^{Tot,\ diss}$ is the total concentration of ligand. This expression has two new parameters, however, the parameter I_{ML} is related to the parameter f in equation (3) since, when I_{ML} is expressed in decimal percent, I_{ML}+ f = 1, hence equation (4) is used in problems seeking to understand complexing capacity in addition to the magnitude of K_{cond} s (Boguta et al. 2016; Esteves Da Silva et al. 1998). For (4), parameter solutions are determined using non-linear regression analysis, plotting I versus $C_M^{Tot,\ diss}$.

Expression (3) was developed to capture non-idealities/deviations from linearity in Stern-Volmer plots. Another commonly used expression to address this issue that also relies on non-linear regression is

$$I_0/I = \left(\frac{1}{\frac{f}{1+K_{cond} \cdot C_M^{Tot,\ diss}} + I_{ML}} \right), \qquad (4\text{-}5)$$

where I_{ML} is decimal (Carraway et al. 1991) and non-linear regression is performed on a I_0 / I versus $C_M^{Tot,\ diss}$ plot. Comparison of results from different equations are useful due to the variability in error structure arising from different functional forms.

When collisional/dynamic quenching occurs simultaneously to complexation between a metal and DOM, nonlinearity of I_0/I versus $C_M^{Tot,\ diss}$ plots (away from x-axis) is observed. The expression used in this case is (Carraway et al. 1991)

$$\frac{I_0}{I} = \left(1 + K_{\text{cond}}^{\text{d}} \cdot C_{\text{M}}^{\text{Tot, diss}}\right) \cdot \left(1 + K_{\text{cond}} \cdot C_{\text{M}}^{\text{Tot, diss}}\right) \quad (4\text{-}6)$$

where $K_{\text{cond}}^{\text{d}}$is the constant for collisional or dynamic quenching and parameters are determined via nonlinear regression (Carraway et al. 1991).

Data treatment and calculations

The R (R Core Team 2019) package staRdom (Pucher et al. 2019), with associated packages in R (Helwig 2019; Massicotte 2019; Wickham et al. 2019; Wickham and Henry 2019), was used for analysis of EEM spectra. Fluorescence peaks and indices calculated include Coble peaks (Coble 1996), the humification index (HIX) (Ohno 2002; Zsolnay et al. 1999), the index of recent autochthonous contribution (BIX) (Fellman et al. 2010; Huguet et al. 2009), and the fluorescence index (FI) (McKnight et al. 2001). HIX is calculated according to $\sum_{\lambda=435-480\text{ nm}} I_{\text{Em}} \Big/ \sum_{\lambda=300-345\text{ nm}} I_{\text{Em}}$ for λ_{Ex} = 254 nm (Ohno 2002). BIX is $I_{\lambda=380\text{ nm}}^{\text{Em}} \Big/ I_{\lambda=430\text{ nm}}^{\text{Em}}$ for λ_{Ex} = 310 nm (Huguet et al. 2009), and FI is $I_{\lambda=380\text{ nm}}^{\text{Em}} \Big/ I_{\lambda=430\text{ nm}}^{\text{Em}}$ for λ_{Ex} = 370 nm (McKnight et al. 2001).

The processing pipeline included data checking, blank subtraction, inner filter effect correction and removal of scattering peaks (see vignette, Pucher 2019). Raman normalisation was not performed, in accordance with findings of Mostofa (Mostofa et al. 2013b). PARAFAC analysis was also conducted and provides similar but different data as from peak picking (Coble peaks), namely that decomposition of spectral components via PARAFAC analysis avoids spectral overlap and can provide exploratory results beyond the pre-determined Coble peaks (Murphy et al. 2013). Normalisation (and subsequent inverse

normalisation) was performed for PARAFAC analysis, and results were subsequently validated via analysis of residuals, split-half analysis, and comparison with similar systems (Bro 1997); OpenFluor was used for the latter (Murphy et al. 2014). SFS data were analysed by linear (Excel) and nonlinear (Origin) regression analysis using equations (4-3), (4-4), (4-5) and (4-6).

Additional data analysis included pair-wise correlation analysis, multiple regression, and principle component analysis (PCA). These were performed using the corrplot, FactoMineR, factoextra, fields, leaps, plot3D, rcorr, and stats calculation and visualisation packages in R (Alboukadel and Fabian 2017; Harrell et al. 2015; Karline 2017; Lumley 2017; Nychka et al. 2017; R Core Team 2019; Sebastien et al. 2008; Taiyun and Viliam 2017). To perform these calculations, results from physical and chemical analysis of water samples were combined with results from analysis of EEM data and results for K_{cond} into a single multivariate data set.

4.2 WATER QUALITY AND CONDITIONS

Results for individual measurements of 22 physical and chemical parameters for the 32 samples in different regions of Taihu are given in Table 4-1 (along with results for $C_{\mathrm{Pb}}^{\mathrm{Tot,\ diss}}$) and for brevity are summarised here. The pH in the lake was somewhat high, ranging from 7.90 to 8.35, which has been attributed to inorganic carbon scavenging of phytoplankton as a result of HABs (Fang et al. 2018; Ma et al. 2014; 2015). The Chl-a concentrations ranged from 7.81 to 239.2 $\mu g \cdot L^{-1}$, with higher Chl-a concentrations occurring in HAB-impacted areas of the lake, and a

Table 4-1. Chemical and physical properties of water samples from Taihu.[1]

Stations	pH	COD_{Mn} (mg/L)	DO (mg/L)	BOD (mg/L)	NH_4^+ (mg/L)	NO_2^- (mg/L)	NO_3^- (mg/L)	TDN (mg/L)	TN (mg/L)	PO_4^{3-} (mg/L)	TDP (mg/L)	TP (mg/L)	Chla (μg/L)	DOC	K (mg/L)	Na (mg/L)	Ca (mg/L)	Mg (mg/L)	Cl^- (mg/L)	SO_4^{2-} (mg/L)	Transp (m)	Cond (μS/cm)	Pb (μg/L)
St0	8.03	5.80	6.57	2.87	0.47	0.052	0.065	0.98	1.98	0.038	0.06	0.18	68	4.48	4.88	32.20	29.87	7.45	35.55	46.22	0.20	465	0.32
St1	7.97	9.56	12.75	7.01	0.12	0.002	0.083	0.68	2.81	0.052	0.08	0.28	135	8.55	4.95	40.15	29.48	7.24	45.24	51.45	0.25	490	0.43
St3	7.96	7.65	11.65	4.68	0.16	0.002	0.073	0.60	2.48	0.039	0.06	0.24	119	5.31	5.01	40.78	25.87	7.13	45.88	51.52	0.20	470	0.39
St4	7.95	11.42	12.40	6.18	0.17	0.003	0.069	0.62	4.00	0.022	0.04	0.36	239	5.36	5.02	41.37	25.63	7.14	46.26	52.20	0.20	470	0.39
St5	7.90	6.18	14.16	3.29	0.28	0.005	0.087	0.63	2.06	0.018	0.04	0.18	79	5.58	5.06	42.34	23.79	7.24	42.26	48.03	0.35	475	0.42
St6	8.18	5.18	4.10	4.58	1.01	0.372	0.673	3.22	3.80	0.093	0.12	0.23	54	4.15	4.91	33.45	33.52	6.60	44.75	54.59	0.25	560	0.44
St7	7.94	4.88	6.51	2.09	0.36	0.016	0.090	0.76	1.57	0.029	0.06	0.14	22	4.85	5.01	39.33	21.81	7.31	44.56	51.86	0.30	440	0.53
St8	8.04	5.89	7.01	3.21	0.37	0.003	0.081	0.58	1.66	0.054	0.08	0.21	28	4.85	5.06	38.75	28.87	7.38	45.43	52.17	0.20	480	0.49
St9	8.07	5.27	7.93	3.05	0.60	0.028	0.081	1.00	1.74	0.048	0.07	0.17	31	4.49	4.90	25.02	28.70	7.47	26.34	41.95	0.25	385	0.45
St10	8.15	5.37	3.67	4.16	0.96	0.209	0.477	2.67	3.32	0.068	0.09	0.20	27	4.31	4.67	31.93	35.10	6.58	40.61	40.28	0.30	460	0.38
St11	8.04	4.98	6.49	3.11	0.06	0.002	0.086	0.48	1.17	0.006	0.02	0.10	18	5.18	4.93	36.51	32.49	7.59	43.55	51.31	0.30	480	0.45
St12	8.19	4.50	7.83	1.73	0.05	0.005	0.072	0.46	1.57	0.008	0.02	0.12	30	3.45	4.68	32.64	32.52	7.13	38.63	46.74	0.25	455	0.69
St13	8.07	6.36	6.81	3.07	0.21	0.001	0.070	0.49	1.88	0.006	0.02	0.15	57	4.36	5.07	43.40	26.11	7.52	48.42	54.88	0.20	490	0.54
St14	8.08	7.12	8.94	5.14	0.23	0.001	0.076	0.58	2.23	0.005	0.02	0.14	101	4.75	4.86	42.79	24.14	7.51	48.64	55.62	0.20	475	0.88
St15	8.11	5.18	6.81	2.73	0.56	0.050	0.074	0.95	1.59	0.045	0.06	0.14	30	4.01	4.83	24.89	29.63	7.67	26.16	41.42	0.25	390	0.36
St16	8.15	5.75	4.48	4.14	0.82	0.275	0.673	2.82	3.54	0.108	0.14	0.26	45	4.39	4.85	27.29	37.23	6.57	35.09	39.75	0.40	445	0.34
St17	8.09	4.46	6.20	2.73	0.55	0.269	0.522	2.49	3.33	0.088	0.12	0.21	32	3.49	4.78	34.97	33.83	7.33	37.85	50.04	0.70	475	0.36
St18	8.05	4.08	7.83	4.50	0.24	0.005	0.081	0.80	2.51	0.099	0.13	0.31	105	5.56	5.07	39.97	32.98	7.58	47.97	50.12	0.25	500	0.68
St19	8.05	6.27	6.67	2.23	0.30	0.007	0.076	0.66	1.90	0.069	0.11	0.25	43	5.01	5.14	39.54	33.01	7.58	46.37	50.76	0.20	500	0.46
St20	8.03	7.12	6.73	3.86	0.20	0.002	0.075	0.59	2.24	0.015	0.03	0.18	59	5.83	5.11	38.95	28.73	7.62	46.76	52.24	0.20	475	0.51
St21	8.06	7.17	7.83	4.00	0.12	0.001	0.078	0.48	2.43	0.009	0.02	0.19	64	4.58	5.05	39.99	25.35	7.37	46.62	52.32	0.15	460	0.37
St22	8.04	5.48	7.75	3.53	0.10	0.002	0.065	0.62	1.53	0.010	0.02	0.10	26	5.93	5.22	39.33	29.88	7.80	47.18	51.03	0.30	485	0.59
St23	8.06	6.22	8.33	3.09	0.08	0.002	0.076	0.48	2.23	0.009	0.02	0.18	54	4.71	5.08	40.03	27.78	7.56	47.31	52.63	0.15	480	0.94
St24	8.17	5.57	8.84	2.43	0.07	0.002	0.077	0.44	1.55	0.009	0.02	0.10	46	4.03	4.84	35.91	30.68	7.40	42.45	50.61	0.20	470	0.40
St25	8.13	5.39	9.46	2.67	0.13	0.002	0.065	0.47	1.62	0.008	0.02	0.10	43	3.98	4.75	32.40	32.66	7.22	38.67	45.63	0.20	455	0.45
St26	8.21	3.91	7.83	1.63	0.06	0.002	0.069	0.45	1.08	0.007	0.01	0.06	17	3.25	4.76	36.40	32.88	7.70	42.96	52.95	0.30	485	0.49
St27	8.16	3.88	7.31	1.31	0.17	0.004	0.091	0.51	1.44	0.008	0.03	0.07	12	3.41	4.90	36.93	31.92	7.65	43.54	53.34	0.35	480	0.41
St28	8.10	3.26	9.26	0.72	0.13	0.013	0.087	0.44	0.92	0.006	0.03	0.03	8	3.76	4.33	35.18	21.90	7.25	40.85	50.31	1.10	420	0.35
St29	8.06	4.68	8.11	4.24	0.10	0.002	0.070	0.43	1.26	0.008	0.02	0.09	24	4.67	4.86	37.79	30.09	7.73	44.39	53.41	0.25	480	0.50
St30	8.06	4.63	8.11	3.17	0.10	0.003	0.094	0.57	1.91	0.008	0.02	0.09	26	4.16	4.83	37.57	28.30	7.58	43.75	52.77	0.20	470	0.60
St31	8.35	6.24	7.05	3.61	0.27	0.002	0.091	0.53	2.37	0.012	0.03	0.15	56	4.31	4.91	40.51	22.52	7.40	46.79	54.57	0.30	420	0.44
St32	8.20	7.28	10.42	4.18	0.33	0.002	0.074	0.59	3.03	0.032	0.05	0.23	111	5.67	5.10	42.21	23.69	7.30	47.64	53.63	0.15	435	0.46

[1] Abbreviations are dissolved oxygen (DO), Biological oxygen demand (BOD), chemical oxygen demand (COD), ammoniacal nitrogen (NH_4^+), nitrate (NO_3^-), nitrite (NO_2^-), total dissolved nitrogen (TDN), total nitrogen (TN), phosphate radical (PO_4^{3-}), total phosphorus (TP), total dissolved phosphorus (TDP), chlorophyll-a (Chl-a), dissolved organic carbon (DOC), chloride (Cl^-), sulfate (SO_4^{2-}) and electrical conductivity (Cond).

number of parameters follow the general motif of being higher in HAB-impacted areas and vice versa. Table 4-1 shows that Na^+ and Cl^- are the dominant ions in the lake, which is an indicator that anthropogenic impacts strongly affect the water quality (Chetelat et al. 2008; Yu et al. 2013).

Regarding Pb, concentrations of $C_{\mathrm{Pb}}^{\mathrm{Tot,diss}}$ in the water at the time of sampling are also in Table 4-1. These levels are low enough to be well below environmental acceptance criteria (lower than the standard concentration for drinking water and aquatic life, WQC set via USEPA), and low enough to be below levels that would have a detectable effect in quenching titrations (verified in this study by testing, data not shown). The low levels of $C_{\mathrm{Pb}}^{\mathrm{Tot,diss}}$ at pHs above ~8.5 are an expected consequence of formation of various inorganic complexes (hydroxy-, carbonato-, pyrophosphate) whose solubility product is exceeded or which more readily flocculate resulting in deposition of Pb into the bottom sediments as insoluble compounds (Fang et al. 2018). Likewise, during periods of lower ambient pH, DOM in freshwater lakes can complex with heavy metals and flocculate in a manner that results in deposition of metals into bottom sediments. Due to pollution inputs into Taihu, including Pb, over time this has resulted in high sediment concentrations of heavy metals (Liu et al. 2012; Niu et al. 2015). Due to the polymictic nature of the lake, storms cause resuspension events that can cause high levels of metals to become available for redissolution as pH values recover (seasonally, post-HAB) to a lower level (Wang et al. 2014; Zheng et al. 2013). There are implications of varying dissolved metal content from the standpoint of ERA. First, it is not unusual, and therefore analytical methods must be adaptable. In the case of low $C_{\mathrm{Pb}}^{\mathrm{Tot,diss}}$, measurements are performed as

described in this manuscript. In the case of higher $C_{\mathrm{Pb}}^{\mathrm{Tot,diss}}$, saturation measurements or competitive ligand exchange techniques are used as part of the titration process (Sander et al. 2015). For the work reported here, which centers on the potential effects of DOM that deviate from standard assumptions used in, e.g. WHAM and the SHM, I sampled when there is potentially a high level of DOM cycling in the lake, inclusive of locally high contributions of allochthonous DOM (i.e. as occurs during HABs). From the standpoint of ERA, the quantities that are calculated in setting WQC involve ascertaining what value of $C_{\mathrm{Pb}}^{\mathrm{Tot,diss}}$, if present, would cause unacceptable risk under variations in ambient conditions.

Figure 4-2 shows selected contour maps for Chl-a, DOC, COD_{Mn}, TN, TP and TN:TP to illustrate these general trends. The higher concentration of the nutrients is the main driver that leads to HABs, which in turn may be associated with elevated Chl-a, COD and DOC concentrations. Chl-a has a higher correlation with COD_{Mn} than BOD, which is likely a result of processes that affect the reworking of organic matter from HABs (note, I treat BOD, COD_{Mn}, DOC, and Chl-a as indicators of OM/primary productivity, correlations are discussed in more detail below). The regions that suffered from HAB are not entirely co-located with the distribution of TN and TP. This is an outcome of transport hydrodynamics in the lake. The predominant inflow of river water from the west/northwest and outflow of water to the east ensures a general trend of mass movement counter-clockwise from the northern part of Taihu to the locale of the largest outflow at the Taipu River. Additionally, in summer the prevailing winds from the southeast or southwest generate surface currents that manifest in localised counter clock-wise rotation (Figure 4-1B, see arrows pointing northeast and northwest to the north and south

of the island in the lake) (Qin et al. 2000; Qin et al. 2007). These simultaneous phenomena have a strong impact on the distribution of HAB and HAB-associated water quality parameters in the northern and western areas of the lake.

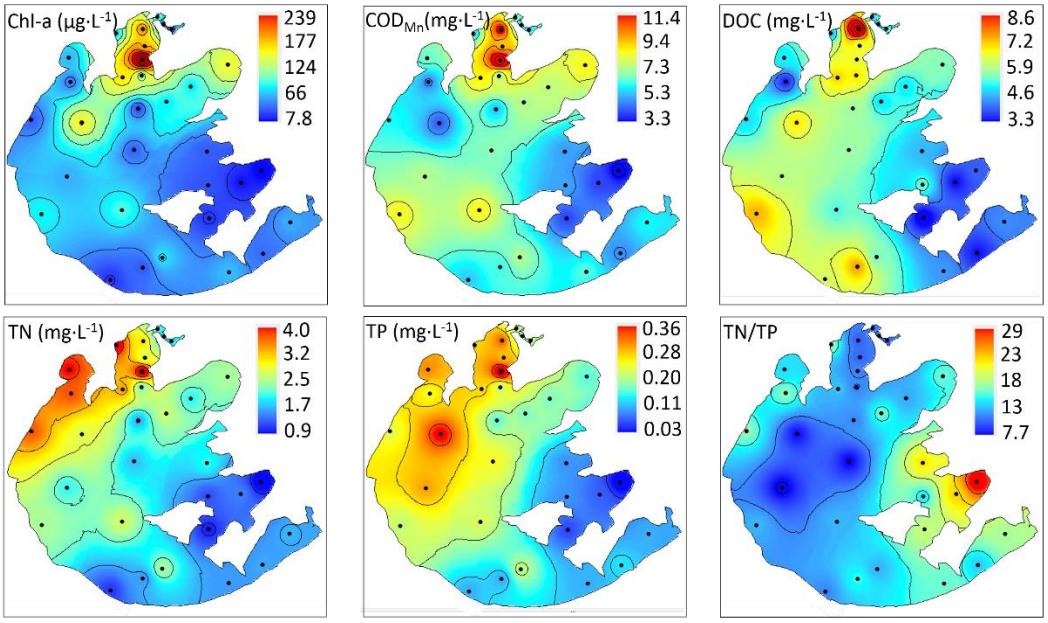

Figure 4-2. Contour maps showing the distribution of selected water quality parameters in Taihu. Abbreviations are chlorophyll-a (Chl-a), chemical oxygen demand (COD_{Mn}), dissolved organic carbon (DOC), total nitrogen (TN), total phosphorus (TP). Chl-a and TN distributions are concentrated in portions of the lake that also suffer most from cyclic HABs.

4.3 The Properties of DOM in Taihu

Fluorescence properties of DOM

A variety of approaches have been used to analyse EEM data and I consider results for three of these here: 1) an early approach adduced by Coble involving quantifying the intensity of local maxima of fluorescence corresponding to different components of DOM (EEM peak picking), 2) calculation of fluorescent indices (FlInd), 3) use of PARAFAC analysis to decompose EEM matrices into different spectral components. The last decade has seen an increasing shift to

PARAFAC analysis of EEMs (Jaffé et al. 2014; Murphy et al. 2013); this approach is analogous to quantification of Coble peaks, however it can reveal the presence of additional local maxima as well as provide improved resolution of the peaks found in analysis of raw EEMs data (see the section on EEM–PARAFAC components of Taihu DOM below for additional information on PARAFAC analysis).

Based on several decades of work on the characterisation of DOM, the common fluorophores in DOM that are identifiable by fluorescence peaks in different regions of EEMs are classified into tyrosine-like (Tyr, amino-sugar), tryptophan-like (Trp, proteins and peptides), and HA/FA-like materials (Mostofa et al. 2013b). Peak nomenclatures typically follow either the early nomenclature of Coble or the more recent terminology of Mostofa (Coble 1996; Mostofa et al. 2013b). In the Mostofa terminology, regions with Peaks A and C are associated with humic substances, with FAs having lower emission wavelengths than HAs for any given sample, and the regions with Peaks T and T_{UV} are associated with protein-like DOM, with the lower emission wavelengths for each region being Tyr-like and higher emission wavelengths being Trp-like, as shown in Figure 4-3. For the Coble terminology (Coble 1996), Coble peaks a, and c are coincident with Mostofa's Peak A and Peak C, respectively. Coble terminology does not encompass Peak T_{UV}, and in Coble terminology the Mostofa Peak T is subdivided into t (higher emission wavelength, Trp-like) and b (lower emission wavelength, tyrosine-like) peaks. Coble terminology also distinguishes a m peak that is a subclass of Mostofa's Peak C region, designating a peak that occurs at a slightly lower excitation wavelength than the primary Peak C. Mostofa recognises

subclasses of the Peak C region (M, M_p and W, see Mostofa et al. 2013b for further details).

The EEMs for the 32 stations are given in Figure 4-4. In Figure 4-4, the EEMs samples from all stations display Peak T_{UV} and Peak T (protein-like DOM), and generally the highest intensities are seen for these peaks, though, even visually it is apparent that for Sts 9 and 15 these contributions are low (particularly in the Tyr-like portion of the EEM spectrum, see EEM for St 9). Sts 9 and 15 are the only two stations that are technically not in Taihu. These stations are in Wuli Bay, which was an arm of Taihu until a gate was built to separate it from Taihu; Wuli Bay is not considered as a watercourse connected to Taihu. All the samples also had a Peak A contribution of varying intensity (e.g. contrast St 9 and St 13), however Peak C is weak or absent from visual inspection of the EEMs for around a third of the samples (e.g. St 13 in). Strong protein-like fluorescence has often been reported in water bodies that experienced HABs (Haas and Wild 2010; Moffett 1995), and protein-like fluorescence is also associated with wastewater, i.e. from wastewater treatment plants (WWTPs, e.g. see Sorensen et al. 2018). Many studies have demonstrated that excretion by HABs may contribute significantly the DOM pool (Bertilsson and Jones 2003; Moffett 1995; Yao et al. 2011; Zhang et al. 2009; Zhang et al. 2007). Since the highly labile DOM leached from algae is consumed very rapidly, the algae-produced DOM is not likely to persist in the environment, and thus except under specific conditions this bioavailable pool of algae-produced DOM that predominates in the HAB-dominated summer environment of Taihu is not expected to make up a significant fraction of the DOM in natural, unimpacted waters (Chen and Wangersky 1996; Hansen et al. 2016; Moreira et al. 2011). A shift in composition violating this

assumption would be one reason for speciation models to fail to predict bioavailability.

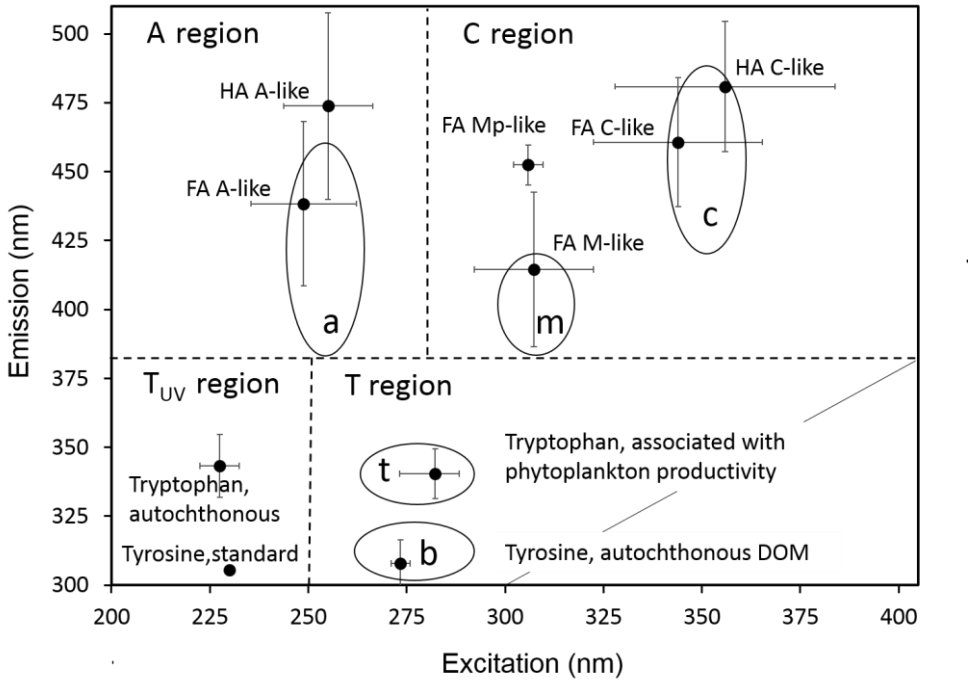

Figure 4-3. Schematic showing locations of EEM peaks reported in the literature for DOM. Regions for Peaks T_{UV}, T, A and C (Mostofa et al. 2013b) in EEMs are separated by dashed lines; error bars are one standard deviation of literature average. The approximate/indicative locations of Coble peaks a, c, b, t, and m are marked with ellipses (Coble, 1996).

Coble peaks and fluorescence indices

Table 4-2 contains results for quantification of Coble peaks and the FlInd. For 27 of 32 samples, the quantification of Coble peaks a, b, c, m, and t shows the order b ≥ t > a > m > c fluorescence, indicating that protein-like (b and t, tyrosine and tryptophan) compounds are the main component of DOM in Taihu at the time of sampling.

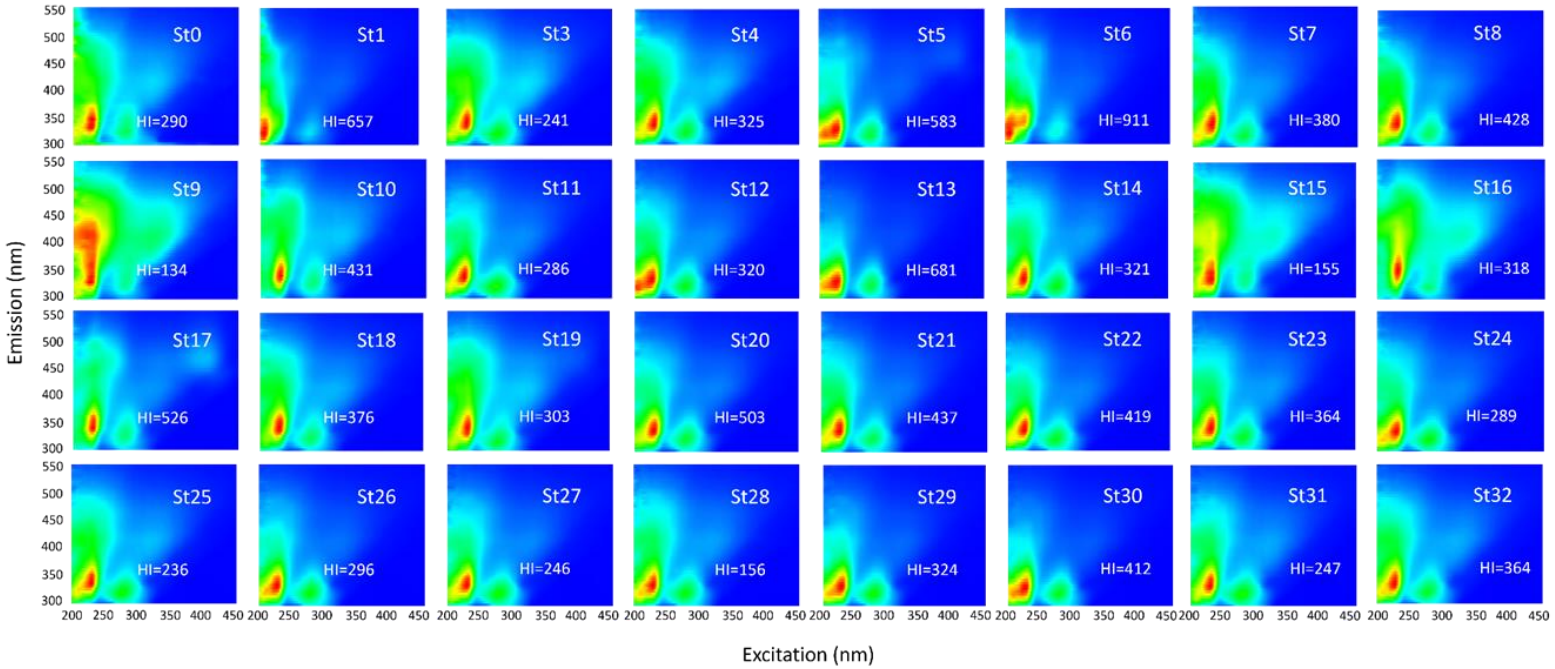

Figure 4-4. EEMs of water samples from 32 stations in Taihu. Note: for clarity in visualising differences in distribution of fluorescence across and between spectra, each EEM has been normalised to a maximum intensity of 100%. The value of HI in each panel represents the highest fluorescence intensity in RFU for non-normalised EEMs.

Two of the five exceptions are Sts 9 and 15, which have the lowest and second lowest, respectively, intensities for Peak T_{UV} and T of all stations. The other exceptions are Sts 10, 16 and 17, along the western Yixin shoreline where the greatest density of water from the Massif region in the western Taihu Basin feeds into Taihu. These stations all have slightly differing relative proportions of b and t, still following the trend a > m > c.

The metrics HIX, BIX, and FI have been developed characterise the origin and transformation degree of DOM (Huguet et al. 2009; McKnight et al. 2001). HIX is based on the concept that emission spectra will shift toward longer wavelengths as humification of DOM proceeds (Fellman et al. 2010). The HIX values for all the samples from Taihu are below 1, which indicates this DOM is mainly associated with biological or autochthonous material with a quite low humification degree (Huguet et al. 2009), which is consistent with findings for Coble peaks and my PARAFAC model (*vide infra*). The average HIX value is 0.52, and only Sts 9, 10, 15, 16 and 17 have a HIX value greater than 0.6. St 17 is near Sts 10 and 16 where there is greater influx, hence a slightly greater allochthonous contribution to DOM may be anticipated at these stations (Zhang et al. 2012).

The BIX index was calculated for characteristic of autochthonous biological activity in water samples. The BIX values in my study range from 0.87 to 1.13. Huguet et al. (2009) showed that values from 0.8 to 1 represent the DOM associated with a strong autochthonous component, and values greater than 1 are indicative of biological production of strongly labile organic matter. Of 32 stations, all have a BIX higher than 0.8, and 24 display a BIX value higher than 1, indicating the presence of freshly released DOM (Huguet et al. 2009). In this study,

the BIX and HIX indices show a small range of values and a negative correlation, indicating that the DOM in Taihu was strongly affected by autochthonous contributions, freshly released in origin and likely caused by the HAB in the lake. These findings might be subject to debate however, for instance, *Microcystis* spp. are typically the dominant genus found in Taihu HABs, and Yang et al. (2016) found that, when growing *Microcystis aeruginosa* in lab culture, BIX values may drop from 1 to ~0.2 in early exponential phase growth (Yang et al. 2016). Similar comments pertain to my results for FI. McKnight et al. (2001) developed the FI for predicting the precursor source and chemical properties of FA. For my samples the FI values range from 1.39-1.71. FI values of <1.9 consistently appear in DOM from rivers that have terrestrially derived DOM sources (McKnight et al. 2001). In terrestrial environments the source of DOC is typically from decomposition of dead organic matter (Camilleri and Ribi 1986). Taihu is a very large lake with many inflowing rivers that may transport HA/FA components of DOM into the lake, however, the FI may not be representative of the source of non-HA/FA components of the DOM.

EEM–PARAFAC components of Taihu DOM

PARAFAC analysis was used to decompose EEMs into components corresponding to DOM fluorophores (Bro 1997; Murphy et al. 2013). Figure 4-5 panels A to D display four different components, designated as Comp1 to Comp4, which are the composite components obtained from PARAFAC analysis; the component breakdowns for each sample are given in Table 4-3.

For PARAFAC, an initial exploratory analysis was performed including scrutiny of model residuals, plots of leverage for each sample, and split-half analysis for the entire data set (both calculated as implemented in R's staRdom).

Table 4-2. Coble peaks and FlInds. Units for Coble peaks are RFU and indices are unitless.

Station	Coble peaks					Indices		
	b	t	a	m	c	FI	BIX	HIX
St 0	115	117	105	83	60	1.55	0.94	0.58
St 1	152	139	112	84	62	1.48	1.01	0.54
St 3	134	107	103	76	58	1.58	1.00	0.56
St 4	157	137	108	85	69	1.71	1.05	0.54
St 5	247	228	117	78	59	1.47	1.01	0.47
St 6	266	265	178	130	86	1.50	1.10	0.57
St 7	157	138	92	73	46	1.43	1.07	0.49
St 8	168	158	94	82	44	1.52	0.92	0.47
St 9	43	59	91	70	55	1.49	0.94	0.76
St 10	139	170	151	111	88	1.48	0.87	0.68
St 11	169	125	78	57	39	1.43	1.04	0.44
St 12	167	141	83	65	43	1.50	1.06	0.46
St 13	291	277	94	68	51	1.54	1.04	0.38
St 14	169	144	96	70	53	1.60	1.06	0.50
St 15	49	70	92	67	50	1.50	0.89	0.74
St 16	105	108	160	120	100	1.57	0.90	0.73
St 17	164	178	170	92	79	1.50	1.04	0.63
St 18	160	148	118	92	63	1.46	0.98	0.55
St 19	148	123	112	84	58	1.54	0.98	0.57
St 20	227	199	113	85	65	1.56	1.04	0.47
St 21	175	155	94	71	49	1.47	1.08	0.47
St 22	203	164	100	74	48	1.62	1.11	0.45
St 23	185	163	102	80	58	1.49	1.08	0.48
St 24	157	131	76	57	41	1.48	1.04	0.45
St 25	132	102	82	62	45	1.51	1.00	0.51
St 26	165	135	69	49	34	1.39	1.13	0.42
St 27	141	110	65	46	35	1.59	1.06	0.44
St 28	87	69	49	35	24	1.39	1.02	0.49
St 29	186	151	67	49	34	1.54	1.09	0.39
St 30	211	181	71	52	37	1.67	1.08	0.38
St 31	148	117	77	58	40	1.50	1.02	0.47
St 32	169	149	104	83	64	1.63	1.03	0.51

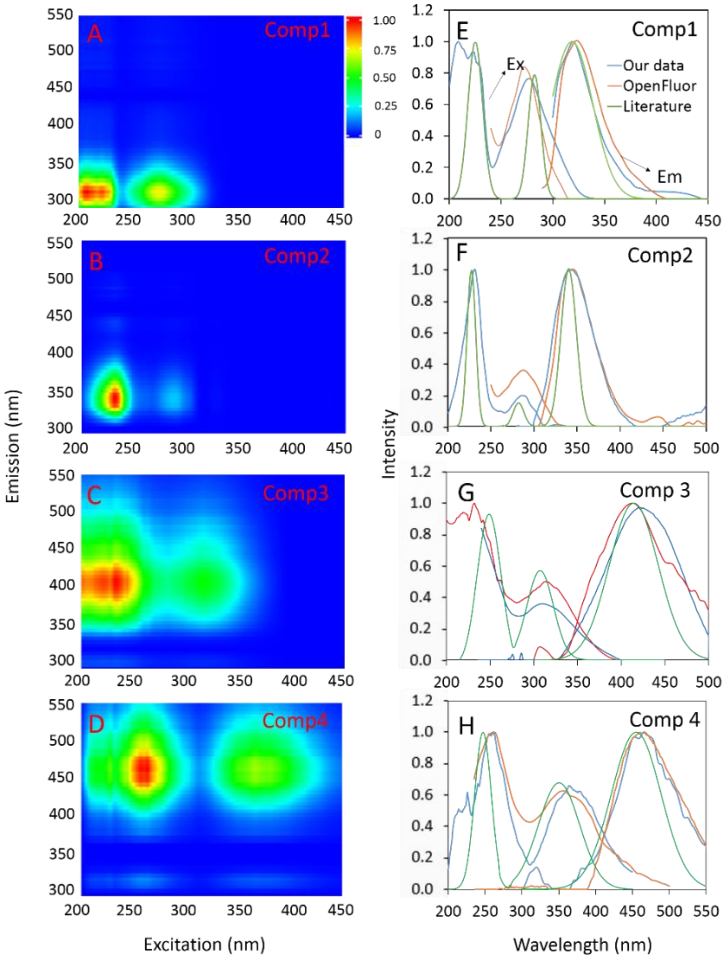

Figure 4-5. Results from PARAFAC analysis of EEM spectra. Panels (A), (B), (C) and (D), respectively, show the composite fluorescence signatures of Comp1 to Comp 4. Panels (E), (F), (G) and (H), respectively, show a comparison of my composite results with representative results published on OpenFlour and a composite of literature data reviewed and compiled by Mostofa et al. (2013b).

Based on leverage, as a metric of how unusual a datum is, outliers were identified and removed from the final calculation that was used to determined underlying composites for each component. Samples from St 0, 6, 9, 10, 15, 16, and 17 had the highest leverage and were classified as outliers. After the calculation of component composites for the remaining samples (base EEM data set), the outlier samples are recalculated to extract the calculated components. The features that cause samples to be outliers are in some cases apparent from visual scrutiny of EEMs in Figure 4-4. For instance, for St 17 the Peak C occurs at a higher

excitation wavelength and for St 9 Peak A is much broader than for samples in the base data set.

Table 4-3. The component breakdowns for each sample by PARAFAC model.

Station	Component (%)			
	Comp1	Comp2	Comp3	Comp4
St 0	20	20	30	30
St 1	20	24	28	27
St 3	18	21	28	33
St 4	21	21	27	31
St 5	28	23	17	32
St 6	19	34	25	22
St 7	23	27	30	20
St 8	24	30	32	15
St 9	12	13	35	40
St 10	12	23	25	40
St 11	27	27	24	22
St 12	30	25	25	20
St 13	38	28	17	17
St 14	25	23	24	28
St 15	14	15	30	41
St 16	8	17	28	47
St 17	12	23	17	49
St 18	19	26	29	26
St 19	18	22	28	32
St 20	25	28	24	24
St 21	24	28	25	22
St 22	26	29	25	20
St 23	24	27	26	23
St 24	27	25	24	24
St 25	22	22	27	29
St 26	31	28	22	19
St 27	27	26	23	23
St 28	26	23	25	26
St 29	33	29	20	18
St 30	37	29	18	17
St 31	25	25	25	25
St 32	23	24	27	27

Figure 4-6 shows the comparison of PARAFAC model output data with the data from Openflour for each component. Openflour is an online repository of

published DOM fluorescence spectra, and it can be searched for quantitative matches with any given set of input spectra; I searched Openfluor using the four components shown in Figure 4-5 as input spectra. Studies have shown that there are now more than 100 published PARAFAC models of DOM and over 500 published PARAFAC components (Murphy et al. 2013; Murphy et al. 2014).

For Comp1, there are 16 studies that agree with both excitation and emission of my data. For Comp2, 2 and 3 studies for the excitation and emission, respectively, agree. Similar results for Comp3 include 12 and 22 studies, respectively, for both excitation and emission peaks. There are 12 data sets that agree with my excitation spectrum for Comp4 and 22 for the emission spectrum. In Figure 4-5, panels E, F, G and H, respectively, show a comparison of my PARAFAC composite results with representative results published on OpenFlour and a composite of literature data reviewed and compiled by Mostofa et al. (2013b). The Mostofa excitation and emission peaks were plot by Using data from Mostofa et al. (2013b), average $\lambda_{Ex,\,max}$, and $\lambda_{Em,\,max}$ and standard deviations were calculated for Tyr, Trp, HA and FA components of DOM and these values were used to construct composite spectra according to

$$I = \sum_i e^{-\left(\frac{(\lambda-\bar{x})^2}{2\cdot s^2}\right)}, \qquad (4\text{-}7)$$

where I is the composite fluorescence intensity, i sums over all peaks in an excitation/emission spectrum, λ is the spectral wavelength for each point reconstructed in the composite, $\bar{x}$ is the average λ_{max} for excitation or emission, and s is the standard deviation of $\bar{x}$.

In Figure 4-5 panels E to H, I compare composite spectra from my results to representative results from the literature obtained from the OpenFlour database (Murphy et al. 2014) and to a composite for each component obtained from the data in the extensive review published by Mostofa et al. (2013b). The spectra of the four components in my study agree very well to those of DOM reported in other aquatic environments based on comparison to published data (see Figure 4-6).

The EEM for Comp1 show peaks at λ_{Ex} 223 and 280 nm / λ_{Em} 320 nm, corresponding to the Peaks T_{UV} and T with aromatic protein/tyrosine-like fluorescence (Mostofa et al. 2013b). This component has been reported to arise from the degradation products of autochthonously-produced DOM, such as phytoplankton (Catalán et al. 2013; Yao et al. 2011; Zhang et al. 2009), and the short WRT for Taihu coupled with cyclic HABs is one reason why the ratio of protein-like to FA/HA-like DOM might be overall higher in Taihu. In the EEM of Comp2, there were two excitation maxima (λ_{Ex} 230 nm and 285 nm) at λ_{Em} 347 nm, consistent with tryptophan-like fluorescence in Peaks T_{UV} and T (Mostofa et al. 2010). Yamashita et al. (2008) reported that Comp2 is comprised of labile components produced by authochthonous biological production. Comp3 has λ_{Ex} 210-240 and 315 nm and λ_{Em} 408 nm, corresponding to the FA-like fluorescence of Peak A and Peak C, respectively (Fu et al. 2010; Parlanti et al. 2000; Zhang et al. 2009). Comp4 is also composed of two peaks with λ_{Ex} 261 and 364 nm / λ_{Em} 465 nm. The first peak lies within the spectral area of Peak A and the second one Peak C region. Both peaks fall into the category of HA-like fluorescence (Mostofa et al. 2005; Ohno and Bro 2006).

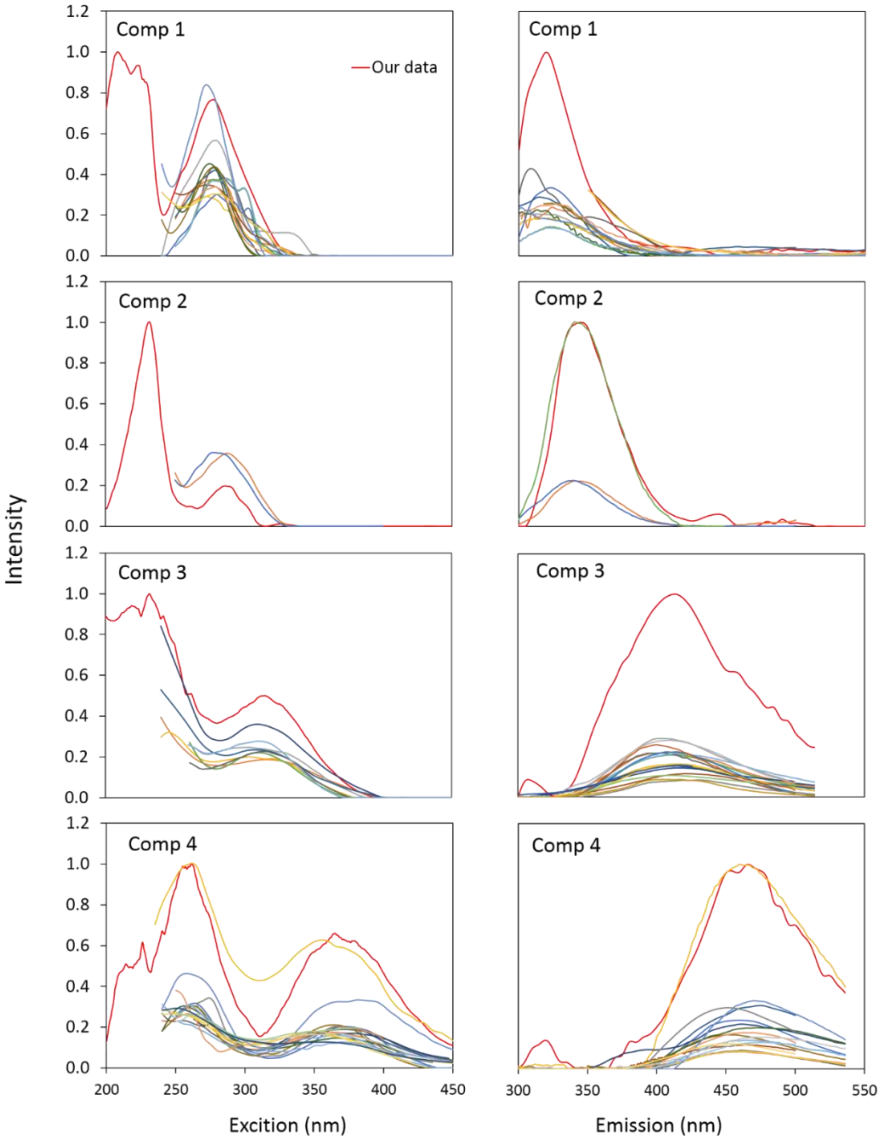

Figure 4-6. A comparison of PARAFAC model output data from this study (red line, all panels) with matching data from Openfluor. Data is given as reported, i.e., the present data and some other data are normalised to a peak maximum of 1, and other data are not. All other lines are literature results of spectra as archived in Openfluor.

Unlike the Coble peaks, I do not see a consistent pattern of progression for the different components to the relative composition of the EEMs. In common with findings for Coble peaks, Sts 9, 10, 15, 16 and 17 have the lowest contributions from the Tyr-like component and Trp-like components. Sts 10, 16 and 17, located at and below the outflow of Zhushan Bay (a polluted bay, Chen 2008), have cumulatively the highest amounts of the HA-like component. Other extrema differ

from those seen in the Coble peaks, for instance St 13 has the greatest amount of the Tyr-like component, and St 6, has the highest amount of both tryptophan-like DOM. St 13 is closest to the city of Wuxi, having a population of 4.9 million people, and St 6 is near the mouth of a tributary, and in Meiliang Bay, which is typically the area of Taihu most polluted/affected by HABs.

Split half is a way to determine if there is internal consistency for calculation results wherein a data set is split into parts, each part is calculated independently, and the results compared. The default split half implementation in staRdom divides samples, i.e. for this study the group of 32 stations, into four subgroups (A, B, C and D), then the subgroups are recombined (AB, AC, AD, BC, BD, and CD, six subgroups). The results from split half analysis (sans outliers) are shown in Figure 4-7, which shows there is reasonable internal consistency of calculated components, particularly since split half analysis becomes more problematic as the number of samples decreases.

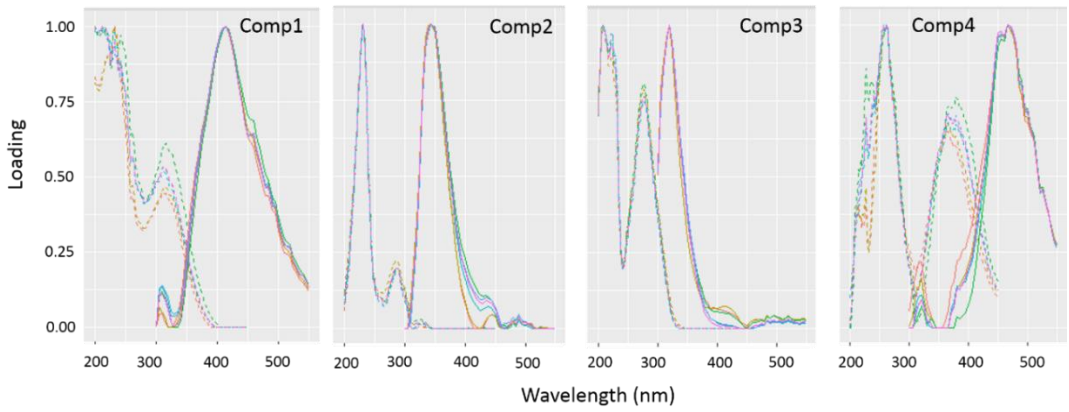

Figure 4-7. Results of split half analysis for Comp1 to Comp4. Each panel shows results for one component and contains plots of results of split half calculations for six subgroups. Excitation spectra are shown as dashed lines, and emission spectra as solid lines. For each component plot, there are six excitation spectra, which correspond by plot color to an emission spectrum of the same subgroup from split half analysis (i.e. colors represent calculation result for each subgroup).

4.4 COMPLEXATION OF LEAD BY TAIHU DOM

Compared with EEM, SFS shows narrower peak widths, is easier to use for identification, and minimises the chance for false determinations or omissions of specific spectral features. Meanwhile, the process of obtaining SFS is much faster than EEM (Dreischuh et al., 2015). SFS is a simple, sensitive and nondestructive technique that has been successfully used to rapidly characterise the interactions between heavy metals and DOM (Esteves Da Silva et al. 1998; Ryan and Weber 1982b; Zhang et al. 2014). Numerous studies have used fluorescence quenching titrations to investigate the binding properties of heavy metals with DOM (e.g. Fu et al. 2007; Manciulea et al. 2009; Wu et al. 2011; Yamashita and Jaffé 2008). Preliminary evaluation confirmed that the samples used for this study were suitable for quenching titration studies (fluorescence quenching was observed after the addition of Pb and that no fluorescence enhancement was observed under the experimental conditions). Figure 4-8A shows an example of fluorescence quenching of DOM by Pb as a function of Pb concentration for St 1 (SFS for the 32 samples are all characterised by a similar spectral shape but by differences in relative intensity, see Figure 4-9). All SFS spectra for this study showed two peaks at wavelengths of λ = 290 nm (Peak I) and λ = 414 nm (Peak II). Figure 4-8B displays a SFS for commercially purchased HA, in which I see that the SFS for HA is considerably more complex than the SFSs for my samples, however, Peaks I and II from my samples have corresponding features in the HA SFS, marked by arrows in each plot. Figure 4-8C shows the modified Stern–Volmer plot for data extracted from Figure 4-8A.

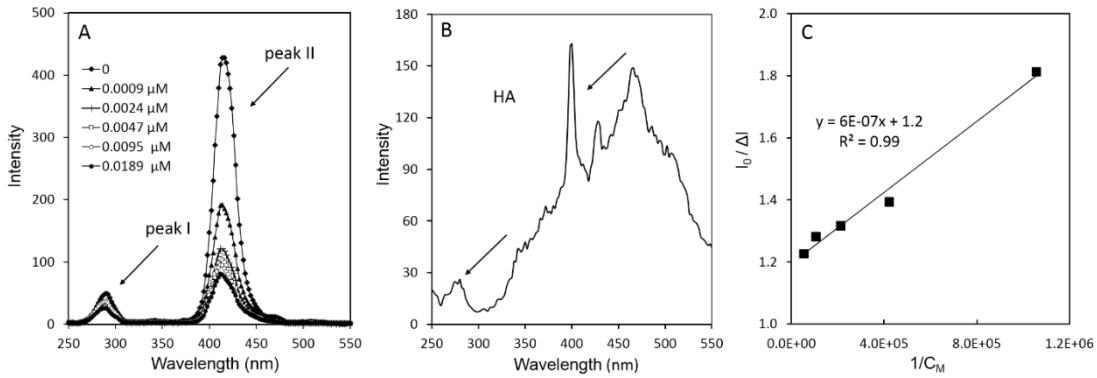

Figure 4-8. Results for SFS quenching experiments. (A) An example of a SFS quenching titration for DOM from St 1 titrated with Pb, (B) the SFS for a commercially available HA with arrows showing the locations of Peak I and Peak II from (A), and (C) a modified Stern–Volmer plot resulting from data in panel A. Note, $\Delta\lambda$ for Peak II vs. Peak I is the same for (A) and (B); λ_{max} Peak I and Peak II in panel B are 15 nm lower than in (A), consistent with natural variations in spectral features (see Figure 4-3).

Figure 4-9 displays SFS for 32 stations in Taihu. All the samples have two differentiated peaks. Peak I is often assigned as originating from Trp-like and tyrosine-like fluorophores (Yu et al. 2016; Zhang et al. 2008), however, both Peak I and Peak II can be found in the SFS of HA result (Figure 4-8). With respect to Peak II, its counterpart is typically not visually apparent on EEMs; this may be an artefact of the relative intensity of scattering peaks bleeding into the shoulder of the EEM Peak T in unprocessed EEMs, whereas Peak II lies in a relatively quiet spectral region. Complicating matters, EEMs and SFS are typically collected with spectrofluorimeter settings that result in different spectral resolution. In this vein, some authors contend that SFS Peak II (shoulder of EEM Peak C) contains polycyclic aromatic structures like flavone and coumarine components that are difficult to discern in EEMs (Smith and Kramer 1999; Zhang et al. 2008).

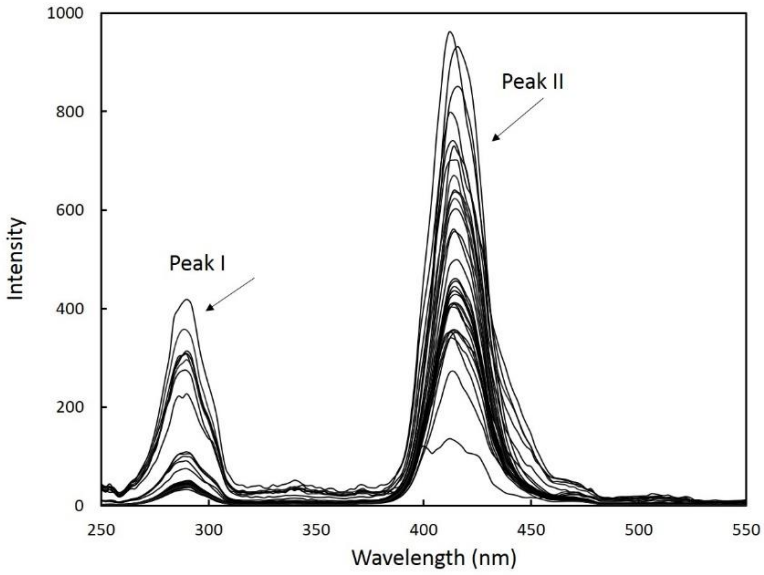

Figure 4-9. SFS of 32 samples from Taihu without added Pb. Each line indicates the SFS of a sample taken from a different Taihu station.

The SFS spectra for 32 stations were analysed using Stern-Volmer analysis as described in Sections 2.5 and 2.6 to obtain f, K_{cond}, and $C_{\text{L}}^{\text{Tot, diss}}$. The binding strength for these fluorophores with metals may vary according to DOM composition (Ryan and Weber 1982a; Zhang et al. 2014) resulting in variations of K_{cond} for different samples. Values of K_{cond} and f based on data from SFS quenching titrations for the samples from 32 stations of Taihu are summarised in Table 4-4 for Peak II. These K_{cond} values vary over a range of 4.64-6.50. These results indicate that Pb has a complexation affinity for DOM that varies by approximately two orders of magnitude, far from fitting the assumption that a constant K_{cond} is universally suitable for speciation models used in ERA. In the present study, I also calculated $C_{\text{L}}^{\text{Tot, diss}}$, however, in many cases the expression used for this was over-parameterised, e.g., see (Esteves Da Silva et al. 1998), hence values for those samples are not reported.

Table 4-4. Parameters governing the complexation of Pb with DOM, calculated from SFS Peak II.[a]

Station	$\log K_{cond}$ [b]	$C_L^{Tot, diss}$ [c]	f (%)	Station	$\log K_{cond}$	$C_L^{Tot, diss}$	f (%)
St0	5.61 ± 0.31	1.9E-06	69	St17	5.40 ± 0.43		84
St1	6.32 ± 0.19	9.3E-07	84	St18	6.04 ± 0.58	6.7E-07	83
St3	5.68 ± 0.20		64	St19	6.00 ± 0.23	9.3E-07	83
St4	6.50 ± 0.02		75	St20	6.13 ± 0.07		81
St5	5.97 ± 0.08		68	St21	5.82 ± 0.14		98
St6	6.18 ± 0.53	5.4E-06	87	St22	6.02 ± 0.02		96
St7	6.04 ± 0.32	4.5E-06	89	St23	5.47 ± 0.16		98
St8	5.49 ± 0.11	5.5E-07	93	St24	6.14 ± 0.28		87
St9	5.92 ± 0.44	2.6E-06	91	St25	6.02 ± 0.16	8.0E-06	98
St10	5.02 ± 0.15		83	St26	6.01 ± 0.54	5.5E-06	99
St11	5.97 ± 0.14		85	St27	4.64 ± 0.25		100
St12	6.41 ± 0.08		88	St28	5.69 ± 0.68	1.4E-05	98
St13	5.74 ± 0.26		88	St29	5.72 ± 0.51		95
St14	5.77 ± 0.44		84	St30	5.52 ± 0.28	1.8E-06	85
St15	5.88 ± 0.32		84	St31	5.94 ± 0.19	5.1E-07	88
St16	5.84 ± 0.18		82	St32	5.79 ± 0.27		98

[a] f is the fraction of I_0 that corresponds to the fluorescent portion of DOM that participates in complexation with DOM (I_0 is the fluorescence intensities of the sample without Pb present); K_{cond} is the conditional stability constant that describes the affinity for Pb to complex with DOM and form Pb-DOM; C_L is the total ligand concentration, i.e. DOM in molar equivalents in terms of complexation with Pb.
[b] Values are given with uncertainty expressed as average of results from different methods (see equations) of parameter determination, where applicable, or standard error from fitting.
[c] Units for total dissolved L in molar.

While various attributions are made to the origin of Peaks I and II, the origins of each are not unequivocally clear. For the majority of samples, a K_{cond} for Peak I was not quantifiable either because the peak itself was too weak or because the progression of changes in signal as a result of titration was small. For those samples for which Peak I K_{cond} was quantifiable, results are given in Table 4-5, along with results from Peak II for comparison. I find, as other authors have commented (Fu et al. 2007; Lu and Jaffe 2001) that K_{cond} from Peak I and Peak II are not greatly different, i.e. given uncertainties known for calculating K_{cond} by any method, ± an order of magnitude is not unreasonable. This observation would seem to suggest that Peak I arises in whole or part from the weaker low wavelength HA emission, as seen in Figure 4-8B.

Table 4-5. Comparison of logK_{cond} calculated from Peak I[a].

Station	Peak I	
	logK_{cond} [b]	f (%)
St0	5.58 ± 0.15	46
St3	5.18 ± 0.03	73
St4	6.00 ± 0.05	33
St25	5.74 ± 0.01	41
St26	5.42 ± 0.46	51

[a] K_{cond} is the conditional stability constant that describes the affinity for Pb to complex with DOM and form Pb-DOM; f is the fraction of I0 that corresponds to the fluorescent portion of DOM that participates in complexation with DOM (I0 is the fluorescence intensities of the sample without Pb present).
[b] values are given with uncertainty expressed as average of results from different methods of parameter determination, where applicable, or standard error from fitting.

Table 4-6 shows the range of values of K_{cond} found in this study in comparison to some representative values of K_{cond} for complexation of specific DOM components with Pb. It is generally accepted for a number of reasons that the binding strength order for components with Pb should be HA > FA > Trp > Tyr, which is reflected in the literature results shown. The ranges for found in this study span all components, though exceeding the literature value for HA shown.

Table 4-6. Comparison of values of logK_{cond} calculated from this study and representative values from literature.

Ligand	logK_{cond}	References
L-Tyrosine	4.19	Weber and Simeon 1971
D-Tyrosine	4.14	
LD-Tyrosine	4.09	
L-Tryptophan	5.11	
D-Tryptophan	5.05	
LD-Tryptophan	5.06	
FA-water	5.10	Saar and Weber 1980
FA-water	5.20	Warwick and Hall 1992
FA-lake water	5.14	
HA	6.11	Ghosh and Banerjee 1997
Peak II/HA	4.64 to 6.50	This study

4.5 Relationships between Water Quality, DOM Properties and Conditional Stability Constants

I used pair-wise correlation analysis, multiple regression, and principal component analysis to perform exploratory investigation of my data (Izenman, 2008). Pair-wise correlation analysis is suitable to explore basic relationships between measured quantities in the sense that no quantity is assumed to be an independent variable on which another depends (in contrast to linear regression analysis). Correlation analysis is often performed using Pearson's *r* as a measure of the strength of a linear relationship between two variables. I used Spearman's ρ for reasons relating to the potential violation of bivariate normality in the dataset. Early work by Kowalski (1972) concludes that the distribution of *r* is not robust when bivariate normality is violated, as is often the case for environmental samples, and since then various studies indicate that for the type of data I have, Spearman's ρ, which correlates for monotonic relationships, is a suitable correlator, also with suitably robust *p*-values (Fowler 1987; Gauthier 2001).

Figure 4-10 shows results for Spearman's ρ from pairwise correlation analysis for parameters including water quality, parameters of DOM characterisation and $\log K_{cond}$ for Pb-DOM complexation. Results are plotted in clusters according to a matrix hierarchical clustering algorithm implemented in R. Table 4-7 gives *p*-values levels corresponding to Spearman's ρ for Figure 4-10. In many cases, I anticipate that some quantities might have strong positive relationships, for instance I find that all dissolved nutrients correlate with total dissolved forms, and the analysis is thus in some cases useful as confirming my understanding of expected trends in the regional system, though, I note that, for a system with as

many varied and complex inputs as Taihu, even these basic relationships should not be accepted as given without testing. In other cases, I find results that might not be considered fully intuitive by all. Thus for instance, no matter how I vary the approach to calculation, I consistently find that Comp1, Comp2, and b and t have strong relationships with each other, as do Comp3, Comp4, and c, a, and m, however these two indicators of DOM type do not have a strong relationship with each other. It would seem a reasonable supposition to expect that all of these constituents of DOM would increase with increasing DOC, and therefore each type would correlate with each other type (as is the case with some nutrient forms). That I do not observe this reinforces my hypotheses at the outset (in choosing to sample Taihu, during the summer) that physically separable contributors to DOM are present (i.e. all forms contribute to DOC, however, protein-like DOM would not correlate with FA/HA-like DOM if they are present from distinct sources with varying source contributions regionally).

In Figure 4-10, I expect there may be some trends based on end-member mixing, from various sources, of conservative quantities (e.g. ions that are not reactive or less reactive), coupled with the imprint of changes in reactive species that reflect dynamic processes in the water column (e.g. changes in nutrients and Chl-a). Accordingly, there are strong relationships between Na^+, K^+, Cl^-, and SO_4^{2-} (bottom right corner, Figure 4-10). A retrospective study of water in Taihu spanning six decades (Yu et al., 2013) reports that inputs from these ions have changed greatly as a result of increases to the surrounding population base and concomitant pollution to the lake. Increases in K^+ have occurred in part due to the large fertilizer load and SO_4^{2-} due to atmospheric deposition of SO_2 (as H_2SO_4) from coal

and combustion byproducts. The ions Na^+ and Cl^- are partly linked to outflow from domestic WWTPs, though Cl^- is also input from industrial pollution and wastewater treatment (Yu et al. 2013), and to some extent all of these ions are associated with mixed pollution sources. While ions represent more conservative tracers of water source and mixing, they are not independent of other quantities, and there are strong relationships between Na^+ and Cl^- with DOC (in part consistent with WWTP sources), and to a lesser extent BOD, COD_{Mn} and Chl-a (HABs), while SO_4^{2-}, Na^+ and Cl^- all have negative associations with NO_2^- (bottom right and left of Figure 4-10, respectively). NO_2^- is one of the most highly correlated parameters with significant relationships ($p < 0.01$) to all dissolved nutrients (positive), as well as COD_{Mn} and DO (left edge, Figure 4-10). One report indicates that NO_2^- concentrations from runoff from the western mountains can be exceptionally high, consistent with the idea that NO_2^- is not associated with ion pollutant signatures (Hampel et al. 2018). There are strong positive relationships between various indicators of DOM/productivity with total nutrients and K^+, all of which fit with expectations of organic matter and agricultural runoff serving as a source of needed carbon and nutrients that drive HABs (bottom left and right, Figure 4-10, for comparison, see for instance Paerl et al. 2011; Xu et al. 2010). Total and dissolved forms of nutrients have generally strong relationships with each other (top and bottom right, Figure 4-10, respectively); in some cases, i.e. NO_2^- correlates with NO_3^-, the two quantities are different, however, correlation is consistent with common provenance. In other cases, the correlation is obviously spurious as, for instance, NO_2^- and NO_3^- are both constituents of TDN.

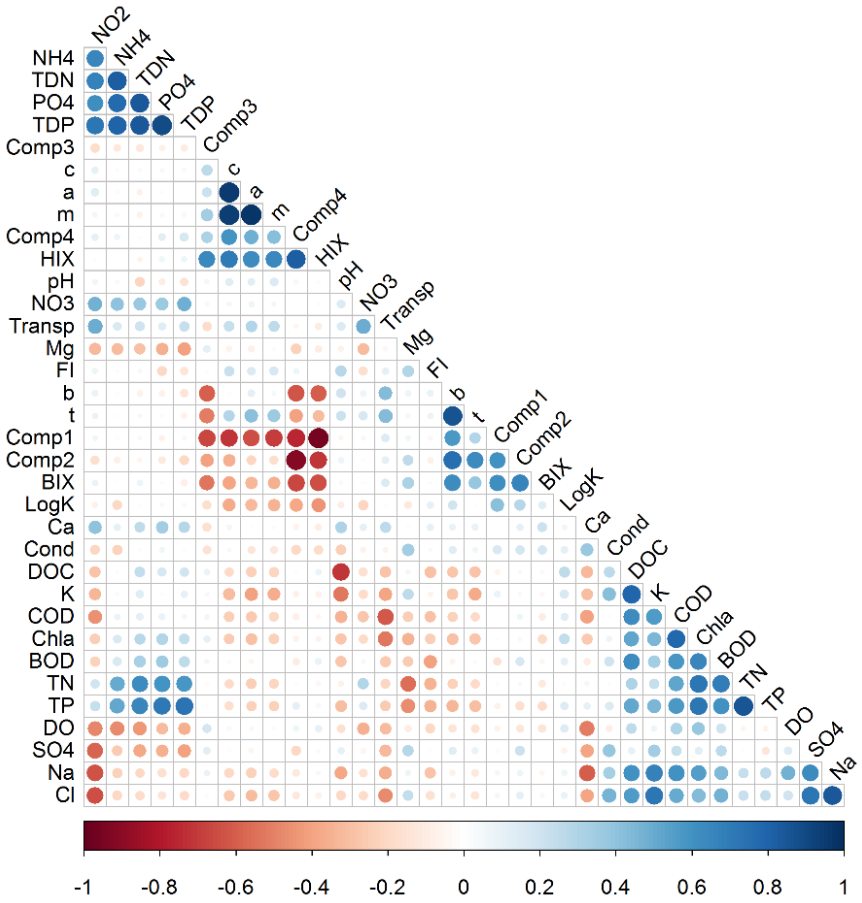

Figure 4-10. Correlation matrix plot showing pairwise-correlation analysis results. The size and degree of coloration of each circle in the matrix is proportional to Spearman's ρ (see color legend at the bottom). The plot is arranged according to post-correlation hierarchical clustering. The p-values associated with each ρ are given by significance level in Table 4-7; for all but two pairs, $\rho > 0.55$ are all associated with $p < 0.001$. For the two exceptions, $0.001 < p < 0.05$. See text for further discussion of clusters.

The theme of common provenance may also be invoked in considering some relationships between PARAFAC components, Coble peaks, and FlInds, though there also begins to be a clear indication of different types of DOM. Comp4, HIX, and Coble peaks a, c, and m, and to a lesser extent Comp3, all show positive relationships with each other and are indicators of FA- and HA-dominated DOM (upper right, Figure 4-10), whereas Comp1, Comp2, BIX, and Coble peaks b, and t show positive relationships with each other and are indicators of protein-dominated DOM (middle right, Figure 4-10, see for instance Coble 1996; Stedmon et al. 2003).

Table 4-7. *p*-value levels associated with values of Spearman's ρ given in Figure 7. *, **, and ***, respectively, represent $p < 0.05$, $0.01 < p < 0.05$, and $p < 0.001$.

	NO2																															
NH4	***	NH4																														
TDN	***	***	TDN																													
PO4	***	***	***	PO4																												
TDP	***	***	***	***	TDP																											
Comp2						Comp2																										
c							c																									
a							***	a																								
m							***	***	m																							
Comp4							***	**	*	Comp4																						
HIX						***	***	***	***	***	HIX																						
pH												pH																				
NO3	**	*	*	*	**								NO3																			
Transp	**												**	Transp																		
Mg				*	*										Mg																	
FI																FI																
b						***				***	***			*			b															
t						**		*	*	*				*			***	t														
Comp1						***	***	***	***	***	***						***		Comp1													
Comp3						*	*			***	***						***	***	***	Comp3												
BIX						**	*		*	***	***						***	*	***	***	BIX											
LogK							*			*	*								*		LogK											
Ca	*																					Ca										
Cond																						*	Cond									
DOC												***												DOC								
K	*							*	*			**		*				*					*	***	K							
COD	**													*								*		***	***	COD						
Chla														**										**	**	***	Chla					
BOD				*																				***	*	***	***	BOD				
TN		**	***	***	***										**											**	***	***	TN			
TP		*	***	***	***										**									**	**	***	***	***	TP			
DO	**	**	*	*									*									**					*			DO		
SO4	***		*	*	*																	*	*								SO4	
Na	***											*		*								***		***	***	***	***	*			***	Na
Cl	***													**								*	**	***	***	**	*	**			***	***

The weak negative relationships of protein-like indicators with BIX is consistent with an autochthonous contribution of these quantities to DOM, while the stronger relationship of HIX with FA/HA-like indicators is more consistent with allochthonous contributions to DOM. The middle portion of Figure 4-10 has a cluster of largely negative relationships wherein FA/HA-dominated DOM is inversely correlated with protein-dominated DOM. DOC does not correlate with any PARAFAC components, Coble peaks, or fluorescence indices. If considering DOC as a heterogeneous and macromolecular system that is generalisable in chemical behavior (i.e., fixed reactivity in respect of metal complexation), as is the case for the ERA speciation models in common use, this might be a surprising result. In contrast, if DOC is considered more in the framework of an assemblage (possibly with separate FA/HA versus aromatic/protein-like constituents, or possibly a wider variation of functional group compositions associated with macromolecules) it is not surprising that DOC does not correlate with any of those parameters. In the latter case, there is no reason why FA/HA composition should be perforce linked to protein-like DOM indicators, and therefore different substituents of DOM would not necessarily correlate with DOC itself. Additionally, reactivity of DOM with metals might vary greatly as well. In keeping with this supposition, $\log K_{cond}$ has among the fewest correlations (ranked in the bottom octile), with ρ only exceeding 0.4 for Comp1 (0.41) and HIX (-0.45). As K_{cond} is the primary parameter of focus for use in speciation models that support ERA, I was interested to further explore any relationships that might exist between the other parameters and K_{cond}.

I performed multiple regression analysis and was not able to find a predictive model for K_{cond} using the entire dataset due to collinearities. Reduction of the dataset resulted in optimal predictivity at 24 parameters (Figure 4-11A). Past this optimum, further reduction in parameters, resulted in inferior correlation and reduction in p-values. As the number of parameters used in prediction was reduced, the number of permutations of parameters that would produce a model of equally good correlation and p-value increases.

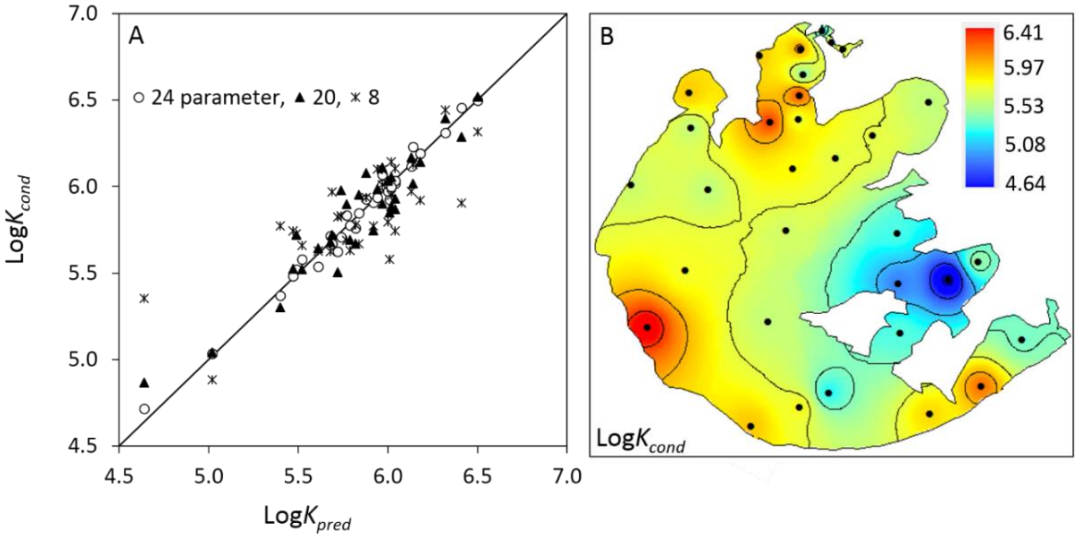

Figure 4-11. Plot showing the results of multiple regression analysis and distribution of logK_{cond}. (A) Result for multiple regression using different numbers of parameters as predictors of K_{cond}, and (B) contour map showing logK_{cond}. For the plots in (A), selected models with 24, 20, and 8 parameters are shown. The R^2, adjusted R^2, and p-values for these are, respectively, 0.98, 0.92, 0.0005 (24 parameters), 0.88, 0.67, 0.0097 (20), 0.59, 0.44, 0.037 (8).

I find that, depending on the level of accuracy desired, eight parameters provide an adequate predictor of K_{cond}, as shown in Figure 4-11A. From permutational analysis of subsets of the data, I find a reasonable degree of variability in the multiple regression equation that will predict K_{cond}, though I consistently find that parameters including a mixture of water chemistry, Coble peaks/PARAFAC components, and FlInd provide similar predictions of K_{cond}, as to those shown in Figure 4-11A. The process of examining multiple regression is useful to support an understanding that K_{cond} depends on water quality parameters and DOC fraction in a rational manner that, as with pairwise correlation results in Figure 4-10, speak to the difference water inputs to the lake as well as processes affecting the diagenesis of DOM. Figure 4-11B shows the variation of logK_{cond} across Taihu; the highest values for logK_{cond} are associated with sites that have strong allochthonous contributions, natural and anthropogenic (Meiliang Bay,

The Taige/Caoqiao Rivers, the Changxin River, and the Tiaoxi River mouths). There is also an area of elevated values near the Taipu River mouth. The Taipu River is the location of Taihu's main outflow, however, this region of the shoreline also historically was the site of extensive and long-standing aquaculture activity (Cao et al. 2007).

Care must be taken when multiple regression is performed, and I used this approach to answer two simple questions: 1) are there combinations of variables that are able to serve as predictors of K_{cond}?, and 2) if so, how parsimonious a model might be used, and with how many permutations?

In theory, I expect that, for so many variables, some combination might predict K_{cond}, and with multiple regression in particular, once finding a model, it is often more instructive to use multiple regression to assess the impact of with input variables can be removed with either positive (improving predictivity) or negligible effects. PCA in contrast, because of the manner in which contributions of different variables occurs, enables a way to test whether there are groupings of subsets of samples that are similar to each other, and different from other subsets, and if so, what relative role K_{cond} has in contributing to these groupings. I found when performing PCA that three main principal components (PC1, PC2 and PC3) account for the majority of the variance in the original data set (see Figures 4-12 and 4-13).

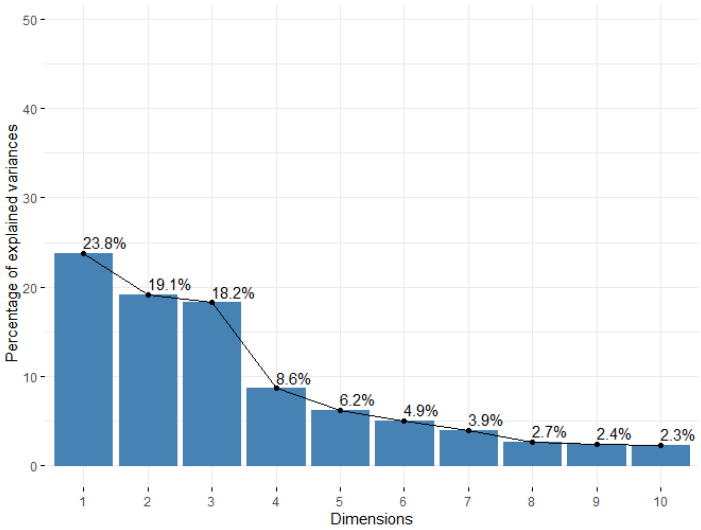

Figure 4-12. Scree plot showing total percent explained variance that each PC accounts for in the input data. Dimensions 1, 2, …,10 represent PC1, PC2, …, PC10, respectively.

Rather than being constituted of a few contributing parameters, PC1-PC3 each have a relatively large number of contributing parameters. PC1 accounts for 24% of the total data set variance and is characterised by low contributions (~4 to <10%) of 12 parameters (nutrients and ions) among 35 parameters. PC2 explains 19% of the total variance and is mainly associated with low contributions (~3 to 8%) of 14 parameters (some DOM components, FlInd, DOM/productivity indicators, total nutrients). PC3 accounts for 13% of the total variance and is again comprised of low contributions (~3 to 10%) of 15 parameters, similar to PC2, however with different degrees of contribution.

Figure 4-14 is a 3-dimensional plot of PC1-PC3 with the different stations labelled. There is one main cluster that is ellipsoidal, the major axis vertices for which may be thought of as endpoints based on the stations nearest to each, i.e. Sts 1 and 4 at one vertex and Sts 26-28 at the other. Some stations nearest to inputs of large rivers off-axis to, or highly separated from, the main cluster. These include St 6, near a river mouth in Meiliang Bay, Sts 9 and 15 in Wuli Bay, and Sts 10, 16, and

17, which are all adjacent to the shoreline where the rivers from the northwestern highlands feed into the lake. For the three PCs, most of the parameters in the dataset contribute overall to one or more PCs, and these parameters therefore constitute a relatively large group of indicators that cumulatively characterise different areas of the lake. A notable exception is K_{cond}. For all three PCs, the contribution of K_{cond} is either one of the lowest, or the lowest, of all parameters.

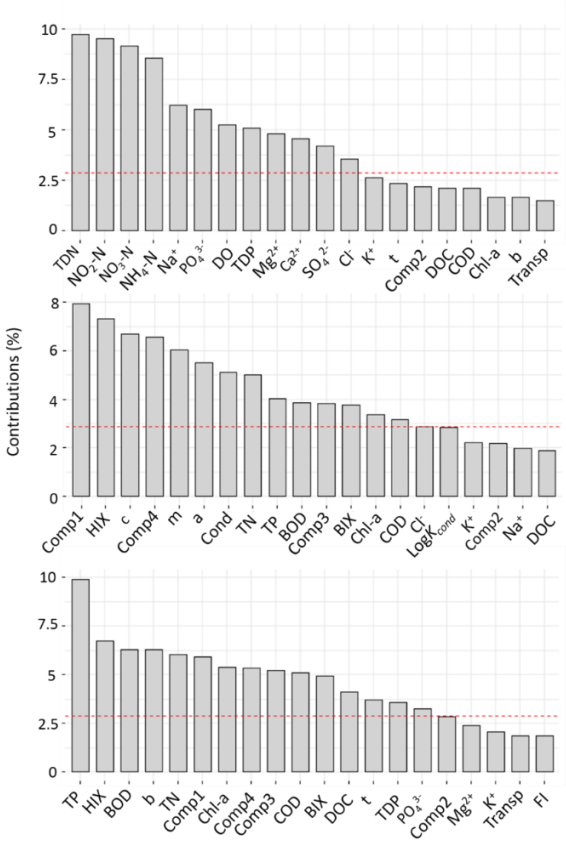

Figure 4-13. Bar plots showing the percent total contribution that each variable makes to principal components. (A) PC1, (B), PC2 and (C) PC3. The dashed red reference line corresponds to the expected value if the contribution where uniform; a contribution above the reference line is often considered as important in contributing to the dimension. For the current data set, the range of percent contribution of each variable is not large (i.e. of a possible range that could approach a maximum near 100%). For data sets wherein particular variables have high contributions, the plot would appear with a smaller number of variables contributing above the reference line and a larger number of variables contributing below the reference line.

Based on analysis of preliminary data prior to performing the present study and a limited elementary effects sensitivity analysis that I performed on the data reported here, I find that results obtained from the methods of multi-variate analysis that I describe are, generally, highly sensitive to minor variations in inputs. As such, I do not believe that, for instance, a single governing formula for prediction of K_{cond}, even in Taihu, would be robust to changing field conditions at the regional level. However, what I also find from this analysis is that there are general trends: correlations between water quality indicators, PARAFAC components, Coble peaks and fluorescence indicators vary in a logical manner, subsets of these different types of parameters seem to consistently produce a multiple regression model that is an adequate predictor of K_{cond}, PCA produces groupings that are reflective of processes in different parts of the lake, with some isolated areas or source inputs being "more different", there are no strong correlations of any single component with K_{cond} and K_{cond} is not a significant contributor to and PCs. Summarising, K_{cond} might be described as an outcome of water composition, in the sense that water chemical properties and DOM indices may serve as predictors of K_{cond}, however, unlike many other parameters, K_{cond} is not a characteristic differentiating water from one station to another. I do not know of another study that has approached the issues here with such a comprehensive data set and from the standpoint of a rapid method that is practically extensible to ERA.

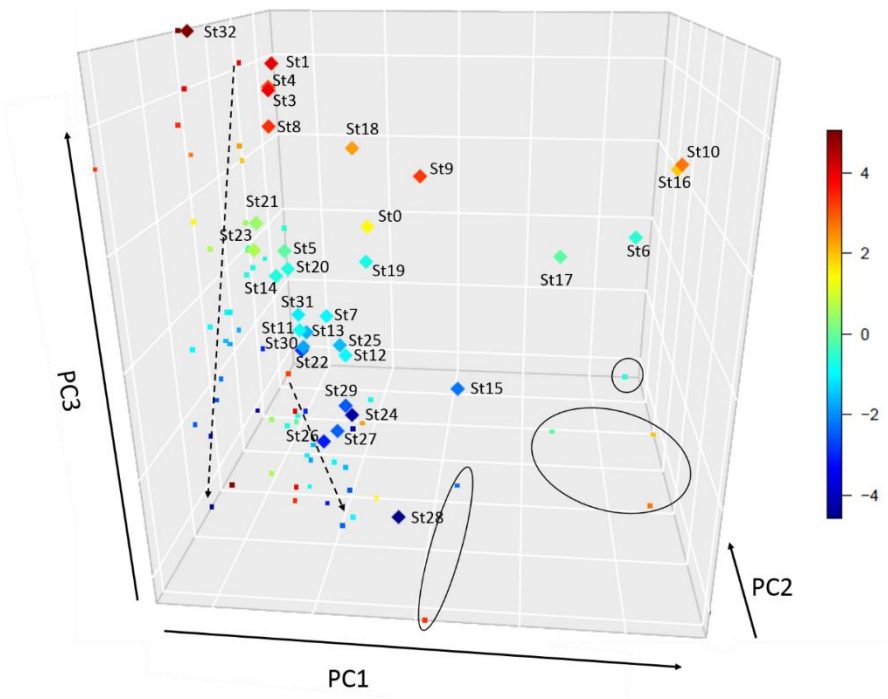

Figure 4-14. Graphical results from PCA analysis. Three-dimensional plot of PC1-PC3, which cumulatively account for the majority of variance in the data set (see Figure 4-12). Diamonds are points for each St, and small squares show the projections of these stations onto the x-y and y-z axes. Black dashed arrows are roughly aligned according to the main circulation trend in Taihu (from Meiliang Bay in the northern part, e.g. St 1, to eastern Taihu, e.g. St 28). Stations not part of the main end-member mixing group, i.e. not following the trend of the dashed black lines, are circled on the x-y projection. These stations correspond to inputs from major rivers as discussed in the text.

4.6 Implications for the Study of DOM on ERA

DOM and Pb-DOM binding, and relationships with these to water quality in Taihu, have been investigated in this study to understand implications for building better speciation models for ERA. Key points are as follows:

- DOM is highly variable across Taihu and reflects different inputs from different regions as well as processes within the lake. Temporal variability is presumably high as well, since I find that during the time of my study

there is a strong HAB contribution to DOM, and HABs are associated with summer conditions.

- I find that K_{cond} for Pb-DOM binding vary by approximately two orders of magnitude across Taihu, and in many cases there is a strong proteinaceous contribution to DOM. Such variable composition and binding strength is consistent with prior findings that a one-size-fits-all approach to metal-DOM binding leads to inaccuracies in commonly used speciation models. Therefore, such generalised approaches need improvement for regional-level ERA in complex watersheds.
- The K_{cond} of Pb-DOM binding can be predicted using the chemical properties of the water together with parameters extracted from fluorescence studies of the DOM present. This approach aids our understanding of conceptual models regarding the provenance and diagenesis of DOM.
- Results from PCA confirm the finding that water quality and DOM composition parameters are strongly interrelated and reflect different inputs, diagenetic and transport processes across the large expanse of Taihu.
- The approach taken here is extensible to any regional setting for freshwater studies, and with particular relevance to bioavailability modelling and ERA.

Overall, results herein suggest that the values of K_{cond} that I obtain fit with our understanding of processes occurring across the lake, and as affected by upstream hydrological inputs and regional-scale transport. The ability to use the

fluorescence methods here in high throughput applications (fluorescence measurement, titration, and data analysis pipelines), is highly attractive for ERA applications, and I do not know of another report that has been as comprehensive and resulted in simultaneously good internal agreement with understanding of the field site and results (K_{cond}) that are obtained in a manner practical enough to implement in ERA studies. I have recently completed a detailed study using the K_{cond}s reported here in ERA models, and I find that the average relative error is vastly improved; I report these results in Chapter 5.

5 NEW APPROACH TO REGIONAL STREAMLINED RISK ASSESSMENT

In Chapter 2, I discussed that speciation modelling should be used in conjunction with biological techniques for validation. Free metal ion (in this case $C_{Pb^{2+}}$) is generally accepted to be the relevant quantity in bioavailability-based ERA (Nys et al. 2014). A BLM speciation model is considered valid if there is a demonstrable correlation between BLM-predicted free metal ion and measured toxicity data, with a factor of ±2 being a benchmark of good predictive capability (USEPA, 2003a, b). However, the metric for BLM is usually for the measurement of metal toxicity, which indirectly reflects Pb bioavailability. In this chapter, I use a whole-cell bioreporter to test the $C_{Pb^{2+}}$ in the waters of Taihu, and I compare this to results from speciation modelling, which is an approach that has not been studied yet in this way and at a regional level. Using a whole-cell bioreporter to measure $C_{Pb^{2+}}$ is of interest since it is comparatively much faster, cheaper and can be performed on high-throughput basis, as well as being a more direct measurement of bioavailability (Belkin 2003; Magrisso et al. 2009; Zhang et al. 2017). A direct approach enables comparison of $C_{Pb^{2+}}$ levels to often well-known

data on, for instance, Genus Mean Acute Values (GMAV is the geometric mean of the species mean acute values for all species in the genus, and the species mean acute value is the geometric mean of the acute toxicity data for an individual species) for toxicity.

The aim of this chapter is to 1) expand upon earlier work in Chapter 3 and determine the $C_{Pb^{2+}}$ in different regions of Taihu using a whole-cell bioreporter; 2) to explore the optimisation of the speciation model (using results from Chapter 4 for all analyses) on the estimation of the free metal concentrations and 3) to compare the measured $C_{Pb^{2+}}$ with the free metal concentrations predicted by speciation modelling.

5.1 Chemical Speciation Calculations for DOC Binding

Speciation calculations were performed using Visual MINTEQ 3.1 (Gustafsson 2014), as described in Chapter 3. The input data for Visual MINTEQ were pH, temperature (of assay), the total concentrations of all inorganic constituents analysed in Taihu water samples as well as total concentrations of all MM constituents and DOM. To represent DOM, either DOC concentration or C_L was used, depending on how DOM was modelled, as described in this section. Speciation modelling is based on thermodynamic principles (Vanbriesen et al. 2010), and therefore requires mole-based units.

Since there is not a fixed chemical formula for DOC and DOC itself is usually reported in weight per volume units, a conversion must occur. For instance, the SHM uses the conversion 1.65 × DOC (mg/L) × 5.33 (mole·mg^{-1} reactive sites) to obtain reactive HA, and these conversion factors of 1.65 and 5.33 are based on

quantities inferred from averages of experimental data (Gustafsson 2001; Gustafsson 2014). In contrast to DOC, values for C_L are determined experimentally and are in units of molar (see for instance Boguta et al. 2016; Sander et al. 2011; Wells et al. 2013). Some values for C_L are given in Chapter 4, however, as described there, some results are not accurate due to problems with overparameterisation. As such, an approach similar to that of the SHM (and WHAM, Tipping 1994) is taken wherein the concentration of active DOC (ADOC, i.e., molar concentration capable of participating in M-DOC binding) is calculated as follows:

$$C_{\mathrm{ADOC}} = f_{\mathrm{ADOC}} * C_{\mathrm{DOC}}, \qquad (5\text{-}1)$$

where C_{ADOC} is the concentration of ADOC in M (unit), f_{ADOC} is the fraction of DOC that is ADOC, in mol mg^{-1}, and the concentration of DOC, in $mg{\cdot}L^{-1}$. The value for f_{ADOC} is determined from experimental data using the average value of C_L reported in Table 4-4 as a measure of ADOC and using the average values of DOC concentration in Table 4-1 that are associated with the same samples.

For the work reported in this chapter, six approaches were used to calculate M-DOC binding, and for simplicity, I give each an abbreviated name, abbreviations and method descriptions as follows:

Method 1) SHM: DOC concentrations were used as direct inputs and DOC-associated speciation was calculated for HA and FA using the SHM, which is what is referred to in this work to as being a one-size-fits-all approach since the FA:HA ratio, number of binding sites per FA/HA component, and M-DOC binding parameters are all assumed invariant in this model. As described in Chapter 3, the SHM assumes a gel-like structure for humic substances and accounts for

metal binding via two discrete types of ligands sites, with an electrostatic submodel and an empirical set of equations to account for extra charge screening within the gel model.

Method 2) Lit K–f C_{L}: Per Chapter 4, four different components of DOC were assumed (Tyr, Trp, FA and HA). Calculations were performed assuming an aqueous-phase reactivity model and using conditional stability constants from the literature ($logK_{\mathrm{cond}}^{\mathrm{Tyr}}$ = 4.14, $logK_{\mathrm{cond}}^{\mathrm{Trp}}$ = 5.07, $logK_{\mathrm{cond}}^{\mathrm{FA}}$ = 5.15, $logK_{\mathrm{cond}}^{\mathrm{HA}}$ = 5.82, Mostofa et al. 2013a; Saar and Weber 1980; Warwick and Hall, 1992; Weber and Simeon, 1971). Ligand concentrations C_{Tyr}, C_{Trp}, C_{FA}, and C_{HA}, were obtained by

$$C_{\mathrm{Comp}} = C_{\mathrm{L}} \times \%Comp, \qquad (5\text{-}2)$$

where C_{Comp} represents C_{Tyr}, C_{Trp}, C_{FA} and C_{HA} and $\%Comp$ is the percentage of each component. This approach is of interest in terms of the dynamics of the result, however, suffers from the flaw that it would presumably underestimate organic ligand concentrations if Peak II (Chapter 4), from which C_{L} concentrations are derived, exclusively represents HA (since f_{ADOC} is calculated using data that pertains to Peak II; see discussion in Chapter 4 regarding the identity of Peak II). This calculation is effectively another, less complicated, one-size-fits-all calculation inasmuch as binding constants are the same in all cases and ligand concentrations are fixed in respect of DOC concentrations.

Method 3) Exp K–f C_{L}: Speciation was calculated as for Method 2 above, however, as a refinement, $K_{\mathrm{cond}}^{\mathrm{Tyr}}$ and $K_{\mathrm{cond}}^{\mathrm{HA}}$ were assumed to be equal to K_{cond} for Peak I (where applicable) and Peak II, respectively, from Table 4-4.

Method 4) Lit K–f HA: This approach is the same as for Method 2 above, only with a variation in specification of ligand concentration to correct for possible error in specifying concentration in Method 2 above. For this approach to calculation, the concentration of C_{ADOC} as determined in equation 5-1 above is assumed equal to C_{HA}, and the concentration of Try, Trp, and FA are estimated according to the concentration of C_{HA} according to

$$C_{\mathrm{Comp}} = C_{\mathrm{HA}} \times (\%Comp/\%HA), \qquad (5\text{-}3)$$

where $\%Comp$ and $\%HA$ are taken from Table 4-3.

Method 5) Exp K–f HA: This approach is the same as for Method 3 above, however using the approach to specifying ligand concentration from Method 4 above.

Method 6) Exp K–C_{L}: A single, generic, "organic" ligand type ($\mathrm{L_{ADOC}}$) was assumed and entered as a new speciation component, and for each St, the ligand binding strength and ADOC were varied using C_{ADOC} (equation 5-1 above) and K_{cond} for Peak II (from Chapter 4) as binding parameters. This approach is different than the SHM in most respects, however shares the assumption that C_{ADOC} can be assumed to be a fixed proportion of DOC. This approach assumes that a single strong(er)-binding proportion of DOM, $\mathrm{L_{ADOC}}$, has overarching effect in determining metal speciation and that K_{cond} for M-$\mathrm{L_{ADOC}}$ binding is variable, which is akin to the approach and generic terminology of strong-metal binding that is used in some work (see Chapman et al. 2009; Maldonado et al. 2005; Sander et al. 2011 as examples).

5.2 SPECIATION RESULTS

Water quality and effect on inorganic Pb speciation

The properties of the water samples collected from 32 stations are shown in Chapter 4, Table 4-1. While DOC in freshwater lakes can complex with heavy metals and strongly affect the metal speciation, inorganic components may also have a large effect on speciation, such that one model in use for prediction of toxicity and use in determining WQC is referred to as the Hardness Model (referring to inorganic constituents contributing to water hardness, see Deforest et al. 2017). The $C_{Pb^{2+}}$ is considered to be the toxic and bioavailable Pb species provoking biological response (Magrisso et al. 2009; Zia et al. 2011) and its concentration will be affected by water quality. When heavy metals combine with anions (e.g. Cl^- and SO_4^{2-}), the free metal ion will be reduced. At the same time, cations in solution will compete for anion binding, inclusive of biotic ligand. All Pb interactions with inorganic species are be affected by the water pH (Tipping et al. 1998). In particular, because of increasing pH in summer in Taihu (Wang et al. 2017), the resulting alkaline environment may contribute to the formation of bis-hydroxy- and/or carbonato- complexes of metal and substantively reduce the $C_{Pb^{2+}}$/bioavailability (Kim et al. 1999).

Cation and anion concentrations vary in different regions of Taihu (Table 5-1), reflecting regional differences at the watershed scale. The ions that vary the most are NH_4^+, NO_2^-, NO_3^-, and PO_4^{3-}. However, for NO_2^-, NO_3^- and PO_4^{3-}, the variation is most likely because the concentrations measured are near LOD. Only the constituents that can bind Pb strongly, such as Cl^- and SO_4^{2-}, will affect the Pb bioavailability. To test the effect of such variability, I chose two stations with the

concentration of Cl^- and SO_4^{2-} that differed the most (Sts 14 and 15) and performed speciation calculations on these stations from pH 6 to 9, the upper limit being within summer ranges found in Taihu.

Table 5-1. Variation of cations and anions in different regions of Taihu.

Ions	Average[a]	Maximum	Minimum	Maximum/Minimum
NH_4^+	0.3	1.0	0.05	19
NO_2^-	0.04	0.4	0.001	378
NO_3^-	0.1	0.7	0.065	10
PO_4^{3-}	0.03	0.1	0.005	23
K^+	4.9	5.2	4.3	1.2
Na^+	37	43	25	1.7
Ca^{2+}	29	37	22	1.7
Mg^{2+}	7.4	7.8	6.6	1.2
Cl^-	43	49	26	1.9
SO_4^{2-}	50	56	40	1.4

[a] Values for average, maximum, and minimum are in $mg \cdot L^{-1}$.

Figure 5-1 shows the calculated speciation variation of inorganic Pb fractions at different pH for Taihu water for the two stations that were picked as examples. The dominant complexes are $PbSO_4$ (aq), $PbCl^+$, $PbOH^+$ and $PbCO_3$ (aq). As can be seen in Figure 5-1, when the pH increases from 6 to 9, $PbSO_4$ and $PbCl^+$ concentrations decrease. However, for $PbOH^+$ and $PbCO_3$, the concentration increases initially with increasing pH, before commencing a decreasing trend. The pH values in Taihu at the time of sampling for this work ranged from 7.90 to 8.35, which implies that Pb^{2+} only accounts for around 10% of the total Pb concentration in this speciation calculation. At 49 $mg \cdot L^{-1}$, the SO_4^{2-} concentration of St 14 is almost twice that of St 15 (26 $mg \cdot L^{-1}$), and the concentration of Cl^- for St 15 compared to St 14 is also higher (ratio of 1.3, St 15 Cl^- is 56 $mg \cdot L^{-1}$; St 14 is 41 $mg \cdot L^{-1}$). However, at pH=8, only 1% more Pb was complexed by SO_4^{2-} and Cl^- in St 14. The results for overall percent of Pb^{2+} speciation in Figure 5-1 are very close to results from an International Union of Pure and Applied Chemistry

(IUPAC) study for inorganic speciation of Pb in freshwater (in the absence of DOC, Powell et al. 2009). For instance, I find that the average fraction of Pb^{2+} at pHs, relevant for Taihu, is around 10% (with no DOM) which is with the same as the fraction of Pb^{2+} reported by Powell et al. (2009) for ~10%. For $PbSO_4$ (aq), in both Powell et al. and my study, the average fraction is around 3%.

In my calculation, and that of Powell et al., higher order Pb hydroxy clusters are neglected (Wang et al. 2009, these equilibria are not in Visual MINTEQ), and therefore the concentration of hydroxy-complexes may be underestimated compared to those of carbonato-complexes at high pH. In the absence of DOC, at high pH the inorganic forms of Pb that are present may vary, but, generally, Pb^{2+} is not a dominant species at higher pH. While the results in Figure 5-1 give a sense of the relative importance of inorganic Pb complexes and almost absent bioavailability of Pb^{2+} at high pH, when DOC is present in solution, it will often become the predominant component that complexes Pb^{2+} (Gustafsson 2011; Ibrahim 2015; Shahid et al. 2012).

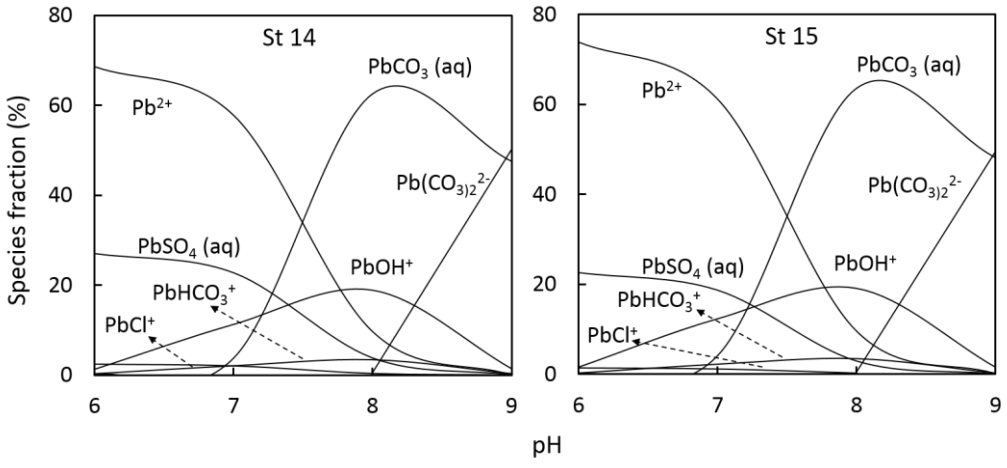

Figure 5-1. Percent of inorganic Pb species versus pH for Pb^{2+} in Taihu water without DOC. The value of $C_{Pb}^{Tot,\ diss}$ was set at 9.7 × 10^{-7} M. Other inputs are the water quality parameters from St 14 and St 15 (the full list of parameters is in Chapter 4, and a description of standard speciation calculation is in Chapter 3).

Pb-DOC speciation variability from different approaches to calculation

The DOC concentration in samples from the 32 Taihu stations is variable, ranging from 3.3 to 8.6 mg·L^{-1}. As described in Chapter 4, the characteristics of DOC (different components and values of K_{cond} for Peak II/HA) are also highly variable in different regions of Taihu. Methods 1-6 for calculating Pb-DOC binding in Section 5.1 were chosen to explore how much variations in DOC characteristics affects Pb-DOC speciation. I also wanted to see which approaches are more accurate for the organic matter in Taihu, which, during active HABs differs greatly from standard assumptions about DOC that are inherent in models such as WHAM and the SHM. Figure 5-2 shows C_{PbDOC} (sum of all fractions) as percent of $C_{Pb}^{Tot,\,diss}$, calculated using the six approaches described in Section 5.1 above. Figure 5-3 shows the variations in the percentage of $C_{Pb}^{Tot,\,diss}$ complexed as Pb-DOC from station-to-station, as calculated by Method 1 to Method 6. Panels A and B are the same data as for Figure 5-2 above, replotted to better see the variations in different stations as a function of method of calculation. Panel C shows summary statistics with relative average magnitude of Pb-DOC and precision for Methods 1 to 6.

In Figures 5-2A and 5-3C (Method 1/SHM), compared with other methods of calculation, there is a much higher concentration of Pb-DOC for all the 32 stations (for St 1, nearly 90% $C_{Pb}^{Tot,\,diss}$ was complexed by DOC).

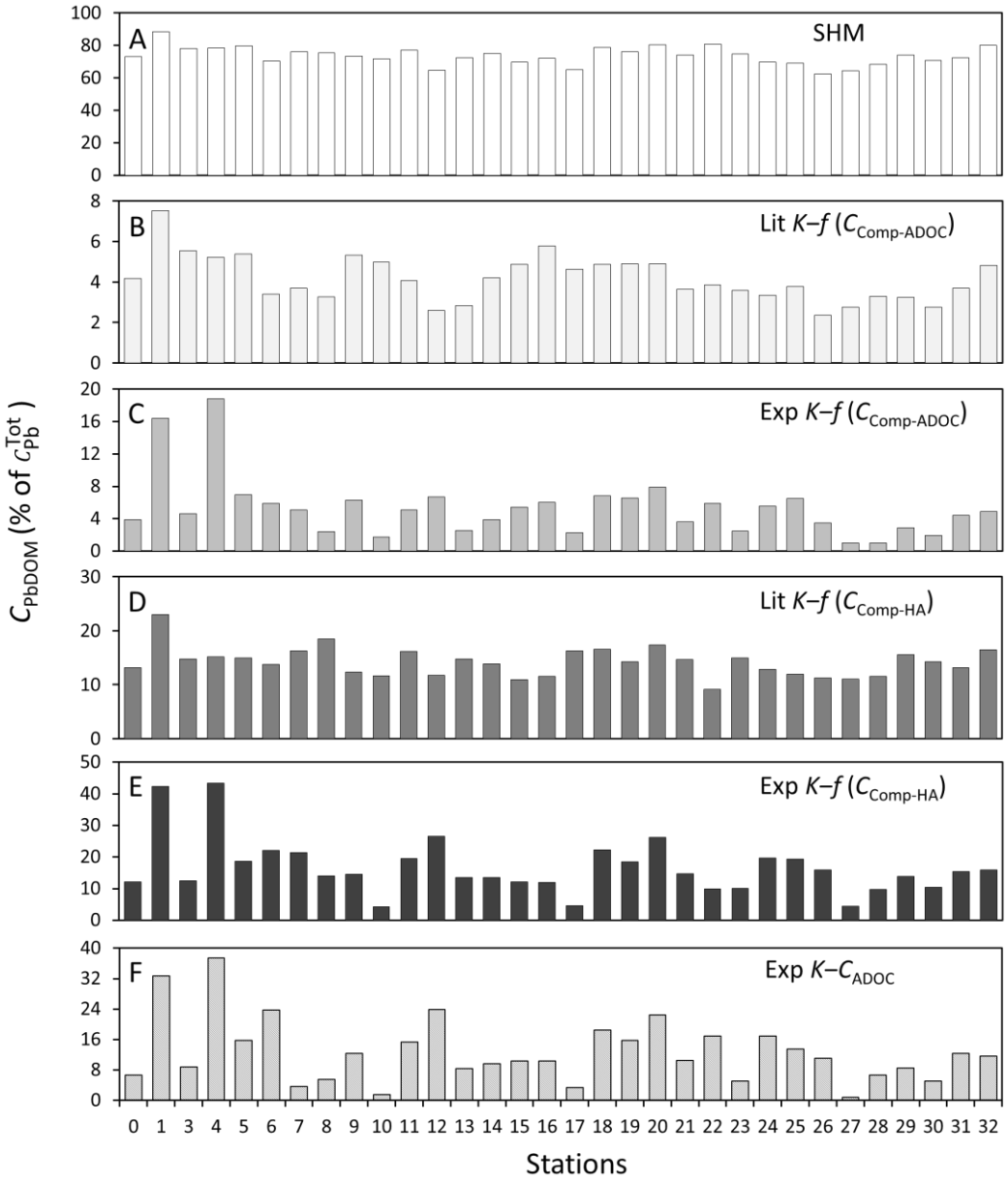

Figure 5-2. Variation in C_{PbDOM} expressed as the percent of $C_{\mathrm{Pb}}^{\mathrm{Tot}}$ for each station in Taihu. C_{PbDOM} speciation was determined by six modeling approaches. For visual clarity, labels on the x-axis correspond to St numbers (i.e. 0, 1, … 32, instead of St 0, St 1, … St 32).

However, for this method the predicted relative amount of Pb complexed as Pb-DOC did not change very much between different stations. In comparison, for Methods 2 and 4 (Figure 5-2B and D, also see Figure 5-3C), the percent of Pb complexed as Pb-DOC is much lower, however, varying the ligand concentrations and not K_{cond} still gives percentages of Pb complexed as Pb-DOC that do not change too much for all the stations. For Methods 3, 5 and 6 (corresponding to

Figure 5-2C, E and F, respectively), the value of Pb-DOC varies a lot (Figure 5-3C) due to the variation of ligand concentrations as well as K_{cond}. The methods have in common much lower active ligand concentrations, ranging from 2.0×10^{-7} to 1.8×10^{-6} M, therefore, the relatively narrow range of active ligand concentration leads to the dominant role of K_{cond} in the complexation of Pb. For all the calculations the concentration of ADOC varies linearly, however K_{cond} varies exponentially, therefore, variations in K_{cond} have much more effect on Pb speciation.

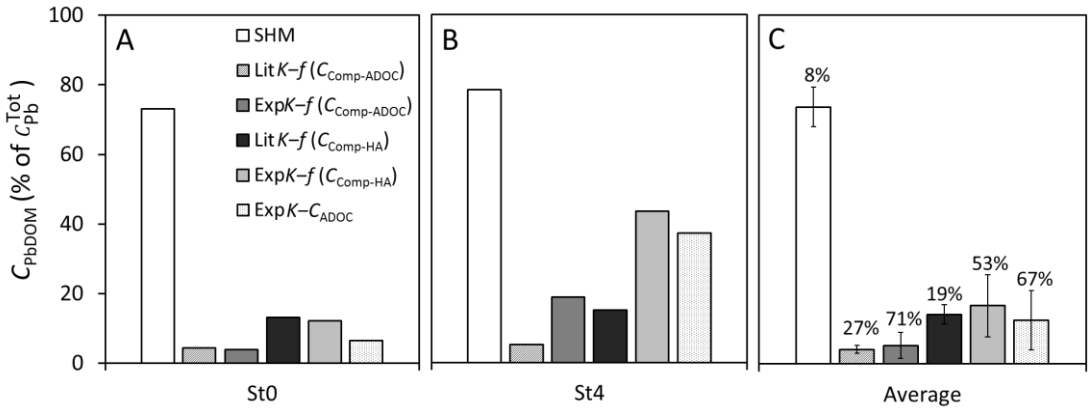

Figure 5-3 Variations in the percent of $C_{\mathrm{Pb}}^{\mathrm{Tot,\ diss}}$ complexed as Pb-DOC. (A) and (B) Pb-DOC variability, St 0 and St 4, respectively, for the six methods of calculation; (C) Summary statistics for the percent of $C_{\mathrm{Pb}}^{\mathrm{Tot,\ diss}}$ complexed as Pb-DOC; error bars show one standard deviation and RSDs are labelled in percent for 32 stations.

Figure 5-4 shows the how proportion of the four components Tyr, Trp, FA and HA vary depending on the method used in this study. In Figure 5-4, two representative stations (panels A and B, I selected St 4 and 10 as representative examples) and summary statistics are shown (Panel C). For Methods 2 to 5, respectively, RSDs for Tyr are 45, 79, 51 and 75%, for Trp are 33, 61, 45 and 59%, for FA are 21, 60, 32 and 58%, for HA are 10, 30, 18 and 29%.

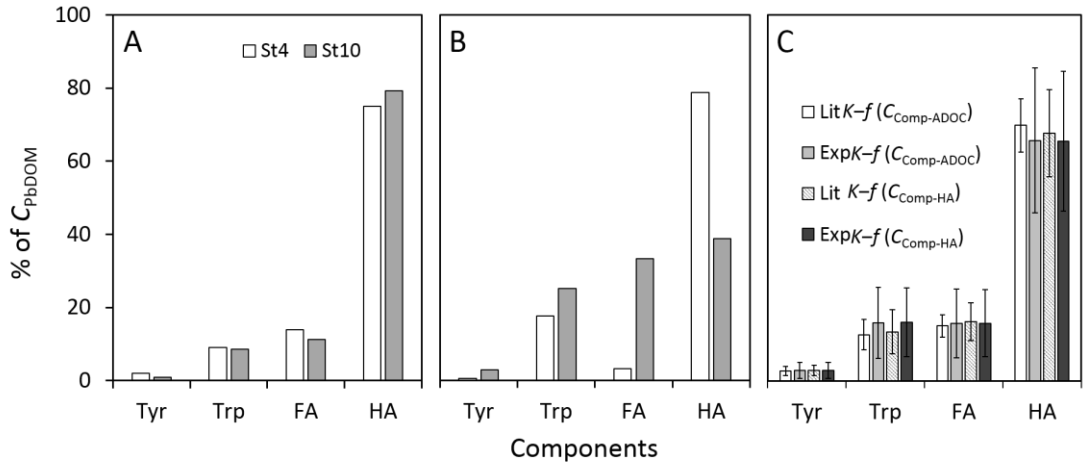

Figure 5-4 Variation of C_{Tyr}, C_{Trp} C_{FA}, and C_{HA} as total percentage of C_{PbDOM}. Representative results for two stations (Sts 4 and 10) are given in (A) and (B), respectively, for Method 2/Lit K–f ($C_{\mathrm{Comp\text{-}ADOC}}$) (which has the lower variability for C_{PbDOM} results from stations-to-station) and Method 5/Exp K–f ($C_{\mathrm{Comp\text{-}HA}}$) (which has the higher variability for C_{PbDOM} results from stations-to-station). C) shows the average variation of C_{Tyr}, C_{Trp} C_{FA}, and C_{HA}, and error bars show the standard deviation of the average.

The overall variability of the four Pb-Comp species in Figure 5-4, on average, is slightly different from that for Pb-DOC variation for Method 2 to Method 5 in Figure 5-3, though in both Figures 5-3 and Figure 5-4, Methods 2 and 4 show lowest variability and Methods 3 and 5 show highest variability. I also notice that Pb-HA shows the highest variation Pb-Tyr is the lowest. The average RSD for $C_{\mathrm{Pb}}^{\mathrm{Tot,\ diss}}$ follows the order Method 2 < Method 4 < Method 3 < Method 5 as shown in Figure 5-4C. Figure 5-4A shows how, for different stations, the calculation of Method 2/Lit K–f ($C_{\mathrm{Comp\text{-}ADOC}}$) leads to a lower variation of C_{PbDOM} (with the largest variability being for C_{PbTry}, being a factor of 2 higher for St 4 than for St 10), whereas for Method 5/Exp K–f ($C_{\mathrm{Comp\text{-}HA}}$) (Figure 5-4B), a higher variation of C_{PbDOM} from station-to-station appears, with the largest variability being for C_{PbFA}, being a factor of 10 higher for St 10 than for St 4. For all the calculations that involve different DOM components, HA is consistently the dominant form of organic matter that complexes Pb (Figure 5-4C).

5.3 TOWARD MODEL VALIDATION: COMPARISON OF MODEL RESULTS TO BIOREPORTER RESPONSE

In this study, I first used the bioreporter assay, as described in Chapter 3 on Taihu water samples directly (data not shown). The bioreporter confirmed results from ICP-MS, i.e. $C_{Pb^{2+}}$ in unspiked samples was below the bioreporter LOD and the background Pb is negligible relative to the level of Pb used in the spike assay. Figure 5-5 shows the bioreporter response, calibrated as Pb^{2+}, for the 32 stations across Taihu. The $C_{Pb^{2+}}$ correlates negatively with DOC, consistent with the idea that, generally speaking, higher DOC concentration in Taihu will bind more Pb, resulting in diminished $C_{Pb^{2+}}$.

Bioavailability/toxicity-based speciation models were validated against biological response, i.e. bioreporter response, for this work. Figure 5-5 shows plots of speciation results for $C_{Pb^{2+}}$ for the six methods of calculation used in this study versus bioreporter-measured $C_{Pb^{2+}}$.

In Figure 5-6, the stations having weaker Pb-ADOC binding (higher Pb bioavailability) lie to the top right of each graph, whereas the stronger Pb-ADOC binding (lower Pb bioavailability) lie to the bottom left. The solid line indicates an exact match between measured and predicted $C_{Pb^{2+}}$, and two dashed lines and the point plotted as a data centroid are discussed further below. Qualitatively, Figure 5-5A shows that there is no relationship between measured $C_{Pb^{2+}}$ and Method 1/SHM data. As discussed above, the K_{cond}s used to describe M-DOC binding are fixed for the SHM, and the results in the figure suggest that the fixed K_{cond}s and/or the manner of determining ligand concentration does not lead to a biologically meaningful result. Methods 2 and 4 display a poor prediction with

flat slopes and no differentiation of predicted results. Visually, Methods 3, 5 and 6 appear much better than other methods, with relatively higher slopes, and most data in the region of the 1:1 line.

There are two features in Figure 5-5 that I have calculated and used as figures of merit to quantitatively evaluate each plot: 1) the distance of the modelled data, as a group (on average), from the biological measurement, and 2) how well the data lines up with the 1:1 line. Table 5-2 shows a summary of the parameters that I used to quantify each. To test the distance of the modelled data from biological measurement, I calculated the % difference of the centroid, which is

$$\Delta_{\text{centroid}}\ (\%) = \frac{\left(C_{\text{Pb}^{2+}}^{\text{Pred,avg}} - C_{\text{Pb}^{2+}}^{\text{Biol,avg}}\right)\times 100}{C_{\text{Pb}^{2+}}^{\text{Biol,avg}}} \qquad (5\text{-}4)$$

where Δ_{centroid} is the % difference of the average $C_{\text{Pb}^{2+}}$predicted from speciation modelling, $C_{\text{Pb}^{2+}}^{\text{Pred, avg}}$ and the average $C_{\text{Pb}^{2+}}$ measure by the bioreporter, ($C_{\text{Pb}^{2+}}^{\text{Biol, avg}}$), averages being over 32 stations. I plotted one centroid in Figure 5-5 panel A to show graphically show what this looks like. Other measures of distance of modelled data to biological response include the average of the RPDs, RPD_{avg}, for predicted versus measured $C_{\text{Pb}^{2+}}$ at each station, and the geometric mean of the RPDs, RPD_{geom}. RPD provides information on the scale of residuals. RPD_{geom} gives a value that will smooth out outliers. I calculated SSR and slope, *m*, of a linear regression of the data as measures of how "linear" the data is, assuming that model-predicted data equals bioreporter data.

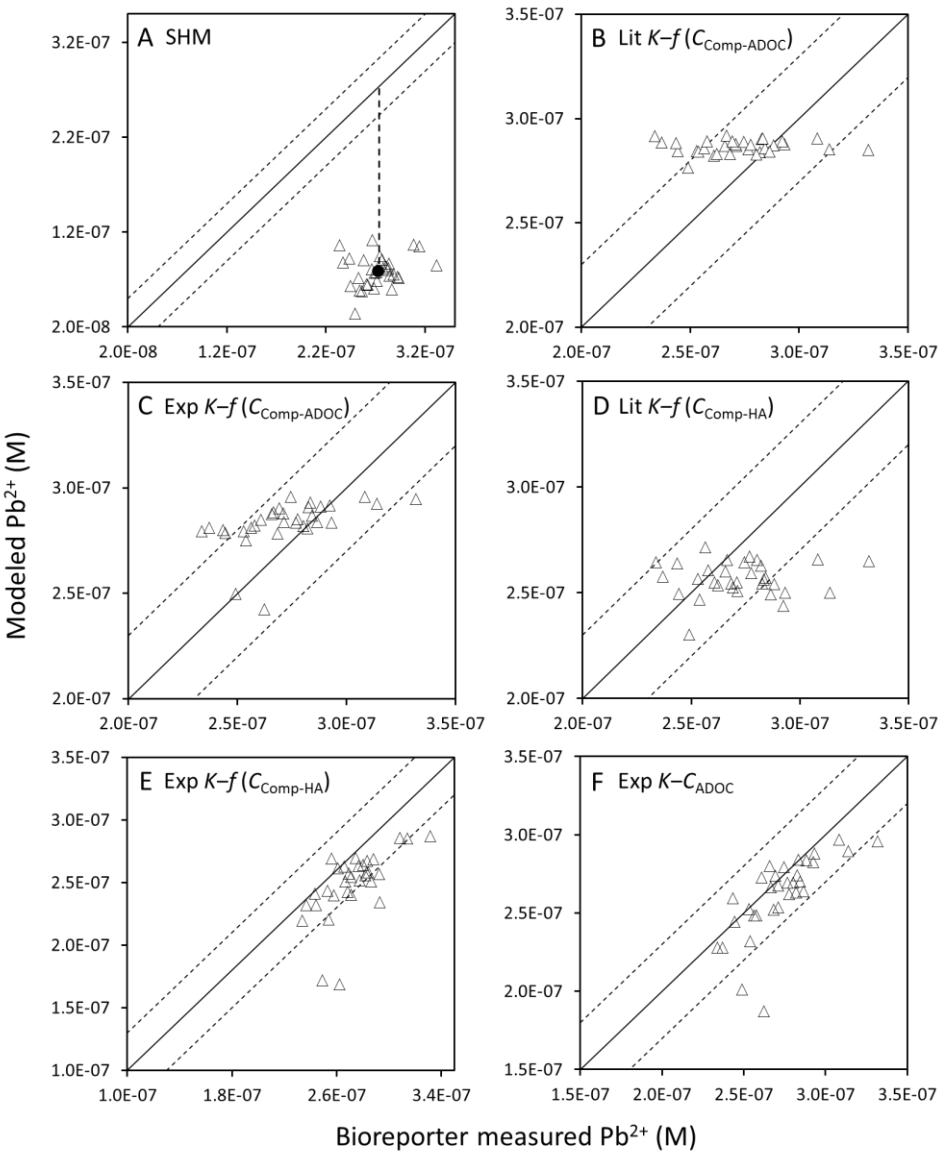

Figure 5-5. Comparison of Pb^{2+} ($C_{Pb^{2+}}$) from speciation calculation and bioreporter measurements. The six panels differ according to the manner in which PbDOM was calculated in the speciation model. The solid line in each plot represents the 1:1 line (predicted bioavailability = biologically measured). Two types of figures of merit are also shown. The two dashed lines represent a factor of twice the average relative percent difference (RPD) for Method 6/Exp K–C_{ADOC}, and the difference in the data centroid (circle) and the 1:1 line is a shown in panel A (dotted line). See text for further details about figures of merit.

Also, in Table 5-2, I calculated the same quantities for data from literature (Ge et al., 2005) for a study that used the WinHumicV and NICA-Donnan models. WinHumicV is based on WHAM (Tipping 1994), so similar in approach as SHM,

and NICA-Donnan gives results for Ge et al. (2005) that are better than, but similar to, those of WinHumicV.

Table 5-2. Summary of the figures of merit used to evaluate plots in Figure 5-6.[a]

Model	$\Delta_{centroid}$	RPD_{avg}	RPD_{geom}	$R_{RPD_{avg}/RPD_{geom}}$	SSR	m
Method 1	-71	111	110	1.0	1.2E-12	0.2
Method 2	5.4	7.5	4.8	1.6	2.1E-14	0.008
Method 3	4.1	6.3	3.9	1.6	1.5E-14	0.2
Method 4	-5.9	8.2	5.9	1.4	1.3E-13	0.1
Method 5	-9	9.5	6.4	1.5	3.2E-14	0.76*
Method 6	-4	5.5	2.8	1.9	1.4E-14	0.84*
NICA-Donnan	136	105	81	1.3	8.9E-14	2.1
WinHumicV	-92	150	120	1.2	1.4E-13	2.4

[a] $\Delta_{centroid}$ is the percent difference of the average $C_{Pb^{2+}}$ predicted from speciation modelling, versus that measured by the bioreporter; RPD_{avg} is average RPD (RPDs calculated as absolute, not), all points; RPD_{geom} is the corresponding geometric mean; R is a ratio (terms in subscript); SSR is the sum of squared residuals; represents for regression sum of squares; m is the slope of a linear regression of the data; Method 1 = SHM; Method 2 = fixed K (literature), $C_{comp} = f(C_L, \%Comp)$; Method 3 = measured K (HA), $C_{comp} = f(C_L, \%Comp)$; Method 4 = fixed K (literature), $C_{comp} = f(HA, \%Comp)$; Method 5 = measured K (HA), $C_{comp} = f(HA, \%Comp)$; Method 6 = measured K (HA), C_L; Data for NICA-Donnan and WinHumicV are form Ge et al. (2005). * indicates H_0: $m - 1$ (slope of 1:1 line) cannot be rejected, $p < 0.05$.

Looking at the results in Table 5-2, for $\Delta_{centroid}$ Method 2 to Method 6 are much better than Method 1 and methods from literature. The RPD_{avg} and RPD_{geom} follow the centroid trend: Method 1 and literature results have an order of magnitude worse RPD on average than for Method 2 to Method 6. Using $\Delta_{centroid}$, RPD_{avg} and RPD_{geom}, Method 6 comes out as the best model, followed by Method 3.

The usual approach to evaluate agreement between predicted and biologically measured data involves setting positive and negative limits of acceptability. The USEPA standard (USEPA 2003a, b) for setting these limits that is used in BLM modelling is too large to be relevant to my results since this standard is based on biological toxicity measurements, which are less direct measurements and consequently have inherently larger uncertainty. Therefore, I decided to set a factor of twice the average RPD value for Method 6 (dashed lines in Figure 5-5)

as nominal guideline for error in prediction. In Figure 5-5, the dashed lines provide an indication of the distance of the data, on average, from the 1:1 line, as well as a sense of linearity for each set of results and the relative number of points that might be characterised as outliers. The value of $R_{\mathrm{RPD_{avg}/RPD_{geom}}}$, in comparison to other values, also provides some indication of outliers. So, for instance, for Method 1, all points are far away from the 1:1 line, the $\mathrm{RPD_{avg}}$ is very high, and the $R_{\mathrm{RPD_{avg}/RPD_{geom}}}$ is 1; when all points are far off of an accurate prediction, none are effectively outliers. In contrast, for Method 6, most of the points fall very close to the 1:1 line, and the $R_{\mathrm{RPD_{avg}/RPD_{geom}}}$, at 1.9, is the highest for all results in Table 5-2 because two points far from the 1:1 line cause a large difference in $\mathrm{RPD_{avg}}$ versus $\mathrm{RPD_{geom}}$.

While the metrics of Method 3 are similar to those of Method 6 in terms of how close the centroid is to the 1:1 line, visually it is apparent that Method 3 is inferior to Method 6 in terms of linearity, which is verified by the SSR and *m*. The SSR is a calculation of how well the data fits the 1:1 line. For Method 1 the SSR is highest (least fit to the 1:1 line), the literature data also high, and Method 2 to Method 6 are better overall. The SSR shows that Method 6 has the closest distance to the 1:1 line (lowest SSR value) followed by Method 3, though the difference in SSR for the two methods is small. However, for Method 6 $m = 0.84$ (not significantly different from $m = 1$, see footnote Table 5-2), whereas $m = 0.24$ for Method 3. I also tested *m* for Method 5 (0.78) and found that it is not significantly different from $m = 1$, the slope of the 1:1 line.

Of the different approaches considered, Method 6 is the best method for incorporating Pb-DOC into speciation modelling and obtaining results that agree

with biological measurement. The Method 6 model uses C_L and K_{cond} that I calculated from Peak II (based on SFS measurements, Chapter 4), which could be representative of HA (*vide supra*). If this is true, then the accuracy of Method 6 implies that HA is the main factor influencing L_{ADOC}, which is also consistent with assumptions in models such as SHM and WHAM. Clearly, however, these one-size-fits-all HA-dominated models do not always work (Figure 5-5A for with SHM; Table 5-2 for literature results), and it would appear that the main differentiator for Method 6 is the use of values of K_{cond}, that are not one-size-fits all and that do vary at a regional level. In contrast to Method 6, while the central tendency measures are as good for Method 5, for linearity it is second best after Method 6, and this approach does assume different components (obtained independently from the experiments used to determine C_L and K_{cond}). Nonetheless, as Figure 5-4 shows, even for Method 5, Pb-HA still dominates. Therefore, for my samples, it appears that HA, or perhaps some fraction of HA with aggregated strong metal-binding characteristics plays a more important role than other components in DOC on Pb binding.

5.4 Implications for Environmental Risk assessment

The main goal of this study was to explore the possibility of using site-specific parameters in chemical speciation models to improve their predictions of Pb speciation to be fit-for-purpose for use in ERA. Primary findings from this part of the work are as follows:

- I have shown that such model optimisation produces results that are much more accurate in their agreement with bioreporter measured $C_{Pb^{2+}}$ than results from one-size-fits-all models in current use for ERA;
- The best agreement between biologically measured bioavailable Pb and model predictions results from modelling ADOC as a single organic ligand type, L_{ADOC}, with aqueous-phase complexation, C_L and K_{cond} for which are rapidly and conveniently assessed from simple fluorescence measurements;
- I conducted this study across the area of Taihu, which, with a 2,400 km^2 surface area, is large enough to reflect regional scale processes. My results offer a good demonstration for a way forward to streamline ERA in freshwater settings.

6 Risk Assessment of Pb Pollution in Lake Sediment

Previous chapters detail work that I have done using a bioreporter to measure the Pb aqueous bioavailability in Taihu, China's third largest freshwater lake (Zhang et al. 2017). Extending this aqueous-phase work to use a bioreporter to assess the $C_{Pb^{2+}}$ in lake sediment is a logical extension of ERA on lake pollution. Studies have shown (*vide supra*) that the sediment in Taihu is heavily polluted by different heavy metals and they usually co-exist. While the bioreporter that I have been using is sensitive to several different types of heavy metals at higher concentrations (the LOD for Zn, Ni, Cu are all higher than $6 \mu \cdot L^{-1}$, which is much higher than $1.2 \mu \cdot L^{-1}$ for Pb and as the metal concentration increases, their influence on bioreporter is also irregular), it is differentially more sensitive to Pb, and thus should be suitable for use to study Pb sediment bioavailability in Taihu. During the course of this work, however, an opportunity arose to investigate a lake system, Brothers Water lake in the United Kingdom (UK), in which Pb is specifically highly accumulated in the sediment (Schillereff et al. 2016). The Pb contamination in this lake is quite high, > 12,000 $mg \cdot kg^{-1}$, and there is a large body of data available for the sediments of this lake, making the lake ideal for the study

needs of my project. This chapter reports results from studies on a core from this lake.

6.1 History of Field Site and Methods used for Sediment Studies

Description of Brothers Water and history of mining impacts

Brothers Water is a small (0.18 km^2), upland lake with a comparatively large catchment (13.01 km^2) in the eastern Lake District of northwest England (54.5066°N, 2.9249°W, Figure 6-1A). There is a single dominant inflow fed by five tributary networks that drain the surrounding upper hills, and this inflow enters Brothers Water at its southeast corner (Figure 6-1). According to historical records, the English Lake District experienced small-scale Bronze Age and Roman Era metal extraction, followed by more extensive Medieval operations (1200–1400) and an intensifying industrial phase from 1550 to ~1940 (Adams 1988). The primary Pb mine whose impacts on Brothers Water have been studied is called Hartsop Hall; it lies 600 m to the southwest of Brothers Water on the east-facing flank of Hartsop-above-How hill. Documentation for mining activities at Hartsop Hall exist for 1696, 1802-1804 (2450 $kg \cdot year^{-1}$ ore), 1830-1832 (6230 $kg \cdot year^{-1}$ ore), 1863-1871 (24,000 $kg \cdot year^{-1}$ ore) and 1931-1942 (Tyler, 1992). Later, during 1931–1942, mechanically enhanced extraction resulted in more efficient Pb recovery from harvested ores, and processing shifted to the larger Greenside Mine (Tyler, 1992). Peak modern production at Hartsop Hall (1863-1871 period) coincides with anecdotal evidence for discoloration of Kirkstone Beck, fish kills and acute livestock poisoning (Tyler, 1992).

In Schillereff et al.'s (2016) work on Brothers Water, they note a consistency with other smaller water-bodies in the area that act as a pollutant sinks for mining-related Pb from upstream, intercepting or "trapping" (Miller et al., 2014) much of the mining-sourced Pb and thus preventing its deposition in larger lakes of the region (e.g. Ullswater, Windermere). Therefore, the first-order lakes like Brothers Water are the primary sink for mining-derived material and for which its sediment cores are a well-preserved reflection of pollutant impacts.

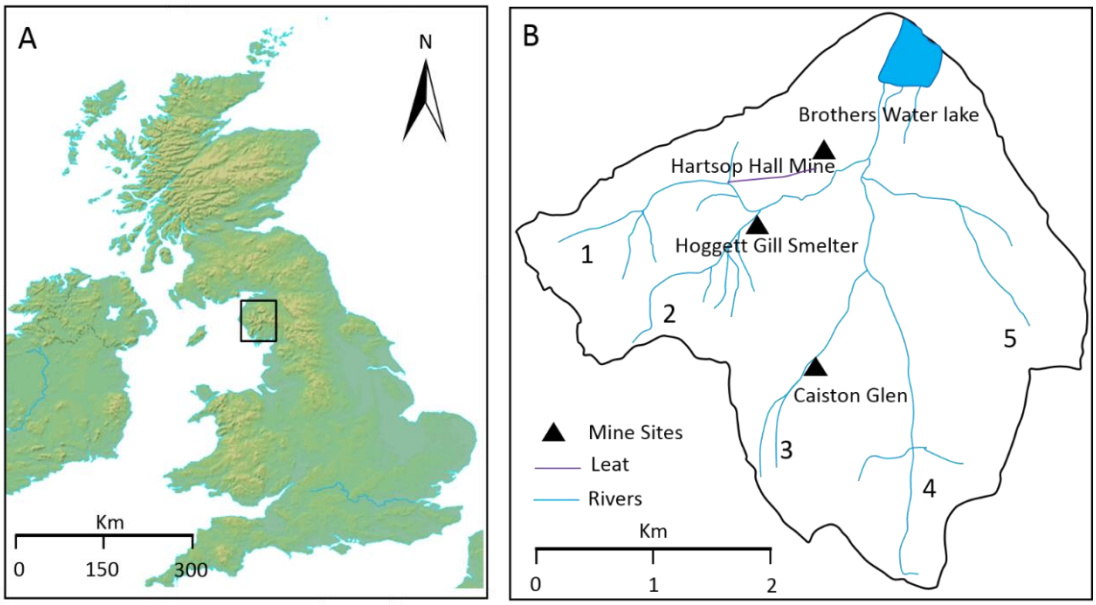

Figure 6-1. Details on geographical context of Brothers Water lake. (A) Location of the English Lake District within the UK. (B) Detail map showing the five tributary systems (for simplicity labelled 1-5 since they are not discussed further in text) that drain into Brothers Water within the catchment (black line). Also show are the locations of ore extraction and processing sites (labelled as Mine Sites) in the Brothers Water catchment and the location of a leat (drainage trench) that cuts through legacy waste heaps from the Hartsop Hall mine.

Waste materials of the mining infrastructure are still visible across the hillslopes at Hartsop Hall Mine even today (Figure 6-2). After rainfall, overland flow incising through spoil piles and remnants of a functioning leat drain directly downslope to the streams (see Figure 6-1B) that are tributaries to Brothers Water. This

overland flow through streams continues to deposit Pb-bearing sediments into the lake, enhancing the Pb concentration in lake sediments (Schillereff et al. 2016). Therefore, it is important to understand risks associated with historical recent and continuing Pb deposition in the lake.

Figure 6-2. The location of Brothers Water and its floodplain relative to Hartsop Hall mine. The view west across the floodplain of Brothers Water highlighting the location of Hartsop Hall mining infrastructure, shaft levels, exposed waste heaps and their proximity to the Kirkstone Beck river that drains into Brothers Water. The shafts/levels were sunk incrementally, with the first ore extracted from shafts at level 1, and with shafts at levels 3 and 4 having been dug during peak mining in the 1860s and 1870s (figure from Schillereff et al. 2016).

Previous work on sampling and analysis of sediments in Brothers Water

Sediment cores of between 24.5 and 339 cm in length were extracted from ten profundal locations in March, 2011, and October, 2012, by Schillereff et al., locations of which are shown in Figure 6-3. I selected sediment core BW11/2, sampled in 2011, for Pb bioavailability study based on the historical depth range it covers, the large differences in distribution of Pb in different sediment layers,

the representation of Pb contamination (notably very high Pb in one layer), and the sufficiency of sample available for study. The core BW11/2 is 339 cm in length and was originally subsampled at 0.5 cm depth, much of the original sample having been used for other analyses, including total Pb and geochronology. I chose thirty-two sediment samples from different layers (ranging from 15 to 202.75 cm depth) of core BW11/2 to use for all the tests in this study. The layers I chose represent the periods of interest from prior to intensive mining activity up to recent times and samples with sufficient material for analysis and varying total sediment Pb concentration, $C_{\mathrm{Pb}}^{\mathrm{Tot,\,sed}}$.

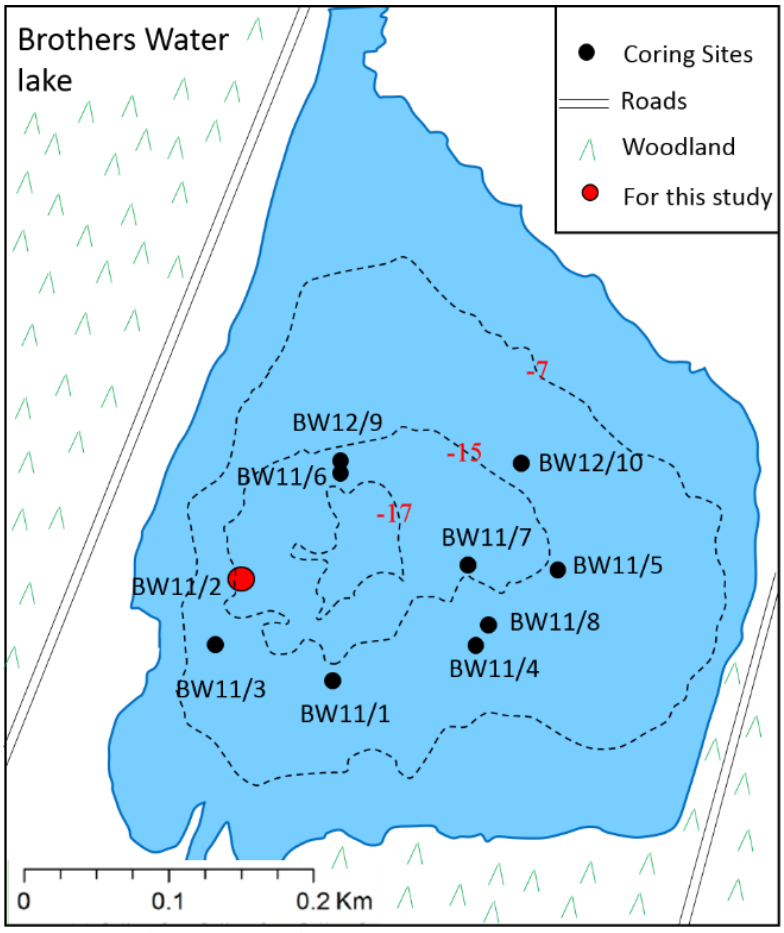

Figure 6-3. Sampling diagram of Brothers Water lake. Selected depth contours (relative to the lake border), locations of the ten 2011/2012 coring sites and relative location of coring site BW11/2 (used in bioavailability studies reported here) are shown.

Selected subsamples from core BW11/2 had been previously dated using multiple isotope techniques. Radiometric measurements for ^{210}Pb, ^{226}Ra, ^{137}Cs and ^{241}Am (Szarlowicz et al. 2019) were conducted by direct gamma assay using Ortec HPGe GWL series well-type coaxial low background intrinsic germanium detectors at the Liverpool Environmental Radioactivity Laboratory (Appleby et al. 1986). Geochronology was based on the convergence of fallout ^{210}Pb with *in situ* ^{226}Ra (radium) activity and artificial radionuclide (^{137}Cs, ^{241}Am, cesium and americium) concentrations associated with known atmospheric releases of these radionuclides to the atmosphere (Schillereff et al. 2016). An age-depth model was then constructed for BW11/2 using thirteen ^{14}C radiocarbon measurements that targeted handpicked terrestrial plant macrofossils (Schillereff et al. 2016).

Percent organic matter (OM) content was determined by thermogravimetry (TGA) as the percentage mass loss during burning between 230 and 530°C using a PerkinElmer STA6000. To determine the mean particle size, samples were treated with 30% H_2O_2 to remove the organic fraction, sonicated to disperse, and measured via laser granulometry, simultaneous to determination of sand, silt and clay content, on a Beckman Coulter LS320 particle size analyser (Schillereff 2015).

Sediment sub-samples taken at 0.25 cm midpoints in 0.5 cm core slices were freeze-dried, and Pb concentrations were measured using a Bruker S2 Ranger ED-XRF. The thirty-two sediment samples from core BW11/2 have $C_{\mathrm{Pb}}^{\mathrm{Tot,\,sed}}$ ranging from 45 mg·kg^{-1} to 10,500 mg·kg^{-1}, spanning a deposition time period from 500 to 2011 A.D. (Schillereff et al. 2016). These different $C_{\mathrm{Pb}}^{\mathrm{Tot,\,sed}}$ in the lake sediments over this period reflect a prior history of varying impacts to the lake watershed from Pb mining. Prior to analysis of Pb bioavailability on the whole

core (for which some subsamples had a limited amount of material available), I selected five samples from the thirty-two for detailed study. These five were chosen to be representative of different periods (before mining, during mining and after mining) and different Pb concentrations.

Methods used to study sediment bioavailability of Pb

In this research, genetically engineered *E. coli* strain zntA, which has the capacity to emit a dose-dependent bioluminescence in response to bioavailable Pb, was used, as described in detail in Section 2.3 in Chapter 2 and Section 3.1 in Chapter 3. For direct-contact sediment assays, 50 µL of bioreporter cell suspension was added to 50 µL of sediment slurry, and the bioluminescence was measured as for solution-phase assays described in Section 3.1, Chapter 3. Sediments slurries were prepared by mixing sediments with water in different proportions, and the technique requires careful mixing and rapid sample transfer to ensure uniform results (i.e., to avoid settling). At the outset of my bioavailability experiments, I knew that the direct-contact sediment assay would pose a number of challenges because of the complex interplay between slurry concentration, attenuation of signal transmittance, LOD, and high Pb concentrations potentially killing the bioreporter. I first performed a series of preliminary experiments with sediments of moderate lead concentrations over slurry concentration ranges from 0.039 to 500 mg sediment·mL^{-1} water to determination the feasible range of slurry concentration (too much sediment attenuates signal, too little sediment reduces Pb available for the bioreporter to sense). Based on these preliminary experiments, I chose to do more detailed experiments using the slurry dilution series: 6.25, 3.125, 1.5626, and 0.7812 mg sediment·mL^{-1} water.

Compared with the measurement of Pb in aqueous-phase, particles in solid-phase materials may block or scatter the luminescence signal produced by the bioreporter. In some cases, it may be possible to neglect these effects and perform direct measurement in the bioreporter/soil slurry, depending on the degree of the effect and the aim of the study (Magrisso et al. 2009). Often neglecting the blocking/scattering effect is unsuitable, and common ways to address this problem include, for instance, measurement after separation of the cells from particulate matter using a polyvinylpyrrolidone density gradient, or measurement of signal loss with post-analysis correction (Magrisso et al. 2009; Pertof et al. 1978). Preliminary testing of BW11/2 samples confirmed that blocking/scattering effects are non-negligible for these samples, and the approach I used herein to correct for effect of the sediment matrix on bioluminescence detection involves measurement of light blocking/scattering, which may vary according to sediment qualities.

To perform experiments to measure blocking, bioreporter response was measured in solution phase and compared to the same exposure in sediment slurries. Since the goal was to measure the physical effect of blocking/scattering and to avoid bioreporter activation during the experiment, I added activated solution-phase bioreporter to a known quantity of sediment and measured the diminution of signal immediately. To perform blocking experiments, first special plates were prepared wherein doses 50 μL of well-mixed sediment slurry was added to wells in a microplate and carefully dried at low temperature (30°C). At the beginning of each experiment, bioreporter was activated as described in Chapter 3 at a dose of 1:1 bioreporter: 0.2 $mg \cdot L^{-1}$ Pb. When the activated bioreporter signal was seen to be nearing the luminescence response maximum,

100 µL of activated reporter solution was transferred to each microtiter plate well with dried sediment and vigorously mixed to suspend the dried sediment into solution. Luminescence measurement was immediately resumed, and the diminution in signal between activated reporter and activated reporter plus sediment was used to quantitate the blocking effect.

Response for bioreporter sediment assays was calculated using the bioreporter calibration curve and correcting for reduction in transmittance as a result of blocking/scattering. The transmittance (T, decimal) of blocking was calculated as

$$T = R_S/R_C \qquad (6\text{-}1)$$

where R_S is the bioluminescence value after adding the sediment, R_C is the bioluminescence value before blocking (control). All experiments were performed with 4 replicates unless otherwise stated.

According to Schillereff et al. (2016), the $C_{Pb}^{Tot,\,sed}$ in in some of the sediments is very high, and an initial issue that I needed to consider was the potential effect of the very high $C_{Pb}^{Tot,\,sed}$ on the bioreporter. From prior work, I have tested the bioreporter response to Pb standards over a large range of Pb from 0 to 400 mg·L^{-1} (Figure 6-4A), and from this it became clear that at around 12.5 mg·L^{-1} Pb the bioreporter response started to decrease and after above 100 mg·L^{-1} Pb the bioreporter is killed, leading to complete absence of signal. Another researcher who is also using this bioreporter has done work that confirmed my interpretation of these findings using a Live/Dead assay (Huang et al. 2013, and unpublished data, personal communication, Boling Li, XJTLU, 2019). Prior to doing direct-contact sediment assays with the bioreporter for research data collection, I first performed some preliminary analysis to see if the very high

sediment concentrations would adversely affect the reporter. Firstly, I made some calculations based on the $C_{\mathrm{Pb}}^{\mathrm{Tot,\ sed}}$ to calculate the level of Pb that the bioreporter would be exposed to assuming 100% bioavailability. Secondly, I prepared a large range of slurry concentrations of sediment and incubated them with the bioreporter. Use of these varying slurry concentrations offered the information whether the bioreporter response was in the region of signal reduction or in the region where signal increased with increasing Pb. By doing this, I found that all of the responses for the slurry concentrations I tested were in the calibration range.

In addition to direct-contact assays, the concentration of $C_{\mathrm{Pb}^{2+}}$ to total Pb ($C_{\mathrm{Pb}}^{\mathrm{Tot,\ desorb}}$) desorbed from different sediment samples was determined after extraction with 50% MM, which is intended to mimic the static solution-phase environment of the sediment assay, i.e. the amount of Pb that is desorbed in the absence of bioreporter over the time course of the bioreporter direct-contact assay. To perform the desorption experiments, sediment sample was added to a solution with 50% MM and 50% ultra-pure water. After 3.5 h of contact, slurries used in desorption were centrifuged (3 min at 10,625 × g) and filtered through a membrane filter (0.45 µm pore size). The filtrate was analysed using both ICP-MS (for $C_{\mathrm{Pb}}^{\mathrm{Tot,\ diss}}$, as described in Section 3.1, Chapter 3) and bioreporter (for $C_{\mathrm{Pb}^{2+}}$, as described in Section 3.1, Chapter 3).

6.2 Effect of Sediment on Bioluminescence Signal Transmittance

Five sediments with $C_{Pb}^{Tot,\ sed}$ in spanning the lowest and highest concentrations (45 mg·kg^{-1} to 10,500 mg·kg^{-1}) from core BW11/2 were chosen for more detailed analysis, beginning with intercomparison of results for how these different sediments affected bioluminescence signal transmittance. Transmittance may vary with the physical properties of the sediment, which vary across the different depths of core BW11/2. When sediments are deposited in lakes, the weathered materials from which they come are subjected to a number of physical and chemical processes that determine sediment properties. Lake sediments are typically comprised of terrestrially-derived clastic material and autochthonous biogenic compounds that can include silicates, carbonate and organic matter (Lowe and Walker 1997). The lithology of BW11/2 core is dominated by silt, with variable sand and organic matter content (Schillereff 2015). The mean particle size of the sediment samples varies with depth and ranges from 6 to 94 μm (Schillereff 2015). The organic matter content varies from 4 to 19%. All these factors (minerology, grain size variation, organic matter content) can cause differences in the blocking/scattering of bioluminescence signal for different sediment samples.

Higher slurry concentrations may increase the effective Pb LOD due to diminution of bioluminescence signal transmittance and associated increase in signal-to-noise. Meanwhile, it is difficult for the bioreporter to sense $C_{Pb^{2+}}$ at lower slurry concentrations since $C_{Pb}^{Tot,\ sed}$, and therefore the maximum potential bioavailable Pb, decreases as the slurry is more diluted. I used the four slurry

concentrations determined in preliminary work as feasible to examine the effects of sediment slurry concentration on bioreporter bioluminescence transmittance. Results for the five sediments that I chose for detailed analysis are displayed in Figure 6-4. Increasing slurry concentrations reduce measured bioluminescence due to the physical blocking and scattering of light by the sediment particles, and, as expected from theory, higher slurry concentrations result in lower light transmission and vice versa. Transmittance, as $\%T$, varies from $\sim 25\%$ to $\sim 75\%$ for the range of slurry concentrations used. As shown in Figure 6-4B, the decrease of $\%T$ from high slurry concentration to low is non-linear, and when plotted as optical density (Figure 6-4C) a linear relationship is apparent. This trend is in a manner consistent with Beer's Law, which is widely used in calculating light fields in dispersion media and in solving problems of the reconstruction of the dispersion medium parameters from the characteristics of scattered radiation (Dick 1998). The results in Figure 6-4 show that small differences in $\%T$ exist from sediment to sediment, as expected given the variations in sediment composition through the core. Uncertainty analysis of 25 replicate experiments (replicates for each individual core subsample) of the type shown in Figure 6-4 suggests that greater accuracy in correcting for transmittance effects is achieved using the sediment-specific T data (RSD less than 10%), except for the highest slurry concentration (with 16.7% for the RSD). At this slurry concentration the relative uncertainty in T is highest, as the overall signal is lowest in all cases, and hence an average value was used for T as being more accurate than individual values.

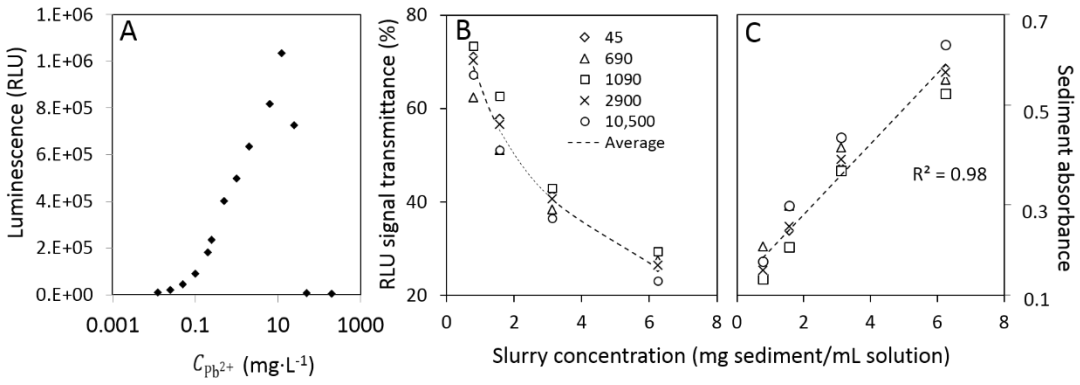

Figure 6-4. Response of bioreporter to Pb and effects of sediment slurry concentration on bioreporter bioluminescence. Bioreporter response to Pb standards over a large range of Pb from 0 to 400 mg·L^{-1} (A), for the five sediments with varying concentrations of $C_{\mathrm{Pb}}^{\mathrm{Tot,\,sed}}$ (concentrations in legend in mg·kg^{-1}) that were chosen for more detailed analysis, figure shows (B) diminution of transmittance, and (C) increase in optical density for blocking/scattering of bioreporter bioluminescence signal. Dashed lines represent average values for all five sediments trialled at each slurry concentration (mg sediment·mL^{-1} solution). For panel B, R^2s from linear regression for each individual sediment are 0.97, 0.99, 0.97, 0.98, and 0.99, for sediments having 45, 690, 1090, 2900, and 10,500 mg·kg^{-1} $C_{\mathrm{Pb}}^{\mathrm{Tot,\,sed}}$, respectively.

6.3 Pb Bioavailability in Lake Sediments

Bioavailable Pb by direct-contact assay compared to solution desorption

Preliminary trials suggested that for the materials used in this study, Pb bioavailability is a function of slurry concentration. Subsequent to determining a feasible range of slurry concentrations from which a useful level of bioluminescence signal could be obtained, the five sediments with $C_{\mathrm{Pb}}^{\mathrm{Tot,\,sed}}$ ranging from 45 to 10,500 mg·kg^{-1} (also representing different sediment ages due to relative positions in the core from which they were taken) were selected to investigate the effect of slurry concentration on Pb bioavailability further. Figure 6-5A displays the relative content of $C_{\mathrm{Pb}^{2+}}$ in these five sediment samples by direct-contact assay for four sediment slurry concentrations. It shows that the

relative content of bioavailable Pb is inversely related to $C_{Pb}^{Tot,\ sed}$ (especially for lower slurry concentration, ranges from 88% bioavailable for 45 mg·kg^{-1} to ~1% for 10,500 mg·kg^{-1} sediment $C_{Pb}^{Tot,\ sed}$). For all the five samples, as the slurry concentration increases, the content of relative $C_{Pb^{2+}}$ decreases. The pattern of decrease would be consistent with various physico-chemical phenomena, desorption for instance. A desorption study found that as the slurry concentration increased, the desorbed metal concentration decreased (Yin et al. 2002), which is quite similar to my findings. Therefore, I decided that it would be of interest to compare the $C_{Pb^{2+}}$ in direct-contact assays to desorbed Pb and, further, to compare what the bioreporter sees as desorbed Pb versus what a chemical test (ICP-MS) result shows.

Results for the $C_{Pb^{2+}}$ in desorption experiment supernatants are shown in Figure 6-5B, and results for ICP-MS analysis for the same solutions are shown in Figure 6-5C. In Figure 6-5B, the trend of the desorption data is consistent with the data from the direct-contact assays in Figure 6-5A, though, since for the 45 mg·kg^{-1} sediment the desorbed $C_{Pb^{2+}}$ in all the four slurry concentrations was lower than the LOD of the bioreporter, it is not possible to calculate the relative amount of desorbed $C_{Pb^{2+}}$ for this sediment. Relative desorption of this low $C_{Pb}^{Tot,\ sed}$ sediment may be simultaneously higher than that for the 690 mg·kg^{-1} sediment on a relative basis and nonetheless lower than the reporter LOD. In this desorption experiment, the sediment: solution ratio significantly affects the distribution of metals between sediment particles and solution. As the amount of sediment mass per volume of solution is changed, so does relative speciation. In their work on soils, Yin et al. (2002) found, consistent with the equilibrium

speciation theory, that at higher soil:solution ratio, Cu showed a stronger disposition to be retained in soil organic matter and was more difficult to dissolve and/or desorb into solution. My results agree with their study.

For the ICP-MS data in Figure 6-5C, all the trends[3] could be said to follows the observed behaviour of the bioreporter in general terms if the data is viewed as being highly "noisy", i.e. as a function of slurry concentration the largest change is for 45 and least change for 10,500 $mg \cdot kg^{-1}$ Pb, as seen for the bioreporter results. The lack of a clear trend for the ICP-MS data would appear to be an artefact of measurement, with possible sampling heterogeneity caused by small sediment quantities, small sample sizes and intra-sample differences in colloidal minerals sampled and/or the amount of Pb associated with same and simultaneous differences in the effect of HNO_3 used to solubilise Pb for ICP-MS measurement. The results from ICP-MS analysis indicate that the concentration of ICP-MS-measured desorbed Pb (total solution-phase Pb) is higher than the bioreporter-measured desorbed Pb in Figure 6-5B, which demonstrates that much of solution-phase Pb is not bioavailable to bioreporter. Studies have demonstrated that both organic matter and inorganic species (solubility of both of which increase with decreasing sediment:solution ratio) bind metals and hence reduce metal bioavailability (Boggs et al. 1985; Mostofa et al. 2013a; Tipping et al. 1998).

[3] In the mathematical sense, an upward or downward shift/pattern in noisy data as function of the independent variable.

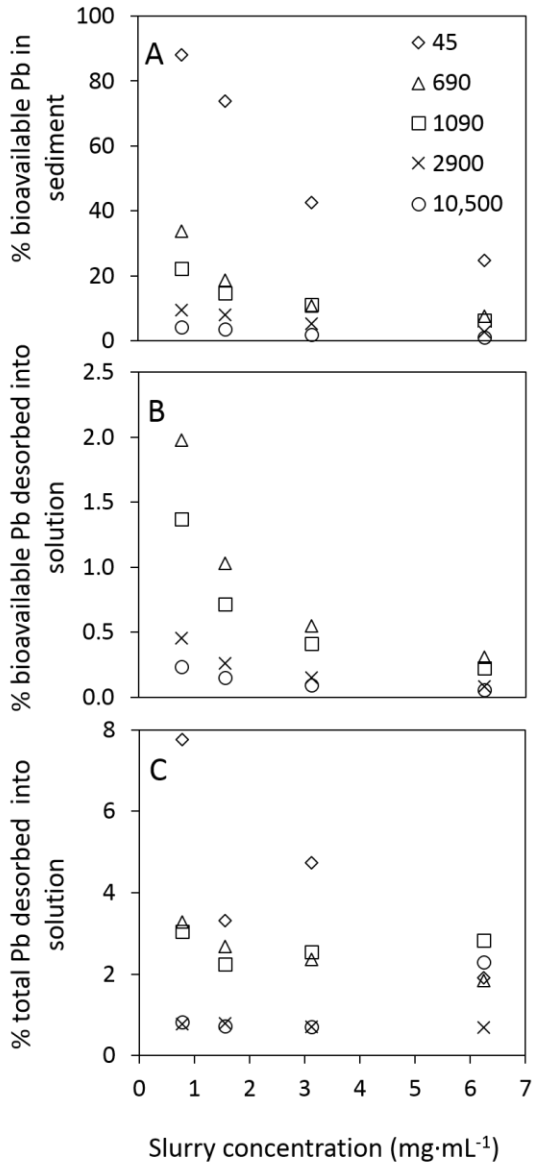

Figure 6-5. Effects of sediment slurry concentration (mg sediment·mL^{-1} solution) on direct-contact assay and solution-desorbed Pb. (A) Relative content of bioavailable Pb in sediment measured by direct-contact assay; (B) Relative content of bioavailable Pb desorbed in supernatants; (C) ICP-MS measured relative content of $C_{Pb}^{Tot,\,sed}$ desorbed in supernatants. Sediment $C_{Pb}^{Tot,\,sed}$ (in mg·kg^{-1}) is given in the legend of (A).

Therefore, in the desorption solution, inorganic and/or organic complexed Pb is not bioavailable and cannot be detected by the bioreporter. However, for the ICP-MS analysis, HNO_3 was added to the solution to effect total digestion before the measurement, and effectively all Pb in solution (including colloidal forms) and are measured as Pb ions. In contrast, results from the direct-contact assay show

that roughly an order of magnitude more Pb is bioavailable when the reporter directly "sees" the sediment, and the direct-contact assay results are higher than the results for static-sink desorption of Pb measured by ICP-MS.

Figure 6-6 shows the relationship between $C_{Pb^{2+}}$ by direct-contact assay versus $C_{Pb^{2+}}$ in desorption supernatant, with a very good linear relationship (R^2 = 0.98) and a slope of 16. This large slope suggests some additional detection mechanism other than simple interrogation of the solution-phase by the reporter, i.e. either the bioreporter can detect some part of the undesorbed Pb on sediment particles (as the reporters and sediment particles likely adhere to each other) or the bioreporter has some part in dynamically influencing Pb desorption in a manner that simultaneously causes uptake into the reporter for further activation of the promoter associated with bioluminescence. Both of these types of phenomena have been confirmed to occur and reported upon in the literature (Magrisso et al. 2009; Tecon et al. 2010).

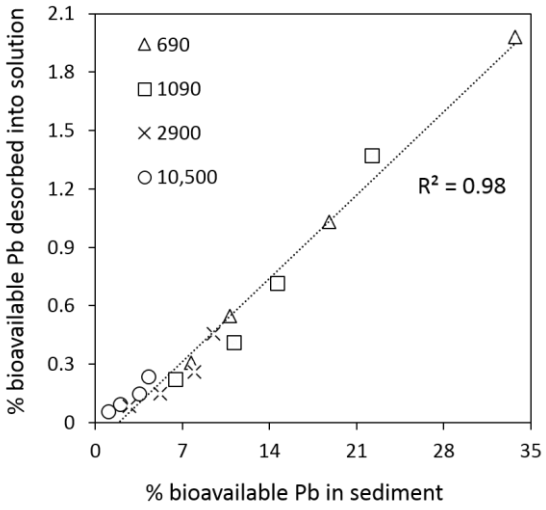

Figure 6-6. Agreement between two types of bioreporter measurements. Correlation between $C_{Pb^{2+}}$ in sediment as measured by direct-contact assay and $C_{Pb^{2+}}$ desorbed into solution for five sediments of different age and with widely differing $C_{Pb}^{Tot,\,sed}$ (listed in the legend in units of mg·kg^{-1}).

Bioaccessible Pb in Brothers Water sediments and implications for ERA

As I discussed above, even though the $C_{\mathrm{Pb}}^{\mathrm{Tot,\ sed}}$ is quite high in some sediment samples, most of the Pb is not bioavailable. However, as indicated in the introduction, bioavailability can be variable. Floods in particular cause disturbances in and change the distribution of lake sediments (Schillereff et al. 2014). During, or as a result of such events, it is quite possible that the Pb in the sediment can be released to the lake water as a result of sediment disturbance/resuspension and enhance the risk of Pb exposure. For results discussed above, decreasing the sediment:solution ratio increases the $C_{\mathrm{Pb}^{2+}}$, and theoretically, as the slurry concentration approaches zero, the limit of an infinite sink environment is reached. While this is not meaningful physically (no sediment means no Pb to measure), it is nonetheless possible to estimate the infinite sink limit from the data. The result would in effect conditionally represent something referred to as bioaccessibility, i.e. an estimate of the amount of Pb that may not be bioavailable at a higher sediment:solution ratio, but which might ultimately become bioavailable, other environmental factors remaining equal. The term bioaccessibility was used by Ruby et al. (1994; 1996) for representing the fraction of a toxicant (or substance) that becomes soluble within the gut or lungs and therefore becomes available for absorption through a membrane (Ruby et al. 1994; 1996). This concept of bioaccessibility has been refined with respect to ERA to indicate that portion of toxic substance that *is* bioavailable or *may become* bioavailable, i.e. from the release or solubilisation of soil- and sediment-associated metals in environmental systems external to the organism (Reeder et al. 2006).

Results from bioavailability for the five selected samples in Figure 6-5A were used for the estimation of bioaccessible Pb. Bioaccessibility was estimated by two graphical methods of plotting, per the exemplars in Figure 6-7; one obtains an intercept from fitting a line, and the other from non-linear fitting to a generalised hyperbolic. The two approaches, having different mathematical forms, are subject to different fitting uncertainty.

Figure 6-8 shows the comparison of $C_{Pb^{2+}}$ and bioaccessible Pb as a function of $C_{Pb}^{Tot,\,sed}$ in the five sediments. Results for estimated bioaccessibility show that 100, 23, 11, and 5% of, respectively, the 45, 690, 1090, 2900, and 10,500 mg·kg^{-1} $C_{Pb}^{Tot,\,sed}$ samples is bioaccessible. For the five sediments chosen for detailed study, the relative content of bioaccessible Pb follows the trend for bioavailable Pb, decreasing as the total Pb content increases. Effectively all of the Pb in the 45 mg·kg^{-1} $C_{Pb}^{Tot,\,sed}$ sediment is ultimately bioaccessible (100%), however only a small fraction of the Pb in the 10,500 mg· kg^{-1} $C_{Pb}^{Tot,\,sed}$ sediment appears to be bioaccessible (5.3%). This finding was not as expected, however, might be rationalised by chemical processes in diagenesis (changes undergone by a sediment after its initial deposition, Jackson 1997). For instance, a higher $C_{Pb}^{Tot,\,sed}$ would theoretically drive the equilibrium position forward for mineralisation reactions. In addition, the potential of mineralisation reactions' being accelerated by high $C_{Pb}^{Tot,\,sed}$, other processes that could also have a role to play in affecting bioaccessibility include sediment accumulation rate (potentially affects diagenetic processes), the amount organic matter (complexes with Pb) and sediment biological activity (affects chemical composition of organic matter, Price 1976).

Figure 6-8B shows the bioavailable Pb in all the sediment samples (above Limit of Quantitation/LOQ) at 6.25 mg·mL^{-1} slurry concentration. I include only points above LOQ here as due to the larger uncertainties associated with the higher slurry concentration. Data in panel B is consistent with data in A, however, the trend is not as clear; there are various reasons why this might be, considering that it is likely that no one mechanism is likely to explain bioavailability. I will discuss this further with respect to sediment grain size distribution below.

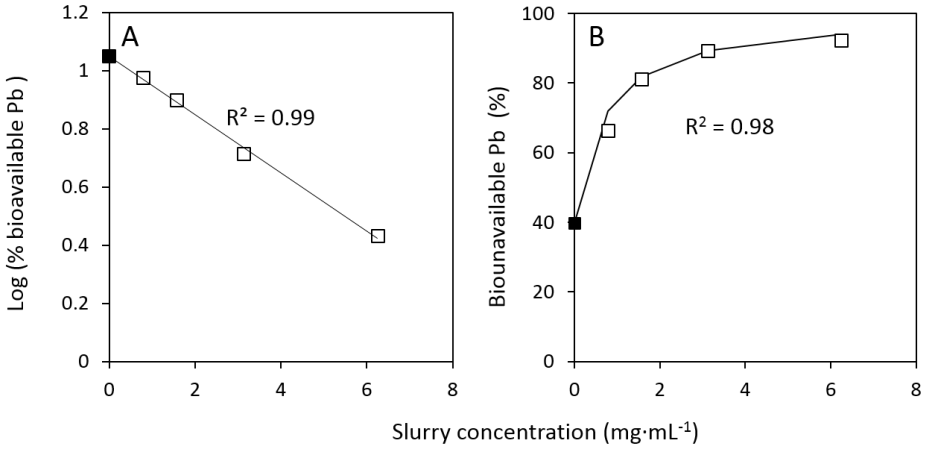

Figure 6-7. An example of graphical methods used for the estimation of bioaccessible Pb. (A) linear regression; (B) non-linear hyperbolic curve. Intercepts shown as filled squares.

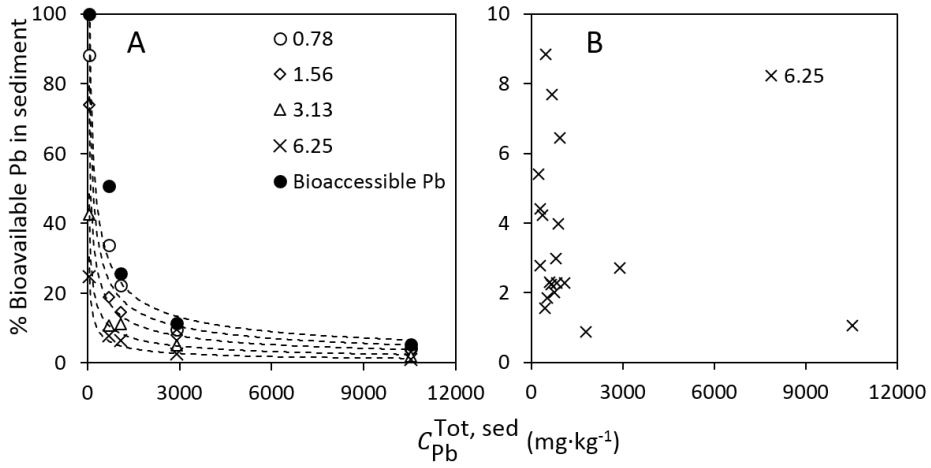

Figure 6-8. Comparison of bioavailable Pb and bioaccessible Pb with $C_{Pb}^{Tot, sed}$ for five sediments. (A) R^2 is 0.95, 0.99, 0.97, 0.96 and 0.91 for 0.78, 1.5626, 3.125and 6.25 mg·mL^{-1} slurry concentrations (given in legend), respectively); (B) bioavailable Pb in all the sediment samples (above LOQ) at 6.25 mg·mL^{-1} slurry concentration.

In Tyler's (1992) analysis of historical mining activity in the Brothers Water watershed, a period of intensive mining happened in the interval of 1863–1871, and Schillereff et al. (2016) showed that this period corresponds to the depth range from 49.5 to 62 cm sediment. The 10,500 mg·kg^{-1} total Pb sediment occurs at 58.75 cm in core BW11/2, which is during this mining period. In my study, I found that most of the Pb in this layer of the sediment is not bioavailable. Notwithstanding my hypothesis regarding the potential relationship between high $C_{\mathrm{Pb}}^{\mathrm{Tot,\,sed}}$ and the concentration of $C_{\mathrm{Pb}^{2+}}$ (inverse relationship in Figures 6-5 and 6-8), during this period, a large amount of Pb was deposited in the lake in the form of ore particles i.e. a form of mineralised Pb. This mineralised Pb would be expected to be less inherently bioavailable. Though once the galena removed from subsurface and exposed to surface, the oxidation processes might render some of the mineralised Pb bioavailable, this process would be limited to surface Pb, and the bulk of the material in particles would remain intact as galena. Nonetheless, for 5.3% bioaccessibility, this implies that 560 mg·kg^{-1} of Pb in the sample with a $C_{\mathrm{Pb}}^{\mathrm{Tot,\,sed}}$ of 10,500 mg·kg^{-1} is bioaccessible, and this is considerably above 400 mg·kg^{-1}, which is the level of acceptable risk to cause cancer for human in soil (in the form of $C_{\mathrm{Pb}}^{\mathrm{Tot,\,sed}}$) assigned by the USEPA (2009). As bioaccessibility in the sense that it is used here is akin to an infinite sink limit, it still nominally represents a conservative approach to risk assessment. *In situ* sediment:solution ratios are much higher than the slurry concentrations used here, though surface layers or layers subject to bioturbation/storm resuspension would still be at issue as sources of bioavailable environmental Pb. Such estimations of bioaccessible Pb could be used as a site-specific risk assessment guideline value

that would be more reasonable than $C_{\mathrm{Pb}}^{\mathrm{Tot,\,sed}}$, yet conservative in relation to variations in actual $C_{\mathrm{Pb}^{2+}}$.

Changing Pb bioavailability in time from the Brothers Water core BW11/2

The full suite of sediment samples (32 samples) was analysed by direct-contact assay at a slurry concentration of 6.25 mg·mL^{-1}, which is the sediment:solution ratio that is closest to *in situ* values while still being feasible to measure. Figure 6-9 presents (A) $C_{\mathrm{Pb}}^{\mathrm{Tot,\,sed}}$ with depth/age, (B) bioavailable Pb and (C), and the amount of bioavailable Pb relative to $C_{\mathrm{Pb}}^{\mathrm{Tot,\,sed}}$. In the discussion here, the variations in measured quantities in Figure 6-9 will be discussed in terms of age.

Panel A shows the $C_{\mathrm{Pb}}^{\mathrm{Tot,\,sed}}$for all Pb measurements in core BW11/2 to 210 cm depth or ~1200 A.D. The core is 351 cm long, dating back to ~500 A.D., after the Roman Era in the UK, and Figure 6-9A shows part of the pre-1507 record wherein the sediment all display a $C_{\mathrm{Pb}}^{\mathrm{Tot,\,sed}}$, which can be classed as the pre-mining baseline.[4] Per Adams (1988), the intensifying industrial phase began in the 1500s, i.e. any mining that occurred in the period of 500-1507 A.D. was relatively modest compared to later. Those samples above the pre-1507 baseline have an average concentration of 860 mg·kg^{-1}, which is 14 times higher than baseline of 62 mg·kg^{-1}. However, the highest record, ~12,400 mg·kg^{-1}, is over ~20,000 times the baseline. There is a first small-peak at ~122 cm/1550 A.D. which looks like there was decidedly mining by this time, with $C_{\mathrm{Pb}}^{\mathrm{Tot,\,sed}}$ increasing thereafter, with some periods of apparent less activity. The first small peak was followed by peaks at

[4] I refer to this as pre-mining baseline, however, since there was Bronze Age and Roman Era mining, and core BW11/2 does not capture the pre-Bronze Age $C_{\mathrm{Pb}}^{\mathrm{Tot,\,sed}}$, what I refer to as baseline here may be relative, and may not be true baseline.

~1612 A.D. 1702 A.D. (which can be attributed to the first big mining activity for which Tyler, 1992, reports documentation in 1696 A.D.) and ~1780 A.D. During early-nineteenth century, approximately the turn of the century to the 1830s, contractual documents indicate that mining ventures at Hartsop Hall experienced a financial pressure and restricted operations (Tyler 1992). The imprint of these small changes can be observed in the BW11/2 Pb profile at 75.75 to 72.25 cm. Mining activity subsequently resumed and reached its peak during the period when water powered milling was introduced (1863 to 1871 A.D.); which is reflected in the large spike starting at 60.75 cm depth/~1870 A.D. and peaking at 58 cm/~1875 A.D. The last period of ore extraction at Hartsop Hall was1931-1942 (38.25 to 34.75 cm). Pb continued to fluctuate after the cessation of mining in 1950 and the average concentration is 810 mg·kg^{-1} which is 12 times higher than the baseline. This is due to the remobilisation of mining waste during flood events (Schillereff et al. 2014; 2016).

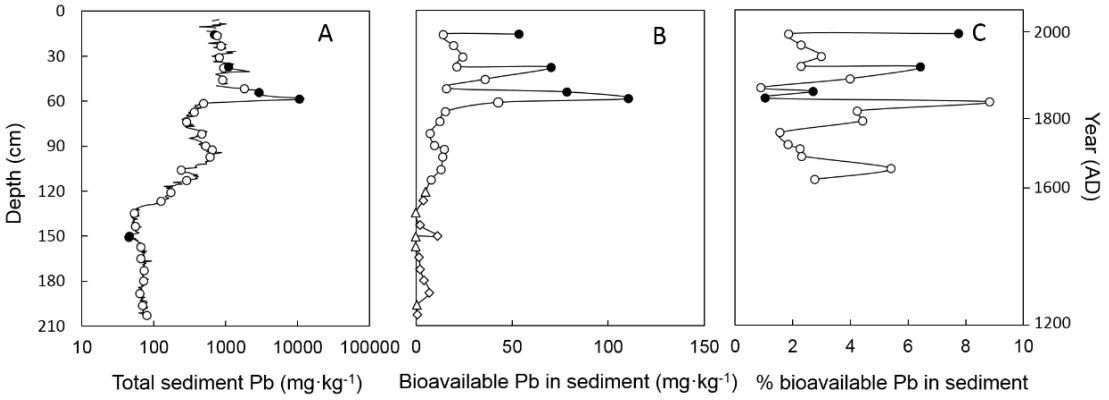

Figure 6-9. Variation of $C_{\mathrm{Pb}}^{\mathrm{Tot,\,sed}}$ and $C_{\mathrm{Pb}^{2+}}$ over time in Brothers Water core BW11/2. Variation of (A) $C_{\mathrm{Pb}}^{\mathrm{Tot,\,sed}}$, (B) $C_{\mathrm{Pb}^{2+}}$ (C) % bioavailable Pb of $C_{\mathrm{Pb}}^{\mathrm{Tot,\,sed}}$. Triangles represent values below LOD, diamonds represent values above LOD but below LOQ, and circles represent values above LOQ. Filled symbols represent the five samples chosen for detailed study.

Panel B indicates that the concentrations of $C_{Pb^{2+}}$ in core BW11/2 above 120.75 cm/1558 A.D. are higher than that in the deeper core. Almost all the samples below 120.75 cm, prior to 1558 A.D., have bioavailable Pb concentrations that are not detectable (below LOD) or low enough as to be below the bioreporter LOQ at the high slurry concentration (resulting in higher LOD and LOQ) used for these experiments. This finding agrees with the data in panel A that shows relatively lower $C_{Pb}^{Tot,\ sed}$ is present below 129.75 cm/1507A.D., there being a lag time between when $C_{Pb}^{Tot,\ sed}$ begins to increase over baseline in the sediment record (~1510) and when sufficient $C_{Pb}^{Tot,\ sed}$ is present for the bioreporter to detect it (~1560). I found that the trend of $C_{Pb^{2+}}$ in the sediment above 120.75 cm/1558 A.D. generally mimics the trend of $C_{Pb}^{Tot,\ sed}$ in panel A, which means that, on an absolute basis, more Pb is bioavailable in higher $C_{Pb}^{Tot,\ sed}$ samples. There is a positive correlation of R^2 = 0.62 for samples above LOD, however, this is highly influenced by two high points. Two samples I studied that do visually do not follow the trend so closely are in Figure 6-9B are the samples at 15.75 cm/1983 A.D. and 150.25 cm /1407 A.D. The former sample has relatively lower $C_{Pb}^{Tot,\ sed}$ and higher $C_{Pb^{2+}}$. This may be a result of the oxidation processes in the top layer of the sediment causing increased dissolved Pb, due to the oxygen exchange between sediment and water being at the top of the sediment column. This sort of phenomena has been observed, for instance by (Masscheleyn et al. 1990), who reported that the total soluble selenium concentrations substantially increased upon oxidation in the upper sediment column near the water-sediment interface. I am unsure what the cause of the increased bioavailability for the 150.25 cm /1407 A.D. sample is, however, this sample is anomalous in at least one way that

I can see. Of the approximately 160 $C_{Pb}^{Tot,\ sed}$ readings for this core prior to 129.75 cm/1507 A.D. that are shown in Figure 6-9A, if I plot the data as a control chart, there is only one period that deviates statistically from control, and this sample falls at the lowest $C_{Pb}^{Tot,\ sed}$ during that period.

Panel C shows the amount of $C_{Pb^{2+}}$ relative to $C_{Pb}^{Tot,\ sed}$ without the data that are under LOQ. The % $C_{Pb^{2+}}$ of $C_{Pb}^{Tot,\ sed}$ in panel C that are above LOQ mimics the trend in Figure 6-8A as shown in Figure 6-8B. This could be because a higher $C_{Pb}^{Tot,\ sed}$ drives the equilibrium position forward for mineralisation reactions, which has been discussed above. So, while absolute bioavailable Pb may correlate weakly with the $C_{Pb}^{Tot,\ sed}$, I simultaneously find that this bioavailable Pb shows a different trend when normalised to $C_{Pb}^{Tot,\ sed}$, such that relative bioavailable Pb is inversely related to $C_{Pb}^{Tot,\ sed}$.

The properties of the sediment samples might also affect the bioavailable fraction of Pb. Figure 6-10 shows correlations between $C_{Pb^{2+}}$ and physical properties of sediment. For panel A, $C_{Pb^{2+}}$ shows the almost no correlation with fraction of sand in the sediment for the selected 32 samples. However, when I deleted the two points with the highest $C_{Pb}^{Tot,\ sed}$, a positive correlation appears, and the R^2 changes from 0.12 to 0.52. In panel B, plotting $C_{Pb^{2+}}$ versus the fraction of silt in sediment, a negative correlation appears when I exclude these two points, and the R^2 changes from 0.10 to 0.56. These data indicate a weak tendency for more sand to lead to more $C_{Pb^{2+}}$, the opposite being true for silt. Studies have demonstrated that heavy metals are very easily desorbed by sandy soil (panel A) and can be strongly stabilised by clay and silt (as shown in panel B, Acosta et al. 2011;

Sheppard and Thibault 1992). I found no relationship between bioavailability and sediment clay content, however, the clay content of these sediments is generally very low, ranging from 3.8 to 10, and averaging 7.3%. Panel C shows that the observations in panels A and B are also reflected in mean particle size, which shows a weak positive correlation, as should be expected since larger mean particle size reflects more sand and smaller particle size reflects more silt. It seems likely to me that that the two points with the highest $C_{\mathrm{Pb}}^{\mathrm{Tot,\,sed}}$ disrupt these weak correlations in Figure 6-10 because these two have higher relative proportions of the Pb-bearing ore mineral galena, from which the mobilisation and bioavailability of Pb may be very different, as I have also hypothesised about earlier in this chapter.

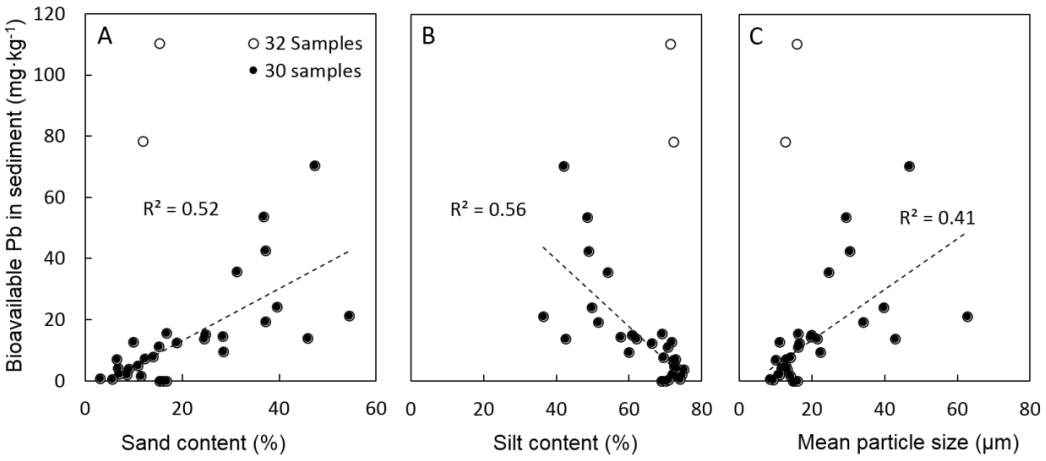

Figure 6-10. Correlation between $C_{\mathrm{Pb}^{2+}}$ and physical properties of sediment. (A)% Sand and (B) % Silt and (C) Mean particle size. Thirty samples are used in linear regressions shown (filled circles), and the two highest $C_{\mathrm{Pb}}^{\mathrm{Tot,\,sed}}$ (2,900 and 10,500 mg·kg^{-1}, open circles) values are not included in the regression.

6.4 Implications on Sediment Study

I have used the Pb-sensitive bioreporter zntA to assess the bioavailable fraction of Pb in the sediments of Brothers Water lake. The percent $C_{\mathrm{Pb}^{2+}}$ varies in

different layers of the sediments and is independent of OM, inversely related to silt content and directly proportional to sand content and mean sediment particle size. There is, at least for some subset of the samples, an inverse relationship between $C_{\mathrm{Pb}}^{\mathrm{Tot,\ sed}}$ and the percent $C_{\mathrm{Pb}^{2+}}$. All of these variations fit with what I know of physico-chemical processes likely at work in the sediment column and the complex nature of factors determining bioavailability. Based on this work, I formulate the following conclusions regarding ERA of the impacted lake sediments:

- The bioreporter can measure over an order of magnitude more $C_{\mathrm{Pb}^{2+}}$ by direct-contact with the sediment slurry than the desorption supernatant. It is thus inaccurate to determine the concentration of bioavailable Pb in sediment by only measuring the Pb desorption into solution. This further demonstrates the dynamic nature and advantage of using a biological rather than a chemical approach to measure bioavailability.
- The absolute amount of bioavailable Pb in the top layer is notably high (53.6 mg·kg^{-1}), which may pose a risk to the aquatic organisms in the lake and the related ecosystem. This result should arouse widespread concern about Pb pollution in Brothers Water lake. However more studies that reated to Pb toxicity to aquatic life in the lake are still needed.

7 EFFECT OF MICRONUTRIENTS ON ALGAL GROWTH – FOCUS ON RISK ASSESSMENT

Eutrophication is a major environmental problem for water resource management (Lewis et al. 2008, 2011; Qin et al. 2007; Tang et al. 2016), and local economies may suffer when a lake experiences HABs (Dodds et al. 2009). It is generally accepted that N and P nutrients are the primary causative factor, however, for systems subject to large anthropogenic perturbation, this may no longer be true, and the role of micronutrients (MNs) are often overlooked. By far the most study of MN limitation is for Fe, the literature for which is extensive (see for instance Kranzler et al. 2013; Moreno-Vivian 1999; Sunda et al. 2005; Vrede and Tranvik 2006). Other MNs are less well-studied than Fe but have been shown to be variously limiting and co-limiting (Bayer et al. 2008; Bonilla et al. 1990; Downs et al. 2008; Hyenstrand et al. 2001; Lewin 1966).

Here I report results from my work on the effects of MNs on algae in Taihu. Rapid development and lack of suitable environmental controls has led to large inputs of pollutants from industry and agricultural waste into Taihu and its tributaries,

intensifying water quality deterioration (Wang et al. 2009). Ergo, this previously oligotrophic, diatom-dominated lake (Chen et al. 2003b,c) is now subject to hypereutrophication, and cyanobacterial HABs have occurred every summer in the northern part of the lake since the mid-1980s (Qin et al. 2007). During the summer of 1990, a large-scale cyanobacterial HAB occurred in Taihu, causing 116 factories to halt work (Guo 2007; Xu et al. 2010). In May, 2007, another large-scale HAB incapacitated a drinking water plant, leading to a water crisis in the city of Wuxi, population 4 million (Guo 2007; Qin et al. 2010). Qin et al. (2007) showed that the extent of HABs in Taihu has expanded throughout the northern, western and central regions of the lake from May through October every year, and this intensity of anthropogenic disturbance to Taihu makes it an interesting field site to study. Further, a better understanding of the factors that promote HABs is essential in order to protect the water resource.

Studies on Taihu often focus on the effects of N and P on algal growth (Paerl et al. 2011; Xu et al. 2010). A recent study by one of my collaborators working on Taihu used short-term nutrient limitation bioassays (NLBs) in small scale mesocosms to study Fe limitation of *Microcystis* spp. in Taihu waters (Xu et al. 2013) and found that Fe was a limiting nutrient under some conditions. So far the emphasis is on cyanobacterial growth as the major risk factor for HABs in Taihu (Chen et al. 2003c; Liu et al. 2011; Paerl et al. 2011). Less emphasis has been on study of *in situ* algal assemblages with multiple species and phyla, and no studies have evaluated the potential that other MNs might play in nutrient limitation in Taihu. A major theme in my work on Pb relates to bioavailability and bioavailability-based risk assessment, and I became interested in the potential links between my colleague's work and mine. Pb is not known to be nutritive, however, many

metals may serve as toxicants or nutrients, depending on concentration (Manahan and Smith 1973; Wu et al. 2017). Either would affect the risk profile for HABs. As a first step, I decided to extent the collaborators work and expand the scope of studies of MN effects on algae in Taihu, with the primary goal being to understand if there are effects, and if so, what the implications might be for HABs.

7.1 Experiments and Laboratory Analysis

Design of experiments

For this study, I employed small-scale mesocosm/NLB experiments. The idea behind mesocosm experiments is to conduct experiments that have an element of control that would be obtainable for lab experiments, hence improving reproducibility, ability to isolate variables, and ability to form more well-defined and tractable hypotheses, while also adding an element of environmental reality that field experiments have and lab experiments lack, i.e. to capture ambient environmental conditions (e.g. diel cycles, temperature conditions, Paerl and Bowles 1987; Piehler et al. 2009; Xu et al. 2010). The particular NLB approach that I used was developed to provide a rapid assessment of nutrient limitation characteristics (Paerl and Bowles 1987; Piehler et al. 2009; Xu et al. 2010) and follows the preceding Taihu work on Fe limitation described in Xu et al. (2013). By doing small-scale mesocosm studies, I was able to perform more trials, however, my experimental design was factorial (Torbjorn et al. 1998), which is a common design, but meant that I had to choose carefully which MNs I would study. I chose to examine the effects of Fe, Cu, Co, B and Mo, with and without

addition of N and P, on *in situ* algal assemblages. I also did N, P, NP, and MNs with/without NP, because I wanted to see the effect of N and P on algal growth separately and check whether these MN are limiting or co-limiting nutrients for algae. The *in situ* assemblage experiments were conducted to simulate the lake environment. I used water and associated algal assemblages from three regions of Taihu that were differentially impacted by HAB, in order to see if observed effects were a function of locale/water chemistry or extant assemblages. I characterised the effect of MNs using traditional methods for chemical (water quality) and biological (microscopic cell counting) analysis, and I supplemented these studies using flow cytometry measurement (FCM) coupled with data-driven analysis.

Study area and sampling sites

I conducted sampling at a time when an HAB was fully developed in the western part of the lake and spreading east, in order to perform NLB experiments when a range of conditions occur in the lake. The three sites that I studied, shown in Figure 7-1, are situated in Meiliang Bay, Gonghu Bay and Xukou Bay, and are part of a long-term monitoring programme.

Meiliang Bay (St 3) is one of the lake's most eutrophic bays with high water turbidity and the occurrence of dense cyanobacterial HABs, particularly in summer. Large amounts of untreated wastewater from factories, residential and agricultural areas are discharged into the bay by the Liangxi and Zhihu Gang rivers, and a strong algal bloom was present at the time of sampling for this study. The west to east spread of HAB is somewhat variable year-to-year, and though I wanted to revisit the sites previously studied for Fe limitation (one of which was

Station 3, Xu et al., 2013), I found that the station in eastern Taihu that these authors studied was already partially impacted by HAB. Hence, I sampled at the nearest eastern station that was not impacted (Station 28, Xukou Bay) at the time of sampling. Gonghu Bay (Station 13) was less affected by HAB than Station 3 at the time of sampling and was chosen as such.

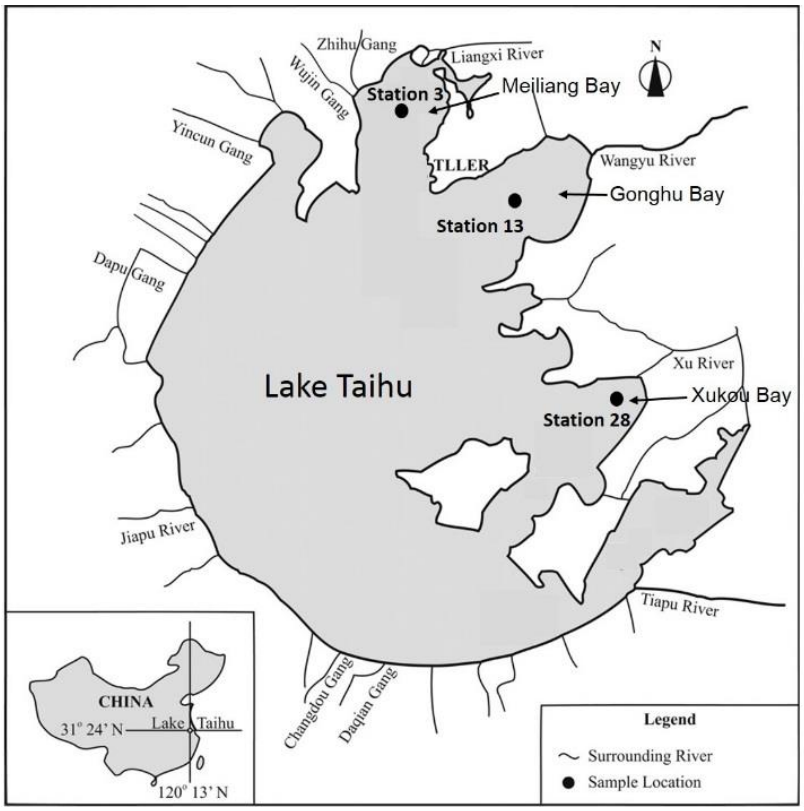

Figure 7-1. Location of sampling sites for small-scale mesocosm MN NLBs in Taihu.

Sample collection and water sample analysis

Water samples from 0.2 m below the surface were collected in August, 2017, into 40-L acid-cleaned polyethylene carboys. The samples were used for NLB experiments (Section 2.5) and water quality analysis. Physical parameters, (WT, pH, and DO) were measured in the field using a YSI 6600 multisensor sonde. Chemical properties were measured in the lab and included DOC, TN, TDN, NH_4^+, NO_3^-, NO_2^-, TP, TDP, PO_4^{3-}, Chl-a. Total dissolved MNs (TDFe, TDCu, TDCo, TDB,

TDMo) were measured as described in Chapter 3. Chl-a was determined as described in Chapter 4, Section 4.1. Phytoplankton samples were preserved with Lugol's iodine solution for storage and were stored in the dark at room temperature until analysis. Algal objects were counted from observations of samples sedimented in a Sedgwick-Rafter chamber and reported as counts (Wang and Wang 1982). The phytoplankton species were identified according to Zhou and Chen (2011).

FCM spectral analysis of single cells was performed using a FACSCalibur (Becton Dickinson, California, USA) with two lasers (argon solid-state, and red diode, excitation at 488 and 635 nm, respectively). For each sample, 800 µL of cell sample was inserted into a 10 mL plastic vial and placed into the flow cytometer with a sample intake speed of 12 $\mu L \cdot min^{-1}$. The sheath fluid was a commercial product (Beckman Coulter Inc., USA), composed of 9.84 $g \cdot L^{-1}$ Na_2SO_4, 4.07 $g \cdot L^{-1}$ NaCl and 0.11 $g \cdot L^{-1}$ procaine hydrochloride, pH 7.0, delivered through a 150 µm nozzle at 4.5 psi. Measurements included forward scatter (FSC), side scatter (SSC) and four fluorescence channels: green fluorescence (FL1, 530/30 nm bandpass, associated with carotenoid fluorescence at λ_{max}= 505-530 nm, Chen et al., 2017; Kleinegris et al., 2010; Steinberg et al., 1995), yellow fluorescence (channel FL2: 585/42 nm bandpass, detects phycoerythrin/PE at λ_{max}= 575 nm, Dennis et al., 2011), red fluorescence (channel FL3: 670 nm/longpass, detects the integrated the red tail of the Chl-a peak, λ_{max}= 650-700 nm, Vincent, 1983) and orange fluorescence (FL4: 661/16 nm bandpass, detects allophycocyanin/APC at λ_{max} = 660 nm, Dennis et al., 2011). Resulting data comprises a six-dimensional algal signature based on variations in size, granularity, carotenoid fluorescence (lower in chlorophytes, for instance, Chen et al. 2017; Steinberg et al. 1995), PE (notably

associated with red algae and cryptophytes, French and Young 1952), APC (characteristically dominant in cyanophytes, Canaani and Gantt 1980) and chlorophyll. For FSC and SSC the amplification gain was set at 1 and measured in the linear mode. For fluorescence channels the amplification gain was set at 1 and measured in the log-mode. Acquisition was set to capture 50,000 total events for each sample. I did all the analyses above at t=0, however, for the NLB experiments, I measured Chl-a, counts, and FCM. Due to limitations in sample volume, I could not do all of the analyses above for all the sample times. Therefore, I did the larger suite of analyses at the beginning to have a good characterisation of my starting point and differences between stations. At the sampling time points of 2 and 4 days, I did the three analyses to see how these particular things were changing with treatment.

Nutrient limitation bioassay experiments

NLB experiments were carried out immediately after sample collection and followed the method of Paerl et al. (2011, also see Haraughty and Burks 1996; Whalen and Benson 2007; and Xu et al. 2013 as examples). The NLB experiment is a form of small-scale and short-term mesocosm study. Mesocosm size, experimental time-scale, design of experiment and quantities measured vary enormously in the literature. A very large number of published studies have employed the approach, however, there remain criticisms. The most systematic work that I know of that addressed such criticisms is a work by Spivak et al. (2011) entitled “Moving on up: can results from simple aquatic mesocosm experiments be applied across broad spatial scales?” These authors note that “Experiments in mesocosms have contributed to our understanding of community ecology and

ecosystem functioning (Fraser and Keddy 1997; Jessup et al. 2004; Spivak et al. 2009), informed theory (Pfisterer and Schmid 2002; Cardinale et al. 2006), and provided insight to global processes (Benton et al. 2007; Duffy 2009; O'Connor et al. 2009)." The authors also point out, however, that munificent criticism of this approach asserts the approach has limited relevance to natural ecosystems (Spivak et al. cite Carpenter 1996; Schindler 1998; and Haag and Matschonat 2001 as examples). To address this controversy, Spivak et al. (2011) considered effects of volume, surface area to volume (shape), and experimental time-scale to determine the generality of algal responses to nutrient enrichment and to determine the extent of relevance of NLB-type mesocosm experiments to large-scale processes, such as eutrophication. These authors also considered results from 1060 NLB experiments subjected to a meta-analysis (Elser et al. 2007). Cumulatively, Spivak et al.'s comprehensive study considered NLB mesocosm experiments spanning a wide range of volumetric (as little as 0.02 L) and temporal (0 to 7 days) scales, and the authors' overall conclusions were that results from mesocosm experiments are applicable to larger scale processes. These conclusions come with caveats. For instance, Spivak et al. observed both volume and shape effects in some cases. These tended to be generally small and disappeared with longer assay times (3 to 7 days). In considering Spivak et al.'s results in the context of my study, while I am not able to unequivocally negate arguments posed by detractors of the NLB mesocosm approach, there is certainly no consensus of opinion invalidating the value of commonly used NLB experiments to real-world environmental processes. Moreover, there is considerable support for the validity of the approach. The NLB method is reasonably tractable for a large factorial experiment such as what I wanted to

perform and therefore I chose this approach as arguably suitable as a screening experiment to identify potential MN effects that might be environmentally relevant and thus merit further study. Additionally, this is the approach that was taken by my collaborator's Hans Pearl and Hai Xu, who had published his findings in a suitable journal with success (Pearl et al. 2015; Xu et al. 2013). It seemed to me that using his method would also enable my work to serve as a comparable extension to his.

For each NLB treatment, I took triplicate water 14 L subsamples from each respective station from the 42-L samples described above and placed each into 1-L transparent, chemically inert, cubitainers that were trace-metal clean, as described in Xu et al. (2013). Nutrient was then added to cubitainers by spiking with concentrated solution to achieve the final concentrations shown in Table 7-1 for each treatment. The treatments were control (no nutrient additions), N, P, combined N and P (NP), single MNs (Fe, Cu, Co, B or Mo), and MN+NP (Fe+NP, Cu+NP, Co+NP, B+NP or Mo+NP). Each treatment was sampled twice (once at 2 days, once 4 days) for analysis (Chl-a, microscopic counts, FCM). Concentrations of N, P, NP, and Fe were based on those used in previous work; concentrations for other MNs were initially targeted at four times projected ambient, based on literature on Taihu or according to other information in literature (Bayer et al. 2008; Procházková et al. 2014; Xu et al. 2013). After nutrient additions, the cubitainers were incubated *in situ* in Taihu near the surface for four days by placing them in a frame at Taihu Laboratory for Lake Ecosystem Research (TLLER). As an exploratory study, I chose this method to examine short-term growth responses of algae, as the issue of long-term phytoplankton succession patterns is undoubtedly more complex.

Table 7-1. Treatment schedule used in Taihu NLB experiments.

Experimental treatment	Nutrient concentration[1]
Control	no addition
N	2.0 mg·L^{-1} N
P	0.20 mg·L^{-1} P
NP	2.0 mg·L^{-1} N + 0.20 mg·L^{-1} mg·L^{-1} P
Fe	200 µg·L^{-1} Fe
Fe+NP	200 µg·L^{-1} Fe + 2.0 mg·L^{-1} N + 0.20 mg·L^{-1} P
Cu	20 µg·L^{-1} Cu
Cu+NP	20 µg·L^{-1} Cu + 2.0 mg·L^{-1} N + 0.20 mg·L^{-1} P
Co	1 µg·L^{-1} Co
Co+NP	1 µg·L^{-1} Co + 2.0 mg·L^{-1} N + 0.20 mg·L^{-1} P
B	18 µg·L^{-1} B
B+NP	18 µg·L^{-1} B + 2.0 mg·L^{-1} N + 0.20 mg·L^{-1} P
Mo	1 µg·L^{-1} Mo
Mo+NP	1 µg·L^{-1} Mo + 2.0 mg·L^{-1} N + 0.20 mg·L^{-1} P

[1]N was added as KNO_3, P was added as $K_2HPO_4 \cdot 3H_2O$, Fe was added as $FeSO_4 \cdot 7H_2O$, Cu was added as $CuSO_4 \cdot 5H2O$, Co was added as $CoCl_2 \cdot 6H_2O$, B was added as H_3BO_3, and Mo was added as $Na_2MoO_4 \cdot 2H_2O$.

Data analyses

One-way ANOVA followed by Tukey's Honest Significant Difference (HSD) post-hoc test was used to test for differences in Chl-a among treatments. The R programming language and environment for statistical computing was used to perform calculations, and the level of significance used was $p < 0.05$ for all tests (Bretz et al. 2011). Additional tests for correlation were performed in Microsoft Excel (Pearson's r and Spearman's ρ, nonparametric). To analyse FCM data I used a data-driven approach. FCM is a high-throughput technology offering rapid simultaneous quantification of multiple cellular characteristics. The ability to measure six or more parameters simultaneously and measure tens of thousands of cells in a few minutes is attractive, however, this "blessing of dimensionality", or the ability to separate groups with higher dimensional data that are not otherwise separable, is complemented by "the curse of dimensionality" (Donoho 2000). To deal with the curse of processing large amounts of multi-dimensional

data, even today FCM data analysis typically utilises a process called gating, which Bashashati and Brinkman (2009), in a recent review, described thus:

> *"Gating is a highly subjective process in which the investigators determine the regions in multiparametric space that contain the 'interesting' data, based on their knowledge of the experimental factors and experience. This is a tedious, time-consuming, and often inaccurate task... to serially select regions in one- and two-dimensional graphical representations of the data... This low-dimensional subsetting ignores the high-dimensional multivariate nature of the data... even relatively minor differences in gating can produce different quantitative results."*

Recently there has been a great deal of effort put into development of data-driven approaches to FCM data analysis, so that data analysis is driven by the structure of the data itself (Finak et al. 2009; Finak et al. 2010) rather than expert opinion (Finak and Gottardo 2011). My use of a data-driven approach was an exploratory effort, and to my knowledge I am the first to use such an approach to study changes in algal assemblages.

To perform data-driven analysis of FCM data, I used FlowMerge (Finak and Gottardo 2011), which is part of the Bioconductor software project for the analysis of FCM data (Huber et al. 2015). FlowMerge is an extension of the Bioconductor FlowClust algorithm (Finak et al. 2009). FlowClust is based on *t*-mixture models with Box-Cox transformation, and when the number of clusters is not known a priori, the Bayesian information criterion (BIC) is used to determine the most appropriate number of clusters inherent in the multi-

dimensional structure of FCM data (Lo et al. 2008, 2009). While this approach is used and works well in many applications, it has been noted that the BIC may overestimate cluster number because the number of mixture components needed to model data may be greater than justified by inherent difference in a sample (Baudry et al. 2010; Finak et al. 2009). This issue has been addressed by application of the entropy-based integrated completed likelihood criterion (ICL). The ICL has been shown to provide a better estimate of the number of clusters, however is not a good model for the underlying data distribution (Baudry et al. 2010). By combining the two approaches, data is first clustered using the *t*-mixture model with Box-Cox transformation, and subsequently the ICL guides remerging mis-split clusters, arriving at a solution that has the suitable fitting properties and a number of clusters that is most likely to represent the number of different types of cells/populations present in a sample (Finak et al. 2009).

7.2 Initial Conditions and Water Quality

Results from water quality analysis, shown in Table 7-2, confirm that the three different stations had the different initial conditions. Turbidity, nutrients (TN, TDN, NH_4^+, TP, TDP, PO_4^{3-}), DOC, and Chl-a are highest for Station 3, intermediate for Station 13 and lowest for Station 28. Some MN concentrations follow this trend. TDFe are relatively high and within the range that a previous study found for Station 3 (10-106 $\mu g \cdot L^{-1}$) but are considerably higher than that study found in the eastern part of the lake (below detection to 3 $\mu g \cdot L^{-1}$, Xu et al. 2013). Other MN values are reasonably low or below detection, as may occur with trace quantities. The nutrients TN and TP are both dominated by organic forms, the majority of which is particulate for N, and presumably P as well, though there is

a small diminution in the percentage of organic forms from Station 3 to Station 28. DOC follows that pattern, and since the predominant drainage pattern and HAB pattern is from west to east, these results are as expected. Most other nutrient forms follow this pattern, however, within analytical uncertainty, NO_3^- is low and essentially static. The TN:TP ratios are similar for Stations 3 and 13 and higher for Station 28, and TDN:TDP ratios are both a factor of ~2 less than the TDN:TDP ratio for Station 28. There have been reports detailing the ability of cyanobacteria to flourish at low TN:TP ratios (Schindler 1977; Smith 1983). The high pH of Taihu is notable and perhaps the best indicator of the degree of its anthropogenic perturbation. The high pH has been attributed to inorganic carbon scavenging of phytoplankton as a result of HABs, part of a vicious cycle conveying competitive advantage on bloom-forming species (Wang et al. 2017). This pH may substantively reduce the bioavailability of MNs due to the formation of bis-hydroxy- and/or carbonato- complexes at high pH that is expected theoretically and has been demonstrated experimentally (Kim et al. 1999; O'Shea and Mancy 1978).

Consistent with prior recent reports, I found that the phytoplankton in Taihu were variable across the lake, dominated by Cyanophyta (blue-green algae/cyanobacteria), Bacilliarophyta (diatoms), Chlorophyta (green algae), Cryptophyta and Euglenophyta (Chen et al., 2003c; Xu et al., 2013). Figure 7-2 shows pie charts with the relative percentages of each phylum and the total counts for each station. Station 3 and Station 13 were dominated by Cyanophyta (> 90% of total counts), however, for Station 3, ~82% of all cyanophytes (*Chroococcus, Microcystis, Nostoc*, and *Oscillaria* spp.) were Microcystis by count, whereas for Station 13, ~90% of all cyanophytes were *Nostoc* spp. by count.

Microcystis and *Nostoc* are non-nitrogen-fixing and nitrogen-fixing genera, respectively, which may affect phytoplankton growth differently between these two stations. Station 28 was dominated by Bacilliarophyta. The total counts for Station 13 are approximately three times that of Station 3, whereas the inverse is true for Chl-a between the two stations.

Table 7-2. Properties of lake water used for NLB experiments[1].

	Parameter	Station 3	Station 13	Station 28
Physical	WT (^{0}C)	30.4	29.8	30.8
	Turbidity (NTU)	124	48	0.5
	pH	9.26	8.91	9.30
Chemical	TN (mg/L)	4.55	2.22	0.62
	TDN (mg/L)	0.80 (18)	0.69 (31)	0.60 (97)
	TKN (mg/L)	4.4 (98)	2.1 (95)	0.5 (84)
	NH_4^+ (mg/L)	0.30 (6.6)	0.26 (12)	0.14 (23)
	NO_3^- (mg/L)	0.10 (2.2)	0.11 (5)	0.09 (15)
	NO_2^- (mg/L)	0.002 (0.04)	0.002 (0.09)	0.01 (1.9)
	TP (mg/L)	0.43	0.18	0.02
	TDP (mg/L)	0.03 (7)	0.02 (11)	0.01 (50)
	DOP+PP (mg/L)	0.42 (97)	0.17 (94)	0.02 (80)
	PO_4^{3-} (mg/L)	0.01 (3)	0.01 (3)	0.004 (20)
	TN:TP	11	12	31
	TDN:TDP	27	35	60
	TDFe (µg/L)	94	68	38
	TDCu (µg/L)	2.9	3.0	1.7
	TDCo (µg/L)	< 0.8	< 0.8	< 0.8
	TDB (µg/L)	< 10	< 10	< 10
	TDMo (µg/L)	3.8	3.7	3.1
	DOC (mg/L)	5.46	4.61	3.83
	DO (mg/L)	12.3	13.0	11.7
Biological	Chl-a (µg/L)	203	73	1.5

1 Values in parentheses are percentages of TN and TP for nitrogen and phosphorus species, respectively; TKN and DOP+PP determined by difference. Abbreviations are surface water temperature (WT), total nitrogen (TN), total dissolved nitrogen (TDN), total Kjeldahl nitrogen (TKN), ammoniacal nitrogen (NH_4^+), nitrate (NO_3^-), nitrite (NO_2^-), total phosphorus (TP), total dissolved phosphorus (TDP), soluble reactive phosphorus (PO_4^{3-}), dissolved organic phosphorus (DOP), particulate phosphorus (PP), total dissolved Fe (TDFe), total dissolved copper (TDCu), total dissolved cobalt (TDCo), total dissolved boron (TDB), and total dissolved molybdenum (TDMo), total dissolved carbon (DOC), dissolved oxygen (DO), and chlorophyll a (Chl-a).

The results in Table 7-2 and Figure 7-2 are consistent with the frequent summer trend in Taihu wherein nutrient enrichment followed by an HAB begins in the western side of the lake and spreads to the east over the course or the summer, per literature cited above on Taihu.

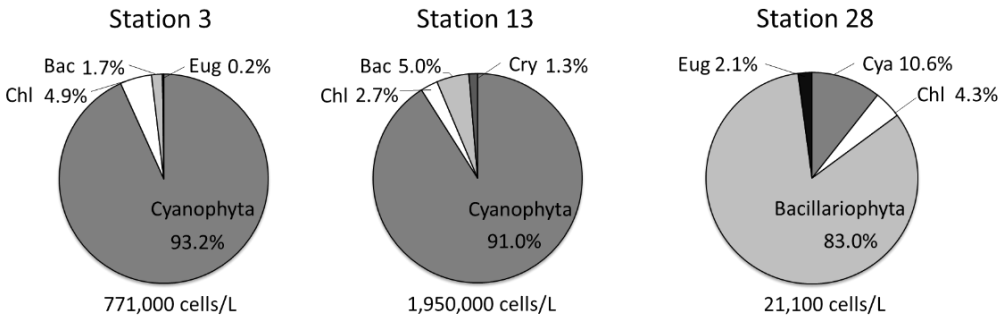

Figure 7-2. Pie charts showing the relative amounts of different phyla present in Taihu at the time of sampling. Abbreviations are Bac = Bacillariophyta; Chl = Chlorophyta; Cry = Cryptophyta; Cya = Cyanophyta; Eug = Euglenophyta). Total counts are given below each pie chart.

7.3 Chl-a Changes in Nutrient Limitation Bioassays

Raw data is provided in Figure 7-3 below, which shows average values for Chl-a for all treatments. Significance in pairwise differences are shown based on Tukey's HSD post hoc tests (a > b > c > d > e > f > g, $p < 0.05$). Where there is a mark with the same letter (such as ab), the null hypothesis, H_0: a-b=0, cannot be rejected, and where different letters are marked (such as a and b) it can be rejected. In assigning letters, the letter a represents the largest average and serves as the point of reference in comparison to the next largest average, and letters are sequentially assigned in this manner thereafter.

Figure 7-4 shows the results from analysis of NLB experiments for Chl-a, which I use as an index of photosynthetic biomass (Billington 1991; Desortová 1981; Flemer 1969; Hallegraeff 1977). To show relative changes, N, P, NP, Fe, Cu, Co, B, and Mo treatments are normalised to the control (panels A, D, and G), and all MN+NP treatments are normalised to NP (panels B, E, and H), i.e. according to expressions 7-1a and 7-1b:

$$\text{Normalised Chl-a}_{\text{N/P,MN}} = \frac{[\text{Chl-a}]_{\text{N/P,MN}}}{[\text{Chl-a}]_{\text{C}}}, \text{ and} \quad (7\text{-}1a)$$

$$\text{Normalised Chl-a}_{\text{MN+NP}} = \frac{[\text{Chl-a}]_{\text{MN+NP}}}{[\text{Chl-a}]_{\text{NP}}}, \quad (7\text{-}1b)$$

where the brackets indicate concentration, the subscripts N/P, MN indicate N, P, NP, or one of the MN treatments, the subscript MN+NP indicates one of the MN treatments also amended with NP, and the subscript NP in 7-1b indicates use of the NP treatment as a control. The rate of change from 0 to 2 days (ΔChl-a$_{0\text{-}2d}$) versus 2 to 4 days (ΔChl-a$_{2\text{-}4d}$) for all treatments, as given in expressions 2a (for diminution) and 2b (for growth) below, is also plotted (panels C, F, and I).

$$\Delta\text{Chl-a}_{t_i - t_{i+2\text{d}}} = \frac{\left([\text{Chl-a}]_{t_i} - [\text{Chl-a}]_{t_{i+2\text{d}}}\right)}{[\text{Chl-a}]_{t_i}} \times 100\%, \text{ and} \quad (7\text{-}2a)$$

$$\Delta\text{Chl-a}_{t_{i+2\text{d}} - t_i} = \frac{\left([\text{Chl-a}]_{t_{i+2\text{d}}} - [\text{Chl-a}]_{t_i}\right)}{[\text{Chl-a}]_{t_{i+2\text{d}}}} \times 100\%, \quad (7\text{-}2b)$$

where the subscript *i* indicates a measurement time point (0, 2 or 4 days) and *i*+2d indicates the reference time point *i* plus 2 days. Generally, for those treatments exhibiting relative increases in Chl-a, average increases are more modest and less variable for Station 3 (average 25% increase, with relative standard deviations/RSDs ranging from 10 to 15%), followed by Station 13 (40% increase and RSDs ranging from 30 to 35%) and Station 28 (average increase of Chl-a by 220%, with RSDs exceeding 100%).

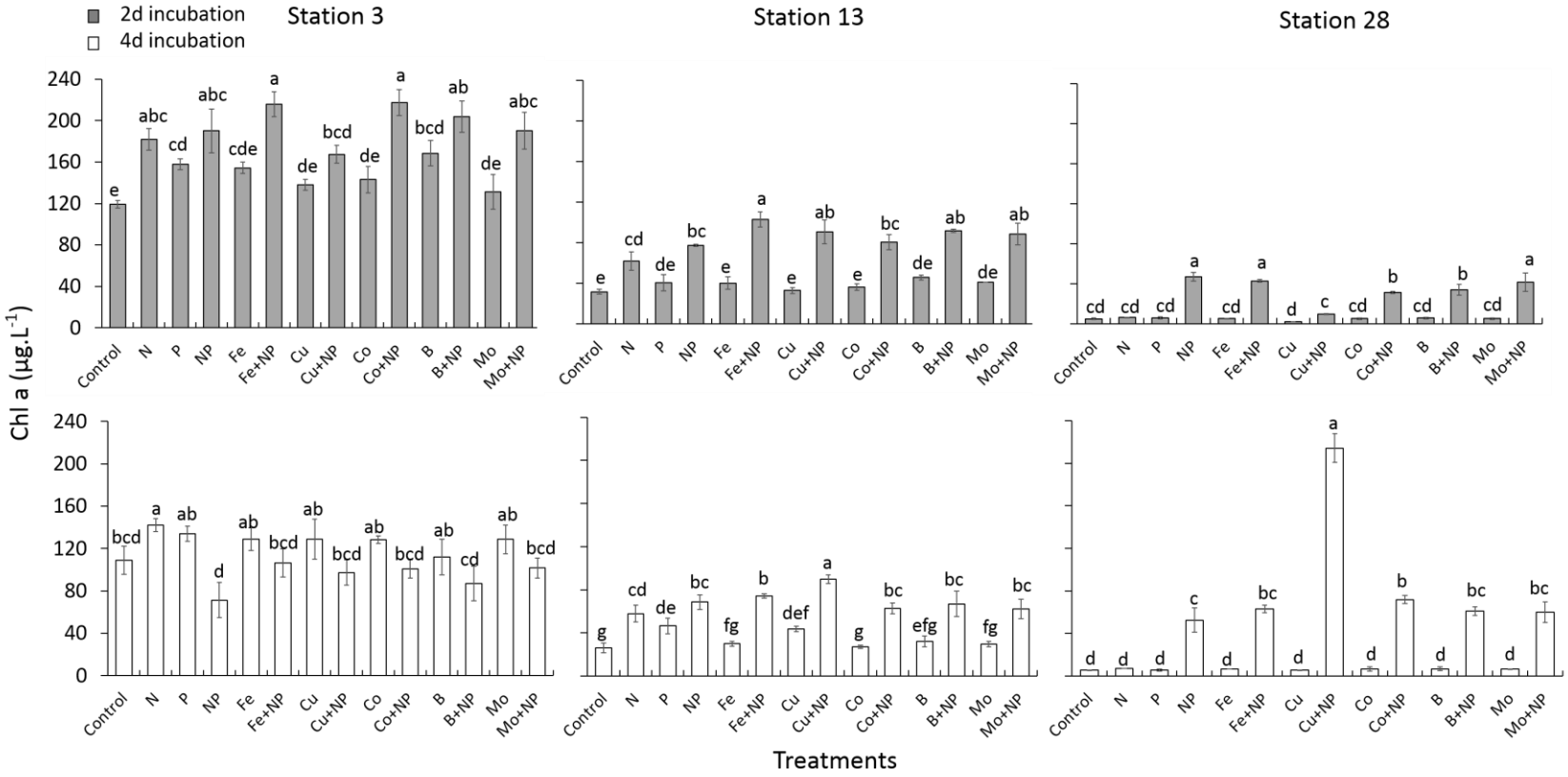

Figure 7-3. Chl-a responses for treatments at the three stations studied and for 2-day and 4-day incubations. Mean values are shown. Error bars represent ±1 standard deviation of triplicate samples. Differences between treatments are shown based on ANOVA Tukey's HSD post hoc tests (a > b > c > d > e > f > g).

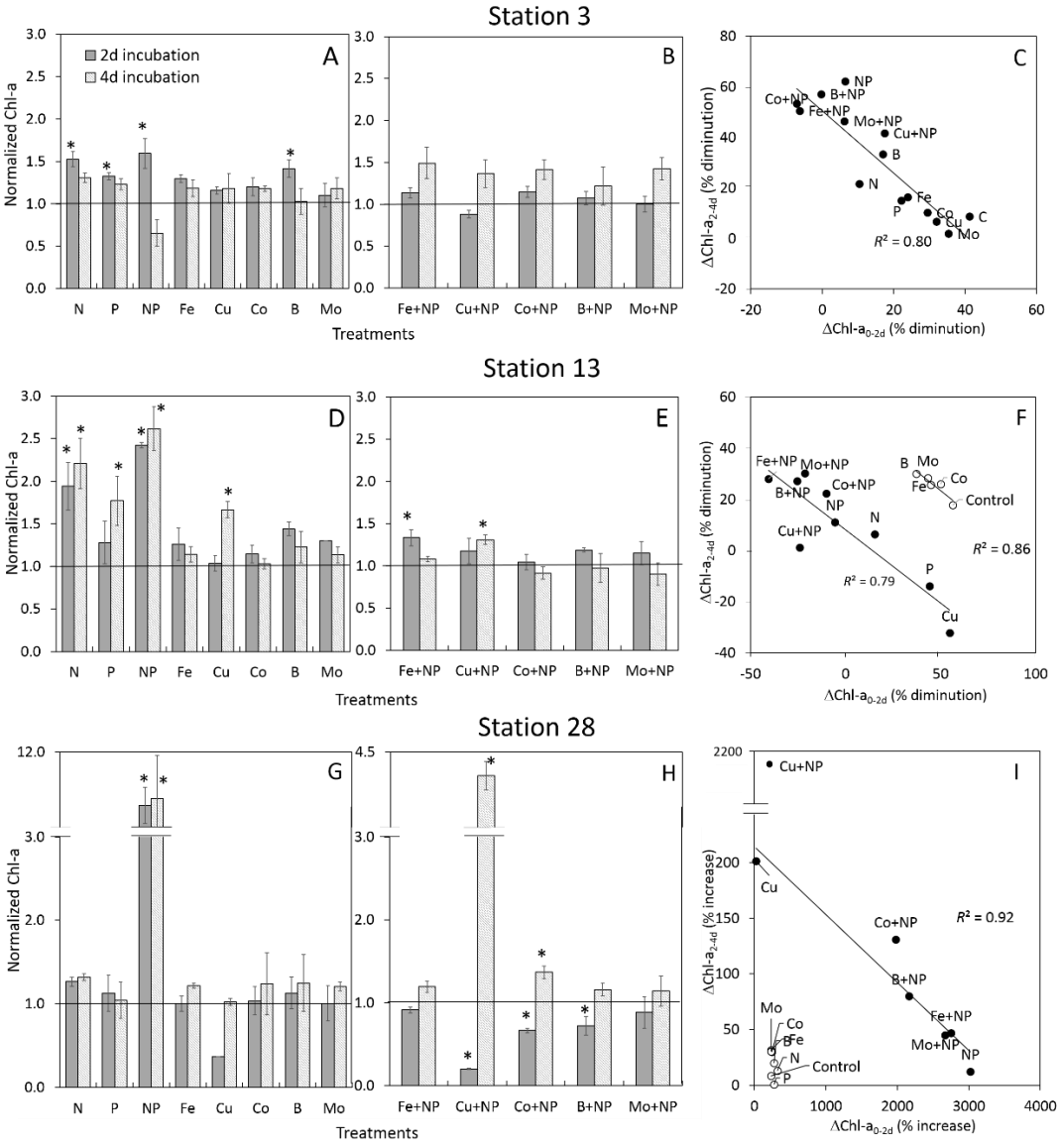

Figure 7-4. Results from Chl-a analysis for Station 3 (top row), Station 13 (middle row) and Station 28 (bottom row). Chl-a concentrations for each station are shown normalised to the control (for N, P, NP, and single MN treatments, panels A, D, and G) or to NP (for all MN+NP treatments, panels B, E, and H). Panels C, F, and I show rate of Chl-a change over 0 to 2 days compared to 2 to 4 days. Asterisks in panels A, B, D, E, G, and H indicate significant ($p < 0.05$) pairwise differences based on a one-way ANOVA/Tukey HSD post-hoc test. Open and filled markers in panels C, F and I are based on apparent groupings as described in the text, and Pearson's r squared (R^2) is given in each. I also calculated Spearman's ρ. Pearson's r and Spearman's for each panel are, respectively, as follows: panel C, -0.89 and -0.91; panel F, -0.89 and -0.75 (for filled markers) or -0.93 and -0.90 (for open markers); panel I, -0.96 and -0.94. For panel I, Cu+NP is treated as a separate class based on Cook's distance. If grouped with other data (filled markers), the correlation coefficients become -0.58 (r) and -0.93 (ρ).

I relate the correlations shown in Figure 7-4C, F, and I to changes in growth phase/growth rate (note – see figure caption for Pearson's *r* and Spearman's ρ). The NLB experiments that I describe are analogous to performing short-term batch culturing under quasi-environmental conditions. Batch systems are highly dynamic with a progression of different phases of population change. Barsanti and Gualtieri (2010) characterise these algal phases in terms of a typical pattern of growth in six phases: lag, acceleration, exponential, early stationary, stationary, and decline (refer to this cited text for more details and cited work). The lag phase represents a period of adjustment or acclimatisation to altered conditions, during which algal growth may not be occurring actively, however most cells are still viable, though not dividing. Laboratory experiments with batch cultivation show that algal growth media inoculated with exponentially growing algae have short lag phases, hence commencement of a NLB experiment need not entail a long lag phase if the algal assemblage initially present is in an active growing state and conditions are not too far altered. After the lag phase, cells transition into active growth through a short phase of growth acceleration until growth reaches the maximum possible that can be supported by a given set of conditions. This maximum growth phase is referred to as the exponential phase since increasing cell density increases in time according to an exponential function. In batch laboratory culture, the exponential phase is reasonably brief, hence the same circumstance would be expected under NLB conditions. In short order, various physical and chemical factors begin to limit growth, such that the cell population enters early stationary phase wherein cell numbers continues to increase, albeit slowly, until gradually growth ends and stationary phase is reached. Growth is highly dependent on parameters such as light intensity, temperature, and

nutrient availability. The former two being equal, as for my NLB experiments, nutrient availability is the primary factor that determines the maximum cell density that will be reached in stationary phase. The cell concentration remains at a constant value during stationary phase until culture collapse (decline) occurs, which is sometimes referred to as negative growth. The crash is rapid initially, however for some cultures a basal cell population may be able to persist for some time. The different stages of algal growth are characterised by different growth rates. The growth rate is characterized as the slope of the growth curve, i.*e.* df/dt, where cell density is a function, *f*, of time, *t*, which in terms of my experimentally measurable intervals is ΔChl-$a_{0\text{-}2d}$ or ΔChl-$a_{2\text{-}4d}$, as given in expressions 2a and 2b in the article text. Figure 7-5 characterizes the relationship between changes in slope/growth rate through different phases of growth.

For the data shown on a normalised basis, one-way ANOVA/Tukey's HSD post-hoc test ($p < 0.05$) pair-wise differences of treatment compared to control or NP are indicated by asterisks in Figure 7-4. For Station 3, few differences are seen, and only at day 2 for P, N, NP, B, and Fe+NP. Both B and Fe have previously been reported to increase *Microcystis* growth (Gerloff 1968; Srivastava et al. 2016). While NP exhibited the highest Chl-a relative to the control by day 2, by day 4 it appears that NP has accelerated the onset of senescence (a term representing a range of processes, mostly in reference to declining/degrading Chl-a associated with late stationary/lysis phases resulting from environmental stresses such as nutrient limitation Louda et al. 1998). Station 3 had the highest nutrients and initial concentrations of Chl-a, and on an absolute basis there is a trend of Chl-a diminution over 4 days, with an inverse correlation (R^2=0.80) between ΔChl-$a_{0\text{-}2d}$ and ΔChl-$a_{2\text{-}4d}$. This observation fits with the idea that, for a late stationary

assemblage, less nutritive treatments (e.g. the control in Figure 7-4C) result in progressive senescence or decline (decreasing growth curve slope) with a diminishing rate of change, whereas more nutritive treatments cause partial reinvigoration or at least retard the onset of senescence (flat to increasing growth curve slope, as for NP/MN+NP treatments in Figure 7-4C), with subsequent senescence after nutrient exhaustion. In terms of growth curve behaviour, larger nutrient concentrations result in larger changes in curvature/rate of change, in comparison to lower concentrations (Gough et al. 2015; Lee et al. 2000; Pinna et al. 2015).

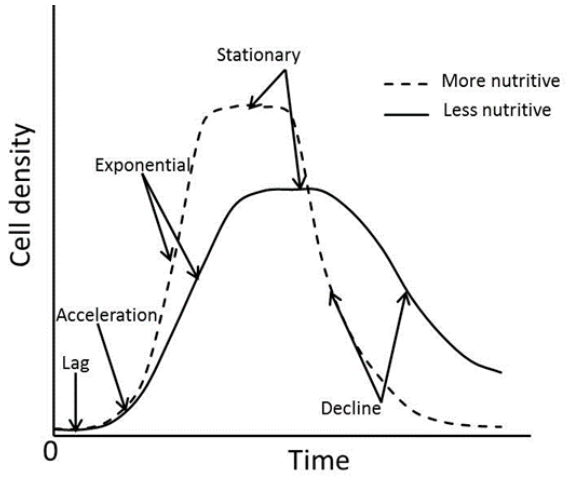

Change in slope as a function of growth phase

Growth phase	Magnitude of slope [a]
Lag	0 → very small
Acceleration	Small
Exponential	Large
Early stationary	Small
Stationary	~ 0
Decline	Large → ~0

[a] The sign of the slope is positive for all phases, except decline, which has a negative slope. When expressed as diminution, all signs are negative except for decline, which is positive.

Figure 7-5. Different phases in algal growth curves. The diagram on the left (per Barsanti and Gualtieri 2010) gives representative algal growth curves and the table on the right shows how the magnitude and sign of the growth curve slope changes. When a given population of algae are growing under very nutritive conditions slopes for each phase are expected to be steeper, the cell density in stationary phase will be higher, and the timing of growth phase transitions may also be affected, as illustrated conceptually in the diagram.

Station 3 was highly impacted by an HAB during the time of this study, the results indicate that NP, MN+NP, and to a lesser extent B have the most effect in supporting the persistence of the HAB. In actual lake conditions *Microcystis* can vertically migrate throughout the shallow water column, optimising its ability to

access favorable conditions to proliferate, which in turn increases its lateral extent; smaller differences I see in mesocosm NLBs might be larger in an open lake.

The Station 13 trend for N and P is similar overall to that of Station 3 in that the order of effect relative to the control is NP > N > P (Figure 7-4), albeit the pattern persists to day 4. Treatments of MN only statistically exceed control/NP treatment for Cu and Fe+NP (day 2) and Cu+NP (day 4). While for most MN/MN+NP, relative Chl-a decreases from day 2 to day 4, the behaviour of Cu/Cu+NP is strikingly different, with Chl-a concentrations increasing for Cu (by 61%) and Cu+NP (by 11%) from day 2 to day 4 relative to the control and NP, respectively. For the scatter plot showing ΔChl-$a_{0\text{-}2d}$ versus ΔChl-$a_{2\text{-}4d}$ for Station 13 (Figure 7-4F), both visually and in terms of R^2, there appears to be two groups with an inverse linear relationship. The first group is the "no-growth" group; though R^2=0.86, it may be more appropriate to view this group as tightly clustered. The second group is all of the remaining treatments. For this group, the NP/MN+NP treatments show growth during over first two days (positive growth curve slope, i.e. a negative ΔChl-$a_{0\text{-}2d}$ value), followed by diminution as nutrients have become exhausted whereas Cu and P show diminution in Chl-a over the first two days with a net increase thereafter. I posit that, as for Station 3, the standing stock for Station 13 is at or nearing decline, and while the NP treatments provoke a reasonably rapid response, P and Cu may undergo lag, i.e. the changes are suggestive of adjustment and/or decline of the standing stock followed by growth.

For Station 28, changes for N and P are not significantly different from the control, however NP together has Chl-a that is almost 10 times that of the control (days 2

and 4). Interestingly, by day 2 for all MN+NP treatments the response is less than that of NP alone, with Cu+NP being a pronounced factor of 4.9 lower. The lower response for single MN is not generalisable, though the response for Cu alone is also much lower, 2.7 times less, than the control. By day 4 all of the control-normalised single MN treatments have increased compared to their values on day 2, and MN+NP treatments are all larger than NP, significantly so for Co and Cu. The treatment Cu+NP has the most pronounced differential effect and is 4 times greater than for NP with a 22-fold increase from day 2 to day 4. The scatter plot for Station 28 (Figure 7-4I) lends the appearance of different behaviors: 1) C, N, P, Fe, Co, B, and Mo; 2) Cu, NP, Fe+NP, Co+NP, B+NP, and Mo+NP; and 3) Cu+NP in a class of its own. Changes for the first group are small and consist of a near-constant ΔChl-$a_{0\text{-}2d}$, followed by small and variable increases in ΔChl-$a_{2\text{-}4d}$. The second group follows the inverse relationship discussed previously for Stations 3 and 13, wherein those greatest increases in ΔChl-$a_{0\text{-}2d}$ (positive growth curve slope) are followed by smaller ΔChl-$a_{2\text{-}4d}$, (in the case of Station 28 possibly indicating onset of stationary phase rather than senescence) and vice versa. Overall, I observe trends in Figures 7-4C, F, and I that are rationalisable in terms of algal growth curves (see Figure 7-5) and appear to result in different groupings based on the initial condition of standing stocks and the relative nutrient value of different treatments. The similarity between Pearson's r and Spearman's ρ are in most cases in good agreement, except when including Cu+NP for Station 28. For Station 28 (filled markers in Figure 7-4I) Spearman's ρ indicates a strong monotonic, if not linear, relationship when including Cu+NP.

With respect to N, P, and NP, the results herein present a unified picture for the stations sampled, spanning the width of Taihu, wherein NP are co-limiting nutrients for HABs, in agreement with previous studies (Dzialowski et al. 2005; Paerl et al. 2015; Xu et al. 2013; Yang et al. 2017). While there is an increasing awareness that MNs and the bioavailability of trace metals play important roles in the carbon and nitrogen metabolism of algae (Baptista and Vasconcelos 2006; Berman-Frank et al. 2001; Juneja et al. 2013; Romero et al. 2013), the state of knowledge is as yet immature, and my primary purpose for this work was to ascertain whether MNs would exhibit effects in a highly disturbed and frequently hypereutrophic system as Taihu. The statistically significant results in Figure 7-4 indicate that MNs may serve both as primary and as co-limiting nutrients in some cases. Results for Cu/Cu+NP (Stations 13 and 28) are most marked, and Fe+NP shows effects for two stations (3 and 13). For Station 28, Cu/Cu+NP appeared to show an inhibitory effect at day 2, whereas by day 4 the maximum increase observed during this study was for Cu+NP. It has long been known that, at high enough concentrations, Cu is an algal biocide, and Cu^{2+} has even been suggested for use in environmental management of HABs at concentrations ranging from 90-500 µg/L (Källqvist and Meadows 1978; Wu et al. 2017). Likewise, the importance of Cu as a MN for algae has long been recognised (Manahan and Smith 1973). Because MN such as Cu are required in very small amounts in the whole algae life cycle, there is frequently only a very small difference between a nutritional, growth-promoting effect and cell toxicity (Procházková et al. 2014). The effect of Cu+NP in Station 28 is unique to my knowledge in the literature.

There has been a growing amount of research into bacterial and algal production of copper-binding ligands called chalkophores and copper-binding siderophores.

These ligands have demonstrated importance in controlling the bioavailability of Cu and may aid organisms to regulate Cu uptake and navigate a narrow divide between nutrition and toxicity (Johnstone and Nolan 2015). Regarding a linked effect with Fe, as early as 1980, McKnight and Morel (1980) published findings wherein Fe limitation resulted in strong secretion of chalkophores by two *Anabaena* species; they speculated that Cu complexes formed with such ligands were likely non-toxic and might convey an advantage to cyanophyte populations. Subsequently, genetic regulatory links between Cu and Fe homeostasis in cyanophytes have been discovered. For example, based on genetic studies employing site-directed mutagenesis, Nicolaisen et al. (2010) have developed a model wherein schizokinen, a siderophore secreted by *Anabaena* spp., is produced and exported under low Fe or high Cu conditions. When the concentrations of both Fe and Cu are low, schizokinen complexes with Fe, increasing Fe bioavailability to the organism. At high Cu/low Fe concentrations, schizokinen complexes Cu in a manner protective to the organism and another Fe transporter is activated. These findings are analogous to findings for *P. aeruginosa* wherein exposure to toxic Cu concentrations resulted in the differential production of siderophores, such that a more Cu-protective effect (bioavailability reduction) is favoured (Braud et al. 2010). In this study, the ambient TDFe for Station 28 averages half that of the other stations (Table 7-2). Since the high Chl-a response of Cu+NP appears previously undocumented, some phytoplankton reportedly have a relatively high cellular Fe requirement (Brand 1991), and the low solubility of environmentally prevalent Fe^{3+} reduces Fe bioavailability, I cannot rule out that Cu treatment induced increased Fe bioavailability followed by growth.

7.4 Effect of Micronutrients on Changes in Algal Assemblages

My purpose in using *in situ* algae was to investigate if any changes in algal assemblages might be observed and if there might be clues as to MN's mediating conditions favouring *Microcystis* over other algae. Figures 7-6 to 7-8 show the changing proportions of algae in response to MN treatments. Disaggregated counts for all species, including species with very low frequency, are given in Figures 7-9 to 7-11. While count data give a sense of changes, some species quantified are colonial and some are not – counting methods address this, arguably, not very successfully (Rott et al. 2007), thus here I have taken a semi-quantitative rather than statistical approach.

For Station 3, changes in total counts and algal assemblages are relatively small; cyanophytes remain dominant, with *Microcystis* spp. averaging 88% of the total cyanophyte counts (Figure 7-6). By day 4, the total counts for both Cyanophyta and Chlorophyta were larger for the single MN treatments in comparison to the corresponding MN+NPs, consistent with the effects discussed for Chl-a with respect to NP.

While Cyanophyta predominated initially for Station 13, followed by Bacillariophyta, then Chlorophtya, the dominant genus was *Nostoc* spp., and changes to the algal populations of Station 13 in response to MN treatment present a more complex picture than that of Station 3 (Figure 7-7).

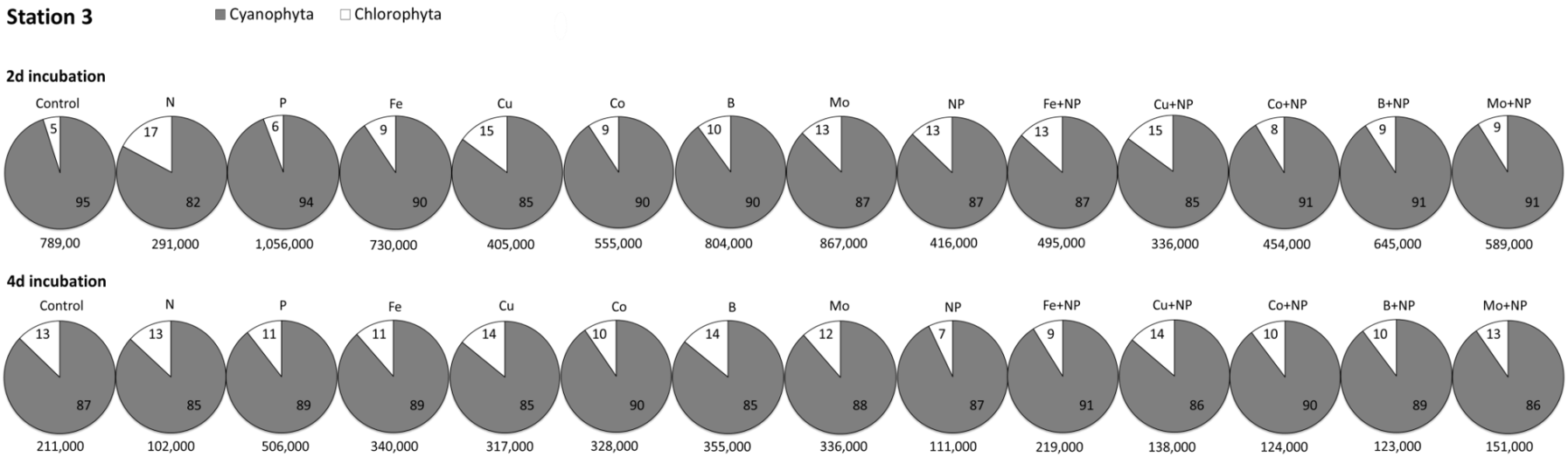

Figure 7-6. Pie charts showing the changing proportions of algae in response to different treatments for Station 3. Numbers on the pies represent %, numbers below are total counts. Phyla whose occurrence is less than 10% at any time are not shown/constitute a negligible fraction, see Figure 7-9.

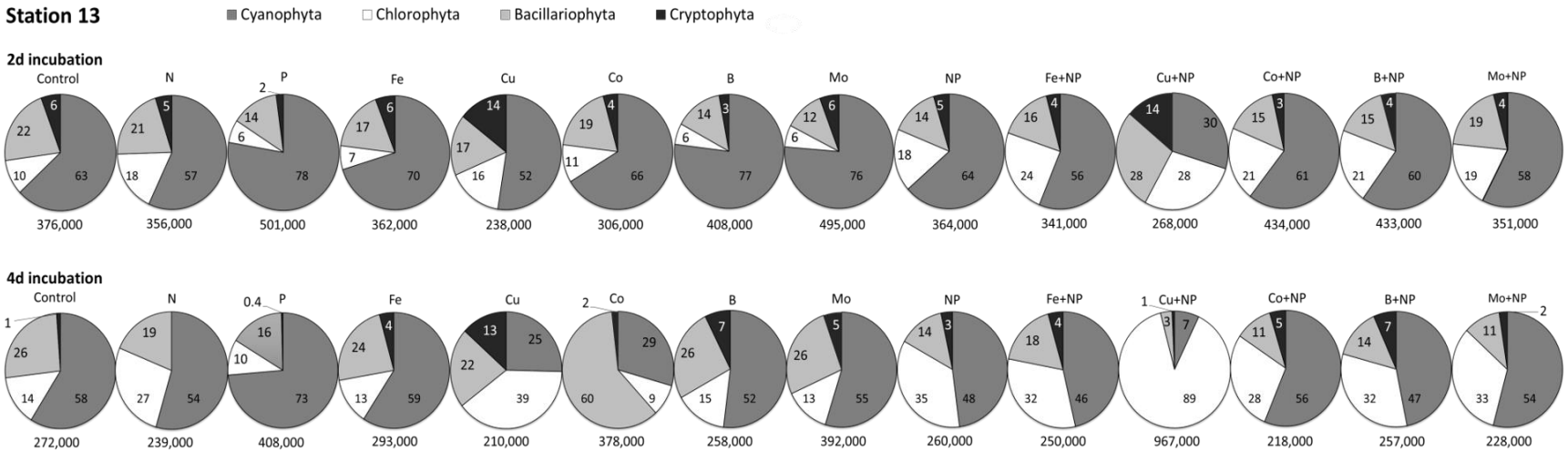

Figure 7-7. Pie charts showing the changing proportions of algae in response to different treatments for Station 13. Numbers on the pies represent %, numbers below are total counts. Phyla whose occurrence is less than 10% at any time are not shown/constitute a negligible fraction, see Figure 7-10.

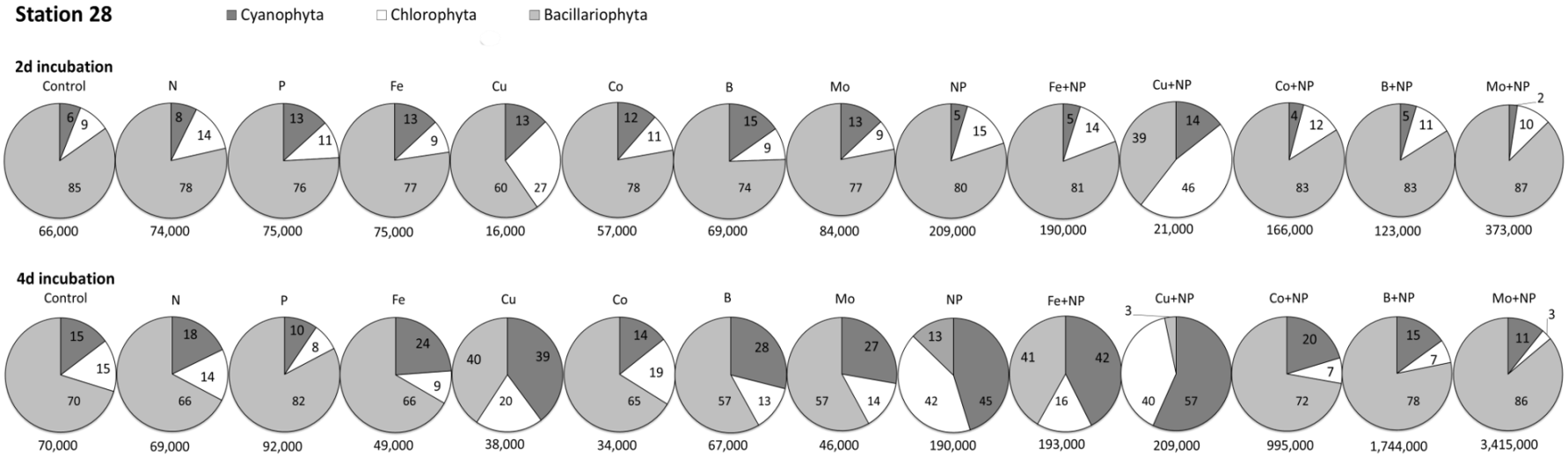

Figure 7-8. Pie charts showing the changing proportions of algae in response to different treatments for Station 28. Numbers on the pies represent %, numbers below are total counts. Phyla whose occurrence is less than 10% at any time are not shown/constitute a negligible fraction, see Figure 7-11.

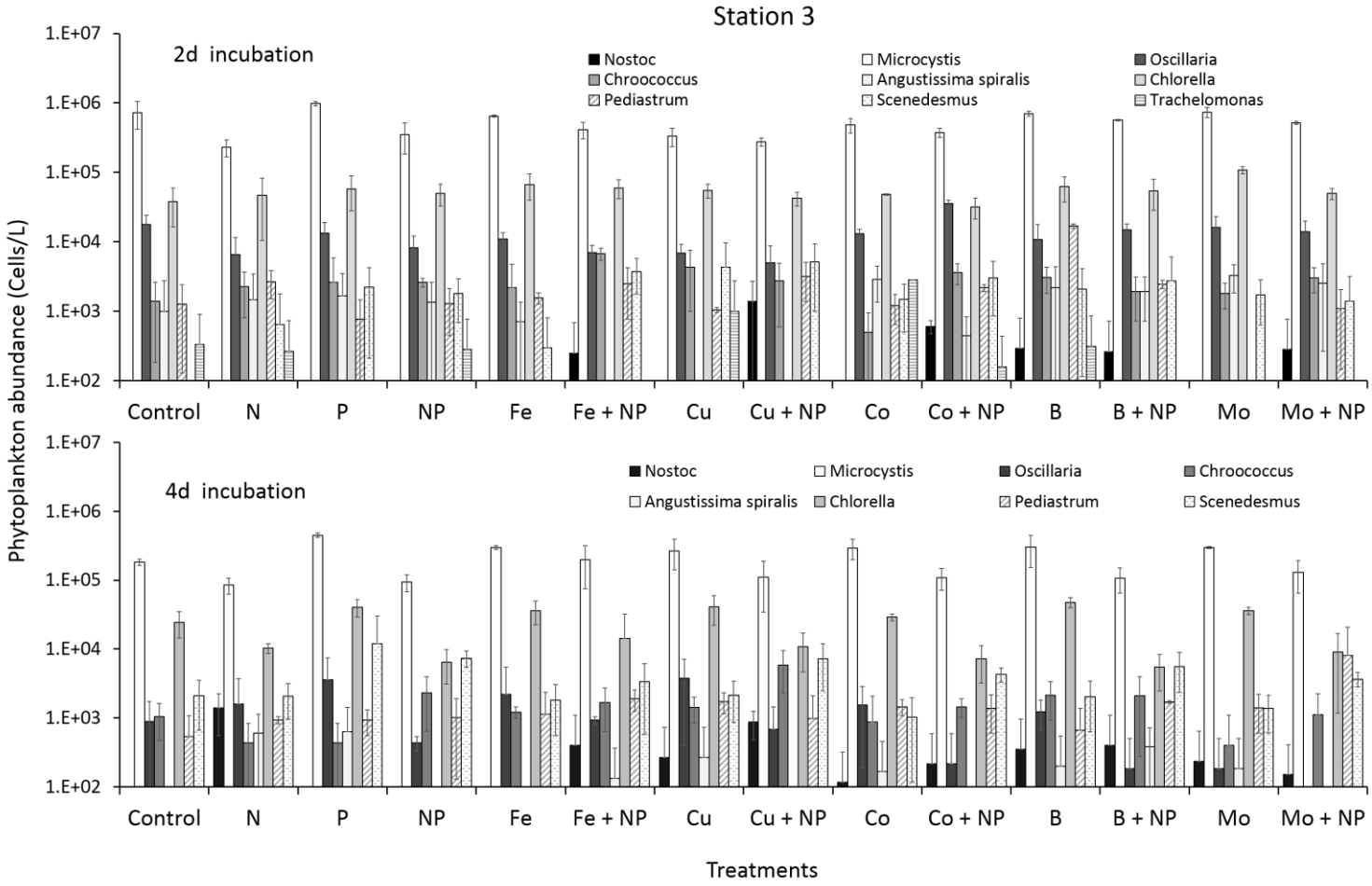

Figure 7-9. Bar charts showing the change of phytoplankton abundance in Station 3 as a function of treatment and treatment time.

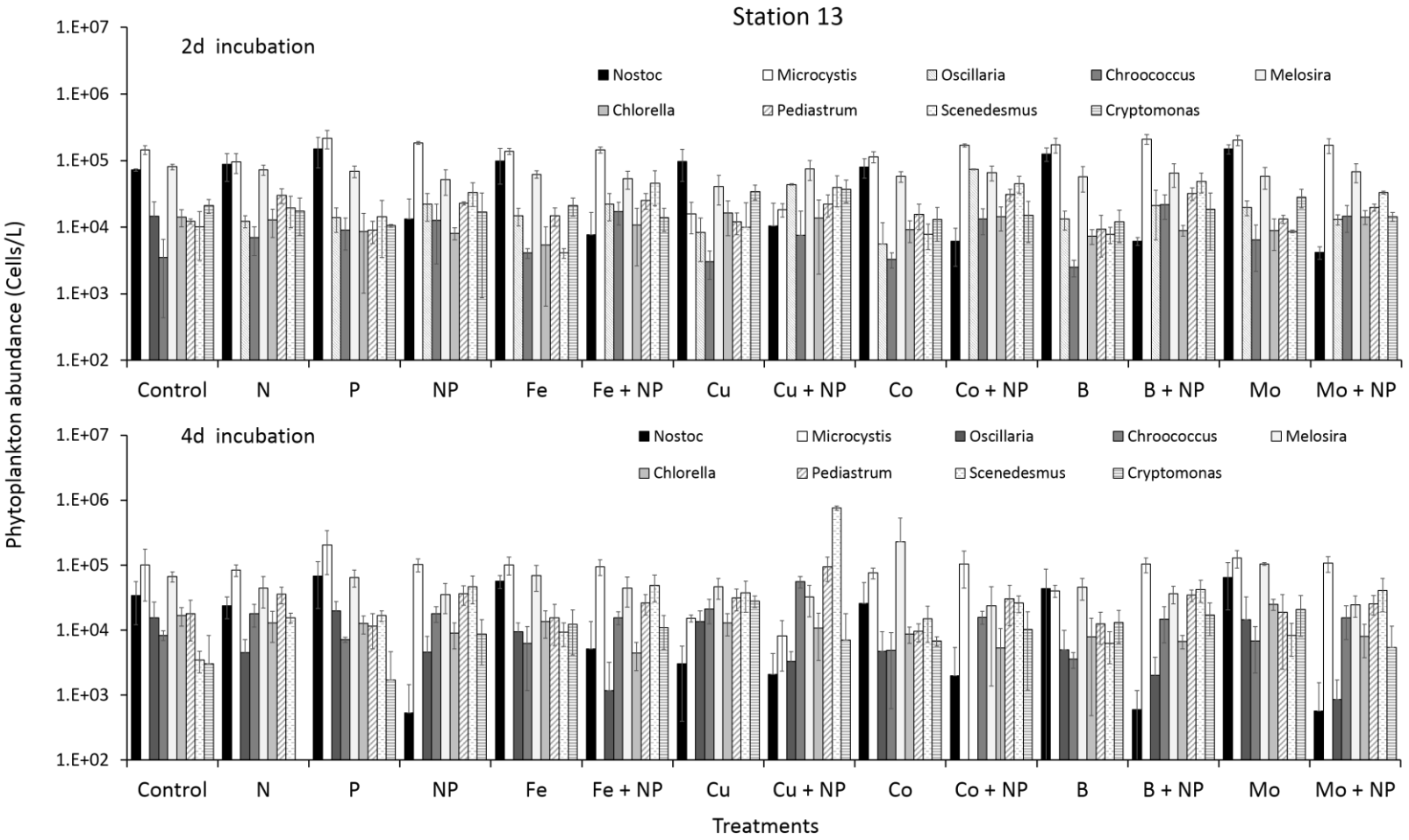

Figure 7-10. Bar charts showing the change of phytoplankton abundance in Station 13 as a function of treatment and treatment time.

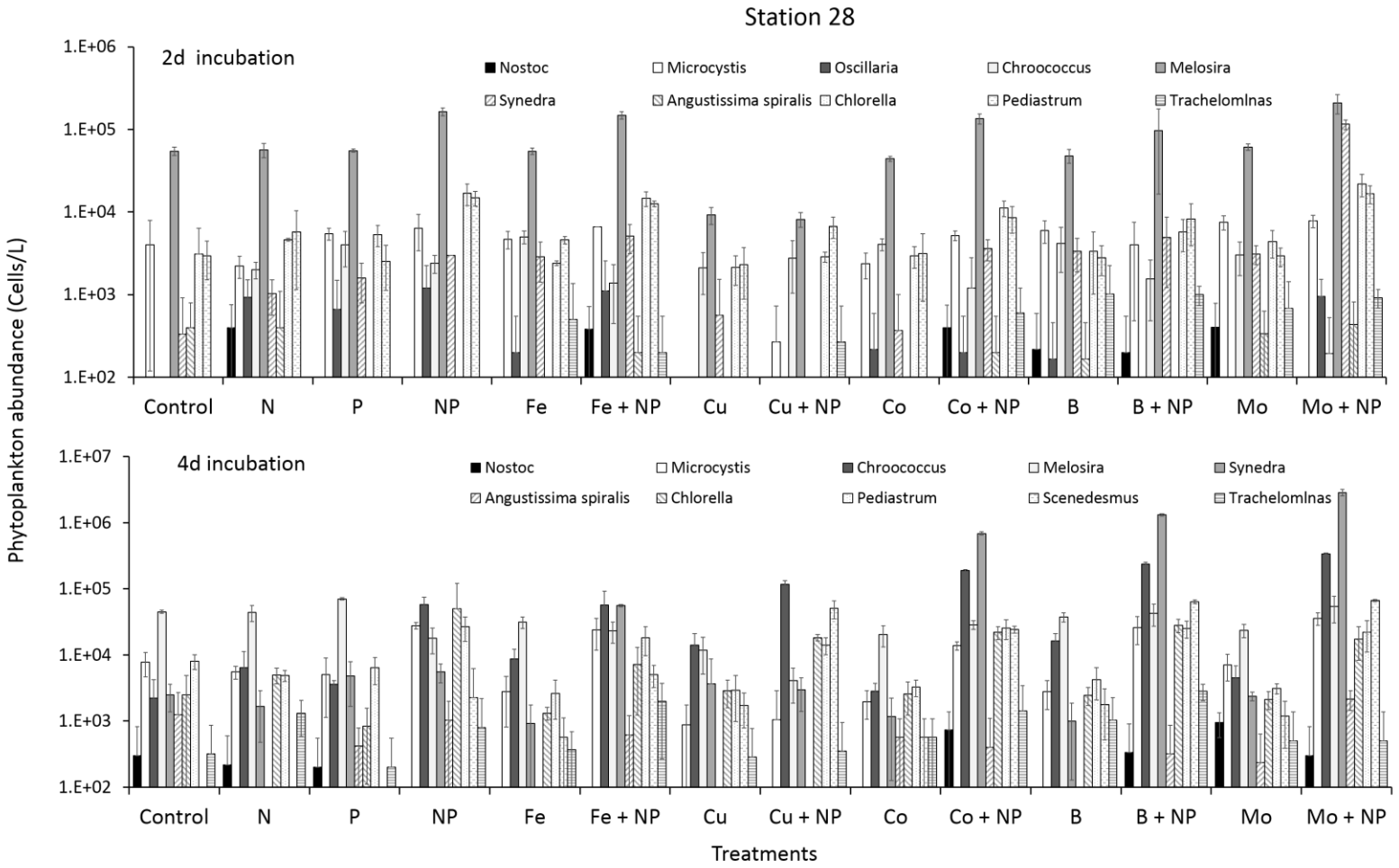

Figure 7-11. Bar charts showing the change of phytoplankton abundance in Station 28 as a function of treatment and treatment time.

The stairstep pattern of Cyanophyta > Bacillariophyta > Chlorophtya in the initial water persisted in the control over 4 days, however the percentage of cyanophytes in the control shifted from 81% *Nostoc* spp./7% *Microcystis* spp. initially to 19% *Nostoc*/39% *Microcystis* by day 2 (12% *Nostoc*/37% *Microcystis* by day 4). This transition from *Nostoc* to *Microcystis* occurred in all treatments as well with varying percentages. The stairstep distribution was observed for the all non-NP treatments in day 2. For NP treatments, by day 2 there was a consistent increase of Chlorophtya relative to Bacillariophyta, with abundance of chlorophtyes being similar or exceeding that of bacillariophytes, a shift which continued to day 4 when all NP/MN+NP treatments save Cu+NP were dominated by cyanophytes, however chlorophytes had become more abundant than bacillariophytes. The change for Cu+NP was dramatic with Chlorophyta becoming 89%, a strikingly apparent visual change under the microscope. Also, by day 4, the most abundant form of cyanophyte was *Chroococcus* spp. for Cu+NP, *Scenedesmus* spp. abundance was 78%, over four times that of any other treatment. For Stations 3 and 13, *Chroococcus* abundance only reached double digits for Cu (Station 3 and 13) and Cu+NP in Station 13. Notable changes in phytoplankton assemblages in single MN treatments were observed for Cu and Co. In the case of Cu, by day 4 the pattern mimicked that of Cu+NP wherein chlorophytes were dominant, followed by cyanophytes (most common form *Chroococcus*), then bacillariophytes. For Co, by day 4 Bacillariophyta became the most abundant type outnumbering Cyanophyta.

For Station 28 the dominant algae in the water column initially were bacilliarophytes (*Melosira* spp., 77%, see Figure 7-11), with another 11 and 4% respectively of cyanophytes and chlorophytes (Figure 7-8). For most treatments,

the pattern of abundance was Bacillariophyta/*Melosira*, followed by Cyanophyta or Chlorophyta. In some cases (control, N, NP, Fe+NP, Cu, Cu+NP, Co+NP, B+NP, Mo+NP) Chlorophyta were more prevalent than Cyanophyta. Cyanophytes were mostly *Microcystis*, except for Cu/Cu+NP, the only treatments that had double-digit abundance of *Chroococcus* (13%). The day 2 total counts for both Cu and Cu+NP were lower than for any other treatment, and Cu+NP was the only treatment wherein chlorophytes dominated (followed by Bacillariophyta, then Cyanophyta). For the original Station 28 water, the small amount of chlorophytes present was equally distributed between *Chlorella* and *Pediastrum* spp. By day 2, the proportion was the same for Cu, and Cu+NP had twice the amount of the latter as the former – by day 4 Cu+NP Chlorophyta was dominated by *Scenedesmus* spp. (24%), the only treatment to have more than 4%. The pattern of abundance by phylum was not greatly changed by day 4 for some treatments, (control, N, P, all of the single MN treatments except for Cu). For NP, Fe+NP and Cu+NP, cyanophytes had become the dominant species, also having a high abundance in Cu, and for NP and Cu+NP Bacillariophyta became a minor component. The treatments NP, Fe+NP, Cu, and Cu+NP at day 4 were the only ones to have *Chroococcus* spp. ~30% or greater (30, 29, 37, 56% respectively, see Figure 7-11). The treatments Co+NP, B+NP, and Mo+NP all showed a similar pattern at 4 days (Bacillariophyta dominant, followed by Cyanophyta, then Chlorophyta) with relatively elevated total counts. These treatments were also distinguished by relatively high amounts of *Synedra* spp. (69, 75, and 84%, respectively, averaging > 2.5 times the highest of all other treatments, see Figure 7-11).

Results from count data are in general accord with Chl-a data in that Station 3 is relatively static, and for Stations 13 and 28 more and varied changes occur,

reflecting potentially complicated succession patterns that depend on the relative distribution of the different species at the start of my experiments and how each respond to treatment. Chlorophyta or Bacillariophyta are able in some cases to expand at the expense of Cyanophyta (for Cu/Cu+NP and Co in Station 13). The most notable change occurring for Stations 13 and 28 is for Cu treatment, singly or with NP. For both stations much higher amounts of *Pediastrum* and/or *Scenedesmus*, species thought to be relatively more tolerant and/or needing Cu (Bilgrami and Kumar 1997; Merchant 1998) appear by day 4 for Cu+NP and to a lesser extent Cu. For Station 13, *Microcystis* diminishes from day 2 to day 4 for Cu/Cu+NP, whereas the opposite occurs for Station 28. The largest increases for *Microcystis* in Station 28 occur for NP, Fe+NP, Cu, and Cu+NP. In view of the relative sensitivity of *Microcystis* to Cu (Horne and Goldman 1974; Zeng et al. 2010), the potential role of Cu and Fe affecting the bioavailability of each other (as discussed for Chl-a above), the lower amount of Fe in the ambient water of Station 28, and the contrasting effect of Cu/Cu+NP on *Microcystis* in Stations 13 versus 28, this again raises the question of to what extent changes seen for Cu relate to Fe. The present results also underscore the desirability of trying to understand how MNs affect succession patterns.

7.5 Flow Cytometry Analysis to Determine Changing Characteristics of Algal Populations

FCM is a promising tool to study changes in size, abundance and community composition. I used FCM in two ways: 1) for univariate analysis, performing estimation of biovolumes and analysis of the FL3/Chl-a channel in comparison to bulk Chl-a analysis, and 2) for data-driven multivariate analysis. Univariate

analysis of FCM data focused on two indicators: FSC and FL3. Per the method of Li and Dickie (2001), I use the FSC signal to estimate a mean equivalent spherical diameter, from which an estimated spherical volume is calculated for each cell, and the sum of all cellular biovolumes is taken as an estimate of the total relative biovolume. As discussed by Dickie and Li, there are various contributors to uncertainty in such an estimation, such as differences in shape and refractive index of cells and uncertainty in size calibration for the flow cytometer. While some uncertainties might cancel, some might propagate, and it is important to keep in mind that this is an estimate. For FL3, this is the channel that is most typically associated with Chl-a fluorescence. For each sample, I summed the total FL3 signal and compare this to results for bulk Chl-a analysis. I wanted to see how these two compare, however, I did not automatically anticipate a correlation due to known changes in fluorescence and photosystem properties for algae under different environmental conditions (Oukarroum 2016).

Figure 7-12 shows results for both univariate analyses, with the sum of end-systolic volume (Σ ESV) versus Chl-a for all stations in the left-hand column and the sum of FL3 versus bulk Chl-a in the right-hand column. Concerning ESV, my hypothesis prior to doing the analysis was that this should show a better correlation for Station 3 than for the other two stations because Station 3 is the least diverse, being primarily constituted of *Microcystis* spp. Further, I hypothesised that, if correlations would be observed, the correlation would be likely better at 2 days than 4 days, as with longer time there might be more differentiation of algae based on treatment effects. The outcome of analysis of ESV was as anticipated, though the correlations were stronger than I expected, and that Station 13 would show as strong of a correlation at 2 days as Station 3 was

unexpected, particularly given the nature of uncertainties in ESV. For both Stations 3 and 13, the correlation is strong on day 2, and much less apparent on day 4. In the case of Station 3, if the treatments NP and Cu+NP are omitted from the group, the correlation is less than for day 2, however still respectable (R^2 = 0.73 on day 4 versus 0.81 for day 2). Without omitting these two treatments, the correlation effectively disappears (R^2 = 0.20). These two treatments did show as being distinct in behavior in terms of Chl-a and cluster analysis. Cook's distance, to measure the influence of individual data points in regression (Mendenhall and Sincich 1996), was calculated. Based on a cut-off of 1 (Cook and Weisberg 1982) the values for NP and Cu+NP are not exceptionally influencing; based on an alternate cut-off of 4/n, there is some difference (Bollen and Jackman 1990); for the limited number of points, the idea that there is a correlation in day 4 should be viewed with caution. Similarly, I find that for Station 13 correlations appear to exist if the treatments are split into two groups: NP/MN+NP and the remainder, and these groups display different behaviors based on other analyses. Grouped together, there is no correlation, hence the trends shown in Figure7-12 for Station 13 on day 4 for the two groups are to be viewed with caution as well. For Station 28, there is no correlation at either time, however, consistent with hypotheses, the apparent scatter in these bivariate plots increases from day 2 to day 4, as treatments show increasing differentiation in response.

Results in Figure7-12 for Chl-a versus FL3 are largely confirmatory to what might be expected. For Station 3, the correlation between Chl-a and FL3 is strong on day 2 (R^2 = 0.81), with a general trend such that more nutritive treatments (N, NP+MN+NP lie at the high endpoint and the remaining treatments at the low endpoint). By day 4 there is a narrow range of values for both Chl-a and FL3,

leading to a clustered appearance in the plot. Taken with other results, this appears likely a result from all treatments having reached limitations to growth. Station 13 shows strong correlations for both day 2 and 4 and in both cases the trend of more nutritive treatments lying at the high endpoint and the remaining treatments at the low endpoint. For Station 28 there are apparent correlations that might be viewed instead potentially as artifacts. Rather than having an actual distribution of values across two endpoints, as for Station 3, day 2, and Station 13, days 2 and 4, the apparent correlations for Station 28 appear to result from two clusters at each endpoint. I note that the apparent correlation shown for Station 28, day 4, results only with deletion of the Cu+NP treatment, which, whether the correlation shown is viewed as an artifact or not, with a Cook's distance of > 2 and taken in the context of the other data, Cu+NP is clearly different in response from other treatments.

Taken together, the results for Chl-a versus FL3 indicate that treatments do cause increasing differentiation over time, and photosystems changes as a result of treatment, i.e. the types of changes that would disrupt potential correlations between Chl-a and FL3, are only potentially in play for Station 28. Further, as the clustering and count results indicate that significant changes are occurring in both algal assemblages and population distribution among growth stages, it is not clear that photosystems changes or large changes in pigment production as a function of growth phases need be invoked to explain the lack of clear correlations for Station 28.

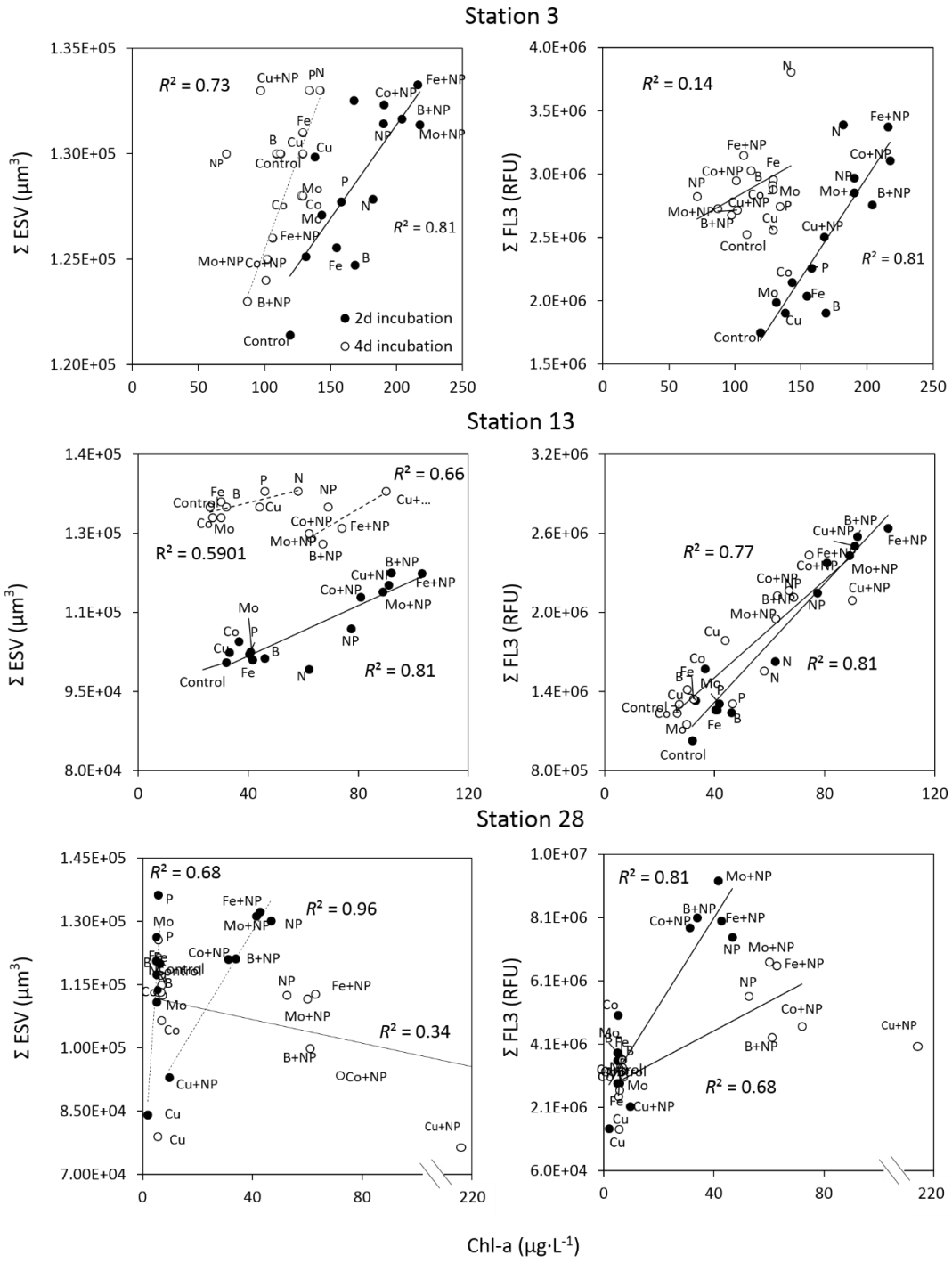

Figure 7-12. Scatter plots showing Chl-a versus univariate FCM data. ESV is derived from FSC in the left-hand column and FL3/Chl-a fluorescence in the right-hand column.

Recently there has been a great deal of effort put into development of techniques to automate the identification of individual populations or groups of cells in mixtures analysed by flow cytometry using clustering algorithms for handling large multivariate data sets (Johnsson et al. 2016). These clustering algorithms

are fundamental in the quest to automate analysis of FCM data (Johnsson et al. 2016). Cluster specification may be determined by, for example, use of a distance function (Euclidean or Mahalanobis), which may in some cases be sensitive to the multi-dimensional "shape" of clusters, or alternately density-based clustering, which can find oddly shaped clusters but it not ideal when populations of varying density occur together (Han et al. 2011). In algal research, as with analyst-driven gating methods, the focus is to "tune" clustering or filtering in such a manner as to successfully identify specific phyta or even species of interest (Dennis et al. 2011; Franklin et al. 2010; Peniuk et al. 2016). When using an algorithm, the algorithm no "preconceived" notion of differentiating, for instance, *Microcystis* spp. from *Chlorella* spp., meaning is not imposed on the results but rather needs to be derived from results. Working with one of the collaborators on my project, I tried a number of algorithms for analysis of FCM data, both data-driven algorithms and algorithms that rely on assumptions or prior knowledge of the data (other methods included *k*-means and DBSCAN, FlowClust, RTAC, and SamSPECTRAL, see Busam et al. 2007; Han et al. 2011; Lo et al. 2008; Zare et al. 2010). Some of these either split the data into overly spheroid multi-dimensional clusters or appeared to produce results that did not perform in a reproducible manner across treatments, stations, and sampling periods. The data-driven approach that I used, FlowMerge, is more robust to handling difficult clustering issues in FCM to provide a final number of clusters most likely representing the number of different types of cells or populations that are "separable"/distinct in a sample (Finak and Gottardo 2011), and on testing proved to be superior in consistent clustering reproducibility across treatments, stations, and sampling

periods. In choosing to use FlowMerge, I opted for a conservative approach that would not overly split clusters.

To perform clustering, I took FCM data files and visually inspected bivariate plots, confirming a large number of changes as a function of time and treatment. Next, I performed clustering on each data file. Clusters are characterised in terms of cluster centers, which is the average value of each of the FCM channels for a given cluster (FSC, SSC, FL1/caroteniod, FL2/PE, FL3/Chl-a, FL4/APC). For the triplicate samples, the average proportion of each cluster and value of each FCM channel was plotted as a function of time. Three main types of cluster, "Cluster 1" (C1), "Cluster 2" (C2), and "Cluster 3" (C3), occurred reproducibly. I found that C1 and C2 were detected in most samples. C1 is characterised by, relative to the other clusters, a high SSC to FSC ratio and very low FL values across all channels. C2 has, relatively, a high FSC to SSC ratio and moderate FL across all channels. C3 is a cluster that appears in many treatments at days 2 and 4, and is characterised by having smaller FSC than C2, smaller SSC than C1, and FL generally higher than C1 but lower than C2. Often, the FlowMerge algorithm (Finak and Gottardo 2011) that I used identified many more clusters than these three, however, as some of these do not appear with high frequency, represent very small proportions of the sample, and often do not cluster repeatedly across replicate samples, I do not discuss them further.

Figure 7-13 shows some representative FCM contour plots, how these compare to cluster plots (the total number of bivariate plots was 3825; see Figure 7-14 for additional selected examples showing more variation in structure), and some

examples of how clusters change as a function of time (see Figures 7-15 to 7-17 for the full 63 plots of this data).

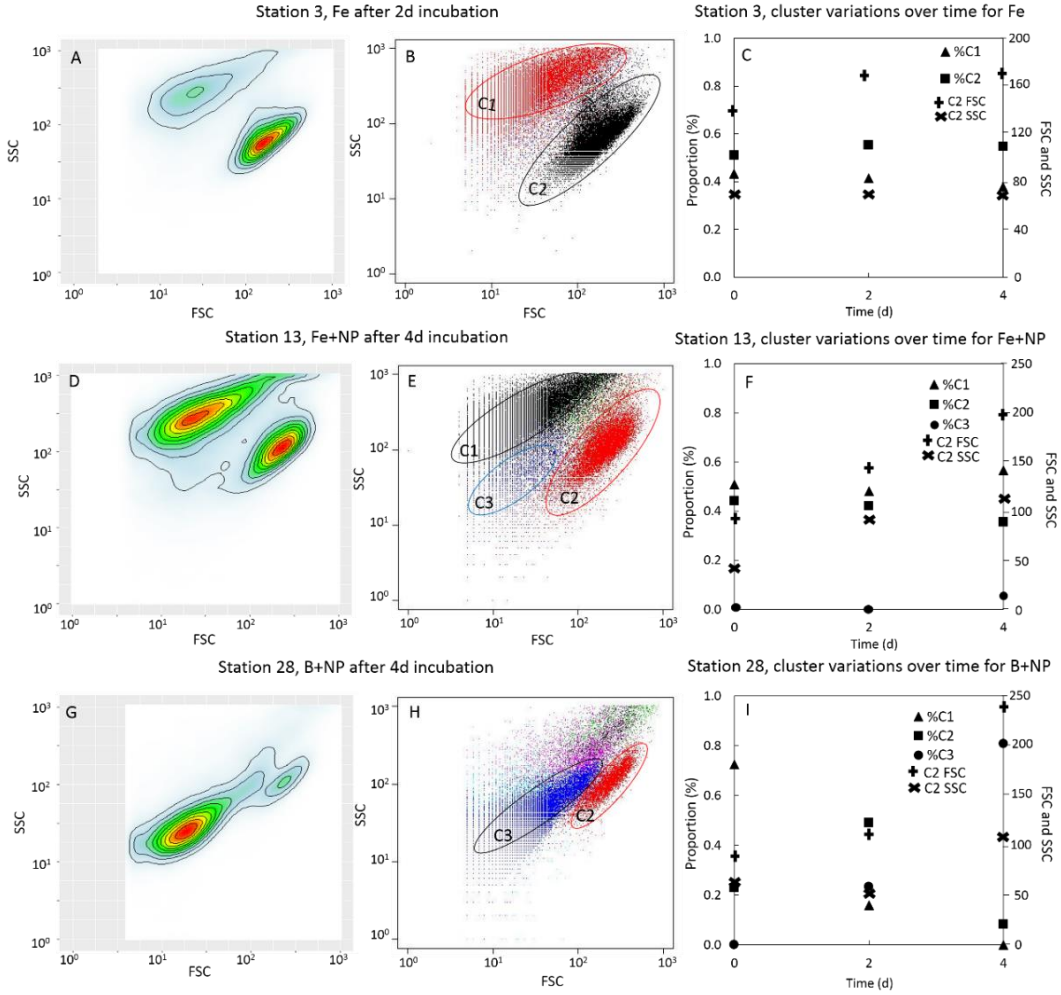

Figure 7-13. Examples of plots from FCM results including bivariate contour plots (panels, A, D, and G), bivariate cluster plots (panels B, E, and H), and plots of cluster variations over time for different treatments (panels C, F, and I). Panels A-C, show plots for Station 3, Fe treatment; this treatment is an example with cells distributed across C1 and C2. Panels D-F, show plots for Station 13, Fe+NP treatment; in this plot C1, C2, and a small C3 are present. Panels G-I, show plots for Station 28, B+NP treatment; this is an example wherein C1 is absent (in multivariate space, which is not necessarily obvious in bivariate space), C2 is small, and C3 is well developed. For panels C, F, and I, FSC and SSC is only shown for one cluster for plot clarity.

Examination of the bivariate contour plots that I constructed in comparison to clustering data suggests that for C1, and especially C2, there might be more

structure in some results than are differentiable by the data-driven clustering approach that I chose. These "buried clusters" likely represent different algal species/phyla (Dennis et al. 2011; Franklin et al. 2010; Peniuk et al. 2016). Regarding C1, FCM reports of features with very low fluorescence for algal samples describe these features in two ways: near zero fluorescence that is characteristic of bacterial heterotrophs, and very low fluorescence signals from algal sources such as debris, or compromised cells that have variously been described as shrunken cells with high granularity/SSC, cells that have lost membrane integrity or cells that have been verified to be dead (Huang et al. 2015; Lopes da Silva et al. 2018; Wang et al. 2016).

For those samples dominated by C1 and C2 (e.g. the initial water samples) C2 is everything else, i.e. predominately cells in the exponential or stationary phase of growth. I observed that C3 is not present in Stations 3, 13, or 28 initially and is only present in some of the day 2 and day 4 samples for which active growth is likely occurring. SSC may increase disproportionately to FSC for dead or dying cells, however for growing cells FSC and SSC are expected to increase together (larger objects scatter more than smaller in the forward and side directions). It is also possible that internal cell structure changes cause variations in SSC signal. Overall, C3's modest FSC, SSC, and FL signatures imply small, but living, cells – the small FSC denoting small(er) relative size, small SSC resulting from smaller side scatter of a small object, and small FL resulting from a smaller volume of pigment contained in small cells. I posit that C3 is newly divided or induction/early exponential phase cells.

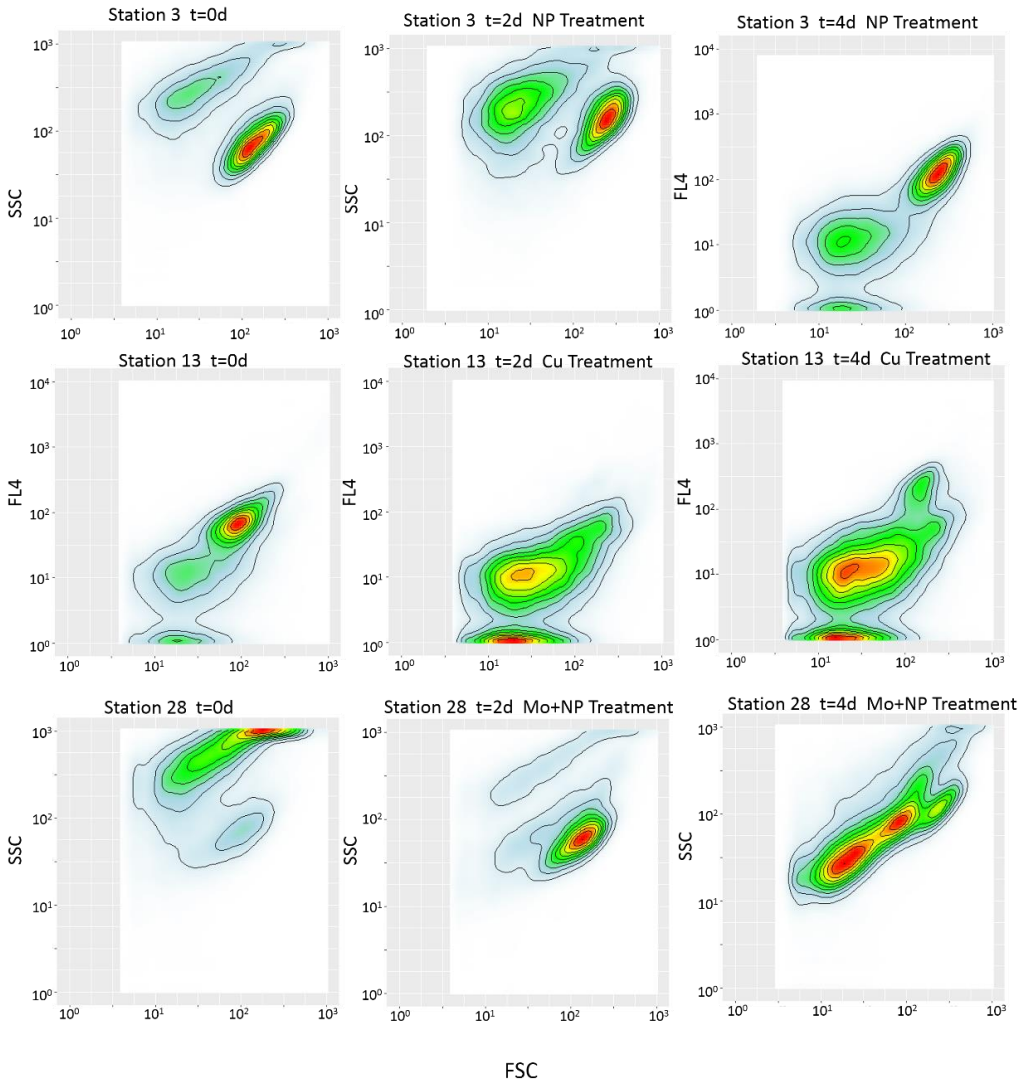

Figure 7-14. Additional selected contour plots for different treatments in different stations.

Clustering results for Station 3 shows the least variability (for greater detail on clustering results, see Figure 7-15). The proportions of C1 initially are 43% and appear to change in two groups. For NP and all MN+NP, the C1 proportion increases by ~6% overall, and the remaining treatments follow the control with the C1 proportion decreasing by ~5% overall. While these are small changes, they appear consistent with microscopic analysis performed in the course of collecting count data for which at day 4 some samples exhibited the appearance of less colorful and/or degraded/fragmented algal cells.

For C2, by day 4, P and single MN treatments have increased in proportion by a small amount (5-10%), while N, NP and NP+MN treatments see overall a slight decrease over this time (the biggest loss is 12% for NP). The decreases in proportions for C2 NP and MN+NP are reflected in the appearance of C3 for these treatments, however, the proportions of C3 for Station 3 are small (maximum 4-6% by day 4). The C3 cluster appears in day 2 for N, NP, Cu+NP, and B+NP, whereas by day 4, C3 has increased for N, NP, Cu+NP, and B+NP and additionally appears for the remaining MN+NP treatments, Fe+NP, Co+NP, and Mo+NP. The highest proportion of C3 is NP, which is the treatment that had notably low bulk Chl-a by day 4. I initially thought that the bulk Chl-a analysis was reflective of an accelerated onset of senescence for NP, however, the FCM results for C3 suggest that instead the appearance of very low bulk Chl-a in day 4 for NP may be related to this treatment's having the highest loss of C2 for NP (the most fluorescent cluster) and greatest gain of C3. The bulk Chl-a for Cu+NP in day 4 was lower than that for NP; while Cu+NP retained a greater proportion of C2 cells, the FL3 (Chl-a) and FL4 channels were relatively flat for this treatment over 4 days in contrast to the other MN+NP treatments. If taken as a group, for C1 the N, NP/MN+NP FSC and SSC are on average slightly smaller than for the remaining treatments (on average 8%), and fluorescence changes even less. Changes for C2 are more pronounced. Over 4 days the C2 FSC, SSC, and FL channels increase for N, NP/MN+NP by 25, 85, and 43%, respectively, as a group average. Over the same time, fluorescence, particularly for FL3 and FL4, is static or decreasing for the other treatments.

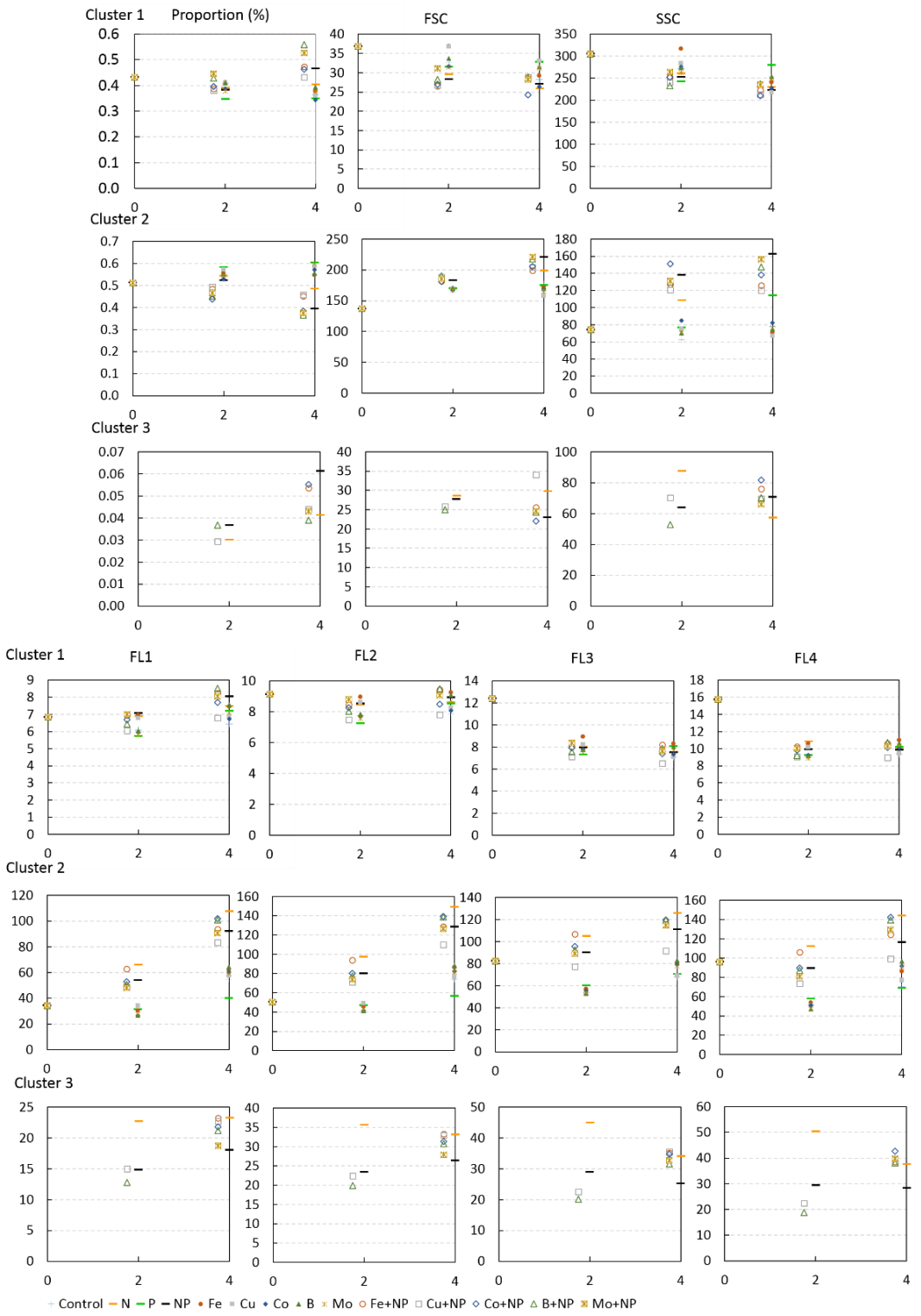

Figure 7-15. Plots from cluster analysis results showing changes in clusters C1, C2, and C3 over time for Station 3. Note, some treatments are plotted at 1.75 and 3.75 days, respectively, instead of 2 and 4 days in order to improve visibility of symbols.

The treatment Cu+NP is unusual in that for FL3 and FL4 its behaviour is more like the non-NP treatments. These averages are for purposes of illustration, however,

there is some variability between the behaviour of different treatments, probably in part as a result of C3 appearing for some N, NP/MN+NP treatments in day 2 and for others in day 4. I note, relative to the discussion for Cu+NP below, that Cu+NP is the only cluster that shows a consistent rise in FSC and all FL channels between day 2 and day 4. The clustering results for Station 3, taken together, are consistent with a picture of nutrient treatment causing modest growth (increases in C2, appearance of C3) for many treatments, with the NP, to a lesser extent N, treatments showing greater changes. Generally, the greater recruitment into C3 by day 4 is associated with larger diminution in Chl-a by day 4.

Figure 7-16 shows details on FL3 versus Chl-a and how Chl-a relates to clustering results. The initial proportion of C1 is similar to Station 3 at 51%, and changes to C1 are also similar as for Station 3 in that changes for the most part are modest and largely not notable except that SSC varies greatly, and not systematically, among treatments. The proportions for C2 increase by ~12% for N over 4 days, while remaining near static for the single MN treatments (minus Cu), and decreasing slightly (6-8%) for NP and the MN+NP treatments (minus Cu+NP).

By day 4, the proportion of C2 in Cu and Cu+NP treatments has decreased by 30 and 32%, respectively, which are the only treatments to have proportions of C2 less than the control. Only 20% of the Cu treatment population is in C2 by day 2. By day 2, C3 appears for NP, B+NP, and Cu+NP, and by day 4, C3 appears for the remaining MN+NP clusters and Cu, with proportions increasing slightly for NP and B+NP. The proportion of all C3 clusters except Cu and Cu+NP is ~5%, whereas for Cu and Cu+NP it is 10% and 28%, respectively.

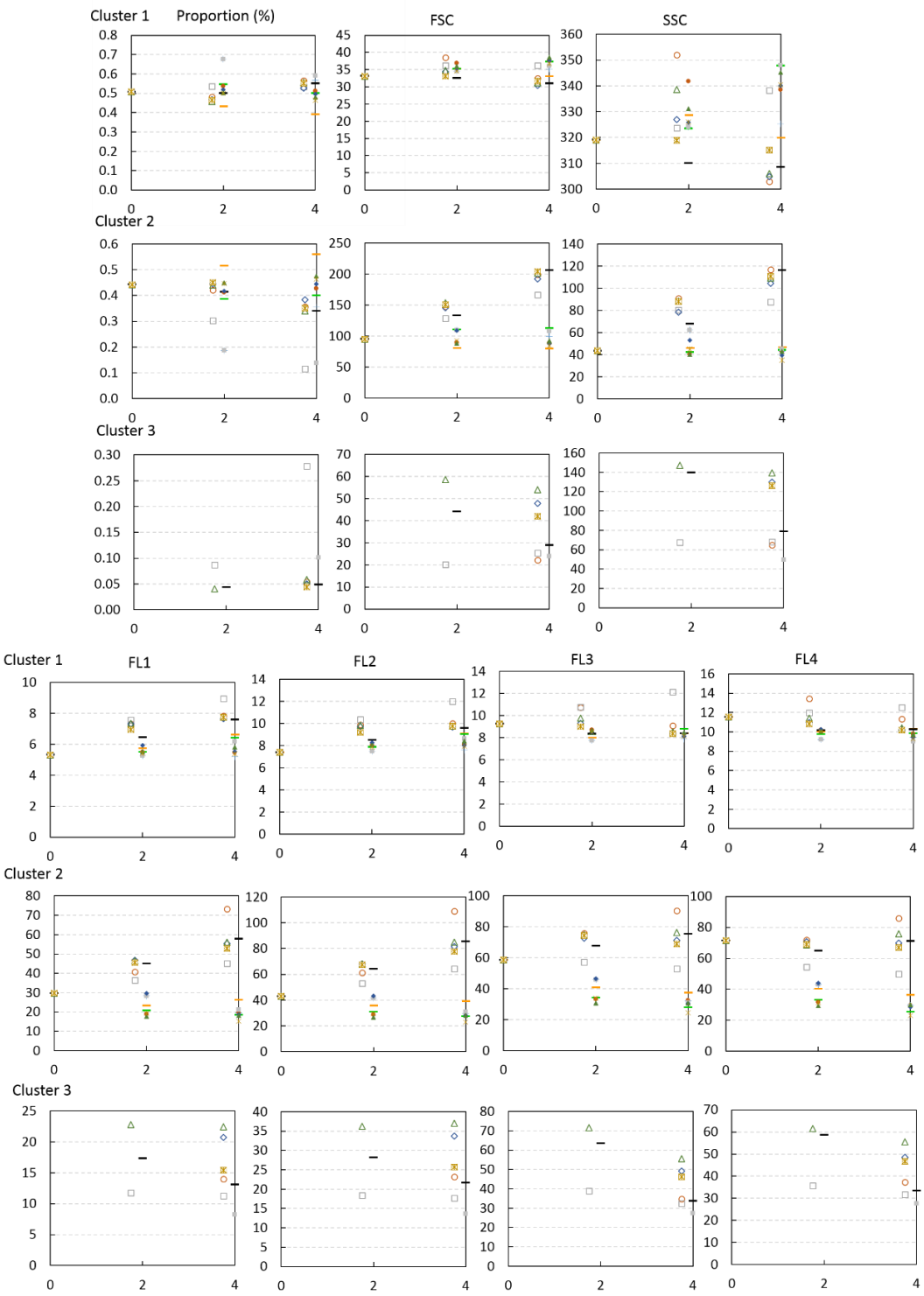

Figure 7-16. Plots from cluster analysis results showing changes in clusters C1, C2, and C3 over time for Station 13. Note, some treatments are plotted at 1.75 and 3.75 days, respectively, instead of 2 and 4 days to improve visibility of symbols.

As with Station 3, it appears that losses in C2 translate to gains in C3. For C2 FSC and SSC are relatively static, except for NP/MN+NP treatments for which FSC and

SSC increase linearly over 4 days. Fluorescence signal is decreasing over 4 days for all but the NP/MN+NP treatments. The proportion of C3 for most treatments is small, however, the appearance of C3 corresponds with a small decrease in bulk Chl-a between day 2 and day 4. Overall, the results from clustering are consistent with the idea that C2 is viable cells that are experiencing nutrient-stimulated growth. The treatments Cu and Cu+NP treatments are unusual in having very high proportions of C3, for which the FSC and FL values are lower than for C2, hence based on the results for NP in Station 3, for which a higher proportion of C3 for NP was associated with a lower bulk Chl-a, it seems that bulk Chl-a would be expected to decrease for Cu and Cu+NP by day 4 for Station 13, and I do see some decrease for Cu. However, the ratio of the fluorescence intensity of C2 to C3 is on average 63% greater for Station 13 than Station 3, which may explain why the bulk Chl-a results do not reflect the higher proportion of C3 for Station 13 Cu and Cu+NP treatments.

For Station 28 (see Figure 7-17), the initial proportion of C1 is 73% and diminishes during treatment much more strongly in comparison to Stations 3 and 13. By day 4, C1 had disappeared for the treatments Co, Co+NP, B, B+NP, and Mo+NP. For all other treatments save N and P, the C1 proportion diminished to < 10%, with N having the highest proportion of C1 at ~16%. This diminution of C1 is most obviously countered by the largest relative increases in Chl-a content from bulk analysis for Station 28. The changes in proportion for C2 are most extreme of the three stations and are mirrored by C3. Proportions change for the control as well, implying that the change in environmental conditions inherent in sampling and redeployment in the cubitainers had an effect on the algae in the control sample. Over the first two days of treatment, proportions of C2 decrease

from 23% to 4-6% for Cu and Cu+NP, remain in the region of starting conditions for P, and for all other treatments a marked increase in the proportion of C2 by an integer factor of 2-3 is observed. Concomitantly by day 2, C3 appears in all treatments except P (for which C3 appears in day 4), however, the proportions of C3 for Cu and Cu+NP (60 to 70%) are twice that of the remaining treatment C3s (11-29%). By day 4, for N, P, Fe, Co, B, and Mo, the proportions of C2 remain high (46 to 66%), whereas the proportions of C2 for NP, Fe+NP, Co+NP, B+NP, and Mo+NP have decreased and are low (6 to 12%), and C2 has disappeared for Cu and Cu+NP. These changes are strongly mirrored in C3; proportions for C3 in day 4 are low for N, P, Fe, Co, B, and Mo (25 to 33%, in contrast to higher proportions for C2 this group), are high for Cu, Cu+NP, NP, Fe+NP, Co+NP, B+NP, and Mo+NP (65-80%, in contrast to low proportions of C2 for this group), and for Cu and Cu+NP, the high proportions of C3 in day 2 increase further to day 4, and C2 disappears for these treatments by day 4. For C2, over four days the FSC of all treatments save Cu and Cu+NP increase, with the group NP, Fe+NP, Co+NP, B+NP, and Mo+NP having FSCs about double the remaining treatments. The SSC follows a similar trend of grouping, however increases more than a factor of two for NP, Fe+NP, Co+NP, B+NP, and Mo+NP and remains flat or decreases slightly for the remainder. The C2 FL channels show similar trends as for FSC, albeit fluorescence shows overall slight decreases for the lower FSC group, while the higher FSC group shows strong increases in all FL channels. The changes in FSC, SSC and FL for C3 are most complex. Generalising, C3 N, P, and all of the single MN treatments do not show marked changes in FSC, SSC, or FL, and FL is lowest and steady across fluorescence channels for Cu. The remaining treatments are variable. For NP, Co+NP, B+NP and Mo+NP, C3 FL decreases (all channels) to a greater or lesser

degree from day 2 to day 4. Only Cu+NP shows a consistent increase in FL from day 2 to day 4, and across all channels. FSC decreases from day 2 to day 4 for Co+NP, B+NP, and Mo+NP. For NP and Fe+NP, FSC increases, however, the largest relative increase by far is for Cu+NP, for which FSC increases by a factor of approximately 2.5 from day 2 to day 4. Large changes in SSC are not observed except for Cu+NP, which increases by a factor of > 4.

Clustering results are consistent with other results, however provide a different perspective. For example, NP in Station 3, Cu/Cu+NP in Stations 13 and 28, and Co+NP, B+NP, and Mo+NP in Station 28 show distinct differences in Chl-a and/or counts that are also apparent in clustering. Notably, Cu+NP behaviour was different in clustering across all stations, and the behaviour, particularly for Station 28, suggests that this treatment is causing a rapid diminution in standing stocks (C2) with rapid new growth (C3) thereafter. I have speculated that the effect of Cu might relate to Fe bioavailability, however, the clustering result suggests another possibility: Cu-sensitive populations are inhibited while less Cu-sensitive populations obtain competitive advantage and grow rapidly in the presence of NP. This would be consistent with changes in assemblages seen from count data. For Station 13 Cu+NP did not favour *Microcystis*, however, for Station 28 it did. I have found only one report detailing longer-term studies on the effect of Cu addition (Zhao et al., 2009), and this report found that Cu does discourage cyanobacteria for a limited time, after which cyanobacterial HAB conditions return. The question of how Cu mediates shifts in assemblages, and whether this relates to Fe, is an interesting topic for further study.

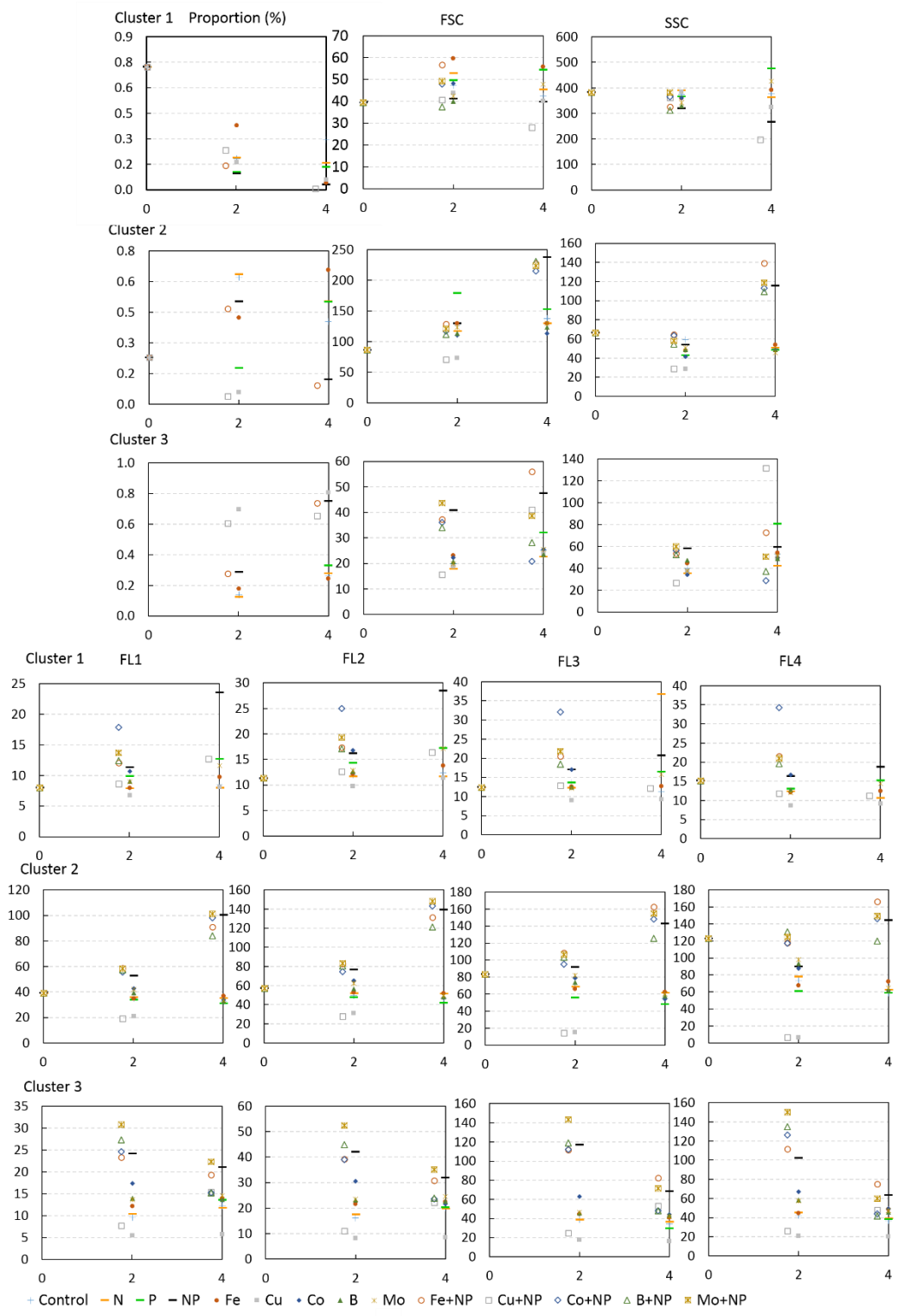

Figure 7-17. Plots from cluster analysis results showing changes in clusters C1, C2, and C3 over time for Station 28. Note, some treatments are plotted at 1.75 and 3.75 days, respectively, instead of 2 and 4 days to improve visibility of symbols.

As the use of a data-driven approach to FCM analysis of phytoplankton is new, I had no expectations about what I might find. I did not find linkages pointing to

contributions of species/phyta. This requires “authentic” samples, posing issues in terms of whether algal cultures are truly axenic, whether culture collection strains are representative of *in situ* counterparts, and whether the effect of distortions imposed by environmental conditions are mimicked in authentic samples. I did find that the results from clustering of FCM data are in many ways in accord with other findings for initial water quality, Chl-a changes, and changes in phytoplankton assemblage: Station 3 represents one endpoint in terms of initial water quality and shows the smallest overall changes in Chl-a and phytoplankton assemblages. Station 28 is in most ways the diametric opposite, with lower initial concentrations of most constituents analysed and having Chl-a and phytoplankton assemblages that changed the most, and quite variably, in response to treatment. Station 13 is intermediate to Stations 3 and 13. Based on my results, it would be reasonable to characterise response to treatment as what is mathematically referred to as an initial value problem – initial water quality parameters and phytoplankton assemblages determine the trajectory of change, and a change in the status quo can potentially result in dramatic outcomes (e.g. Cu+NP in Station 28). Given the high efficiency with which data-driven FCM can be performed, it would be of interest to pursue further studies in future to develop and better understand the utility of this approach.

7.6 Implications for Controlling Harmful Algal Blooms

The results presented here show that MN treatment effects on algae varied spatially and among algal groups in Taihu, with key points being as follows:

- There is a growing body of molecular biological data that documents homeostatic links between MNs (herein I discussed Fe and Cu) and possible mechanisms of molecular control of the bioavailability of MNs. Simultaneously, there is an emerging body of literature 1) documenting the importance of Fe in controlling algal phytoplankton growth, and 2) propounding the use of Cu as an algal biocide. Given the strong effects for Cu that I report here are mutually consistent through the Chl-a, count, and FCM data, and given that a role for Fe cannot be ruled out in causing these effects, more research into MNs and how they interact with N, P, and other MNs should be pursued to explore new interventions for effective management of HABs. Notably, the very nature of the "micro" in micronutrient may hold promise as being more amenable to intervention (for instance, to help one species outcompete another) over regional scales.

- In view of the stimulatory effect that Cu exhibited, inclusive of the cyanobacteria *Microcystis* spp., management of HABs with Cu as an algal biocide may be inadvisable. The data in my study are not sufficiently exhaustive to demonstrate that copper sulfate treatments, and the resulting copper concentrations in treated water, have the potential to promote *Microcystis* spp. growth, however, they do lend basis for invoking the best-practice Precautionary Principle in environmental management. A better understanding of the role of Cu in affecting algal phytoplankton is needed before implementing its widespread use in an environment where it might stimulate growth rather than retard it.

- Results from data-driven analysis of FCM are in accord with the Chl-a and counting data, and this approach holds promise for development of more efficient and reliable ways to investigate growth-related changes in algal communities.

8 CONCLUSIONS AND WIDER IMPLICATIONS

This chapter revisits and draws together the key findings of Chapters 3 to 7 and assesses the extent to which the key research questions (Chapter 1) have been addressed. Additionally, I consider the limitations of the work and its future potential.

8.1 SUMMARY AND CONCLUSIONS

Chapter 3: Whole-cell bioreporters and risk assessment of environmental pollution: A proof-of-concept study using lead

In this chapter my goal was to see if bioreporter results would agree with results from speciation modelling, as this agreement is what would be needed in order to use bioreporter endpoints in ERA. To within current standards of accuracy, my results in this study demonstrate that bioreporter combined with speciation modelling is certainly suitable for extension to larger scale ERA. These results were an important first step to taking my work further.

Chapter 4: The Effect of DOM in Taihu on Pb binding

Having achieved very promising results in the first part of the study, my original plan was to extend the approach to a regional scale in Taihu and perform model validation studies. Initial attempts failed, and it appeared that the manner in which DOM is specified in the speciation models was the cause. Therefore, I had to redesign and add a new part to the study to see if I could find a way to account for DOM variability in speciation modelling. Based on the approach that I designed to determine site-specific binding characteristics for Pb-DOM, I demonstrated that, indeed, the K_{cond} for Pb-DOC binding in Taihu varied over two orders of magnitude at the time of sampling, consistent with my hypothesis that high variability in K_{cond} was responsible for my problems with speciation model validation. Since the trends that I observed in my site-specific measured K_{cond} for Pb-DOC binding varied in a manner consistent with what I knew of the field site, I was optimistic that the values could lead to a more accurate modelling result. Furthermore, the fluorescence-based approach I designed for the investigation of DOM properties and K_{cond} for Pb-DOM binding is simple, rapid, and can be conducted in a high throughput format, which is highly attractive for ERA and makes it a suitable approach to account for DOM variability in ERA modelling.

Chapter 5: New approach to regional streamlined risk assessment

After I determined, through the work described in Chapter 4, that my problems with regional-scale validation of ERA models was likely due to problems in how models specified DOM, the next step was to return to the issue of model validation. Now I also needed to alter the models in order to answer my fundamental

question about how using a bioreporter in conjunction with standard modelling approaches would perform in a freshwater ERA context. For this work, I compared a one-size-fits-all approach to Pb-DOM complexation to different methods of implementing site-specific variations in modelling. I improved the procedures to the speciation model and found model optimised results using the methods that I developed in Chapter 4 are much more accurate in their agreement with bioreporter-measured $C_{Pb^{2+}}$. With a 2,400 km^2 surface area, and a history of extreme impacts, Taihu is a suitable system for me to conclude that the streamlined approach to ERA that I developed has performed well in a first regional-scale freshwater demonstration.

Chapter 6: Risk assessment of Pb pollution in lake sediment

My initial project plan included studies on water/sediment interactions, which is interesting, complicated, and highly relevant to Taihu given its seasonally variable pH, the extreme sediment contamination in some regions, and the effect storms have on resuspension since it is a polymictic lake. These detailed studies were no longer feasible due to the delays caused by not being able to use one-size-fits-all speciation models for the aqueous-phase studies. An excellent opportunity arose through University of Liverpool collaborators to do studies on sediments from Brothers Water lake in the UK, a much simpler lake system that is severly impacted by centuries of Pb-mining in the immediate vicinity. In this work, I found that, for $C_{Pb}^{Tot,\ sed}$ variations from < 50 mg·kg^{-1} to > 10,000 mg·kg^{-1}, there was an inverse relationship between $C_{Pb}^{Tot,\ sed}$ and the percent bioavailable Pb in the tested samples, and that bioavailable Pb increase with increasing sand content and particle size, with a negative relationship to silt content. The relative

bioavailable Pb (in %) was low (averaging 4%), and the absolute bioavailable Pb averaged 35 mg·kg^{-1} (from ~1645 to ~1985 A.D.), compared to an average $C_{\mathrm{Pb}}^{\mathrm{Tot,\ sed}}$ of 1490 mg·kg^{-1} over the same period. Bioaccessible Pb will be higher than this, on the other hand, the infinite sink assumptions that I used to project bioaccessibility are not present in the natural environment. These results can offer a reference for government oversight on dealing with the Pb pollution in this and comparable lakes. One very interesting result was that the bioreporter is able to measure a much higher concentration of bioavailable Pb by direct contact with the sediment slurry than by indirectly measuring desorbed Pb in supernatant under the same conditions. This further demonstrates the advantage of using a biological rather than traditional chemical approach to measure metal bioavailability.

Chapter 7: Effect of micronutrients on algae and implications regarding the risk of harmful algal blooms

This work presented an opportunity to examine the effect of heavy metals/MNs in the environment from a different risk perspective, i.e. that of how MNs affect algae and potentially contribute to HAB formation. Investigations of HABs in lakes have been on-going for decades, and with Taihu being an important water source in China, HABs have aroused more and more attention. The absence of any significant focus on MNs potential as stimulating factor of HABs was both intriguing and challenging. My results show that MN effects on algae varied spatially and among algal groups in Taihu. Overall, the amounts of MN that I used are relatively low in the context of the anthropogenic impacts to Taihu, and I observed some effects that, to my knowledge, have not previously been reported,

particularly for Cu, which effect I could not rule out as being linked with Fe. My results show that it is important to further understand the effects of bioavailability of MNs to algae and factors such as links in homeostatic processes of multiple MNs (here Fe and Cu), for effective management of HABs. Given the stimulatory effect that Cu exhibited, inclusive of the cyanobacteria *Microcystis* spp., management of HABs with Cu as an algal biocide may be contraindicated.

8.2 Limitations and Further Work

The majority of my work centered on using bioavailability-based biological methods combined with speciation modelling to demonstrate an approach to streamlining ERA. Results for both water and sediments studies were highly promising, and in particular my regional-scale demonstration project well exceeded current applicable standards for accuracy. The major limitation to this work that I see is that the variation of DOM properties in natural aquatic systems strongly affects modelling metal-DOM interactions, which thereby affect the ERA conclusions, for instance in using modelling to set WQC. The fluorescence method I used in this study for the charactisation of DOC has been described by some as semi-quantitative. Even though, I found the method that I used is fit for regional-scale ERA in a first demonstration project, it is essentical to validate my work to a much larger scale. For the sediment work one limitation is that the sediment:solution ratio affects singal transmittance of the bioreporter luminescence and hence affects the detecion of bioavailavle Pb in the sediment, especially for the sediment with low $C_{\mathrm{Pb}}^{\mathrm{Tot,\ sed}}$. Therefore, future work is needed to further optimise the interplay between sediment:solution ratio, effective LOD, and $C_{\mathrm{Pb}}^{\mathrm{Tot,\ sed}}$.

I found statistically significant effects of limitation or co-limitation for B, Co, Cu and Fe on the stimulation of algal growth, though even for Mo there appeared in some cases to be shifts in algal assemblages related to Mo treatment. As the purpose of the initial study was to see if there would be observable effects, the major limitation in this work is lack of more detailed information about why and how MNs might affect HABs. Given the unusual results that I observed for Cu and the known homeostatic links between Cu and Fe, how Cu stimulates algal growth and how Cu affects the utilisation of Fe by phytoplankton needs to be further studied. I have found that results from data-driven analysis of FCM demonstrate that this approach holds promise for development of more efficient and reliable ways to investigate growth-related changes in algal communities. Due to the diversity of algal abundance/community composition and response to nutrients in different regions of Taihu, I conclude that a one-size-fits-all approach to management of HABs is arguably inappropriate for a system such as Taihu.

Some parts of my work have been published in highly respected journals (Environmental Pollution, Water Research), which means that my work has gained acceptance by academics. Meanwhile, my work is extensible for use in high throughput formats and in a cost-effective manner, which is highly attractive for ERA applications. Therefore, I believe that my work could be of great value for environmental practitioners in countries where bioavailability-based ERA is already accepted and in use. At the end of this thesis, I strongly urge all humans to stop consuming mindlessly and reducing the pollution on the earth. Fundamentally, while development of streamlined approaches to ERA are increasingly urgent, this is what, in environmental science, is referred to as an "end of the (waste) pipe" solution. I hope that my work nonetheless could raise

environmental awareness about the perils of the incessant human consumption that causes pollution and the need to reduce pollution at the source by reducing consumption.

9 LITERATURE CITED

Acosta JA, Jansen B, Kalbitz K, Faz A, Martínez-Martínez S (2011) Salinity increases mobility of heavy metals in soils. Chemosphere 85:1318–1324

Adams J (1988) Mines of the lake district fells. Dalesman, Lancaster

Adriano DC (2001) Trace elements in terrestrial environments: Biogeochemistry, bioavaibility, and risks of metals, second ed. Springer-Verlag, New York

Ahlström H, Cornell SE (2018) Governance, polycentricity and the global nitrogen and phosphorus cycles. Environ Sci Policy 79:54–65

Ahmed IA, Hamilton-Taylor J, Bieroza M, Zhang H, Davison W (2014) Improving and testing geochemical speciation predictions of metal ions in natural waters. Water Res 67:276–291

Al-Anizi AA, Hellyer MT, Zhang D (2014) Toxicity assessment and modelling of Moringa oleifera seeds in water purification by whole cell bioreporter. Water Res 56:77–87

Alboukadel K, Fabian M (2017) factoextra: Extract and visualize the results of multivariate data analyses. R package version 1.0.5. https://CRAN.R-project.org/package=factoextra.

Allison JD, Brown DS, Novogradac KJ (1991) MINTEQA2/PRODEFA2, a geochemical assessment model for environmental systems. : version 3.11. EPA/600/3-91/021, UEPA, Washington, DC

Anderson DM, Glibert PM, Burkholder JM (2002) Harmful algal blooms and eutrophication:Nutrient sources, composition, and consequences. Estuaries 25:704–726

Andersen RA (2005) Algal culturing techniques. 1st ed. Elsevier/Academic Press, Burlington, Massachusets

APHA (1995) Standard methods for the examination of water and wastewater, 19th ed. American Public Health Association American Water Works Association, Water Environment Federation, Washington, DC

Appleby PG, Nolan PJ, Gifford DW, Godfrey MJ, Oldfield F, Anderson NJ, Battarbee RW (1986) ^{210}Pb dating by low background gamma counting. Hydrobiologia 143:21–27

Arbildua JJ, Villavicencio G, Urrestarazu P, Opazo M, Brix KV, Adams WJ, Rodriguez PH (2017) Effect of Fe (III) on pseudokirchneriella subcapitata at circumneutral pH in standard laboratory tests is explained by nutrient sequestration. Environ Toxicol Chem 36:952–958

Attina TM, Trasande L (2013) Economic costs of childhood lead exposure in low- and middle-income countries. Environ Health Persp 121:1097–1102

Avio CG, Gorbi S, Milan M, Benedetti M, Fattorini D, d'Errico G, Pauletto M, Bargelloni L, Regoli F (2015) Pollutants bioavailability and toxicological risk from microplastics to marine mussels. Environ Pollu 198:211–222

Axler RP, Gersberg RM, Goldman CR (1980) Stimulation of nitrate uptake and photosynthesis by molybdenum in Castle Lake, California. Can J Fish Aquat Sci 37:707–712

Azhar N, Ashraf MY, Hussain M, Hussain F (2006) Phytoextraction of lead (Pb) by EDTA application through sunflower (Helianthus annuus L.) cultivation: Seedling growth studies. Pak J Bot 38:1551–1560

Baken S, Degryse F, Verheyen L, Merckx R, Smolders E (2011) Metal complexation properties of freshwater dissolved organic matter are explained by its aromaticity and by anthropogenic ligands. Environ Sci Technol 45:2584–2590

Baker A (2001) Fluorescence excitation-emission matrix characterization of some sewage-impacted rivers. Environ Sci Technol 35:948–953

Baker A, Ward D, Lieten SH, Periera R, Simpson EC, Slater M (2004) Measurement of protein-like fluorescence in river and waste water using a handheld spectrophotometer. Water Res 38:2934–2938

Baptista MS, Vasconcelos MT (2006) Cyanobacteria metal Interactions: requirements, toxicity, and ecological implications. Crit Rev Microbiol 32: 127–137

Barsanti L, Gualtieri P (2010) Algae: anatomy, biochemistry, and biotechnology, 2nd ed. Taylor & Francis Group/CRC Press, Boca Raton, Florida

Bashashati A, Brinkman RR (2009) A survey of flow cytometry data analysis methods. Adv BMC 2009:120–138

Baudry JP, Raftery AE, Celeux G, Lo K, Gottardo R (2010) Combining mixture components for clustering. J Comput Graph Sta 19:332–353

Bayer TK, Schallenberg M, Martin CK (2008) Investigation of nutrient limitation status and nutrient pathways in Lake Hayes, Otago, New Zealand: A case study for integrated lake assessment. New Zeal J Mar Fre Res 42:285–295

Belkin S (2003) Microbial whole-cell sensing systems of environmental pollutants. Curr Opin Microbiol 6:206–212

Benedetti MF, Riemsdijk WHV, Koopal LK (1996) Humic substances considered as a heterogeneous donnan gel phase. Environ Sci Technol 30:1805–1813

Benton TG, Solan M, Travis JMJ, Sait SM (2007) Microcosm experiments can inform global ecological problems. Trends Ecol Evol 22:516–521

Berman-Frank I, Cullen JT, Shaked Y, Sherrell RM, Falkowski PG (2001) Iron Availability, Cellular Iron Quotas, and Nitrogen Fixation in Trichodesmium. Limnol Oceanogr 46:1249–1260

Bertani G (2004) Lysogeny at mid-twentieth century: P1, P2, and other experimental systems. J Bacteriol 186:595–600

Berthon G (1995) The stability constants of metal complexes of amino acids with polar side chains. Pure Appl Chem 67:1117–1240

Besunder, J.R., Anderson, R.N., Super, D., 1996. Comparison of DMSA+EDTA vs. BAL+EDTA in lead (Pb) poisoned Children(C). Clin Pharmacol Ther 59:146–146

Bertilsson S, Jones Jr JB (2003) Supply of dissolved organic matter to aquatic ecosystems: autochthonous sources. In: Findlay SEG, Sinsabaugh RL (eds), Aquatic ecosystems: interactivity of dissolved organic matter. Academic Press, Amsterdam, pp, 3–24

Biello D (2009) Can the world's most polluted places ever be cleaned?" (http://www.scientificamerican.com/podcast/episode.cfm?id=can-the-worlds-most-polluted-places-09-10-29&SID=mail&sc=emailfriend).Scientific American. Retrieved 21 November 2013

Bilgrami KS, Kumar S (1997) Effects of copper, lead and zinc on phytoplankton growth. Biol Plantarum 39:315–317

Billington N (1991) A comparison of three methods of measuring phytoplankton biomass on a daily and seasonal basis. Hydrobiologia 226:1–15

Birdwell JE, Engel AS (2010) Characterization of dissolved organic matter in cave and spring waters using UV-Vis absorbance and fluorescence spectroscopy. Org Geochem 41:270–280

Blaurockbusch E (2014) Comparison of chelating agents DMPS, DMSA and EDTA for the diagnosis and treatment of chronic metal exposure. Brit J Med Med Res 4:1821–1835

Bo L, Wang D, Li T, Li Y, Zhang G, Wang C, Zhang S (2015) Accumulation and risk assessment of heavy metals in water, sediments, and aquatic organisms in rural rivers in the Taihu Lake region, China. Environ Sci Pollut Res 22:6721–6731

Boggs SJ, Livermore D, Seitz MG (1985) Humic substances in natural waters and their complexation with trace metals and radionuclides: a review. TRAIL 25:1-99

Boguta P, Pieczywek P, Sokołowska Z (2016) A comparative study of the application of fluorescence excitation-emission matrices combined with parallel factor analysis and nonnegative matrix factorization in the analysis of Zn complexation by humic acids. Sensors 16:1760

Boija S, Almesåker A, Hedenström E, Bylund D, Edlund H, Norgren M (2014) Determination of conditional stability constants for some divalent transition metal ion-EDTA complexes by electrospray ionization mass spectrometry. J Mass Spectrom 49:550–556

Bollen KA, Jackman RW (1990) Regression diagnostics: an expository treatment of outliers and influential cases. In: Fox J, Long JS (eds) Modern methods of data analysis. Sage Publications, Newbury Park, California, pp. 257–291

Bonilla I, Garcia-González M, Mateo P (1990) Boron requirement in cyanobacteria. Plant Physiol 94:1554–1560

Bontidean I, Mortari A, Leth S, Brown NL, Karlson U, Larsen MM, Vangronsveld J, Corbisier P, Csöregi E (2004) Biosensors for detection of mercury in contaminated soils. Environ pollut 131:255–262

Bradberry S, Vale A (2009) Dimercaptosuccinic acid (succimer; DMSA) in inorganic lead poisoning. Clin Toxicol 47:617–631

Brand LE (1991) Minimum iron requirements of marine phytoplankton and the implications for the biogeochemical control of new production. Limnol Oceanogr 36:1756–1771

Braud A, Geoffroy V, Hoegy F, Mislin GL, Schalk IJ (2010) Presence of the siderophores pyoverdine and pyochelin in the extracellular medium reduces toxic metal accumulation in Pseudomonas aeruginosa and increases bacterial metal tolerance. Environ Microbiol Rep 2:419–425

Bretz F, Hothorn T, Westfall PH (2011) Multiple comparisons using R. Chapman & Hall/CRC, Boca Raton, FL

Briggs D (2003) Environmental pollution and the global burden of disease. Brit Med Bull 68:1-24

Bro R (1997) PARAFAC. Tutorial and applications. Chemometr Intell Lab 38:149–171

Bruins MR, Kapil S, Oehme FW (2000) Microbial resistance to metals in the environment. Ecotoxicol Environ Safe 45:198–207

Busam S, Mcnabb M, Wackwitz A, Senevirathna W, Beggah S, van der Meer JR, Wells M, Breuer U, Harms H, Chem A (2007) Artificial neural network study of whole-cell bacterial bioreporter response determined using fluorescence flow cytometry. Anal Chem 79:9107–9114

Cabaniss SE (1992) Synchronous fluorescence spectra of metal-fulvic acid complexes. Environ Sci Technol 26:1133–1139

Camilleri JC, Ribi G (1986) Leaching of dissolved organic carbon (DOC) from dead leaves, formation of flakes of DOC, and feeding on flakes by crustaceans in mangroves. Mar Biol 91:337–344

Campbell BM, Beare DJ, Bennett EM, Hall-Spencer JM, Ingram JSI, Jaramillo F, Ortiz R, Ramankutty N, Sayer JA, Shindell D (2017) Agriculture production as a major driver of the Earth system exceeding planetary boundaries. Ecol Soc 22:8

Canaani OD, Gantt E (1980) Circular dichroism and polarized fluorescence characteristics of blue-green algal allophycocyanins. Biochem 19:2950–2956

Cao L, Wang W, Yang Y, Yang C, Yuan Z, Xiong S, Diana J (2007) Environmental impact of aquaculture and countermeasures to aquaculture pollution in China. Environ Sci Pollut Res Int 14:452–462

Cardinale BJ, Srivastava DS, Duffy JE, Wright JP, Downing AL, Sankaran M, Jouseau C (2006) Effects of biodiversity on the functioning of trophic groups and ecosystems. Nature 443:989–992

Carpenter SR (1996) Microcosm experiments have limited relevance for community and ecosystem ecology. Ecol 77:677–680

Carraway ER, Demas JN, DeGraff BA, Bacon JR (1991) Photophysics and photochemistry of oxygen sensors based on luminescent transition-metal complexes. Anal Chem 63:337–342

Carstea EM, Baker A, Bieroza M, Reynolds DM, Bridgeman J (2014) Characterisation of dissolved organic matter fluorescence properties by PARAFAC analysis and thermal quenching. Water Res 61:152–161

Catalán N, Obrador B, Felip M, Pretus JL (2013) Higher reactivity of allochthonous vs. autochthonous DOC sources in a shallow lake. Aquat Sci 75:581–593

Caussy D, Gochfeld M, Gurzau E, Neagu C, Ruedel H (2003) Lessons from case studies of metals: investigating exposure, bioavailability, and risk. Ecotoxicology and Environmental Safety 56, 45–51

Cavet JS, Borrelly GP, Robinson NJ (2003) Zn, Cu and Co in cyanobacteria: selective control of metal availability. FEMS Microbiol Rev 27P165–181

Celen I, Buchanan JR, Burns RT, Robinson RB, Raman DR (2007) Using a chemical equilibrium model to predict amendments required to precipitate phosphorus as struvite in liquid swine manure. Water Res 41:1689–1696

Chaffin JD, Bridgeman TB, Bade DL (2013) Nitrogen constrains the growth of late summer cyanobacterial blooms in Lake Erie. Adv Microbiol 3:16–26

Chakraborty P, Babu PVR, Acharyya T, Bandyopadhyay B (2010) Stress and toxicity of biologically important transition metals (Co, Ni, Cu and Zn) on phytoplankton in a tropical freshwater system: An investigation with pigment analysis by HPLC. Chemosphere 80:548–553

Chapman CS, Capodaglio G, Turetta C, Van den Berg CMG (2009) Benthic fluxes of copper, complexing ligands and thiol compounds in shallow lagoon waters. Mar Environ Res 67:17–24

Chen C, Jiang X, Zhan Y, Jin X, Zhao Z (2011) Speciation distribution and potential ecological risk assessment of heavy metals in sediments of Taihu Lake. China Environ Sci 31:1842–1848

Chen J, Wei D, Pohnert G (2017) Rapid estimation of astaxanthin and the carotenoid-to-chlorophyll ratio in the green microalga Chromochloris zofingiensis using flow cytometry. Mar Drugs 15:1–23

Chen KL, Elimelech M (2007) Influence of humic acid on the aggregation kinetics of fullerene (C 60) nanoparticles in monovalent and divalent electrolyte solutions. J Colloid Interf Sci 309:126

Chen W (2008) Analysis of the zooplankton. In: Qin B (ed), Lake Taihu, China: dynamics and environmental change, Springer, Dordrecht, pp, 254-264

Chen W, Wangersky PJ (1996) Rates of microbial degradation of dissolved organic carbon from phytoplankton cultures. J Plankton Res 18:1521–1533

Chen W, Westerhoff P, Leenheer JA, Booksh K (2003a) Fluorescence excitation-emission matrix regional integration to quantify spectra for dissolved organic matter. Environ Sci Technol 37:5701–5710

Chen Y, Fan C, Teubner K, Dokulil M (2003b) Changes of nutrients and phytoplankton chlorophyll- a in a large shallow lake, Taihu, China: an 8-year investigation. Hydrobiologia 506-509:273–279

Chen Y, Qin B, Teubner K, Dokulil MT (2003c) Long-term dynamics of phytoplankton assemblages: Microcystis-domination in Lake Taihu, a large shallow lake in China. J Plankton Res 25:445–453

Chetelat B, Liu CQ, Zhao Z, Wang Q, Li S, Li J, Wang B (2008) Geochemistry of the dissolved load of the Changjiang Basin rivers: anthropogenic impacts and chemical weathering. Geochim Cosmochim Ac 72:4254–4277

Chi Q, Zhu G, Langdon A (2007) Bioaccumulation of heavy metals in fishes from Taihu Lake, China. J Environ Sci 19:1500–1504

Chow CW, Fabris R, Drikas M (2004) A rapid fractionation technique to characterise natural organic matter for the optimisation of water treatment processes. J Water Supply Res T 53:85–92

Christensen JB, Botma JJ, Christensen TH (1999) Complexation of Cu and Pb by DOC in polluted groundwater : A comparison of experimental data and predictions by computer speciation models (WHAM and MINTEQA2). Water Res 33:3231–3238

Clifford M, Mcgeer JC (2010) Development of a biotic ligand model to predict the acute toxicity of cadmium to Daphnia pulex. Aquat Toxicol 98: 1-7

Coble P, Lead J, Baker A, Reynolds D, Spencer R (2014) Aquatic Organic Matter Fluorescence. In P. Coble, J. Lead, A. Baker, D. Reynolds, R. Spencer (eds.), Aquatic organic matter fluorescence (Cambridge Environmental Chemistry Series). Cambridge University Press, Cambridge

Coble PG (1996) Characterization of marine and terrestrial DOM in seawater using excitation-emission matrix spectroscopy. Mar Chem 51:325–346

Coble PG, Green SA, Blough NV, Gagosian RB (1990) Characterization of dissolved organic matter in the Black Sea by fluorescence spectroscopy. Nature 348: 432–435

Coles CA, Yong RN (2006) Humic acid preparation, properties and interactions with metals lead and cadmium. Eng Geol 85:26–32

Conley DJ, Paerl HW, Howarth RW, Boesch DF, Seitzinger SP, Havens KE, Lancelot, C, Likens GE (2009) Controlling eutrophication: nitrogen and phosphorus. Science 323:1014-1015

Cook RD, Weisberg S (1982) Residuals and influence in regression. Chapman & Hall, New York.

Correll DL (1998) Role of phosphorus in the eutrophication of receiving waters: A review. J Environ Qual 27:261–266

Cory RM, McKnight DM (2005) Fluorescence spectroscopy reveals ubiquitous presence of oxidized and reduced quinones in dissolved organic matter. Environ Sci Technol 39:8142–8149

Crea F, Falcone G, Foti C, Giuffrè O, Materazzi S (2014) Thermodynamic data for Pb^{2+} and Zn^{2+} sequestration by biologically important *S*-donor ligands, at different temperatures and ionic strengths. New J Chem 38:3973–3983

Critto A, Suter GW (2009) Environmental Risk Assessment. Encyclopedia of Corporate Social Responsibility 11:1027-1037

D'Andrilli J, Chanton JP, Glaser PH, Cooper WT (2010) Characterization of dissolved organic matter in northern peatland soil porewaters using ultra high resolution mass spectrometry. Org Geochem 41:791–799

Dang TC, Fujii M, Rose AL, Bligh M, Waite TD (2012) Characteristics of the freshwater cyanobacterium Microcystis aeruginosa grown in iron-limited continuous culture. Appl Environ Microbiol 78:1574

De Schamphelaere KA, Janssen CR (2002) A biotic ligand model predicting acute copper toxicity for Daphnia magna: the effects of calcium, magnesium, sodium, potassium, and pH. Environ Sci Technol 36:48–54

De Wever A, Muylaert K, Langlet D, Alleman L, Descy JP, André L, Cocquyt C, Vyverman W (2010) Differential response of phytoplankton to additions of nitrogen, phosphorus and iron in Lake Tanganyika. Freshwater Biol 53:264–277

De La Gala Morales M, Ariño C, Díaz-Cruz JM, Esteban M (2014) Study of the complexation of Pb(II) with meso-2,3- Dimercaptosuccinic Acid (DMSA) and 2,3-Dimercapto-1-propanesulfonic acid (DMPS) using a bismuth-bulk rotating disk electrode. Electroanal 26:1912–1919

Dee KT (2016) Dissolved organic carbon (DOC) characterisitics in metal-rich waters and implications for copper aquatic toxicity. Dissertation, Colorado School of Mines

Deepthike HU, Tecon R, Vankooten G, Van der Meer JR, Harms H, Wells M, Short J (2009) Unlike PAHs from Exxon Valdez Crude oil, PAHs from Gulf of Alaska coals are not readily bioavailable. Environ Sci Technol 43:5864–5870

Deforest DK, Santore RC, Ryan AC, Church BG, Chowdhury MJ, Brix KV (2017) Development of biotic ligand model-based freshwater aquatic life criteria for lead following US Environmental Protection Agency guidelines. Environ Toxicol Chem 36:2965–2973

Dennis MA, Landman M, Wood SA, Hamilton D (2011) Application of flow cytometry for examining phytoplankton succession in two eutrophic lakes. Water Sci Technol 64:999–1008

Desortová B (1981) Relationship between chlorophyll- a concentration and phytoplankton biomass in several reservoirs in Czechoslovakia. Int Rev Hydrobiol 66:153–169

Di Toro DM, Allen HE, Bergman HL, Meyer JS, Paquin PR, Santore RC (2001) Biotic ligand model of the acute toxicity of metals. 1. Technical basis. Environ Toxicol Chem 20: 2383–2396

Dick VP (1998) Applicability limits of Beer's Law for dispersion media with a high concentration of particles. Appl Opt 37:4998–5004

Ding Y (2009) Development of a whole-cell based biosensor technique for assessment of bioavailability and toxicity of heavy metals in soil. University of Bedfordshire

Dodds WK, Bouska WW, Eitzmann JL, Pilger TJ, Pitts KL, Riley AJ, Schloesser JT. Thornbrugh DJ (2009) Eutrophication of U.S. freshwaters: analysis of potential economic damages. Environ Sci Technol 43:12–19

Donoho DL (2000) High-Dimensional Data Analysis: The curses and blessings of dimensionality, Lecture delivered at the “Mathlathematical Challenges of the 21st Century” conference of The American Math. Society, Los Angeles, August 6-11

Downs TM, Schallenberg M, Burns CW (2008) Responses of lake phytoplankton to micronutrient enrichment: a study in two New Zealand lakes and an analysis of published data. Aquat Sci 70:347–360

Dreischuh T, Gateva S, Serafetinides A, Genova T, Borisova E, Zhelyazkova A, Semyachkina-Glushkovskaya O, Penkov N, Keremedchiev M, Vladimirov B (2015) 18th International School on Quantum Electronics: Laser physics and applications - excitation-emission matrices (EEMs) and synchronous fluorescence spectroscopy (SFS) investigations of gastrointestinal tissues. Proceedings of SPIE - The International Society for Optical Engineering 9447, 94470X-94470X-94476

Du YJ, Wei ML, Reddy KR, Liu ZP, Jin F (2014) Effect of acid rain pH on leaching behavior of cement stabilized lead-contaminated soil. J Hazard Mater 271:131–140

Duffy JE (2009) Why biodiversity is important to the functioning of real-world ecosystems. Front in Ecol Environ 7:437–444

Dzialowski AR, Wang SH, Lim NC, Spotts WW, Huggins DG (2005) Nutrient limitation of phytoplankton growth in central plains reservoirs, USA. J Plankton Res 27:587–595

Ebina J, Tsutsui T, Shirai T (1983) Simultaneous determination of total nitrogen and total phosphorus in water using peroxodisulfate oxidation. Water Res 17:1721–1726

Egorova LG (1972) Complex-forming properties of 2,3-dimercaptosuccinic acid. Complex formation of lead with dimercaptosuccinic acid stereoisomers. Khimiko-Farmatsevticheskii Zhurnal 42:2240–2245

Elser JJ, Bracken MES, Cleland EE, Gruner DS, Harpole WS, Hillebrand H, Ngai JT, Seabloom EW, Shurin JB, Smith JE (2007) Global analysis of nitrogen and phosphorus limitation of primary producers in freshwater, marine and terrestrial ecosystems. Ecol Lett 10:1135–1142

Esteves Da Silva JC, Machado AA, Oliveira CJ, Pinto MS (1998) Fluorescence quenching of anthropogenic fulvic acids by Cu(II), Fe(III) and UO_2^{2+}. Talanta 45:1155–1165

Evans JC, Prepas EE (1997) Relative importance of iron and molybdenum in restricting phytoplankton biomass in high phosphorus saline lakes. Limnol Oceanogr 42:461–472

Fairbrother A, Wenstel R, Sappington K, Woo W (2007) Framework for metals risk assessment. Ecotoxicol Environ Safe 68:145–227

Fairman R, Mead CD, Williams WP (1999) Environmental risk assessment: approaches, experiences and information, Environmental issue report No 4., EEA (European Environment Agency)

Fang F, Gao Y, Gan L, He X, Yang L (2018) Effects of different initial pH and irradiance levels on cyanobacterial colonies from Lake Taihu, China. J Appl Phycol 30:1–17

Fang X, Fernando Q (1995) Stereoisomeric selectivity of 2,3-dimercaptosuccinic acids in chelation therapy for lead poisoning. Chem Res in Toxicol 8:525–536

Fasurová N, Pospíšilová L (2010) Characterization of soil humic substances by ultraviolet-visible and synchronous fluorescence spectroscopy. Appl Mech Mate 303–306:2221–2226

Fellman JB, Hood E, Spencerc RGM (2010) Fluorescence spectroscopy opens new windows into dissolved organic matter dynamics in freshwater ecosystems: A review. Limnol Oceanogr 55:2452–2462

Finak G, Bashashati A, Brinkman R, Gottardo R (2009) Merging mixture components for cell population identification in flow cytometry. Adv BMC 2009:38–49

Finak G, Gottardo R (2011) FlowMerge: Cluster Merging for Flow Cytometry Data. R package version 2.28.0. http://www.bioconductor.org/packages/release/bioc/html/flowMerge.html

Finak G, Perez JM, Weng A, Gottardo R (2010) Optimizing transformations for automated, high throughput analysis of flow cytometry data. BMC 11:546

Flemer DA (1969) Chlorophyll analysis as a method of evaluating the standing crop of phytoplankton and primary productivity. Chesapeake Sci 10:301–306

Fowler RL (1987) Power and robustness in product-moment correlation. Appl Psych Meas 11:419–428

Franklin NM, Stauber JL, Lim RP (2010) Development of multispecies algal bioassays using flow cytometry. Environ Toxicol Chem 23:1452–1462

Fraser LH, Keddy P (1997) The rate of experimental microcosms in ecological research. Trends Ecol Evol 12:478–481

French CS, Young VK (1952) The fluorescence spectra of red algae and the transfer of energy from phycoerythrin to phycocyanin and chlorophyll. J Gen Physiol 35:873–890

Frenich AG, González FE, Juan AM, Vidal JM (2007) Thermodynamics, Solubility and Environmental Issues. Letcher TM (Ed) Thermodynamics, Solubility and Environmental Issues, Elsevier, Amsterdam, pp 429-444

Fu J, Hu X, Tao X, Yu H, Zhang X (2013) Risk and toxicity assessments of heavy metals in sediments and fishes from the Yangtze River and Taihu Lake, China. Chemosphere 93:1887–1895

Fu P, Mostofa KM, Wu F, Liu CQ, Li W, Liao H, Wang L, Wang J, Mei Y (2010) Excitation-emission matrix characterization of dissolved organic matter sources in two eutrophic lakes (Southwestern China Plateau). Geochem J 44:99–112

Fu P, Wu F, Liu C, Wang F, Li W, Yue L, Guo Q (2007) Fluorescence characterization of dissolved organic matter in an urban river and its complexation with Hg(II). Appl Geochem 22:1668–1679

Gauthier TD (2001) Detecting trends using Spearman's rank correlation coefficient. Environ Forensics 2:359–362

Ge Y, Ying G, Macdonald D, Sauvé S, Hendershot W (2005) Modeling of Cd and Pb speciation in soil solutions by WinHumicV and NICA-Donnan model. Environ Modell Softw 20:353–359

Gerloff GC (1968) The comparative boron nutrition of several green and blue-green algae. Physiol Plantarum 21: 369–377

Ghosh R, Banerjee DK (1997) Complexation of trace metals with humic acids from soil, sediment and sewage. Chem Spec Bioavailab 9:15–19

Glass JB, Wolfesimon F, Elser JJ, Anbara FD (2010) Molybdenum–nitrogen co-limitation in freshwater and coastal heterocystous cyanobacteria. Limnol Oceanogr 55:667–676

Goldman CR (1964) Primary productivity and micro-nutrient limiting factors in some North American and New Zealand lakes. Internationale Vereinigung für theoretische und angewandte Limnologie: Verhandlungen 15:365–374

Goldman CR (1966) Molybdenum as an essential micronutrient and useful watermass marker in Castle Lake, California, In Chemical Environment in the Aquatic Habitat, Proceedings I.B.P-Symposium, 10–16, October 1966, pp. 229–238.

Goldman CR (1972) The Role of Minor Nutrients in Limiting the Productivity of Aquatic Ecosystems. In: Likens GE (ed), Proceedings of the Symposium on Nutrients and Eutrophication:The Limiting-nutrient Controversy. Am Soc Limnol Oceanogr, pp. 21-41

Gong Z, Lin Z (2009) Strategy of flood control in Taihu Basin. In: Zhang C, Tang H (eds), Advances in water resources and hydraulic engineering. Proceedings of 16th IAHR-APD Congress and 3rd Symposium of IAHR-ISHS, Volume 6, Springer, Berlin, Heidelberg, pp. 1011–1016

Gough R, Holliman PJ, Cooke GM, Freeman C (2015) Characterisation of algogenic organic matter during an algal bloom and its implications for trihalomethane formation. Sustainability Water Qual Ecol 6:11–19

Grandjean P (2010) Even low-dose lead exposure is hazardous. Lancet 376:855–856

Grandjean P, Bellange M (2017) Calculation of the disease burden associated with environmental chemical exposures: application of toxicological information in health economic estimation. Environ Health 16:123

Grandjean P, Landrigan PJ (2014) Neurobehavioural effects of developmental toxicity. Lancet Neurol 13:330–338

Granéli E, Haraldsson C (1993) Can increased leaching of trace metals from acidified areas influence phytoplankton growth in coastal waters? Ambio 22:308–311

Guo L (2007) Doing Battle With the Green Monster of Taihu Lake. Science 317:1166

Gustafsson JP (2001) Modeling the acid-base properties and metal complexation of humic substances with the stockholm humic model. J Colloid Interf Sci 244: 102–112

Gustafsson JP (2011) Modelling lead (II) sorption to ferrihydrite and soil organic matter. Environ Chem 8:485–492

Gustafsson JP (2014) Visual MINTEQ ver. 3.1. vminteq.lwr.kth.se. Accessed February 2019

Haag D, Matschonat G (2001) Limitations of controlled experimental systems as models for natural systems: a conceptual assessment of experimental practices in biogeochemistry and soil science. Sci Total Environ 277:199–216

Haas AF, Wild C (2010) Composition analysis of organic matter released by cosmopolitan coral reef-associated green algae. Aquat Biol 10:131–138

Hallegraeff GM (1977) A comparison of different methods used for the quantitative evaluation of biomass of freshwater phytoplankton. Hydrobiologia 55:145–165

Hampel JJ, McCarthy MJ, Gardner WS, Zhang L, Xu H, Zhu G, Newell SE (2018) Nitrification and ammonium dynamics in Taihu Lake, China:seasonal competition for ammonium between nitrifiersand cyanobacteria. Biogeosciences 15:733–748

Han J, Kamber M, Pei J (2011) Data mining: concepts and techniques. Third Edition. Morgan Kaufmann Publishers, Chapter 10 and 12, 443–491 and 543–581

Hansen AM, Kraus TE, Pellerin BA, Fleck JA, Downing BD, Bergamaschi BA (2016) Optical properties of dissolved organic matter (DOM): Effects of biological and photolytic degradation. Limnol Oceanogr 61:1015–1032

Hao Y, Chen L, Zhang X, Zhang D, Zhang X, Yu Y, Fu J (2013) Trace elements in fish from Taihu Lake, China: Levels, associated risks, and trophic transfer. Ecotoxicol Environ Safe 90:89–97

Haraughty SJ, Burks SL (1996) Nutrient limitation in Lake Tenkiller, Oklahoma. J Freshwater Ecol 11:91–100

Harrell Jr FE, et al (2015) Hmisc: Harrell Miscellaneous. R package version 3.16-0. http://CRAN.R-project.org/package=Hmisc.

Harris WR, Chen Y, Stenback J, Shah B (1991) Stability constants for dimercaptosuccinic acid with bismuth(III), zinc(II), and lead(II). J Coord Chem 23, 173–186

Harvey F (2007) Planet's most polluted sites unveiled (https://www.ft.com/cms/s/0/1d4c0916-6156-11dc-bf25-0000779fd2ac.html). The Financial Times

Havens KE, Fukushima T, Xie P, Iwakuma T, James RT, Takamura N, Hanazato T, Yamamoto T (2001) Nutrient dynamics and the eutrophication of shallow lakes Kasumigaura (Japan), Donghu (PR China), and Okeechobee (USA). Environ Pollut 111:263–272

He XS, Xi BD, Zhang ZY, Gao RT, Tan WB, Cui DY, Yuan Y (2015) Composition, removal, redox, and metal complexation properties of dissolved organic nitrogen in composting leachates. J Hazard Mater 283:227–233

Heibati M, Stedmon CA, Stenroth K, Rauch S, Toljander J, Säve-Söderbergh M, Murphy KR (2017) Assessment of drinking water quality at the tap using fluorescence spectroscopy. Water Res 125:1–10

Heijerick DG, De Schamphelaere KA, Van Sprang PA, Janssen CR (2005) Development of a chronic zinc biotic ligand model for Daphnia magna. Ecotox Environ Safe 62:1–10

Helwig NE (2019) Multiway: Component models for multi-way data. https://CRAN.R-project.org/package=multiway.

Hill MK (2010) Understanding environmental pollution. Cambridge University Press

Horne AJ, Goldman CR (1974) Suppression of nitrogen fixation by blue-green algae in a eutrophic lake with trace additions of copper. Science 183:409–411

Huang F, Dang Z, Guo CL, Lu GN, Gu RR, Liu HJ, Zhang H (2013) Biosorption of Cd(II) by live and dead cells of *Bacillus cereus* RC-1 isolated from cadmium-contaminated soil. Colloid Surfac B 107:11–18

Huang H, Xiao X, Anas G, Wu J, Nie Z, Peng C, Xu X, Shi J (2015) Effects of natural flavonoids on photosynthetic activity and cell integrity in Microcystis aeruginosa. Toxins 7:66–80

Huang W (2004) The pollutant budget in Lake Taihu. In Qin B, Hu W, Chen W (eds), Process and mechanism of environmental changes of Lake Taihu. Science Press, Beijing, pp, 21–28 (in Chinese)

Huber W, Carey VJ, Gentleman R, Anders S, Carlson M, Carvalho BS, Bravo HC, Davis S, Gatto L, Girke T (2015) Orchestrating high-throughput genomic analysis with Bioconductor. Nat Methods 12:115–121

Hudson N, Baker A, Reynolds D (2007) Fluorescence analysis of dissolved organic matter in natural, waste and polluted waters-a review. River Res Appl 23:63–649

Huguet A, Vacher L, Relexans S, Saubusse S, Froidefond JM, Parlanti E (2009) Properties of fluorescent dissolved organic matter in the Gironde Estuary. Organic Geochem 40:706–719

Hyenstrand P, Rydin E, Gunnerhed M, Linder J, Blomqvist P (2001) Response of the cyanobacterium Gleotrichia echinulata to iron and boron additions – an experiment from Lake Erken. Freshwater Biol 46:735–741

Ibrahim IAA (2015) Chemical characterization and mobility of metal species in fly ash-water system. Water Sci 29:109–122.

ISO (1992) Water quality measurement of biochemical parameters spectrophotometric determination of chlorophyll-a concentration. Ginebra, International Organization for Standardization, pp. 1–6

Ivanikova NV, McKay RML, Bullerjahn GS, Sterner R (2007) Nitrate utilisation by phytoplankton in Lake Superior is impaired by low nutrient (P, Fe) availability and seasonal light limitation– a cyanobacterial bioreporter study. J Phycol 43:475–484

Ivask A, Green T, Polyak B, Mor A, Kahru A, Virta M, Marks R (2007) Fibre-optic bacterial biosensors and their application for the analysis of bioavailable Hg and As in soils and sediments from Aznalcollar mining area in Spain. Biosens Bioelectron 22:1396–1402

Izenman AJ (2008) Modern multivariate statistical techniques: regression, classification, and manifold learning. In: Casella G, Fienberg S, Olkin I (eds) Springer Texts in Statistics Series. Springer Science+Business Media, New York, pp, 633-666

Jackson JA (1997) Glossary of Geology. In: Jackson JA (ed), 5th revised and enlarged edn. Springer, Berlin

Jaffé R, Boyer J, Lu X, Maie N, Yang C, Scully N, Mock S (2004) Source characterization of dissolved organic matter in a subtropical mangrove-dominated estuary by fluorescence analysis. Mar Chem 84:195–210

Jaffé R, Cawley KM, Yamashita Y (2014) Applications of excitation emission matrix fluorescence with parallel factor analysis (EEM-PARAFAC) in assessing environmental dynamics of natural dissolved organic matter (DOM) in aquatic environments: a review. In: Fernando RO (ed), Advances in the physicochemical characterization of dissolved organic matter: impact on natural and engineered systems, ACS 1160:27–73

Janssen CR, Heijerick DG, De Schamphelaere KAC, Allen HE (2003) Environmental risk assessment of metals: tools for incorporating bioavailability. Environ Int 28:793–800

Jessup CM, Kassen R, Forde SE, Kerr B, Buckling A, Rainey PB, Bohannan BJM (2004) Big questions, small worlds: microbial model systems in ecology. Trends Ecol Evol 19:189–197

Jia J, Li H, Zong S, Jiang B, Li G, Ejenavi O, Zhu J, Zhang D (2016) Magnet bioreporter device for ecological toxicity assessment on heavy metal contamination of coal cinder sites. Sensor Actuat B Chem 222:290–299

Jiang X, Wang W, Wang S, Zhang B, Hu J (2012) Initial identification of heavy metals contamination in Taihu Lake, a eutrophic lake in China. J Environ Sci 24:1539–1548

Jin Z, Cheng H, Chen L, L X, Zhu G, Zhuang G, Qian N (2010) Concentrations and contamination trends of heavy metals in the sediment cores of Taihu Lake, East China, and their relationship with historical eutrophication. Ac Geochim 29:33–41

Johnsson K, Wallin J, Fontes M (2016) BayesFlow: latent modeling of flow cytometry cell populations. BMC Bioinformatics 17:25

Johnstone TC, Nolan EM (2015) Beyond iron: non-classical biological functions of bacterial siderophores. Dalton Trans 44:6320–6339

Joumard R, Chiron M, Delsey J, Lambert J (1983) Lead file: car fuel additives. Costs 29:68

Juneja A, Ceballos RM, Murthy GS (2013) Effects of environmental factors and nutrient availability on the biochemical composition of algae for biofuels production: a review. Energies 6:4607–4638

Källqvist T, Meadows BS (1978) The toxic effect of copper on algae and rotifers from a Soda Lake (Lake Nakuru, East Africa). Water Res 12:771–775

Karline S (2017) plot3D: Plotting multi-dimensional data. R package version 1.1.1. https://CRAN.R-project.org/package=plot3D.

Kessler N, Schauer JJ, Yagur-Kroll S, Melamed S, Tirosh O, Belkin S, Erel Y (2012) A bacterial bioreporter panel to assay the cytotoxicity of atmospheric particulate matter. Atmos Environ 63:94–101

Khokhotva O, Waara S (2010) The influence of dissolved organic carbon on sorption of heavy metals on urea-treated pine bark. J Hazard Mater 173:689–696.

Kikuchi T, Fujii M, Terao K, Jiwei R, Lee YP, Yoshimura C (2017) Correlations between aromaticity of dissolved organic matter and trace metal concentrations in natural and effluent waters: A case study in the Sagami River Basin, Japan. Sci Total Environ 576:36–45

Kim JP, Hunter KA, Reid MR (1999) Factors influencing the inorganic speciation of trace metal cations in fresh waters. Mar Freshwater Res 50:367–372

Kinzig AP, Socolow RH (1994) Human impacts on the nitrogen cycle. Phys Today 47:24–31

Kleinegris DMM, van Es MA, Janssen M, Brandenburg WA, Wijffels RH (2010) Carotenoid fluorescence in Dunaliella salina. J Appl Phycol 22:645–649

Kohlmeier S, Mancuso M, Deepthike U, Tecon R, van der Meer JR, Harms H, Wells M (2008) Comparison of naphthalene bioavailability determined by whole-cell biosensing and availability determined by extraction with Tenax. Environ Pollut 156:803–808

Kothawala DN, Stedmon CA, Müller RA, Weyhenmeyer GA, Köhler SJ, Tranvik LJ (2014) Controls of dissolved organic matter quality: evidence from a large-scale boreal lake survey. Global Change Biol 20:1101–1114

Kowalczuk P, Durako MJ, Young H, Kahn AE, Cooper WJ, Gonsior M (2009) Characterization of dissolved organic matter fluorescence in the South Atlantic Bight with use of PARAFAC model: Interannual variability. Mar Chem 113:182–196

Kowalski CJ (1972) On the effects of non-normality on the distribution of the sample product-moment correlation coefficient. J R Stat Soc C-Appl 21:1-12

Kranzler C, Rudolf M, Keren N, Schleif E (2013) Iron in cyanobacteria. In: F. Chauvat and C. Cassier-Chauvat (eds.), Advances in Botanical Research: Genomics of Vyanobacteria. Volume 65. Academic Press, Amsterdam, Netherlands, pp. 57–105

Kujawinski EB, Longnecker K, Blough NV, Vecchio RD, Finlay L, Kitner JB, Giovannoni SJ (2009) Identification of possible source markers in marine dissolved organic matter using ultrahigh resolution mass spectrometry. Geochimica et Cosmochimica Acta 73:4384–4399

Lakowicz JR (2006) Principles of fluorescence spectroscopy, 3rd edition, Springer, Berlin

Larson CA, Liu H, Passy SI (2015) Iron supply constrains producer communities in stream ecosystems. FEMS Microbiol Ecol 91: fiv041

Lasat MM (2002) Phytoextraction of toxic metals: A review of biological mechanisms. J Environ Qual 31:109–120

Lee SJ, Jang MH, Kim HS, Yoon BD, Oh HM (2000) Variation of microcystin content of Microcystis aeruginosa relative to medium N:P ratio and growth stage. J Appl Microbiol 89:323–329

Leenheer JA, Croué JP (2003) Peer Reviewed: Characterizing aquatic dissolved organic matter. Environ Sci Technol 37:18A–26A

Lerche I, Glaesser W (2006) Environmental risk assessment. Springer-Verlag, Berlin, Heidelberg

Lévêque C (2001) Lake and Pond Ecosystems. Encyclopedia of Biodiversity, 458-466

Lewin JC (1966) Boron as a growth requirement for diatoms. J Phycol 2:160–163

Lewis WM Jr, Wurtsbaugh WA, Paerl HW (2011) Rationale for control of anthropogenic nitrogen and phosphorus to reduce eutrophication of inland waters. Environ Sci Technol 45:10300–10305

Lewis WM Jr, Saunders III JF, McCutchan JH Jr (2008) Application of a nutrient-saturation concept to the control of algal growth in lakes. Lake Reserv Manage 24:41–46

Li J, Jia C, Ying L, Tang S, Shim H (2015) Multivariate analysis of heavy metal leaching from urban soils following simulated acid rain. Microchem J 122: 89–95

Li WKW, Dickie PM (2001) Monitoring phytoplankton, bacterioplankton and virioplankton in a coastal inlet (Bedford Basin) by flow cytometry. Cytom 44:236–246

Liu E, Birch GF, Shen J, Yuan H, Zhang E, Cao Y (2012) Comprehensive evaluation of heavy metal contamination in surface and core sediments of Taihu Lake, the third largest freshwater lake in China. Environ Earth Sci 67:39–51

Liu EF, Shen J, Zhu YX, Xia WL, Pan HX, Jin ZD (2004) Heavy metals and nutrients pollution in sediments of Taihu Lake. Acta Sedimentology Sinica 22:507–512(in Chinesse)

Liu X, Lu X, Chen Y (2011) The effects of temperature and nutrient ratios on Microcystis blooms in Lake Taihu, China: An 11-year investigation. Harmful Algae 10:337–343

Lo K, Brinkman R, Gottardo R (2008) Automated Gating of flow cytometry data via robust model-based clustering. Cytom Part A 73A:321–332

Lo K, Hahne F, Brinkman RR, Gottardo R (2009) FlowClust: a Bioconductor package for automated gating of flow cytometry data. BMC Bioinformatics 10:145

Lopes da Silva T, Passarinho PC, Galriça R, Zenóglio A, Armshaw P, Pembroke JT, Sheahan C, Reis A, Gírio F (2018) Evaluation of the ethanol tolerance for wild and mutant Synechocystis strains by flow cytometry. Biotechnol Rep 17(C):137–147

Louda JW, Li J, Liu L, Winfree MN, Baker EW (1998) Chlorophyll-a degradation during cellular senescence and death. Org Geochem 29:1233–1251

Lowe JJ, Walker M (1997) Reconstructing quaternary environments, 3rd edn. Routledge, Taylor & Francis Group, London & New York

Lu X, Jaffé R (2001) Interaction between Hg(II) and natural dissolved organic matter: a fluorescence spectroscopy based study. Water Res 35:1793–1803

Lumley T (2017) leaps: Regression subset selection. R package version 3.0. https://CRAN.R-project.org/package=leaps.

Ma J, Qin B, Gao G, Zhu G, Hai X, Niu H, Paerl HW, Deng J, Brookes JD, Pan W (2014) Environmental factors controlling colony formation in blooms of the cyanobacteria Microcystis spp. in Lake Taihu, China. Harmful Algae 31:136–142

Ma J, Qin B, Wu P, Zhou J, Niu H (2015) Controlling cyanobacterial blooms by managing nutrient ratio and limitation in a large hyper-eutrophic lake: Lake Taihu, China. J Environ Sci 27:80–86

Magrisso S, Belkin S, Erel Y (2009) Lead bioavailability in soil and soil components. Water Air Soil Poll 202:315–323

Magrisso S, Erel Y, Belkin S (2008) Microbial reporters of metal bioavailability. Microb Biotechnol 1: 320–330

Maldonado MT, Strzepek RF, Sander S, Boyd PW (2005) Acquisition of iron bound to strong organic complexes, with different Fe binding groups and photochemical reactivities, by plankton communities in Fe-limited subantarctic waters. Global Biogeochem Cy 19:1–13

Manahan SE, Smith MJ (1973) Copper micronutrient requirement for algae. Environ Sci Technol 7:829–833

Manciulea A, Baker A, Lead JR (2009) A fluorescence quenching study of the interaction of Suwannee River fulvic acid with iron oxide nanoparticles. Chemosphere 76:1023–1027

Marhaba TF (2000) Fluorescence technique for rapid identification of DOM fractions. J Environ Eng 126:145–152

Masscheleyn PH, Delaune RD, Patrick WH (1990) Transformations of selenium as affected by sediment oxidation-reduction potential and pH. Environ Sci Technol 24:91–96

Massicotte P (2019) EemR: Tools for pre-processing emission-excitation-matrix (EEM) fluorescence data. https://github.com/PMassicotte/eemR.

McKnight DM, Boyer EW, Westerhoff PK, Doran PT, Kulbe T, Andersen DT (2001) Spectrofluorometric characterization of dissolved organic matter for indication of precursor organic material and aromaticity. Limnol Oceanogr 46:38-48

Mcknight DM, Morel FMM (1980) Copper complexation by siderophores from filamentous blue-green algae. Limnol Oceanogr 25:62–71

Mendenhall W, Sincich T (1996) A second course in statistics: regression analysis, 5th Edition. Prentice-Hall, Upper Saddle River, New Jersey

Merchant S (1998) Synthesis of metalloproteins involved in photosynthesis: plastocyanin and cytochromes. In: Rochaix JD, Goldschmidt-Clermont M, Merchant S (eds), The molecular biology of chloroplasts and mitochondria in chlamydomonas. Kluwer Academic Publishers, Dordrecht, The Netherlands, pp. 597–611

Mergeay M, Nies D, Schlegel HG, Gerits J, Charles P, Van GF (1985) *Alcaligenes eutrophus* CH34 is a facultative chemolithotroph with plasmid-bound resistance to heavy metals. J Bacteriol 162:328–334

MHPRC (2006) Standards for drinking water quality (GB-5749-2006). Ministry of Health of the People's Republic of China, Beijing

MHPRC (2016a) Water quality: Determination of water inorganic anions (F^-, Cl^-, NO_2^-, Br^-, NO_3^-, PO_4^{3-}, SO_3^{2-}, SO_4^{2-}) – Ion Chromatography (HJ84-2016). Ministry of Health of the People's Republic of China, Beijing

MHPRC (2016b) Water quality: Determination of water soluble cations (Li^+, Na^+, NH_4^+, K^+, Ca^{2+}, Mg^{2+}) – Ion Chromatography (HJ812-2016). Ministry of Health of the People's Republic of China, Beijing.

Miller H, Croudace IW, Bull JM, Carol J, Dix J, Taylor R (2014) A 500 year sediment lake record of anthropogenic and natural inputs to Windermere (English Lake District) using double-spike lead isotopes, radiochronology, and sediment microanalysis. Environ Sci Technol 48:7254–7263

Moffett JW (1995) Temporal and spatial variability of copper complexation by strong chelators in the Sargasso Sea. Deep Sea Res PT I 42:1273–1295

Molot LA, Li G, Findlay DL, Watson SB (2010) Iron-mediated suppression of bloom-forming cyanobacteria by oxine in a eutrophic lake. Freshwater Biol 55:1102–1117

Molot LA, Watson SB, Creed IF, Trick CG, McCabe SK, Verschoor MJ, Sorichetti RJ, Powe C, Venkiteswaran JJ, Schiff SL (2014) A model novel for cyanobacteria bloom formation: the critical role of anoxia and ferrous iron. Freshwater Biol 59:1323–1340

Moreira I, Bianchini I, Vieira A (2011) Decomposition of dissolved organic matter released by an isolate of *Microcystis aeruginosa* and morphological profile of the associated bacterial community. Braz J Biol 71:57–63

Moreno-Vivian C, Cabello P, Martinez-Luque M, Blasco R, Castillo F (1999) Prokaryotic nitrate reduction: molecular properties and functional distinction among bacterial nitrate reductases. J Bacteriol 181:6573–84

Mostofa KMG, Honda Y, Sakugawa H (2005) Dynamics and optical nature of fluorescent dissolved organic matter in river waters in Hiroshima prefecture, Japan. Geochem J 39:257–271

Mostofa KMG, Liu CQ, Feng X, Yoshioka T, Vione D, Pan X, Wu F (2013a) Complexation of dissolved organic matter with trace metal ions in natural waters. In: Mostofa et al. (eds) Photobiogeochemistry of Organic Matter, Environ Sci Eng, Springer, Berlin, Heidelberg, pp 769–849

Mostofa KMG, Wu F, Liu CQ, Fang WL, Yuan J, Ying WL, Wen L, Yi M (2010) Characterization of Nanming River (southwestern China) sewerage-impacted pollution using an excitation-emission matrix and PARAFAC. Limnol 11:217–231.

Mostofa KMG, Yoshioka T, Mottaleb A, Vione D (2013b) Fluorescent dissolved organic matter in natural waters. In: Mostofa KMG et al. (eds), Photobiogeochemistry of Organic Matter, Environ Sci Eng, Springer, pp 429–559

Mueller KK, Lofts S, Fortin C, Campbell PG (2012) Trace metal speciation predictions in natural aquatic systems: incorporation of dissolved organic matter (DOM) spectroscopic quality. Environ Chem 9:356–368

Muralikrishna IV, Manickam V (2017) Chapter Eight - Environmental Risk Assessment. In: Muralikrishna IV, Manickam V (Eds) Environmental Management. Elsevier, Butterworth-Heinemann, pp 135-152

Murphy KR, Stedmon CA, Graeber D, Bro R (2013) Fluorescence spectroscopy and multi-way techniques. PARAFAC. Anal Methods 5:6557–6566

Murphy KR, Stedmon CA, Wenig P, Bro R (2014) OpenFluor–an online spectral library of auto-fluorescence by organic compounds in the environment. Anal Methods 6:658–661

Murphy T, Lean DRS, Nalewajko C (1976) Blue-green algae: Their excretion of iron selective chelators enables them to dominate other algae. Science 192:900–902

Nagai T, Imai A, Matsushige K, Fukushima T (2006) Effect of iron complexation with dissolved organic matter on the growth of cyanobacteria in a eutrophic lake. Aquat Microb Ecol 44:231–239

Ndu U, Mason RP, Zhang H, Lin S, Visscher PT (2012) The Effect of Inorganic and Organic Ligands on the Bioavailability of Methylmercury as Determined by a mer-lux Bioreporter. Appl Environ Microbiol 78:7276–7282

Ndungu, K (2012) Model predictions of copper speciation in coastal water compared to measurements by analytical voltammetry. Environ Sci Technol 46, 7644-7652

Neculita CM, Dudal Y, Zagury GJ (2011) Using fluorescence-based microplate assay to assess DOM-metal binding in reactive materials for treatment of acid mine drainage. J Environ Sci 23:891–896

Nicolaisen K, Hahn A, Valdebenito M, Moslavac S, Samborski A, Maldener I, Wilken C, Valladares A, Flores E, Hantke K (2010) The interplay between siderophore secretion and coupled iron and copper transport in the heterocyst-forming cyanobacterium Anabaena sp. PCC 7120. Biochimica et Biophysica Acta 1798:2131–2140

Niu Y, Jiao W, Yu H, Niu Y, Pang Y, Xu X, Guo X (2015) Spatial evaluation of heavy metals concentrations in the surface sediment of Taihu Lake. Inter J Env Res and Pub Heal 12:15028–15039

Niyogi S, Wood CM (2004) Biotic ligand model, a flexible tool for developing site-specific water quality guidelines for metals. Environ Sci Technol 38:6177–6192.

Norse D (2005) Non-Point pollution from crop production: global, regional and national issues. Pedosphere 15:499–508

North RL, Guildford SJ, Smith REH, Twiss MR, Kling HJ (2008) Nitrogen, phosphorus, and iron colimitation of phytoplankton communities in the nearshore and offshore regions of the African Great Lakes. Verh Internat Verein Limnol 30:259–264

Nychka D, Furrer R, Paige J, Sain S (2017) fields: Tools for spatial data. R package version 10.0, https://github.com/NCAR/Fields.

Nys C, Janssen CR, Mager EM, Esbaugh AJ, Brix KV, Grosell M, Stubblefield WA, Holtze K, De Schamphelaere KA (2014) Development and validation of a biotic ligand model for predicting chronic toxicity of lead to *Ceriodaphnia dubia*. Environ Toxicol Chem 33:394–403

O'Connor MI, Piehler MF, Leech DM, Anton A, Bruno JF (2009) Warming and resource availability shift food web structure and metabolism. PLoS Biol 7:e1000178

O'Shea TA, Mancy KH (1978) The effect of pH and hardness metal ions on the competitive interaction between trace metal ions and inorganic and organic complexing agents found in natural waters. Water Res 12:703–711

Ohno T (2002) Fluorescence inner-filtering correction for determining the humification index of dissolved organic matter. Environ Sci Technol 36:742–746

Ohno T, Bro R (2006) Dissolved organic matter characterization using multiway spectral decomposition of fluorescence landscapes. Soil Sci Soc Am J 70:2028–2037

Orihel DM, Schindler DW, Ballard NC, Wilson LR, Vinebrooke RD (2016) Experimental iron amendment suppresses toxic cyanobacteria in a hypereutrophic lake. Ecol Appl 26:1517–1534

Oukarroum A (2016) Change in photosystem II photochemistry during algal growth phases of Chlorella vulgaris and Scenedesmus obliquus, Curr Microbiol 72:692–699

Paerl HW, Bowles ND (1987) Dilution bioassays: Their application to assessments of nutrient limitation in hypereutrophic waters. Hydrobiologia 146:265–273

Paerl HW, Xu H, Hall NS, Rossignol KL, Joyner AR, Zhu G, Qin B (2015) Nutrient limitation dynamics examined on a multi-annual scale in Lake Taihu, China: implications for controlling eutrophication and harmful algal blooms. J Freshwater Ecol 30:5–24

Paerl HW, Xu H, Mccarthy MJ, Zhu G, Qin B, Li Y, Gardner WS (2011) Controlling harmful cyanobacterial blooms in a hyper-eutrophic lake (Lake Taihu, China): The need for a dual nutrient (N & P) management strategy. Water Res 45:1973–1983

Palma LD, Mecozzi R (2007) Heavy metals mobilization from harbour sediments using EDTA and citric acid as chelating agents. J Hazard Mater 147:768–775

Parlanti E, Wörz K, Geoffroy L, Lamotte M (2000) Dissolved organic matter fluorescence spectroscopy as a tool to estimate biological activity in a coastal zone submitted to anthropogenic inputs. Organic Geochem 31:1765–1781

Pastircakova K (2004) Determination of trace metal concentrations in ashes from various biomass materials. Energy Educ Sci Technol 13:97–104

Peniuk GT, Schnurr PJ, Allen DG (2016) Identification and quantification of suspended algae and bacteria populations using flow cytometry: applications for algae biofuel and biochemical growth systems. J Appl Phycol 28:95–104

Pertof H, Laurent CT, Laas T, Kagedal L (1978) Density gradients prepared from colloidal silica particles coated by polyvinylpyrrolidone (Percoll). Anal Biochem 88:271–282

Pfisterer AB, Schmid B (2002) Diversity-dependent production can decrease the stability of ecosystem functioning. Nature 416:84–86

Piehler MF, Dyble J, Moisander PH, Chapman AD, Hendrickson J, Paerl HW (2009) Interactions between nitrogen dynamics and the phytoplankton community in Lake George, Florida, USA. Lake Reserv Manage 25:1–14

Pinna A, Pezzolesi L, Pistocchi R, Vanucci S, Ciavatta S, Polimene L (2015) Modelling the stoichiometric regulation of C-Rich toxins in Marine Dinoflagellates. PloS ONE 10:e0139046

Pollingher U, Kaplan B, Berman T (1995) The impact of iron and chelators on Lake Kinneret phytoplankton. J Plankton Res 17:1977–1992

Powell KJ, Brown PL, Byren RH, Gajda T, Hefter G, Leuz AK, Sjöberg S, Wanner H (2009) Chemical speciation of environmentally significant metals with inorganic ligands. Part 3: The Pb^{2+} + OH^-, Cl^-, CO_3^{2-}, SO_4^{2-}, and PO_4^{3-} systems: (IUPAC Technical Report). Pure Appl Chem 81:2425–2476

Price NB (1976) Chapter 30 – Chemical diagenesis in sediments. In: Riley JP, Chester R (eds), Chemical oceanography, 2nd edn. Academic Press, London

Procházková G, Brányiková I, Zachleder V, Brányik T (2014) Effect of nutrient supply status on biomass composition of eukaryotic green microalgae. J Appl Phycol 26:1359–1377.

Pucher M (2019) staRdom vignette: PARAFAC analysis of EEM data to separate DOM components in R, https://cran.r-project.org/web/packages/staRdom/vignettes/PARAFAC_analysis_of_EEM.html.

Pucher M, Wünsch U, Weigelhofer G, Murphy K, Hein T, Graeber D (2019) staRdom: versatile software for analying spectroscopic data of dissolved organic matter in R. Water 11:2366

Pure Earth (Blacksmith Institute) and Green Cross (2015) World's worst pollution problems: Top six toxic threats. Pure Earth and Green Cross, New York, Zurich

Qin B, Hu W, Chen W, Fan C, Zhou Z (2000) Studies on the hydrodynamic processes and related factors in Meiliang Bay, northern Taihu Lake, China. J Lake Sc 12: 327–334 (in Chinese)

Qin B, Hu WP, Chen WM (2004) Process and mechanism of environmental changes of the Taihu Lake. Science Press, Beijing (in Chinese)

Qin B, Xu P, Wu Q, Luo L, Zhang Y (2007) Environmental issues of Lake Taihu, China. Hydrobiologia 581:3–14

Qin B, Zhu G, Gao G, Zhang Y, Li W, Paerl HW, Carmichael WW (2010) A drinking water crisis in Lake Taihu, China: linkage to climatic variability and lake management. Environ Manage 45:105–112

Qu W, Dickman M, Wang S (2001) Multivariate analysis of heavy metal and nutrient concentrations in sediments of Taihu Lake, China. Hydrobiologia 450: 83-89

R Core Team (2019) R: A Language and environment for statistical computing. R Foundation for Statistical Computing, Vienna, Austria. URL https://www.R-project.org/.

Rajeshkumar S, Liu Y, Zhang X, Ravikumar B, Bai G, Li X (2017) Studies on seasonal pollution of heavy metals in water, sediment, fish and oyster from the Meiliang Bay of Taihu Lake in China. Chemosphere 191:626

Rasmussen LD, Sørensen SJ, Turner RR, Barkay T (2000) Application of a mer-lux biosensor for estimating bioavailable mercury in soil. Soil Biol Biochem 32:639–646

Reeder RJ, Schoonen MAA, Lanzirotti A (2006) Metal speciation and its role in bioaccessibility and bioavailability. Rev Mineral Geoch 64:59–113

Ren ZL, Tella M, Bravin MN, Comans RNJ, Dai J, Garnier JM, Sivry Y, Doelsch E, Straathof A, Benedetti MF (2015) Effect of dissolved organic matter composition on metal speciation in soil solutions. Chem Geol 398:61–69

Reuter JH, Perdue EM (1977) Importance of heavy metal-organic matter interactions in natural waters. Geochimica Et Cosmochimica Acta 41:325–334

Riether KB, Dollard MA, Billard P (2001) Assessment of heavy metal bioavailability using Escherichia coli zntAp::lux and copAp::lux-based biosensors. Appl Microbiol Biotechnol 57:712–716

Ripp S, Layton A. Sayler G (2011) The microbe as a reporter: microbial bioreporter sensing technologies for chemical and biological detection. In: Sen K, Ashbolt NJ (eds). Environmental Microbiology: current technology and water applications. Caister Academic Press; Norfolk, pp. 281–308

Romero IC, Klein NJ, Barada L, Vo J, Liss AM, Cutter L, Gunderson T, Tiahlo M, Glass JB, Sañudo-Wilhelmy S (2011) Trace metal co-limitation controls on

nitrogen fixation in lakes with varying trophic status, ASLO Aquatic Sciences Meeting.

Romero IC, Klein NJ, Sañudo-Wilhelmy SA, Capone DG (2013) Potential trace metal co-limitation controls on N_2 fixation and NO_3 uptake in lakes with varying trophic status. Front Microbiol 4:54

Rose NL, Boyle JF, Du Y, Yi C, Dai X, Appleby PG, Bennion H, Cai S, Yu L (2004) Sedimentary evidence for changes in the pollution status of Taihu in the Jiangsu region of eastern China. J Paleol 32:41–51

Rott E, Salmaso N, Hoehn E (2007) Quality control of Utermöhl-based phytoplankton counting and biovolume estimates-an easy task or a Gordian knot? Hydrobiologia 578:141–146

Roussel H, Ten-Hage L, Joachim S, Le Cohu R, Gauthier L, Bonzom JM (2007) A long-term copper exposure on freshwater ecosystem using lotic mesocosms: Primary producer community responses. Aquat Toxicol 81:168–182

Ruby MV, Davis A, Nicholson A (1994) In situ formation of lead phosphates in soils as a method to immobilize lead. Environ Sci Technol 28:646–654

Ruby MV, Davis A, Schoof R, Eberle S, Sellstone CM (1996) Estimation of lead and arsenic bioavailability using a physiologically based extraction test. Environ Sci Technol 30:422–430

Rueter JG, Petersen RR (1987) Micronutrient effects on cyanobacterial growth and physiology. New Zeal J Mar Fresh 21:435–445

Ryan DK, Weber JH (1982a) Copper(II) complexing capacities of natural waters by fluorescence quenching. Environ Sci Technol 16:866–872

Ryan DK, Weber JH (1982b) Fluorescence quenching titration for determination of complexing capacities and stability constants of fulvic acid. Anal Chem 54:986–990

Saar RA, Weber JH (1980) Lead(II)-fulvic acid complexes. Conditional stability constants, solubility, and implications for lead(II) mobility. Environ Sci Technol 14:877–880

Sanchez NP, Skeriotis AT, Miller CM (2014) A PARAFAC-based long-term assessment of DOM in a multi-coagulant drinking water treatment scheme. Environ Sci Technol 48:1582–1591

Sander SG, Buck KN, Wells M (2015) The effect of natural organic ligands on trace metal speciation in San Francisco Bay: implications for water quality criteria. Mar Chem 173:269–281

Sander SG, Hunter KA, Hauke H, Mona W (2011) Numerical approach to speciation and estimation of parameters used in modeling trace metal bioavailability. Environ Sci Technol 45:6388–6395

Sandmann G, Böger P (1980) Copper deficiency and toxicity in Scenedesmus. Zeitschrift für Pflanzenphysiologie 98:53–59

Santore RC, Di Toro DM, Paquin PR, Allen HE, Meyer JS (2001) Biotic ligand model of the acute toxicity of metals. 2. Application to acute copper toxicity in freshwater fish and Daphnia. Environ Toxicol Chem 20:2397–2402

Sarkar SD, Blom JF, Bethuel Y, Jüttner F, Gademan K (2016) Allelopathic activity of the iron chelator anachelin–a molecular hybrid with a dual mode of action. Helv Chim Acta 99:760–773

Sekar M, Sakthi V, Rengaraj S (2004) Kinetics and equilibrium adsorption study of lead (II) onto activated carbon prepared from coconut shell. J Colloid Interface Sci 279, 307–313.

Schallenberg M, de Winton MD, Verburg P, Kelly DJ, Hamill KD, Hamilton DP, Dymond JR (2013) Ecosystem services of lakes. In: Dymond JR (ed), Ecosystem services in New Zealand. Manaaki Whenua Press, Lincoln, New Zealand, pp. 203–225

Schillereff DN (2015) Lake sediment records of flood frequency and magnitude. PhD Thesis, University of Liverpool

Schillereff DN, Chiverrell RC, Macdonald N, Hooke JM (2014) Flood stratigraphies in lake sediments: a review. Earth Sci Rev 135:17–37

Schillereff DN, Chiverrell RC, Macdonald N, Hooke JM, Welsh KE (2016) Quantifying system disturbance and recovery from historical mining-derived metal contamination at Brotherswater, northwest England. J Paleolimnol 56:1–17

Schindler DW (1977) Evolution of phosphorus limitation in lakes. Science 195:260–262

Schindler DW (1998) Replication versus realism: the need for ecosystem-scale experiments. Ecosystems 1:323–334

Sebastien L, Julie J, Francois H (2008) FactoMineR: An R package for multivariate analysis. J Stat Softw 25:1–18

Selifonova O, Burlage R, Barkay T (1993) Bioluminescent sensors for detection of bioavailable Hg(II) in the environment. Appl Environ Microbiol 59:3083–90

Shahid M, Dumat C, Aslam M, Pinelli E (2012) Assessment of lead speciation by organic ligands. Chem Spec Bioavailab 24:248–252

Shen J, Liu E, Zhu Y, Hu S, Qu W (2007) Distribution and chemical fractionation of heavy metals in recent sediments from Lake Taihu, China. Hydrobiologia 581:141–150

Sheppard MI, Thibault DH (1992) Desorption and extraction of selected heavy metals from soils. Soil Sci Soc of Am J 56:415–423

Shrivastava A (2011) Methods for the determination of limit of detection and limit of quantitation of the analytical methods. Chronicles of Young Scientists 2:21–25

Sillanpää M, Oikari A (1996) Assessing the impact of complexation by EDTA and DTPA on heavy metal toxicity using microtox bioassay. Chemosphere 32:1485–1497

Singh PK (2001) Complexation equilibria and evaluation of thermodynamic parameters of bivalent metal complexes of glutathione. India Chem 40A:1339–1343

Sisombath NS (2014) Complex formation of Pb(II) with cysteine, penicillamine and N-acetylcysteine. Master's thesis, University of Calgary.

Smayda TJ, Reynolds CS (2001) Community assembly in marine phytoplankton: application of recent models to harmful *dinoflagellat*e blooms. J Plankton Res 23:447–461

Smith DS, Cooper CA, Wood CM (2017) Measuring biotic ligand model (BLM) parameters in vVitro: copper and silver binding to rainbow trout gill cells as cultured epithelia or in suspension. Environ Sci Technol 75: 1–9

Smith DS, Kramer JR (1999) Fluorescence analysis for multi-site aluminum binding to natural organic matter. Environ Int 25:295–306

Smith LED, Siciliano G (2015) A comprehensive review of constraints to improved management of fertilizers in China and mitigation of diffuse water pollution from agriculture. Agr Ecosyst Environ 209:15–25

Smith VH (1983) Low nitrogen to phosphorus ratios favor dominance by blue-green algae in lake phytoplankton. Science 221:669–671

Sohm JA, Webb EA, Capone DG (2011) Emerging patterns of marine nitrogen fixation. Nat Rev Microbiol 9:499–508

Song L, Qin JG, Su S, Xu J, Clarke S, Shan Y (2012) Micronutrient requirements for growth and hydrocarbon production in the oil producing green alga Botryococcus braunii (Chlorophyta). PLoS ONE 7:e41459

Song N, Zhong X, Li B, Li J, Wei D, Ma Y (2014a) Development of a multi-species biotic ligand model predicting the toxicity of trivalent chromium to barley root elongation in solution culture. PloS One 9:64–68

Song Y, Bo J, Tian S, Hui T, Liu Z, Li C, Jia J, Huang WE, Xu Z, Li G (2014b) A whole-cell bioreporter approach for the genotoxicity assessment of bioavailability of toxic compounds in contaminated soil in China. Environ Pollut 195:178–184

Sorensen JPR, Baker A, Cumberland SA, Lapworth DJ, MacDonald AM, Pedley S, Taylor RG, Ward JST (2018) Real-time detection of faecally contaminated drinking water with tryptophan-like fluorescence: defining threshold values. Sci Tot Environ 622-623:1250–1257

Sorichetti RJ, Creed IF, Trick CG (2016) Iron and iron-binding ligands as cofactors that limit cyanobacterial biomass across a lake trophic gradient. Freshwater Biol 61:146–157

Spivak AC, Canuel EA, Duffy JE, Richardson JP (2009) Nutrient enrichment and food web composition affect ecosystem metabolism in an experimental seagrass habitat. PLoS ONE, 4:e7473

Spivak AC, Vanni MJ, Mette E (2011) Moving on up: Can results from simple aquatic mesocosm experiments be applied across broad spatial scales? Freshwater Biol 56:279–291

Srivastava A, Ko SR, Ahn CY, Oh HM, Ravi AK, Asthana RK (2016) Microcystin biosynthesis and mcyA expression in geographically distinct Microcystis strains under different nitrogen, phosphorus, and boron regimes. Biomed Res Int 2016:1–13

Stedmon CA, Markager S, Bro R (2003) Tracing dissolved organic matter in aquatic environments using a new approach to fluorescence spectroscopy. Mar Chem 82:239–254

Steffen W, Richardson K, Rockström J, Cornell SE, Fetzer I, Bennett EM, Biggs R, Carpenter SR, Vries WD, Wit CAD (2015) Planetary boundaries: Guiding human development on a changing planet. Science 348:1259855

Steinberg CEW, Schafer H, Siedler M, Beisker W (1995) Ataxonomic assessment of phytoplankton integrity by means of flow cytometry, In: Seiler JP, Kroftova O, Eybl V (eds), Archives of toxicology:toxicology–from cells to man, Proceedings of the 1995 EUROTOX Congress, August 27–30, Prague, pp. 417–436

Stephen CE, Mount DI, Hansen DJ, Gentile JR, Chapman GA, Brungs WA (1985) Guidelines for deriving numerical national water quality criteria for the protection of aquatic organisms and their uses. (PB85-22704945) US Environmental Protection Agency, Washington, DC.

Sterner RW, Smutka TM, Mckay RML, Qin X, Brown ET, Sherrell RM (2004) Phosphorus and trace metal limitation of algae and bacteria in Lake Superior. Limnol Oceanogr 49:495–507

Stoddard JL (1987) Micronutrient and phosphorous limitation of phytoplankton abundance in Gem Lake, Sierra Nevada, California. Hydrobiologia 154:103–111

Sud D, Mahajan G, Kaur M (2008) Agricultural waste material as potential adsorbent for sequestering heavy metal ions from aqueous solutionse A review. Bioresour Technol 99:6017–6027

Sun S, Huang Y (1993) Lake Taihu. China Ocean Press, Beijing (in Chinese)

Sun SC, Mao R (2008) An introduction to Lake Taihu. In: Qin B (ed) Lake Taihu, China: dynamics and environmental change, Springer, Dordrecht, pp. 1-67

Sunda WG, Price NM, Morel FMM (2005) Trace metal ion buffers and their use in culture studies. In: R.A. Andersen (ed.) Algal Culturing Techniques. 1st ed. Elsevier, Academic Press, Burlington, pp. 35–64

Szarlowicz K, Stobinski M, Hamerlik L, Bitusik P (2019) Origin and behavior of radionuclides in sediment core: a case study of the sediments collected from man-made reservoirs located in the past mining region in Central Slovakia. Environ Sci Pollut Res 26:7115–7122

Taiyun W, Viliam S (2017) R package "corrplot": visualization of a correlation matrix (Version 0.84). Available from https://github.com/taiyun/corrplot.

Tang C, Li Y, Acharya K (2016) Modeling the effects of external nutrient reductions on algal blooms in hyper-eutrophic Lake Taihu, China. Ecol Eng 94:164–173

Tecon R, Wells M, Van der Meer JR (2010) A new green fluorescent protein-based bacterial biosensor for analysing phenanthrene fluxes. Environ Microbiol 8:697–708

Tewari BB (2005) Determination of mixed stability constants of lead(II)/uranyl(II)-NTA-cysteine complexes by paper electrophoresis. B Chem Soc Ethiopia 19:257-265

Tipping E (1994) WHAMC-A chemical equilibrium model and computer code for waters, sediments, and soils incorporating a discrete site/electrostatic model of ion-binding by humic substances. Compu Geosci 20:973–1023

Tipping E (1998) Humic ion-binding model VI: an improved description of the interactions of protons and metal ions with humic substances. Aquat Geochem 4:3–47

Tipping E, Lofts S, Lawlor AJ (1998) Modelling the chemical speciation of trace metals in the surface waters of the Humber system. Sci Total Environ 210–211: 63

Tong S, Von Schirnding YE, Prapamontol T (2000) Environmental lead exposure: a public health problem of global dimensions. B World Health Organ 78: 1068

Torbjorn L, Elisabeth S, Lisbeth A, Bernt T, Rolf B (1998) Experimental design and optimization. Chemometr Intell Lab 42:3-40

Trang P, Berg M, Viet P, Van Mui N, van der Meer J (2005) Bacterial bioassay for rapid and accurate analysis of arsenic in highly variable groundwater samples. . Environ Sci Technol 39:7625–7630

Twiss MR, Auclair JC, Charlton MN (2000) An investigation into iron-stimulated phytoplankton productivity in epipelagic Lake Erie during thermal stratification using trace metal clean techniques. Journal Canadien Des Sciences Halieutiques Et Aquatiques 57:86–95

Twiss MR, Gouvêa SP, Bourbonniere RA, Mckay RML, Wilhelm SW (2005) Field investigations of trace metal effects on Lake Erie phytoplankton productivity. J Great Lakes Res 31:168–179

Tyler I (1992) Greenside: a tale of lakeland miners. Red Earth Publications, Cumbria

USEPA (2003a) The biotic ligand model: Technical support document for its application of the evaluation of Water Quality Criteria for Copper: US Environmental Protection Agency, Washington, DC

USEPA (2003b) Draft update of ambient water quality criteria for copper, Report No. EPA-822-R-03-026. US Environmental Protection Agency, Washington, DC

USEPA (2007a) Guidance for evaluating the oral bioavailability of metals in soils for use in human health risk assessment (OSWER 9285.7-80, May 2007) US Environmental Protection Agency, Washington, DC

USEPA (2007b) Update of ambient water quality criteria for copper, Report No. EPA-822-F-07-001: US Environmental Protection Agency, Washington, DC

USEPA (1992) Definitions and general principles for exposure assessment. Guidelines for exposure assessment. US Environmental Protection Agency Washington, D.C

USEPA (2002) Edition of the drinking water standards and health advisories. US Environmental Protection Agency Washington, DC

USEPA (2009) Regional Screening Level (RSL) - Generic Tables. US Environmental Protection Agency, Washington, DC

USEPA (2017) National recommended water quality criteria -Aquatic Life Criteria Table. US Environmental Protection Agency, Washington, DC

USEPA (2016) Draft estuarine/marine copper aquatic life ambient water quality criteria. US Environmental Protection Agency Washington, DC

USEPA (1979) Methods for chemical analysis of water and wastes Washington, DC

USNRC (1983) Risk Assessment in the Federal Government: Managing the Process, National Academy Press, Washington, DC, March, 1983

USNRC (2003) Bioavailability of Contaminants in Soils and Sediments: Processes, Tools, and Applications. The National Academies Press, Washington, DC.

Uzun L, Türkmen D, Yılmaz E, Bektaş S, Denizli A (2008) Cysteine functionalized poly(hydroxyethyl methacrylate) monolith for heavy metal removal. Colloid Surface A 330:161–167

Vacek J, Petřek J, Kizek R, Havel L, Klejdus B, Trnková L, Jelen F (2004) Electrochemical determination of lead and glutathione in a plant cell culture. Bioelectrochemistry 63:347–351

Van der Meer JR, Belkin S (2010) Where microbiology meets microengineering: design and applications of reporter bacteria. Nat Rev Microbiol 8:511–522

Vanbriesen JM, Small M, Weber C, Wilson J (2010) Modelling chemical speciation: thermodynamics, kinetics and uncertainty. In: Hanrahan G (ed) Modelling of pollutants in complex environmental systems. Vol. 2, Advanced topics in environmental science, ILM Publications. pp. 133–149

Verschoor MJ, Powe CR, McQuay E, Schiff SL, Venkiteswaran JJ, Li J, Molot LA (2017) Internal iron loading and warm temperatures are preconditions for cyanobacterial dominance in embayments along Georgian Bay, Great Lakes. Canadian J Fisheries Aquat Sci 74:1439–1453

Vincent W (1983) Fluorescence properties of the freshwater phytoplankton: Three algal classes compared. Br Phycol Bull 18:5–21

Vrede T, Tranvik LJ (2006) Iron constraints on planktonic primary production in oligotrophic lakes. Ecosyst 9:1094–1105

Wang C, Bi J, Fath BD (2017) Effects of abiotic factors on ecosystem health of Taihu Lake, China based on eco-exergy theory. Sci Rep 7:42872

Wang J, Pang Y, Li L, Huang Y, Jia J, Zhang P, Kou X (2014) The regularity of wind-induced sediment resuspension in Meiliang Bay of Lake Taihu. Water Sci Technol 70:167–174

Wang J, Wang J (1982) Collection, counting and quantification of phytoplankton. Reservoir Fisheries 4:58–63 (In Chinese)

Wang L, Cai Y, Fang L (2009) Pollution in Taihu Lake China: causal chain and policy options analyses. Front Earth Sci China 3:437–444

Wang X, Jiang C, Szeto YT, Li HK, Yam KL, Wang X (2016) Effects of Dracontomelon duperreanum defoliation extract on Microcystis aeruginosa: physiological and morphological aspects. Environ Sci Pollu Res Int 23:8731–8740

Wang YY, Chai YL, Chang H, Peng XY, Shu YD (2009) Equilibrium of hydroxyl complex ions in Pb^{2+}-H_2O system. Trans Nonferrous Met Soc China 19:458–462

Wang S, Zhang J (2006) Blood lead levels in children, China. Environ Res 101:412

Ward TJ, Rausina GA, Stonebraker PM, Robinson WE (2002) Apparent toxicity resulting from the sequestering of nutrient trace metals during standard Selenastrum capricornutum toxicity tests. Aquat Toxicol 60:1–16

Warwick P, Hall T (1992) High-performance liquid chromatographic study of nickel complexation with humic and fulvic acids in an environmental water. Analyst 117:151–156

Weber OA, Simeon V (1971) Chelation of some bivalent metal ions by racemic and enantiomeric forms of tyrosine and tryptophan. BBA-biomembranes 244:94–102

Wells M (2012) Polycyclic aromatic hydrocarbon (PAH) sensitive bacterial biosensors in environmental health. In: Hunter RJ, Preedy VR (Eds), Biosensors and the Environment Health. CRC Environmental Health Series, Enfield, New Hampshire

Wells M, Buck KN, Sander SG (2013) New approach to analysis of voltammetric ligand titration data improves understanding of metal speciation in natural waters. Limnol Oceanogr Meth 11:450–465

Whalen SC, Benson PM (2007) Influence of nutrient reduction, light and light-nutrient interactions on phytoplankton biomass, primary production and community composition in the Neuse River, USA. Fund Appl Limnol 168:257–270

Wickham H, Francois R, Henry L (2019) Dplyr: A grammar of data manipulation. https://CRAN.R-project.org/package=dplyr.

Wickham H, Henry L (2019) Tidyr: Easily Tidy Data with 'Spread()' and 'Gather()' Functions. https://CRAN.R-project.org/package=tidyr.

Wu FC, Tanoue E, Liu CQ (2003) Fluorescence and amino acid characteristics of molecular size fractions of DOM in the waters of Lake Biwa. Biogeochem 65:245–257

Wu H, Wei G, Xiao T, Lin L, Ming L (2017) Species-dependent variation in sensitivity of Microcystis species to copper sulfate: implication in algal toxicity of copper and controls of blooms. Sci Rep 7:40393

Wu J, Zhang H, He PJ, Shao LM (2011) Insight into the heavy metal binding potential of dissolved organic matter in MSW leachate using EEM quenching combined with PARAFAC analysis. Water Res 45:1711–1719

Wurtsbaugh WA, Horne A (1983) Iron in eutrophic Clear Lake, California: its importance for algal nitrogen fixation and growth. Can J Fish Aquat Sci 40:1419–1429

Xu H, Paerl HW, Qin BQ, Zhu GW, Gao GA (2010) Nitrogen and phosphorus inputs control phytoplankton growth in eutrophic Lake Taihu, China. Limnol Oceanogr 55:420–432

Xu H, Zhu G, Qin B, Paerl HW (2013) Growth response of *Microcystis* spp. to iron enrichment in different regions of Lake Taihu, China. Hydrobiologia 700:187–202

Xu P, Qin B (2005) Water quantity and pollutant fluxes of the surrounding rivers of Lake Taihu during the hydrological year of 2001–2002. J Lake Sci 17:213–218 (in Chinese)

Yamashita Y, Jaffé R (2008) Characterizing the interactions between trace metals and dissolved organic matter using excitation−emission matrix and parallel factor analysis. Environ Sci Technol 42:7374–7379

Yamashita Y, Jaffé R, Maie N, Tanoue E (2008) Assessing the dynamics of dissolved organic matter (DOM) in coastal environments by excitation emission matrix fluorescence and parallel factor analysis (EEM-PARAFAC). Limnol Oceanogr 53:1900–1908

Yang C, Liu Y, Zhu Y, Zhang Y (2016) Insights into the binding interactions of autochthonous dissolved organic matter released from *Microcystis aeruginosa* with pyrene using spectroscopy. Mar Pollut Bull 104:113–120

Yang J, Gao H, Glibert PM, Wang Y, Tong M (2017) Rates of nitrogen uptake by cyanobacterially-dominated assemblages in Lake Taihu, China, during late summer. Harmful Algae 65:71–84

Yang S, Liu P (2010) Strategy of water pollution prevention in Taihu Lake and its effects analysis. J Great Lake Res 36:150–158

Yao X, Zhang Y, Zhu G, Qin B, Feng L, Cai L, Gao G (2011) Resolving the variability of CDOM fluorescence to differentiate the sources and fate of DOM in Lake Taihu and its tributaries. Chemosphere 82:145–155

Ye X, Fu H, Guidotti T (2007) Environmental exposure and Children's health in China. Archives Environ Occup Health 62:61–73

Yin Y, Impellitteri CA, You SJ, Allen HE (2002) The importance of organic matter distribution and extract soil:solution ratio on the desorption of heavy metals from soils. Sci Total Environ 287:107–119

Yoon Y, Kim S, Chae Y, Jeong SW, An YJ (2016a) Evaluation of bioavailable arsenic and remediation performance using a whole-cell bioreporter. Sci Total Environ 547:125–131

Yoon Y, Kim S, Chae Y, Kang Y, Lee Y, Jeong SW, An YJ (2016b) Use of tunable whole-Cell bioreporters to assess bioavailable cadmium and remediation performance in soils. PloS One 11:1–16

Yu H, Song Y, Pan H, Peng J, Gao H, Liu R (2016) Synchronous fluorescence spectroscopy combined with two-dimensional correlation and principle component analysis to characterize dissolved organic matter in an urban river. Environ Monit Assess 188:579

Yu T, Zhang Y, Meng W, Hu X (2012a). Characterization of heavy metals in water and sediments in Taihu Lake, China. Environ Monit Assess 184:4367–4382

Yu T, Zhang Y, Hu X, Meng W (2012b) Distribution and bioaccumulation of heavy metals in aquatic organisms of different trophic levels and potential health risk assessment from Taihu lake, China. Ecotoxicol Environ Safe 81:55–64

Yu T, Zhang Y, Wu F, Meng W (2013) Six-decade change in water chemistry of large freshwater Lake Taihu, China, Environ Sci Technol 47:9093–9101

Zare H, Shooshtari P, Gupta A, Brinkman RR (2010) Data reduction for spectral clustering to analyze high throughput flow cytometry data. BMC Bioinformatics 11:1–16

Zeng J, Liuyan Y, Xiong W (2010) High sensitivity of cyanobacterium Microcystis aeruginosa to copper and the prediction of copper toxicity. Environ Toxicol Chem 29:2260

Zhang T, Lu J, Ma J, Qiang Z (2008) Fluorescence spectroscopic characterization of DOM fractions isolated from a filtered river water after ozonation and catalytic ozonation. Chemosphere 71:911–921

Zhang X, Chen Q (2011) Spatial-temporal characteristic of water quality in Lake Taihu and its relationship with algal bloom. J Lake Sci 23:339–347 (in Chinese)

Zhang X, Qin B, Deng J, Wells M (2017) Whole-cell bioreporters and risk assessment of environmental pollution: A proof-of-concept study using lead. Environ Pollut 229:902–910

Zhang Y, Dijk MA, Liu M, Zhu G, Qin B (2009) The contribution of phytoplankton degradation to chromophoric dissolved organic matter (CDOM) in eutrophic shallow lakes: Field and experimental evidence. Water Res 43:4685–4697

Zhang Y, Qin B, Zhu G, Zhang L, Yang L (2007) Chromophoric dissolved organic matter (CDOM) absorption characteristics in relation to fluorescence in Lake Taihu, China, a large shallow subtropical lake. Hydrobiologia 581:43–52

Zhang Y, Yin Y, Liu X, Shi Z, Feng L, Liu M, Zhu G, Gong Z, Qin B (2012) Spatial-seasonal dynamics of chromophoric dissolved organic matter in Lake Taihu, a large eutrophic, shallow lake in China. Organic Geochem 42:510–519

Zhang Y, Zhang Y, Yu T (2014) Quantitative characterization of Cu binding potential of dissolved organic matter (DOM) in sediment from Taihu Lake using multiple techniques. Front Environ Sci Eng 8:666–674

Zhao XL, Song LR, Zhang XM (2009) Effects of copper sulfate treatment on eutrophic urban lake phytoplankton communities. Acta Hydrobiologica Sinica 33:596–602 (In Chinese)

Zheng S, Wang P, Chao W, Hou J, Jin Q (2013) Distribution of metals in water and suspended particulate matter during the resuspension processes in Taihu Lake sediment, China. Quatern Int 286:94–102

Zhou F, Chen J (2011) Freshwater Microbial and Zoobenthos Map (Second Edition). Chemical Industry Press, Beijing (In Chinese)

Zia MH, Codling EE, Scheckel KG, Chaney RL (2011) In vitro and in vivo approaches for the measurement of oral bioavailability of lead (Pb) in contaminated soils: A review. Environ Pollut 159:2320–2327

Zsolnay A, Baigar E, Jimenez M, Steinweg B, Saccomandi F (1999) Differentiating with fluorescence spectroscopy the sources of dissolved organic matter in soils subjected to drying. Chemosphere 38:45–50